WESTERN SYDNEY
UNIVERSITY

Hawkesbury Institute
for the Environment

ENVIRONMENTAL REGULATION OF ENERGETICS OF C_4 PHOTOSYNTHESIS

Julius Ver Morales Sagun

A thesis submitted in fulfilment of the requirements for the degree of Doctor of Philosophy

Hawkesbury Institute for the Environment

Western Sydney University

Australia

July 2019

This thesis is dedicated to my parents and supervisors for their endless support and encouragement.

ACKNOWLEDGEMENTS

It is with great pleasure that I wish to express my utmost gratitude to my principal supervisor, Assoc Prof Oula Ghannoum whose expertise was invaluable in the formulating of the research topic and for her continuous encouragement, advice, and guidance. She has been a source of generosity, insight and inspiration; guiding me in all my efforts throughout my candidature. I owe my research achievements to her enthusiastic supervision. I acknowledge with great gratitude my co-supervisor Prof Fred Chow (Australian National University) for giving me the opportunity to conduct my research at his lab and for sharing his knowledge regarding light photosynthesis and instrumentations. Successful completion of this thesis would not have been possible without their invaluable insights and comments on my work.

I gratefully acknowledge the Western Sydney University and the Australian Research Council for granting me the Postgraduate Research Award. I also acknowledge the vibrant Hawkesbury Institute for the Environment and the ARC Centre of Excellence for Translational Photosynthesis for providing a stimulating academic environment and a platform to interact with renowned researches in Photosynthesis.

I acknowledge with great gratitude Prof Murray Badger (Australian National University) for teaching me how to operate the MIMS and for his valuable scientific comments and discussion on research ideas. I am also thankful for all the people of von Caemmerer lab and Whitney lab for their assistance throughout my experiments at ANU.

My gratitude also goes to staff at the Hawkesbury Institute for the Environments, Dr David Harland, Patricia Hellier, Lisa Davison, Jenny Harvey, Gavin McKenzie, David Thompson and Kerri Sherriff for their generous support on administrative and laboratory work. I wish to thank my research group colleagues Fiona Koller, Walter Israel, Samantha Prior, Urs Benning, Yazen Al-Salman, Dr Sachin Chavan, Dr Bala Sonawane, Dr Clémence Henry, Dr Alex Watson-Lazowski, Dr Christie Foster, and Dr Javier Cano Martin for their friendship and support throughout my candidature. I am thankful to all my PhD colleagues at WSU and ANU. As always, my heartfelt gratitude goes to my family members for their love and constant support throughout my life and for motivating me to pursue an academic career.

STATEMENT OF AUTHENTICATION

The work presented in this thesis is, to the best of my knowledge and belief, original except as acknowledged in the text. I hereby declare that I have not submitted this material, either in full or in part, for a degree at this or any other institution.

TABLE OF CONTENTS

ACKNOWLEDGEMENTS ..... **iii**
STATEMENT OF AUTHENTICATION ..... **iv**
TABLE OF CONTENTS ..... **v**
LIST OF FIGURES ..... **xi**
LIST OF TABLES ..... **xiii**
LIST OF SUPPLEMENTARY TABLES ..... **xiv**
LIST OF SUPPLEMENTARY FIGURES ..... **xv**
ABBREVIATIONS ..... **xvi**
GENERAL ABSTRACT **1**
CHAPTER 1 ..... **4**
GENERAL INTRODUCTION **4**
1.1 C_3 Photosynthesis **5**
1.1.1 Light dependent reactions **5**
1.1.2 Light independent reactions or Calvin cycle **5**
1.2 Photorespiration **6**
1.3 C_4 photosynthesis **7**
1.3.1 Biochemistry, physiology and anatomy **8**
1.3.2 C_4 photosynthesis subtypes **10**
1.3.2.1 NADP-ME type *10*
1.3.2.2 NAD-ME type *11*
1.3.2.3 PCK type *11*
1.4 Quantum yield and the distribution of C_3 and C_4 plants **12**
1.5 Energetics of C_3 and C_4 photosynthesis **14**
1.5.1 Energetics of C_3 photosynthesis **14**
1.5.2 Energetics of NADP-ME subtypes **15**
1.5.3 Energetics of NAD-ME subtypes **16**
1.5.4 Energetics of PCK subtypes **16**
1.6 Alternative electron flows **19**
1.6.1 Cyclic electron flow around PSI **19**
1.6.2 Mehler reaction **20**
1.6.3 Quantification of the magnitudes of CEF and Mehler reaction **21**
1.7 Environmental responses of the light reactions of C_4 photosynthesis **25**
1.7.1 Responses to shade **25**

1.7.2 Responses to low CO_2 28
1.8 Knowledge gaps 30
1.9 Aims and objectives 32
1.10 Thesis outline and structure 34
CHAPTER 2 35
CYCLIC ELECTRON FLOW AND LIGHT PARTITIONING BETWEEN THE TWO PHOTOSYSTEMS IN LEAVES OF PLANTS WITH DIFFERENT FUNCTIONAL TYPES 35
ABSTRACT 36
2.1 INTRODUCTION 37
2.2 MATERIALS AND METHODS 40
2.2.1 Plant culture 40
2.2.2 Membrane inlet mass spectrometry (MIMS) 40
2.2.3 Measurement of ETR1 40
2.2.4 Determination of fI and calculation of CEF 42
2.2.5 Data analysis 44
2.3 RESULTS 45
2.3.1 Comparing two methods for estimating the fraction of absorbed light partitioned to PSI (f_I) 45
2.3.2 The response of ETR1 and CEF in C_3 and C_4 grass species to shade 46
2.3.3 Rates of CEF of other species in response to irradiance 47
2.4 DISCUSSIONS 48
2.4.1 The use of CEF inhibitors is unreliable for f_I estimation in leaves of C_4 grasses… 48
2.4.2 Advantages of simultaneous measurement of Chl fluorescence and gas exchange rate under low irradiances for f_I determination 49
2.4.3 Comparison of f_I across a wide range of species and in response to shade 49
2.4.4 CEF at increasing irradiance 50
2.4.5 Induction of CEF among different species (C_3 and C_4 grasses, gymnosperms, ferns, and liverwort) under high light 50
2.4.6 Capacity for CEF among the C_4 subtypes 51
2.4.7 Induction of CEF in shade-grown C_3 and C_4 species 51
2.5 CONCLUSIONS 53

CHAPTER 3 67

OXYGEN EXCHANGE AND MEHLER REACTION IN LEAVES OF C_3 AND C_4 PLANTS 67

ABSTRACT 68

3.1. INTRODUCTION 69

3.2. MATERIALS AND METHODS 73

3.2.1 Plant culture 73

3.2.2 Membrane inlet mass spectrometry 73

3.2.3 Definitions 74

3.2.4 Calculation of assimilation quotient (*AQ*), rates of Rubisco carboxylation (V_c) and oxygenation (V_o), and Mehler reaction (*Me*) 74

3.2.5 Data analysis 75

3.3 RESULTS 76

3.3.1 Light dependence of oxygen exchange 76

3.3.2 Estimates of *AQ*, V_o, V_c, V_o/V_c, and *Me* under high pCO_2 77

3.3.3 Estimates of V_o, V_c, V_o/V_c, and *Me* at Γ 78

3.4 DISCUSSIONS 80

3.4.1 O_2 exchange of control-grown C_3 and C_4 grasses at high pCO_2 80

3.4.2 O_2 exchange of gymnosperms, liverwort and fern at high pCO_2 81

3.4.3 O_2 exchange of shade-grown grasses at high pCO_2 82

3.4.4 O_2 exchange at the CO_2 compensation point 83

3.5 CONCLUSIONS 85

CHAPTER 4 100

EFFECTS OF LOW LIGHT INTENSITY ON THE ENERGETICS OF CLOSELY RELATED C_3, C_3-C_4 AND C_4 GRASSES 100

ABSTRACT 101

4.1. INTRODUCTION 102

4.2. MATERIALS AND METHODS 105

4.2.1. Plant culture 105

4.2.2. Leaf gas exchange and chlorophyll fluorescence measurements 105

4.2.3. Electrochromic signal to determine the photosystem stoichiometry 105

4.2.4. Quantification of functional PSII by the oxygen yield per single turn-over flash…… 107

4.2.5. Estimation of steady-state cyclic electron flux (CEF) around PSI using custom-built equipment 107

4.2.5.1. LEF_{O2} measurement 107
4.2.5.2. ETR1 measurement from redox kinetics of P700 107
4.2.6. Measurements of leaf reflectance, transmittance and absorptance 109
4.2.7. Chlorophyll fluorescence using Dual-PAM 109
4.2.8. Quantum yield for CO_2 uptake and assimilation quotient calculations 111
4.2.9. Carotenoid and chlorophyll analysis and quantification by HPLC 111
4.2.10. Activity of Rubisco, PEPC, NADP-ME, NAD-ME and PCK 112
4.2.11. Data analysis 113
4.3. RESULTS 114
4.3.1 Photosynthetic rate and PSII content 114
4.3.2 Using electrochromic signal to determine the photosystem stoichiometry 114
4.3.3 Leaf electron fluxes 114
4.3.4 Custom-built unit versus commercial equipment for measuring leaf electron fluxes 115
4.3.5 Leaf optical properties 116
4.3.6 Activity of photosynthetic enzymes 117
4.3.7 Quantum yield and assimilation quotient 117
4.4 DISCUSSIONS 118
4.4.1 Photosynthetic characteristics and responses to shade in the C_3 and C_3-C_4 species 118
4.4.2 Overall comparison among C_4 species 119
4.4.3 The two NADP-ME species had higher CEF and QY relative to other C_4 species… 119
4.4.4 The NAD-ME species had the lowest energy efficiency and sensitivity to LL relative to other C_4 species 121
4.4.5 Changes in leaf pigments and absorptance under shade reflect composition of light harvesting complexes rather than increased photoprotection 121
4.4.6 Comparison between custom-built and commercial equipment 123
4.5 CONCLUSIONS 125
CHAPTER 5 145
ACCLIMATION OF C_4 PHOTOSYNTHETIC LIGHT REACTIONS TO LOW LIGHT AND LOW CO_2 145
ABSTRACT 146
5.1 INTRODUCTION 147
5.2 MATERIALS AND METHODS 150

5.2.1. Experimental set-up 150
5.2.2. Photosynthesis measurement 150
5.2.3. Dual-PAM measurements 151
5.2.4. Leaf reflectance, transmittance and absorptance measurements 152
5.2.5. Quantum yield for CO_2 uptake (*QY*) 153
5.2.6. Quantification of functional PSII by the oxygen yield per single turn-over flash……..... 153
5.2.7. Carotenoid and chlorophyll analysis and quantification by HPLC 153
5.2.8. Content of Rubisco and activity of PEPC, NADP-ME, NAD-ME and PCK…… 154
5.2.9. Leaf dry mass 155
5.2.10. Statistical analysis 155
5.3 RESULTS 157
5.3.1. Leaf gas exchange under low light and low CO_2 157
5.3.2. PSII content 157
5.3.3. Effect of low light and low [CO_2] on energy distribution of light absorbed by PSI and PSII 158
5.3.4. Rates of various electron transports under low light and low [CO_2] 159
5.3.5. LMA and Rubisco content 159
5.3.6. Activity of C_4 cycle enzymes in C_4 plants 160
5.3.7. Pigment content and composition in leaves under low light and low [CO_2]……..... 160
5.3.8. Leaf optical properties and the *QY* under low light and low [CO_2] 161
5.3.9. Quantum yield for CO_2 uptake (*QY*) under low light and low [CO_2] 161
5.4 DISCUSSIONS 162
5.4.1. Photosynthetic rate was down-regulated in greater extent under low light than under low [CO_2]: C_3, C_3-C_4, and C_4 pathways 162
5.4.2. Efficiency of light reactions in PSI and PSII was down-regulated in greater extent under low light than under low [CO_2]: C_3, C_3-C_4, and C_4 pathways 163
5.4.3. Light-harvesting processes was down-regulated in greater extent under low light than under low [CO_2]: C_3, C_3-C_4, and C_4 pathways 164
5.4.4. Photosynthetic enzymes in the C_4 species were more affected by low light than by low CO_2 166
5.5 CONCLUSION 167

CHAPTER 6 ..... **181**
GENERAL DISCUSSIONS **181**
6.1. Overall thesis summary **182**
6.2. Overall thesis conclusions **183**
6.2.1. Experimentally derived f_I is important for the accurate estimation of the rates of electron fluxes through PSI **184**
6.2.2. Magnitude of Mehler reaction was negligible in high light-grown plants but was greatly stimulated in shade-grown plants **185**
6.2.3. Efficiency of light reactions of photosynthesis in C_3, C_3-C_4 and C_4 species were down-regulated under long-term shade exposure **186**
6.2.4. Efficiency of photosynthesis and light reactions in PSI and PSII were down-regulated more under low light than under low CO_2 in C_3, C_3-C_4, and C_4 species… **187**
6.2.5. Simultaneous measurements of CO_2 and O_2 fluxes enabled the estimation of the capacity for the photosynthetic reduction of nitrate (NO_3^-) among plant species as reflected by the assimilation quotient (*AQ*) **188**
6.3. Future Outlook **189**
REFERENCES **195**

LIST OF FIGURES

Figure 1. 1 Light-dependent and light independent reactions of photosynthesis 6
Figure 1. 2 Carboxylase and oxygenase activities of Rubisco. 7
Figure 1. 3 Profiles of modelled atmospheric CO_2 and O_2 partial pressures 8
Figure 1. 4 Anatomy of C_4 leaves and the C_4 photosynthetic pathway 9
Figure 1. 5 NADP-ME subtype 10
Figure 1. 6 NAD-ME subtype 11
Figure 1. 7 PCK subtype 12
Figure 1. 8 Global distribution of C_3 and C_3 grasses 13
Figure 1. 9 Quantum yield for CO_2 uptake (QY) in different photosynthetic pathways 14
Figure 1. 10 The leaf temperature dependence of the absorbed quantum yield for CO_2 uptake 15
Figure 1. 11 Minimum requirements for ATP and NADPH in subtypes of C_4 photosynthesis 18
Figure 1. 12 Cyclic electron flow around PSI 19
Figure 1. 13 The Mehler reaction 20
Figure 1. 14 Simultaneously collected values for ETR1 utilizing Y(I) obtained by the P700+ signal and ETR2(O2) based on gross oxygen fluxes measured with membrane inlet mass spectrometry (MIMS) 23
Figure 1. 15 Net CO_2 and O_2 exchange, $^{16}O_2$ evolution and $^{18}O_2$ uptake of wild-type and anti-SSu measured with MIMS 24
Figure 1. 16 Acclimation of the light-harvesting complexes in leaf to varying growth irradiance 26
Figure 1. 17 Decrease of photosynthetic activity and alterations in pigment composition the course of CO_2 starvation in tobacco 30
Figure 2. 1 Electron fluxes through PSII in response to measurement irradiance 61
Figure 2. 2 Corrected electron fluxes using experimentally derived f_I 62
Figure 2. 3 Cyclic electron flux around PSI (CEF) in response to irradiance 63
Figure 2. 4 Various electron fluxes of control plants measured at 1000 µmol photons m^{-2} s^{-1} (HL) and shade-grown plants measured at 200 µmol photons m^{-2} s^{-1} (LL) 64
Figure 3. 1 Light dependence of O_2 exchange in leaf discs of control and shade-grown plant species 91
Figure 3. 2 Rate of gross O_2 uptake at high pCO_2 and at compensation point 92
Figure 3. 3 Gross O_2 uptake rate at high pCO_2 and corresponding O_2 uptake in the dark 93
Figure 3. 4 Rates of Rubisco oxygenation (V_o) and carboxylation (V_c), and capacity for Mehler reaction (Me) at high pCO_2 and under increasing irradiance 94
Figure 3. 5 Assimilation quotient (AQ) at high pCO_2 and under increasing irradiance 95
Figure 3. 6 Rates of Rubisco oxygenation (V_o*) and carboxylation (V_c*), and capacity for Mehler reaction (Me*) at compensation point (Γ) and under increasing irradiance 96
Figure 4. 1 CO_2 assimilation, functional PSII content, PSII/PSI ratio, and the quantum yield for CO_2 uptake 134
Figure 4. 2 Various electron fluxes in leaves of control and shade-grown C_3, C_3-C_4 and C_4 grasses 135

Figure 4. 3 Leaf average spectral absorptance 136
Figure 4. 4 Content of chlorophyll and carotenoids in leaf 137
Figure 4. 5 Activities of the C_4 decarboxylases 138
Figure 5. 1 Various electron fluxes in leaves of C_3, C_3-C_4 and C_4 species under low light and low [CO_2] 174
Figure 5. 2 Acclimation of photosynthetic enzymes leaf of C_3, C_3-C_4 and C_4 species under low light and low [CO_2] 175
Figure 5. 3 Contents of chlorophyll and carotenoids in leaf of C_3, C_3-C_4 and C_4 species under low light and low [CO_2] 176
Figure 5. 4 Average leaf spectral absorptance at 400 nm to 800 nm of C_3, C_3-C_4 and C_4 species under low light and low [CO_2] 177
Figure 5. 5 Absorbed quantum yield for CO_2 uptake at saturating irradiance and at growth irradiance in leaf of C_3, C_3-C_4 and C_4 species under low light and low [CO_2] 178
Figure 6. 1 Low [CO_2] and shade acclimation of physiological parameters in C_3, C_3-C_4 and C_4 species 192
Figure 6. 2 Absorbed quantum yields for CO_2 uptake (QY_{1000}) by C_3, C_3-C_4 and C_4 species under shade and low [CO_2] environments 193
Figure 6. 3 The assimilation quotient (AQ_{1000}) of C_3, C_3-C_4 and C_4 species grown under shade 194

LIST OF TABLES

Table 2. 1 The fraction of absorbed light partitioned to PSI (f_I) 54
Table 2. 2 Statistical summary 56
Table 3. 1 Statistical summary 86
Table 4. 1 Statistical summary 126
Table 4. 2 Parameters measured using Licor and custom-built equipment (as described in MM) in representative species of C_3, C_3-C_4, and C_4 plants.....127
Table 4. 3 Content of leaf pigments in representative C_3, C_3-C_4, and C_4 species 129
Table 4. 4 Activities of Rubisco, PEPC and decarboxylases and soluble protein content.....131
Table 5. 1 Statistical summary 168
Table 5. 2 Parameters derived from *A*–*C*i curve, light response curve, Dual-PAM measurements, and LMA in leaf of C_3, C_3-C_4 and C_4 species 170
Table 5. 3 Pigment composition in leaves C_3, C_3-C_4 and C_4 species 172

LIST OF SUPPLEMENTARY TABLES

Table 2. S 1 Fraction of absorbed light partitioned to PSI (f_I) under increasing irradiances. ..57
Table 2. S 2 Responses of various electron fluxes to increasing irradiance.....58
Table 3.S 1 Summary of CO_2 and O_2 exchange data of C_3 and C_4 species grown at high light (CONTROL) and SHADE 88
Table 3.S 2 Summary of CO_2 and O_2 exchange data of gymnosperms, liverwort and fern species.....90
Table 4. S 1 Dual-PAM parameters 133

LIST OF SUPPLEMENTARY FIGURES

Figure 2. S 1 Cross sectional diagram of the gas exchange cuvette 65
Figure 2. S 2 An example of the determination of energy conversion efficiency in PSI by Saturating Pulse method of Dual-PAM (Klughammer & Schreiber, 2008) 66
Figure 3.S 1 Summary of the differences in main gas fluxes occurring in an illuminated leaf. 97
Figure 3.S 2 Cross-sectional diagram of the gas exchange cuvette. 98
Figure 3.S 3 Typical gas exchange traces of gross O_2 evolution, gross O_2 uptake and net CO_2 uptake measured using MIMS. 99
Figure 4. S 1 The amplitude of the fast rise in the EC signal 139
Figure 4. S 2 An example of changes in the oxidation state of P700 in leaf segments 140
Figure 4. S 3 An example of HPLC chromatogram of leaf extract 141
Figure 4. S 4 Relationships between photosynthetic rate at 1000 µmol photons m^{-2} s^{-1} (A_{1000}) and various electron transport fluxes using custom built equipment. 142
Figure 4. S 5 Average leaf spectral absorptance for control (A) and shade-(B) grown plants 143
Figure 4. S 6 Relationship between total leaf chlorophylls and total leaf carotenoids 144
Figure 5. S 1 Photosynthetic CO_2 response curves (A-C_i) of C_3, C_3-C_4 and C_4 species under low light and low [CO_2] 179
Figure 5. S 2 Photosynthetic light response curves of C_3, C_3-C_4 and C_4 species under low light and low [CO_2] 180

ABBREVIATIONS

$[CO_2]$	-	level of CO_2 concentration (ppm)
ΔpH	-	pH gradient
3-PGA	-	3-phosphoglycerate
A	-	CO_2 assimilation rate (µmol CO_2 m^{-2} s^{-1})
A_{sat}	-	saturated CO_2 assimilation rate (µmol CO_2 m^{-2} s^{-1})
Abs	-	leaf absorptance
A-C_i	-	Response of CO_2 assimilation rate to interecllular CO_2 concentration
ADP	-	Adenosine diphosphate
AL	-	Actinic light (µmol photons m^{-2} s^{-1})
AQ	-	Assimilation quotient (mol CO_2 mol^{-1} O_2)
ATP	-	Adenosine triphosphate
BSC	-	Bundle-sheath cell
C_3	-	C_3 photosynthesis pathway
C_4	-	C_4 photosynthesis pathway
CCM	-	Carbon concentrating mechanism
CEF	-	Rate of cyclic electron flux around Photosystem I (µmol electron m^{-2} s^{-1})
Chl	-	Chlorophyll
CSR	-	CO_2 saturated rate (µmol CO_2 m^{-2} s^{-1})
Cyt b_6f	-	Cytochrome b_6f complex
e^-	-	Electron
ETR1	-	Electron transport rate through Photosystem I
ETR2	-	Electron transport rate through Photosystem II
Fd	-	Ferredoxin
f_I	-	fraction of the absorbed white light partitioned to Photosystem I
f_{II}	-	fraction of the absorbed white light partitioned to Photosystem II
F_v/F_m	-	Maximum quantum yield of Photosystem II
G3P	-	Glyceraldehyde 3-phosphate
HL	-	High light intensity (µmol photons m^{-2} s^{-1})
I	-	Irradiance (µmol photons m^{-2} s^{-1})
K_{cat}	-	Rubisco catalytic activity (s^{-1})

LEF_{O2}	-	Rate of linear electron flow through Photosystem II and I (µmol electron m^{-2} s^{-1})
LHC	-	Light harvesting complexes
LHCI	-	Light harvesting chlorophyll-protein complex of Photosystem I
LHCII	-	Light harvesting chlorophyll-protein complex of Photosystem II
LL	-	Low light intensity (µmol photons m^{-2} s^{-1})
LMA	-	Leaf mass per area
LSU	-	Rubisco large subunit
LUE	-	Light use efficiency
MC	-	Mesophyll cell
MDH	-	Malate dehydrogenase
Me	-	Rate of Mehler reaction (µmol electron m^{-2} s^{-1})
MIMS	-	Membrane inlet mass spectrometry
ML	-	Medium light intensity (µmol photons m^{-2} s^{-1})
NAD-ME	-	Nicotinamid adenine dinucleotide malic enzyme
NADPH	-	Nicotinamide adenine dinucleotide phosphate
NADP-ME	-	Nicotinamide adenine dinucleotide phosphate malic enzyme
NPQ	-	Non-photochemical quenching
P680	-	Photosystem II reaction centre
P700	-	Photosystem I reaction centre
PC	-	Plastocyanin
PCK	-	Phosphoenolpyruvate carboxykinase
pCO_2	-	CO_2 partial pressure
PEPC	-	Phosphoenolpyruvate carboxylase
PET	-	Photosynthetic electron transport
PG	-	Phosphoglycolate
P_m	-	Maximum photo-oxidisable P700 content
PMF	-	Proton-motive force
PPDK	-	Pyruvate orthophosphate dikinase
PQ	-	Plastoquinone
PQH2	-	Plastoquinol
PSI	-	Photosystem I
PSII	-	Photosystem II
qP	-	Coefficient of photochemical quenching

QY	-	Quantum yield for CO_2 uptake (mol CO_2 mol^{-1} photons)
R^2	-	Regression coefficient
R_d	-	Rate of mitochondrial respiration under dark (µmol O_2 m^{-2} s^{-1})
R_l	-	Rate of mitochondrial respiration under light (µmol O_2 m^{-2} s^{-1})
Rubisco	-	Ribulose-1, 5-bisphosphate carboxylase/ oxygenase
RuBP	-	Ribulose-1, 5-bisphosphate
s.e.	-	Standard error
sFR	-	Strong far-red light
SL	-	Saturating light intensity (µmol photons m^{-2} s^{-1})
SP	-	Saturating pulse
TTFA	-	Thenoyltrifluoroacetone
V_c	-	Rate of Rubisco carboxylation (µmol CO_2 m^{-2} s^{-1})
V_o	-	Rate of Rubisco oxygenation (µmol O_2 m^{-2} s^{-1})
wFR	-	Weak far-red light
Y(II)	-	Photochemical yield of photosystem II
Y(I)	-	Photochemical yield of photosystem I
Y(NA)	-	fraction of overall P700 that cannot be oxidized by a saturation pulse
Y(ND)	-	fraction of overall P700 that is oxidized in a given state due to a lack of donors
Γ	-	CO_2 compensation point
LC	-	Low CO_2 concentration (ppm)
C_i	-	Intercellular CO_2 concentration
PAR	-	Photosynthetic active radiation
CABP	-	2-carboxyarabinitol 1,5- bisphosphate

GENERAL ABSTRACT

Many studies have been aimed at understanding the biochemistry and significance of C_4 pathway since its discovery. It has become well established that this pathway enables the plant to photosynthesize at a higher rate than C_3 photosynthesis under conditions of high temperatures and limited water supply. This is because of the CO_2 concentrating mechanism (CCM) in C_4 photosynthesis achieved by a series of anatomical and biochemical adaptations which allow the operation of two photosynthetic cycles, C_4 and C_3, across the outer mesophyll (MC) and inner bundle-sheath cells (BSC) to saturate Rubisco with CO_2 in the BSC. CCM minimizes photorespiration where oxygen competes with CO_2 uptake which consumes additional energy and decreases productivity. Most importantly, the activity rate of C_4 photosynthesis is also higher under high light intensities thus it is not surprising to find C_4 plants in open and arid habitats leading them to an agricultural and ecological importance. C_4 photosynthesis is also traditionally grouped into three classical subtypes based on the major C_4 acid decarboxylation step in the BSC: NADP malic enzyme (NADP-ME), NAD-malic enzyme (NAD-ME), and PEP carboxykinase (PCK).

In view of the relative abundance of C_4 plants in high light environments, it is interesting to ascertain what physiological factors associated with C_4 photosynthesis might make it favourable in those environments. One reason is the differences in the maximum quantum yield for CO_2 uptake (QY), which is the leaf-level ratio of photosynthetic carbon gain to absorbed photons. Under elevated temperature (>25^{o}C) and ambient CO_2 concentrations, previous studies showed that C_3 species had lower QY than C_4 species and among C_4 subtypes, NAD-ME subtype had the lowest. Lower QY of C_3 species is due to photorespiration, however, causes of differences in the QY among C_4 subtypes are not clear. One reason for this variation is the efficiency of light energy conversion reactions (termed energetics) in MC and BSC which is associated with distinct composition, activity and/or efficiency of light-harvesting complexes (LHC) and electron transport components. Limited information is available explaining the connection between energetics under varying environmental conditions and QY among C_4 subtypes.

The main aim of this thesis was to investigate the plasticity of the components and activities of the light reactions of photosynthesis in representative species of C_3, C_3-C_4, and the three subtypes of C_4 species under environmental conditions that may affect the photosynthetic quantum yield such as low light and low CO_2.

The outcomes of this study contribute significant insights towards understanding of the known differences in QY and evolution of the three C_4 biochemical subtypes. This was achieved by addressing the following specific objectives: (i) establish a new method which can give a more reliable estimation of the partitioning of the absorbed light between the two photosystems in leaf; (ii) use this new method to quantify the magnitude of various electron fluxes *in vivo* in leaf; (iii) investigate the acclimation of the light reactions of photosynthesis under long-term exposure to shade as measured by the rates of various electron fluxes, stoichiometry of photosystems and composition of pigments; and (iv) investigate the acclimation of the light reactions of photosynthesis to long-term exposure to low light combined with low CO_2 condition in C_3 and C_3-C_4 species and among C_4 species with different biochemical subtypes. These objectives were accomplished in four different experimental chapters.

Chapters 2 and 3 aimed for the development of a new method which gave a more reliable estimation of the rates of electron fluxes in the leaf based on membrane inlet mass spectrometry (MIMS) and chlorophyll fluorescence method using a Dual-PAM/F. This method was used to experimentally determine the portion of the absorbed light that goes to PSI (f_I) which was needed to calculate cyclic electron flux (CEF) in leaves of plants with different functional types. It was shown that the majority of C_4 species examined had f_I of 0.6 which is higher than what is usually assumed. The C_3 grass had f_I of 0.4 which is lower compared to the model C_3 species. Other species such as liverwort and fern had f_I of 0.5 while gymnosperms had lower f_I. It was also shown that these values can change depending on the growing conditions such as irradiance. Since the method also measures gross O_2 evolution and uptake, this enabled us to estimate the capacity for Mehler reaction. We found that O_2 uptake of all high-light grown C_3 and C_4 species, including the gymnosperms, liverwort and fern measured under high irradiances had no significant difference with the rate of dark O_2 uptake. This suggests that these species have low or virtually no potential for the Mehler reaction and that the O_2 uptake was mainly due to photorespiration or mitochondrial respiration. However, O_2 uptake of shade-grown C_4 plants under high light was significantly higher compared to dark O_2 uptake, suggesting enhanced operation of Mehler reaction having 20-50% of the maximum electron flow.

Chapter 4 investigated the differences in the efficiency of light harvesting complexes (LHC) in leaves of representative species of C_4 plants together with C_3 and C_3-C_4 species to elucidate if the high photosynthetic QY observed in C_4 grasses and the variations in QY among the subtypes are associated with differences in the activity and stoichiometry of the photosystems

and/or pigment composition. This chapter also investigated how changes in the light intensity during growth induce changes in the components of the light reactions thus altering the relative light absorption and energy conversion efficiency by PSI and PSII. Results showed that NAD-ME species were generally outperformed by NADP-ME and PCK species and even by C_3 and C_3-C_4 species under shade as reflected by a great decrease in the activities and composition of the light harvesting components, absorptance and efficiency.

Chapter 5 further investigated the plasticity of light harvesting components under changing environmental conditions such as low light, low CO_2 and the combination of these two conditions to also provide insight into the physiology of C_4 plants under the low CO_2 conditions that led to their evolution. This chapter demonstrated that low light influenced the changes in the activities of photosystem complexes and the rate of photosynthesis to a greater extent than low CO_2 in C_3, C_3-C_4 and C_4 species. This was evident by heightened decreases in yield efficiency of PSI and PSII and down-regulation of various electron transport rates. Growth under low light also caused great reduction in photosynthetic enzyme content and activities in C_3, C_3-C_4 and C_4 species, whereas growth under low CO_2 had a limited effect. Among all photosynthetic types, C_4 species were observed to be less plastic under low light compared to C_3 and C_3-C_4 species in terms of photosynthesis rate. C_3 and C_3-C_4 species were observed to be less plastic under low light in terms of PSI and PSII efficiency.

In conclusion, this PhD project demonstrated that the observed high QY of C_4 species particularly the NADP-ME species based on the published studies might be associated with the comparatively greater plasticity adjustments in the light harvesting components of leaf under varying environmental conditions. This is very important acclimation characteristic as it maximises light energy absorption while preventing photo-inhibition under stress conditions such as long-term shade exposure. This ensures the light reactions can still provide the right ATP/NADPH ratio even under limited supply of light energy. Understanding how the mechanisms of the photosynthetic light reactions acclimate under low light condition gives us insights on the role of light energy conversion in the significant advantage of certain plants under shade.

CHAPTER 1

GENERAL INTRODUCTION

1.1 C_3 Photosynthesis

Photosynthesis is a series of processes in which sunlight powers the biosynthesis of carbohydrates. This process is divided into two types of reaction: the light dependent reactions (**Figure 1. 1A**) and the light independent reactions or Calvin cycle (**Figure 1. 1B**).

1.1.1 Light dependent reactions

The main function of these reactions is to produce ATP and NADPH, which are used to reduce CO_2 during the dark reactions (**Figure 1. 1A**). This takes place in the thylakoid membranes where protein-pigment complexes are located. There are four major protein complexes in the thylakoid membrane that are linked and work together during the process: Photosystem II (PSII), Cytochrome b_6f complex (cyt b_6f), Photosystem I (PSI), and ATP synthase. The first in the chain is the PSII reaction centre (P680) which uses light energy to split water and releases oxygen and proton within the granal lumen, and electrons to reduce the small molecule plastoquinone (PQ) to plastoquinol (PQH_2). Further this cycle produces reduced plastocyanin (PC) on the lumen side while also pumping protons from the stroma into the lumen. Reduced PC donates electrons to the reaction centre of PSI (P700). Light induced excitement of PSI leading to the reduction of ferredoxin which is capable of reducing $NADP^+$ to yield NADPH. The proton-motive force (PMF) drives a flow of protons through a transmembrane enzyme complex, ATP synthase, generating ATP from ADP on the stromal side of the membrane. This process is also termed as linear electron flow (LEF). Sometimes an organism has all the reductive power (NADPH) that it needs to synthesize new carbon skeletons, but still needs ATP to power other activities in the chloroplast. In this case, ATP is produced without the involvement of PSII through cyclic electron flow around PSI (CEF) and Mehler reaction, wherein proton gradient is generated across the membrane using the mechanisms of photosynthesis (**Figure 1. 1A**). These three modes of electron transport (LEF, CEF, and Mehler reaction) are all coupled to ATP synthesis (Allen, 2003; Lodish *et al.*, 2008).

1.1.2 Light independent reactions or Calvin cycle

In the light independent reactions or Calvin cycle, the enzyme Rubisco combines CO_2 with a five-carbon sugar, ribulose 1,5-bisphosphate (RuBP), to yield two molecules of a three-carbon compound, 3-phosphoglycerate (3-PGA). In the presence of ATP and NADPH produced during the light-dependent stages, 3-PGA is reduced to glyceraldehyde 3-phosphate (triose phosphate). Five out of the six molecules of the glyceraldehyde 3-phosphate produced are

used to regenerate RuBP (Calvin, 1962). The remaining triose phosphates are used in the synthesis of sucrose and starch and other C-skeletons (**Figure 1. 1B**) (Allen, 2003; Ghannoum *et al.*, 2005; Lodish *et al.*, 2008).

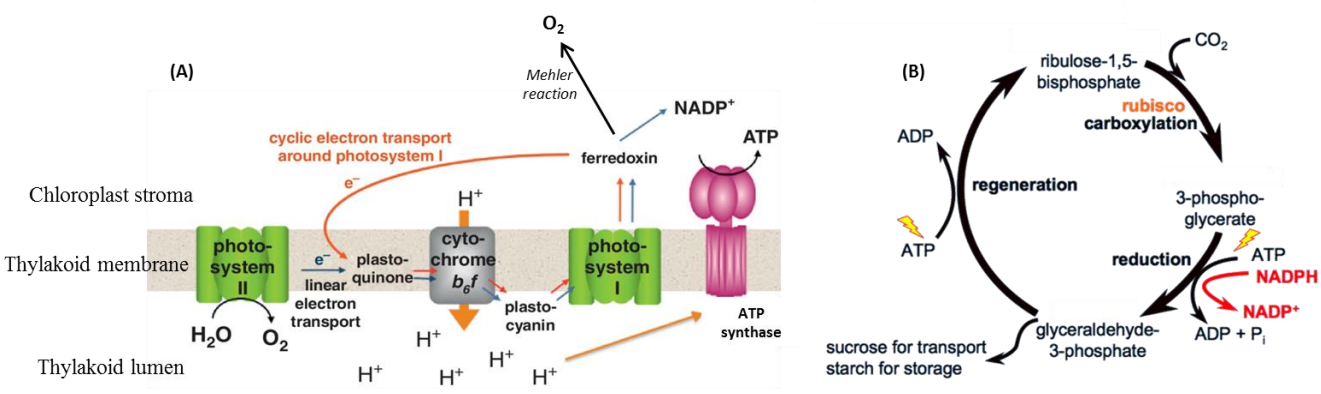

Figure 1. 1 Light-dependent and light independent reactions of photosynthesis

(A) Light-dependent reactions of photosynthesis and the proteins involved in the process which occur in thylakoid membrane of chloroplasts. **(B)** Dark reactions or the Calvin cycle occurring in three stages: 1. carboxylation, where the enzyme Rubisco incorporates carbon dioxide into an organic molecule, 2. Reduction, where the organic molecule is reduced, and 3.regeneration, where RuBP, the molecule that starts the cycle, is regenerated so that the cycle can continue (Lodish *et al.*, 2008).

1.2 Photorespiration

Rubisco is an important biological enzyme because it catalyses the primary chemical reaction by which inorganic carbon enters the biosphere (**Figure 1. 2**). Reflecting its importance, Rubisco is also the most abundant protein in leaves, accounting for about 50% of soluble leaf protein in C_3 plants (20–30% of total leaf nitrogen). Rubisco can also fix oxygen together with RuBP, resulting in one molecule each of 3-phosphoglycerate and 2-phosphoglycolate (Leegwood *et al.*, 2000; von Caemmerer & Quick, 2006). Phosphoglycolate has no known metabolic purpose and toxic at higher concentrations for the plant (Anderson, 1971). It therefore has to be processed in a metabolic pathway called photorespiration which demands additional ATP and leads to a net loss of CO_2 (**Figure 1. 2**). Thus, the efficiency of C_3 photosynthesis can be decreased by 40% under unfavorable conditions including high temperatures and aridity which trigger the oxygenation process (Ehleringer *et al.*, 1991). Photorespiratory fluxes are higher under high temperature conditions because the specificity of Rubisco for CO_2 relative to O_2 decreases with temperature and the solubility of O_2 in

aqueous solutions such as the cytoplasm and the chloroplast stroma is less affected by higher temperatures than the solubility of CO_2 (Ku & Edwards, 2004). The oxygenase reaction of Rubisco may be a relic of the evolutionary history of this enzyme, which evolved more than 3 billion years ago when atmospheric CO_2 concentrations were high and oxygen concentrations were low (Gowik & Westhoff, 2011). With the increase of oxygen and decrease of carbon dioxide concentrations in the atmosphere, certain plant species evolve to perform C_4 photosynthesis (Tcherkez *et al.*, 2006).

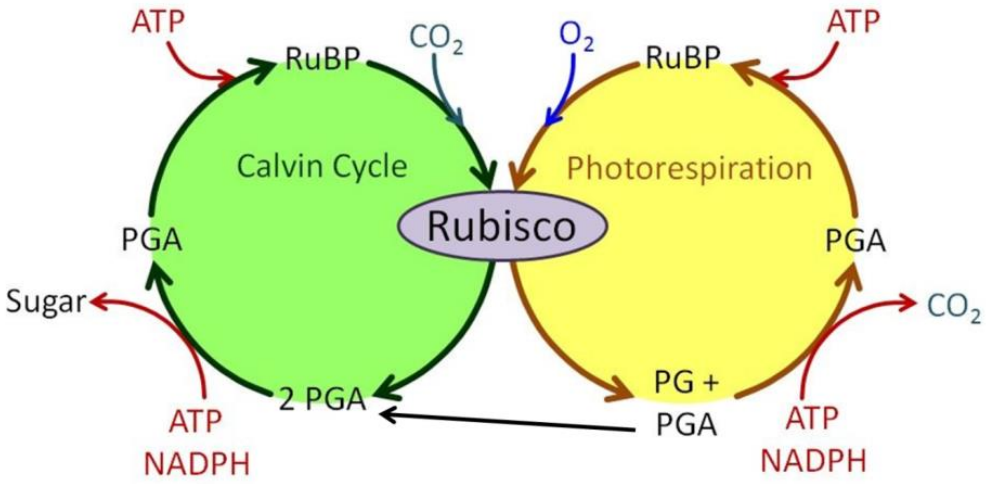

Figure 1. 2 Carboxylase and oxygenase activities of Rubisco.

1.3 C_4 photosynthesis

The period over which C_4 photosynthesis is postulated to have arisen in the grasses, and later in other groups, is characterized by progressive climate deterioration and falling atmospheric CO_2 levels (**Figure 1. 3**) (Christin *et al.*, 2008; Gowik & Westhoff, 2011; Sage, 2004). Atmospheric models estimate that CO_2 levels were three- to five fold greater than today during the mid-Cretaceous, and gradually declined to below current levels by Miocene/Pliocene times (5–15 million years ago) before reaching a low point in the later Pleistocene (Berner & Kothavala, 2001).

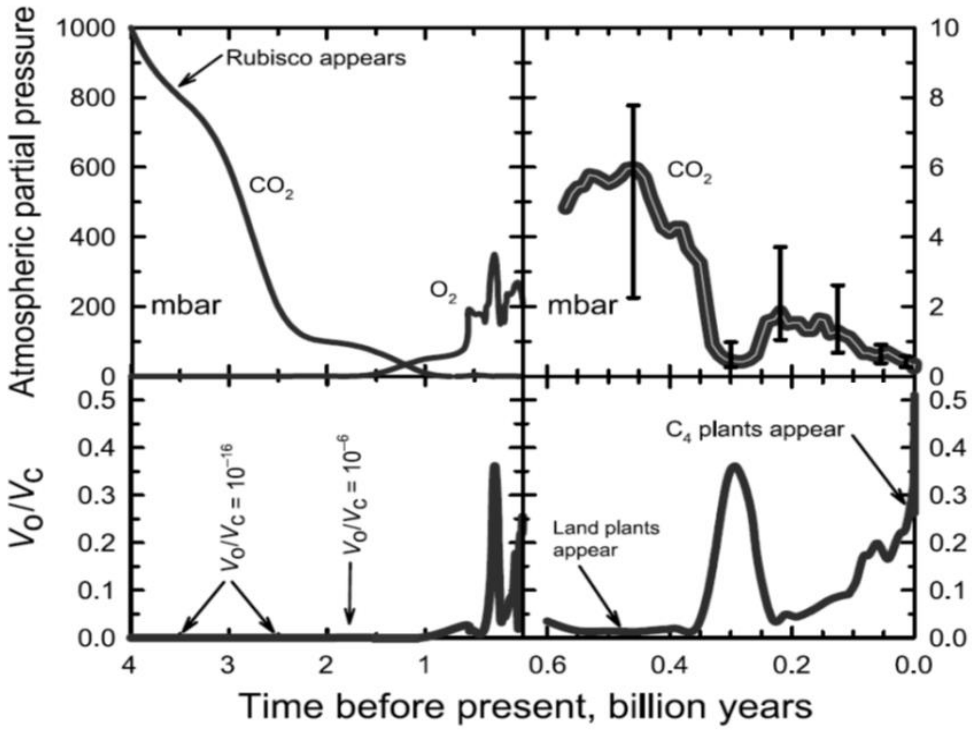

Figure 1. 3 Profiles of modelled atmospheric CO_2 and O_2 partial pressures

Profiles of modelled atmospheric CO_2 and O_2 partial pressures (in mbar) over the history of the earth and corresponding estimates of relative oxygenation potential for C_3 photosynthesis (Sage, 2004).

1.3.1 Biochemistry, physiology and anatomy

The establishment of C_4 photosynthesis includes several biochemical and anatomical modifications of C_3 photosynthesis allowing the concentration of CO_2 at the site of Rubisco, reducing photorespiration. In most C_4 plants the CO_2 concentration mechanism (CCM) is achieved by a specialized leaf cell arrangement called Kranz anatomy, involving 2 cell types: the mesophyll cells (MC) and the bundle sheath cells (BSC) (**Figure 1. 4**) (Edwards *et al.*, 2004; Gowik & Westhoff, 2011; Sage, 2004). In a C_3 leaf, the palisade MC typically form a layer in the upper part of the leaf; the corresponding MC in a C_4 leaf are usually arranged in a ring around the BSC. While the BSC of C_4 plants have chloroplasts, those of C_3 leaves usually lack them. Since Rubisco is housed inside the BSC, it works more efficiently than in C_3 plants because it operates under high CO_2 concentration. Consequently C_4 plants need less of this enzyme, which is by far the most abundant protein in leaves of C_3 plants. This leads to better nitrogen-use efficiency (NUE) of C_4 compared to C_3 plants (Oaks, 1994). Additionally, C_4 plants exhibit better water-use efficiency (WUE) than C_3 plants. Due to the CO_2

concentration mechanism, C_4 plants can keep their stomata more closed. Thus water loss by transpiration is reduced (Long, 1999).

In the MC of C_4 plants, CO_2 is converted to bicarbonate by carbonic anhydrase (CA) and initially fixed by phosphoenolpyruvate carboxylase (PEPC) using PEP as CO_2 acceptor, resulting into oxaloacetate (OAA), a 4-C acid. Oxaloacetate is rapidly converted to the more stable C_4 acids malate or asparate that diffuse to the BSC. Here, CO_2 is released by one of three different decarboxylating enzymes, which define the three basic biochemical subtypes of C_4 photosynthesis, NADP-dependent malic enzyme (NADP-ME), NAD-dependent ME (NAD-ME), and PEP carboxykinase (PEPCK or PCK). The released CO_2 is refixed by Rubisco, which exclusively operates in the BSC of C_4 plants. The 3-C compound resulting from CO_2 release diffuses back to the MC where the primary CO_2 acceptor PEP is regenerated by pyruvate orthophosphate dikinase (PPDK) by the use of two molecules of ATP (**Figure 1. 4**) (Hatch, 1987).

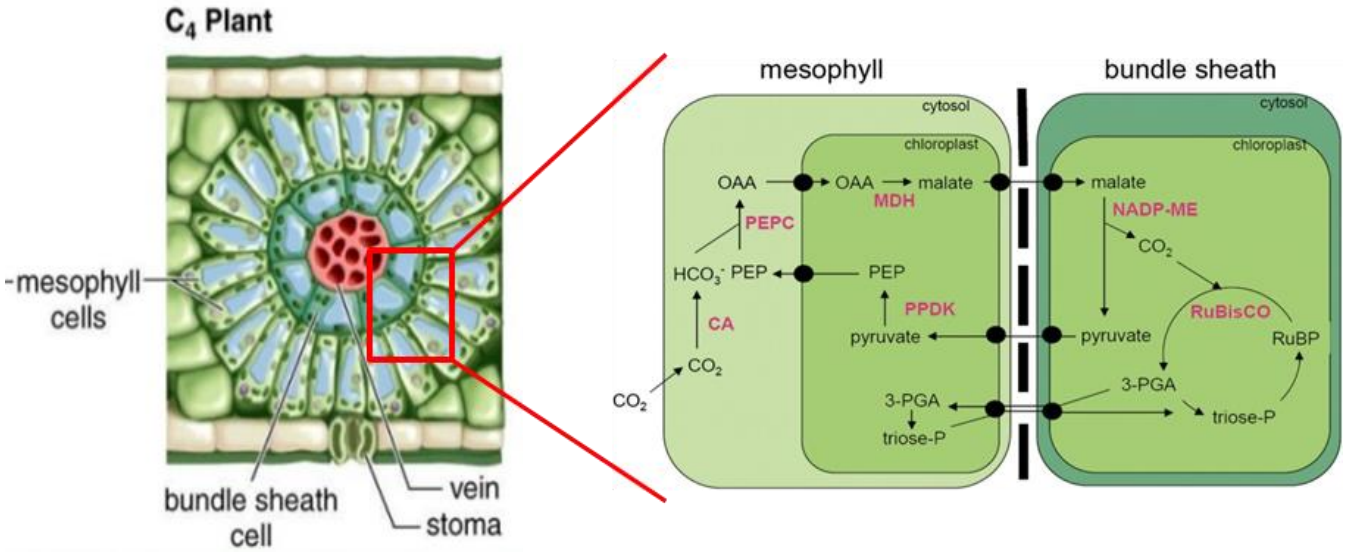

Figure 1. 4 Anatomy of C_4 leaves and the C_4 photosynthetic pathway

A schematic diagram showing the arrangements of BSC and MC (Kranz anatomy) and the schematic diagram of the C_4 photosynthetic pathway occurring in these two types of cells. CA: carbonic anhydrase; PEP: phosphoenolpyruvate; OAA: oxaloacetate; 3-PGA: 3-phosphoglycerate ; RuBP: ribulose 1,5-bisphosphate; PEPC: PEP carboxylase; MDH: malate dehydrogenase; PPDK: pyruvate phosphate dikinase; NADP-ME: NADP malic enzyme.

1.3.2 C_4 photosynthesis subtypes

C_4 plants have three subtypes based on the primary decarboxylating enzymes present in BSC. These are the NADP-malic enzyme (NADP-ME), NAD-malic enzyme (NAD-ME), and PEP carboxykinase (PEPCK or PCK) types. Although PEP-CK operates as a secondary decarboxylase in many C_4 species (Furbank, 2011; Leegood & Walker, 2003; Sharwood *et al.*, 2014; Wang *et al.*, 2014), the primary decarboxylase is generally associated with a suite of anatomical, biochemical and physiological features (Ghannoum *et al.*, 2011; Gutierrez *et al.*, 1974; Hattersley, 1992). Clear differences in leaf ultrastructure, morphological arrangements of BS chloroplasts, biochemistry of the MC and BSC and transport of metabolites between the two cell types exist among the C_4 subtypes (**Figure 1. 5** to **Figure 1. 7**) (Gowik & Westhoff, 2011; Kanai & Edwards, 1999; Romanowska & Drożak, 2006):

1.3.2.1 NADP-ME type

Bundle sheath (BS) chloroplasts are usually arranged in a centrifugal position relative to the vascular bundle, and have thylakoid membranes with reduced grana stacking. OAA, formed by carbon fixation by PEPC in the cytoplasm, is transported to mesophyll (M) chloroplasts, where most of it is reduced to malate. These acids are then exported to BSC. In BS chloroplasts, malate is decarboxylated by NADP-ME where CO_2 is released and used in Calvin cycle (Kanai & Edwards, 1999) (Error! Reference source not found.).

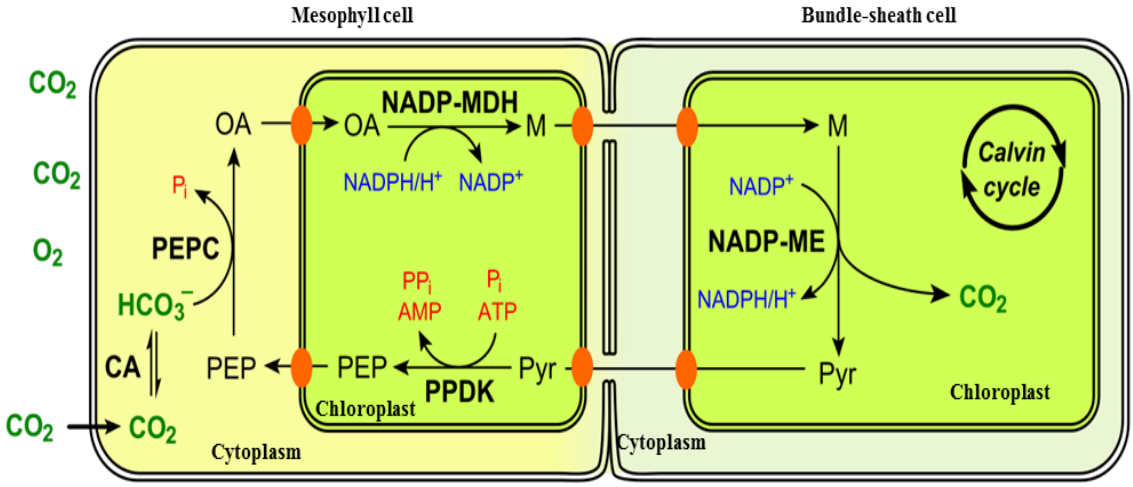

Figure 1. 5 NADP-ME subtype

The major metabolites and decarboxylating enzyme in the NADP-ME subtype. Adapted from Hatch (1987). Abbreviations: **CA**, carbonic anhydrase; **PEPC**, PEP carboxylase; **NADP-MDH**, NADP-malate dehydrogenase; **NADP-ME**, NADP malic enzyme; **PPDK**, Pyruvate phosphate dikinase; HCO_3^-, carbonic acid; PEP, Phosphoenolpyruvate; OA; oxaloacetate; M, Malate; Pyr, Pyruvate.

1.3.2.2 NAD-ME type

Both BS chloroplasts and mitochondria are located together in a centripetal position relative to the vascular bundle. BS chloroplasts also have thylakoid membranes with developed grana stackings. Aspartate is the main product of CO_2 fixation in the MC cytoplasm. It is then transported to BSC mitochondria, where it is deaminated to produce OA. OA is then reduced to malate which will be decarboxylated by NAD-ME to produce CO_2 (for Calvin cycle in BS chloroplasts) and pyruvate (Kanai & Edwards, 1999) (**Figure 1. 6**).

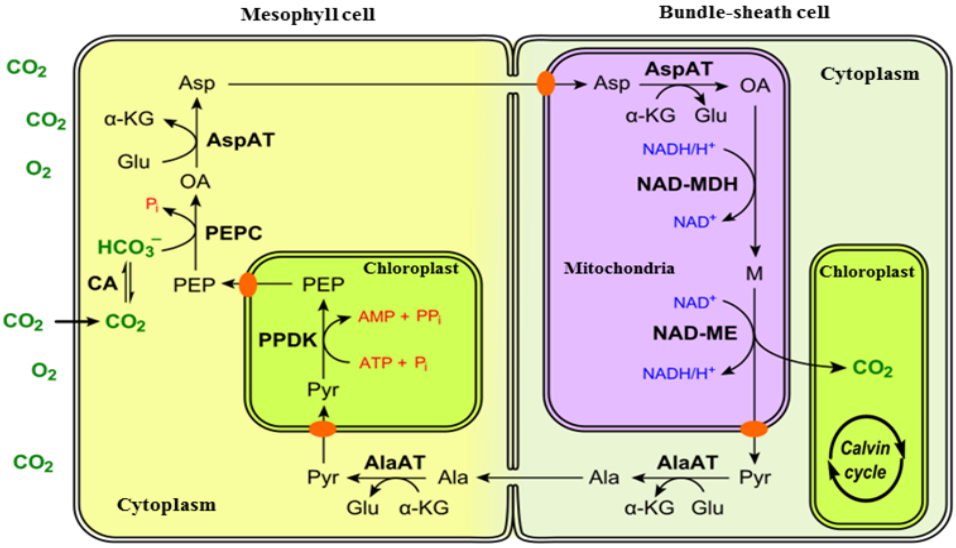

Figure 1. 6 NAD-ME subtype

The major metabolites and decarboxylating enzyme in the NAD-ME subtype. Adapted from Hatch (1987). Abbreviations: **CA**, carbonic anhydrase; **PEPC**, PEP carboxylase; **AspAT**, Aspartate aminotransferase; **NAD-MDH**, NAD-malate dehydrogenase; **NAD-ME**, NAD malic enzyme; **AlaAT**, Alanine aminotransferase; **PPDK**, Pyruvate phosphate dikinase; HCO_3^-, carbonic acid; PEP, Phosphoenolpyruvate; OA; oxaloacetate; M, Malate; Pyr, Pyruvate: Asp, Aspartate; Ala, Alanine.

1.3.2.3 PCK type

BS chloroplasts of also have well- developed grana stacks and are arranged evenly or in a centrifugal position. PCK in the BS cytoplasm is the main decarboxylation enzyme, but BS mitochondria also contain some activities of NAD-ME. Aspartate transported from M cytoplasm to BSC is deaminated and decarboxylated by PCK, whereas malate transported to BS mitochondria is decarboxylated by NAD-ME. Both CO_2 released during decarboxylation are used in Calvin cycle in BS chloroplast (Kanai & Edwards, 1999) (**Figure 1. 7**).

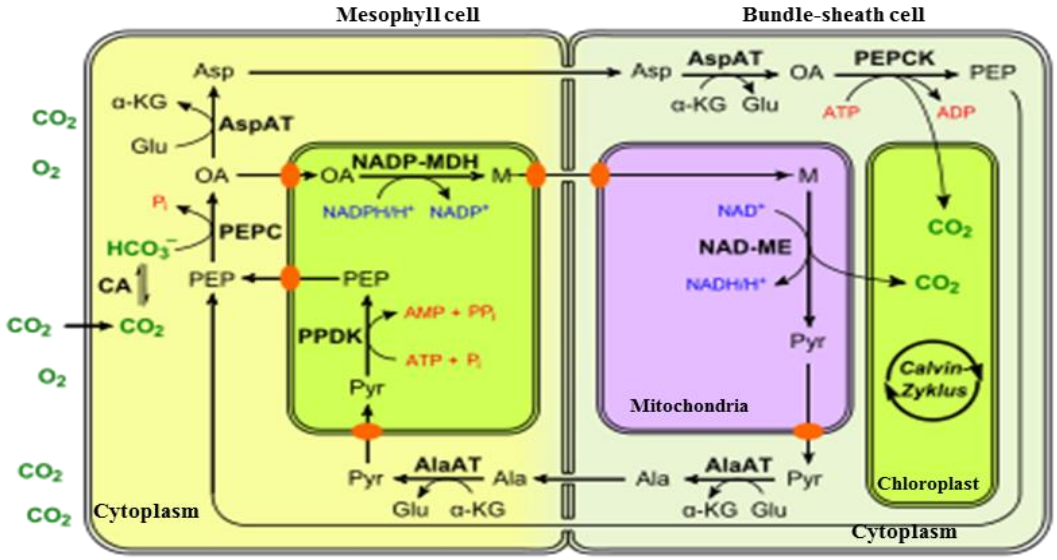

Figure 1. 7 PCK subtype

The major metabolites and decarboxylating enzyme in the PCK subtype. Adapted from Hatch (1987). Abbreviations: **CA**, carbonic anhydrase; **PEPC**, PEP carboxylase; **AspAT**, Aspartate aminotransferase; **PEPCK**, PEP carboxykinase; **NAD-MDH**, NAD-malate dehydrogenase; **NAD-ME**, NAD malic enzyme; **AlaAT**, Alanine aminotransferase; **PPDK**, Pyruvate phosphate dikinase; HCO_3^-, carbonic acid; PEP, Phosphoenolpyruvate; OA; oxaloacetate; M, Malate; Pyr, Pyruvate: Asp, Aspartate; Ala, Alanine.

1.4 Quantum yield and the distribution of C_3 and C_4 plants

The emergence of ecosystems dominated by C_4 species has transformed the biosphere; although comprising only 3% of vascular plant species, they account for some 25% of terrestrial photosynthesis (Still *et al.*, 2003). C_4 grasses commonly dominate warm-climate grasslands and savannas (**Figure 1. 8A**). These patterns correlate best with temperature (Edwards *et al.*, 2010). According to Sage *et al.* (1999), the principal determinants of C_4 success are the growing season temperature and availability of moderate-to-high light levels. In general, higher temperatures favour the growth of C_4 plants over that of C_3 plants in arid or semiarid regions (Ehleringer, 1978; Ehleringer *et al.*, 1997; Hattersley, 1983, 1992; Osmond *et al.*, 1982) (**Figure 1. 8B**).

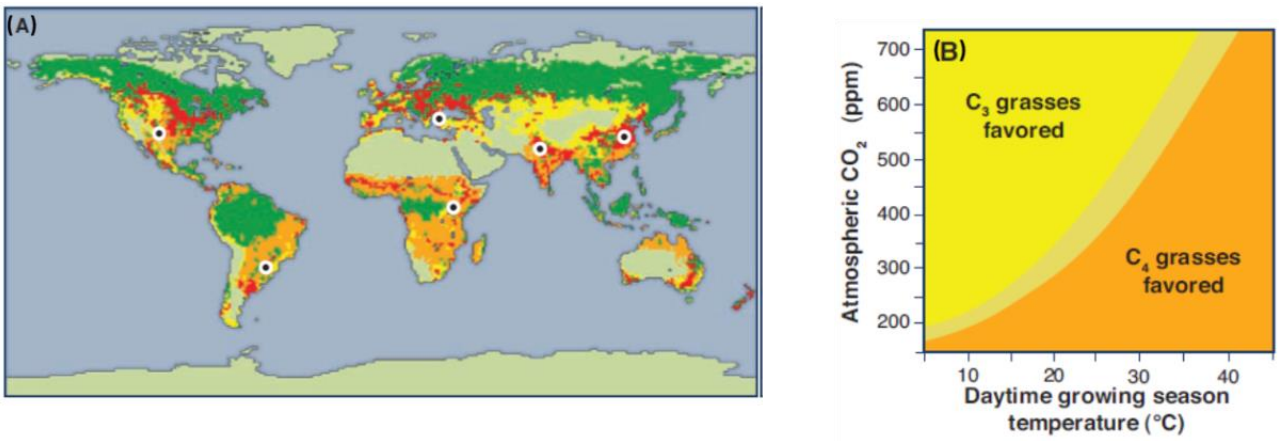

Figure 1. 8 Global distribution of C_3 and C_3 grasses

(A) Global distribution of C_4 (orange) or C_3 (yellow) grasses in forests (green) and woodlands, savannas, and grassland. Cropland (red) and shrubs, desert, bare ground, and ice (beige/brown) are also shown. White circles with black dots in the center indicate the regions in which the geological history of C_4 grasslands is best described. **(B)** The predicted atmospheric CO_2 and growing-season temperature conditions that favour the growth of C_3 or C_4 grasses, based on the quantum yield of photosynthesis, a measure of the inefficiency caused by photorespiration (Edwards *et al.*, 2010).

It was hypothesized by Ehleringer (1978) that the main physiological explanation for a temperature control on C_3/C_4 distributions is the quantum yield (QY). The QY is the ratio of moles of CO_2 assimilated to moles of photosynthetic active radiation (PAR) absorbed by a leaf (Ehleringer & Björkman, 1977). The hypothesis states that a higher QY should translate to a higher efficiency of light use at the canopy scale, and thus a higher capacity for growth and reproduction. Ehleringer & Pearcy (1983) surveyed the QY of a large number of C_4 species and found values ranging from 0.052 to 0.069 mol CO_2 per photons (**Figure 1. 9**).

However, their result suggested that QY of C_4 grass species are not temperature or irradiance dependent as compared to C_3 grasses. They observed that there was no significant decrease in the QY of both NAD-ME and NADP-ME type C_4 species over a 20 to 40°C leaf temperature range (**Figure 1. 10A**). In contrast, in a C_3 plant the QY is higher under normal atmospheric conditions but decreases under photorespiratory conditions (**Figure 1. 10B**). Importantly, QY appear to differ between C_4 grasses with different biochemical subtypes (**Figure 1. 9**).

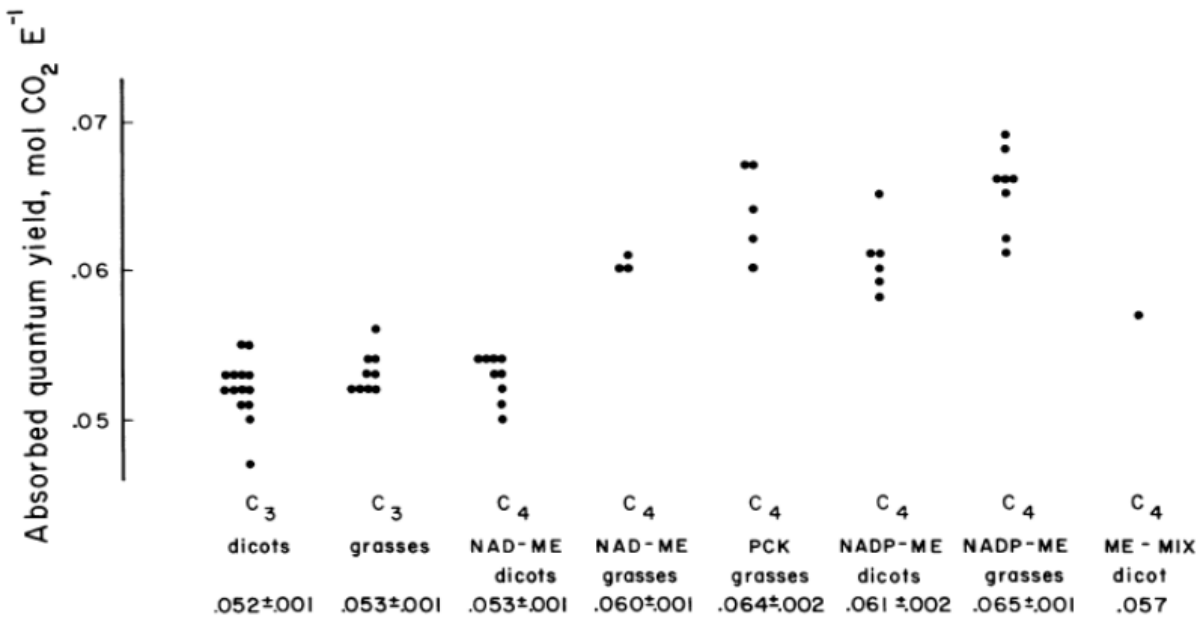

Figure 1. 9 Quantum yield for CO_2 uptake (QY) in different photosynthetic pathways

Quantum yield for CO_2 uptake (QY) in monocot and dicot plants with different photosynthetic pathways. Measurements were made at a leaf temperature of 30^{o}C, 330 ppm CO_2 and 21 kPa O_2 (Ehleringer & Pearcy, 1983).

1.5 Energetics of C_3 and C_4 photosynthesis

To understand why C_4 subtypes have different QY, it is important to understand the theoretical minimum energy requirements among C_4 subtypes.

1.5.1 Energetics of C_3 photosynthesis

In C_3 plants, 3 ATP and 2 NADPH per CO_2 fixed are used in the absence of photorespiration (Edwards & Walker, 1983). Twelve protons generated during light reaction will give 3 ATP molecules through the action of ATP synthase (Allen, 2003; Kramer & Evans, 2011). Photorespiration increases the requirements for both ATP and NADPH in addition to the requirements in the Calvin cycle. A recent study showed that the ATP/ NADPH ratio required for C_3 photosynthesis with photorespiration varied from 1.51 to 1.67 (Kramer & Evans, 2011).

In vivo, the energy requirement in C_4 photosynthesis should be further increased in comparison to C_3 photosynthesis, since ATP and NADPH for other metabolic pathways, such as nitrate assimilation or sucrose synthesis, and ATP for re-fixing CO_2, which is not captured by Rubisco and leaks out from BSC, are needed (Kanai & Edwards, 1999). CO_2 leakage from

BSC is unavoidable and if 10% of CO_2, which is fixed by PEPC and supplied to Rubisco, leaks from BSC during decarboxylation, 0.2 more ATP are needed (Amthor, 2010). Each subtype also involves different processes for the transport of metabolites to BSC and decarboxylation in BSC. As a result, they show different energy requirements (**Figures 1. 5** to **1. 7**) (Hatch, 1987; Kanai & Edwards, 1999).

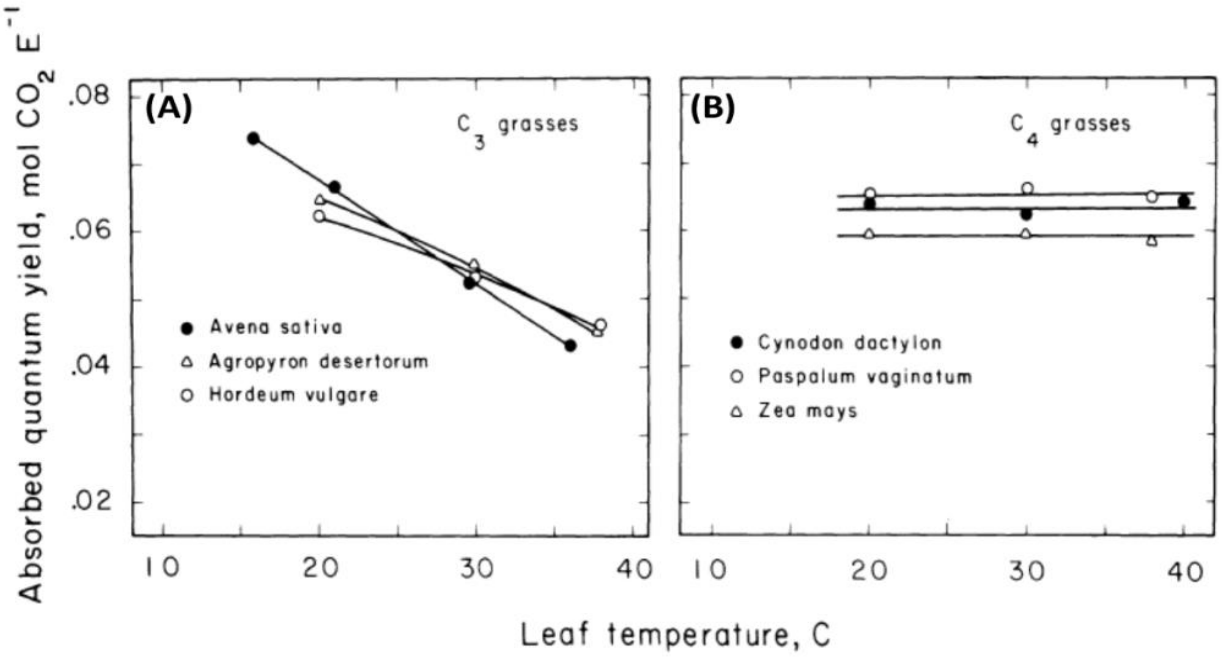

Figure 1. 10 The leaf temperature dependence of the absorbed quantum yield for CO_2 uptake

The leaf temperature dependence of the absorbed quantum yield for CO_2 uptake in **(A)** C_3; and **(B)** C_4 grasses. Measurements were made under normal atmospheric conditions (330 µl CO_2, 21% O_2) (Ehleringer & Pearcy, 1983).

1.5.2 Energetics of NADP-ME subtypes

The minimum energy required for CO_2 assimilation in NADP-ME and NAD-ME subtypes is 5 ATP and 2 NADPH per CO_2, since two ATP per CO_2 are needed for the regeneration of PEP by PPDK, in addition to the energy required in the C_3 cycle (3 ATP and 2 NADPH) (Kanai & Edwards, 1999).

In NADP-ME subtype, it is thought that BSC require more ATP than MC, since NADPH would be supplied through the decarboxylation of malate by NADP-ME, and thus the photosynthetic electron transport (PET) in BS chloroplasts would only require the production of ATP (**Figure 1. 11A**) (Edwards & Walker, 1983; Hatch, 1987; Kanai & Edwards, 1999).

This assumption is supported by the finding that the BS chloroplasts of most NADP-ME species either completely lack or have less grana with little activity for PSII, which is indispensable for the production of ATP and NADPH in LEF (Chapman *et al.*, 1980; Gutierrez *et al.*, 1974; Romanowska *et al.*, 2006; Woo *et al.*, 1970). Moreover, the fact that the enzymes of the reductive phase of the Calvin cycle, such as glyceraldehyde 3-phosphate dehydrogenase and triose phosphate isomerase, are found in both M and BS chloroplasts in NADP-ME species suggests that 3-phosphoglycerate (3- PGA) is reduced in chloroplasts in both types of cells (Friso *et al.*, 2010; Kanai & Edwards, 1999; Majeran *et al.*, 2005). If half of the overall reduction of 3-PGA occurs in M chloroplasts, one NADPH per CO_2 would be consumed for the reduction of one 3-PGA in BS chloroplasts, which can be provided by the decarboxylation of malate. As a result, 2 ATP should be supplied by the PET in BS chloroplasts, 1 for the reduction of 3-PGA and the other for the regeneration of RuBP (**Figure 1. 11A**) (Edwards & Walker, 1983; Hatch, 1987; Kanai & Edwards, 1999; Sage *et al.*, 1999). On the other hand, 2 NADPH, one for the reduction of 3-PGA transported from the BSC and the other for the production of malate from OAA by NADP-malate dehydrogenase (NADP-MDH), and at least 3 ATP, 2 for the regeneration of PEP at least and 1 for the reduction of 3-PGA, are required in the MC in NADP-ME C_4 photosynthesis (**Figure 1. 11A**) (Edwards & Walker, 1983; Hatch, 1987; Kanai & Edwards, 1999; Sage *et al.*, 1999).

1.5.3 Energetics of NAD-ME subtypes

In NAD-ME species, the enzymes that are involved in the reductive phase of the Calvin cycle are also found in both M and BS chloroplasts (Kanai & Edwards, 1999). However, unlike in NADP-ME C_4 photosynthesis, in NAD-ME C_4 photosynthesis there is no mechanism to transport NADPH from mesophyll chloroplasts to BS chloroplasts. Therefore, one NADPH and two ATP are required in BSC and 1 NADPH and 3 ATP in MC, at least, if it is assume that the reduction of 3-PGA equally occurs in M and BS chloroplasts (**Figure 1. 11B**) (Hatch, 1987; Kanai & Edwards, 1999).

1.5.4 Energetics of PCK subtypes

Unlike the other two subtypes of C_4 photosynthesis, the PCK subtype produces a portion of the ATP required for PEP regeneration by respiratory electron transport coupled with the CCM. As shown in **Figure 1. 11C**, malate decarboxylation occurs in mitochondria of BSC in PCK species simultaneously with the decarboxylation of OAA in cytosol. As a result of malate decarboxylation, NADH is released and oxidized in the respiratory chain of BS mitochondria to produce ATP, which is supplied to the cytosol to energize PCK. Malate

decarboxylation also results in the release of pyruvate, which is transported to M chloroplasts and regenerated to PEP by PPDK with ATP (**Figure 1. 11C**) (Kanai & Edwards, 1999; Wang *et al.*, 2014). Previous studies have shown that the ATP required for PCK is exclusively produced by NADH oxidation in the respiratory electron chain which is coupled with malate decarboxylation in BS mitochondria (Burnell & Hatch, 1988; Carnal *et al.*, 1993). Therefore, at least 28.6% of OAA produced by PEPC in MC should be converted into malate, under the assumption that 2.5 ATP are produced by the oxidation of one NADH in respiratory electron transport (Kanai & Edwards, 1999). In this case, 0.29NADPH are required for malate production by NADP-MDH and 0.57 ATP are required for the regeneration of PEP from pyruvate by PPDK in M chloroplasts to drive NAD-ME-dependent decarboxylation. As a result, the minimum energy requirements for PCK C_4 photosynthesis are 3.57 ATP and 2.29 NADPH, which are both slightly higher than the energy requirement in the C_3 cycle (Kanai & Edwards, 1999). If 3-PGA is reduced equally in M and BS chloroplasts, the energy requirements are 1.57 ATP and 1.29 NADPH in MC and 2 ATP and 1 NADPH in BS cells per CO_2 (**Figure 1. 11C**), indicating that a higher ATP/NADPH ratio is required in BSC compared to MC in PCK subtype.

However, a consensus has not been established on the ratio of OAA which is converted to malate by NADP-MDH in MC in PCK subtype (Koteyeva *et al.*, 2015). If 50% of OAA is converted to malate, the minimum energy requirements for PCK subtype are 4 ATP and 2.5 NADPH, of which 2 ATP and 1.5 NADPH are required in MC and 2 ATP and 1 NADPH are required in BSC per CO_2 (Hatch, 1987; Wang *et al.*, 2014). In this case, the ATP produced from NADH in the mitochondrial electron transport chain exceeds the consumption by PCK by 0.75 ATP per CO_2 (**Figure 1. 11C**). These additional ATPs needed during C_3 and C_4 photosynthesis can be provided by the enhancement of cyclic electron flow around PSI (CEF) and by Mehler reaction.

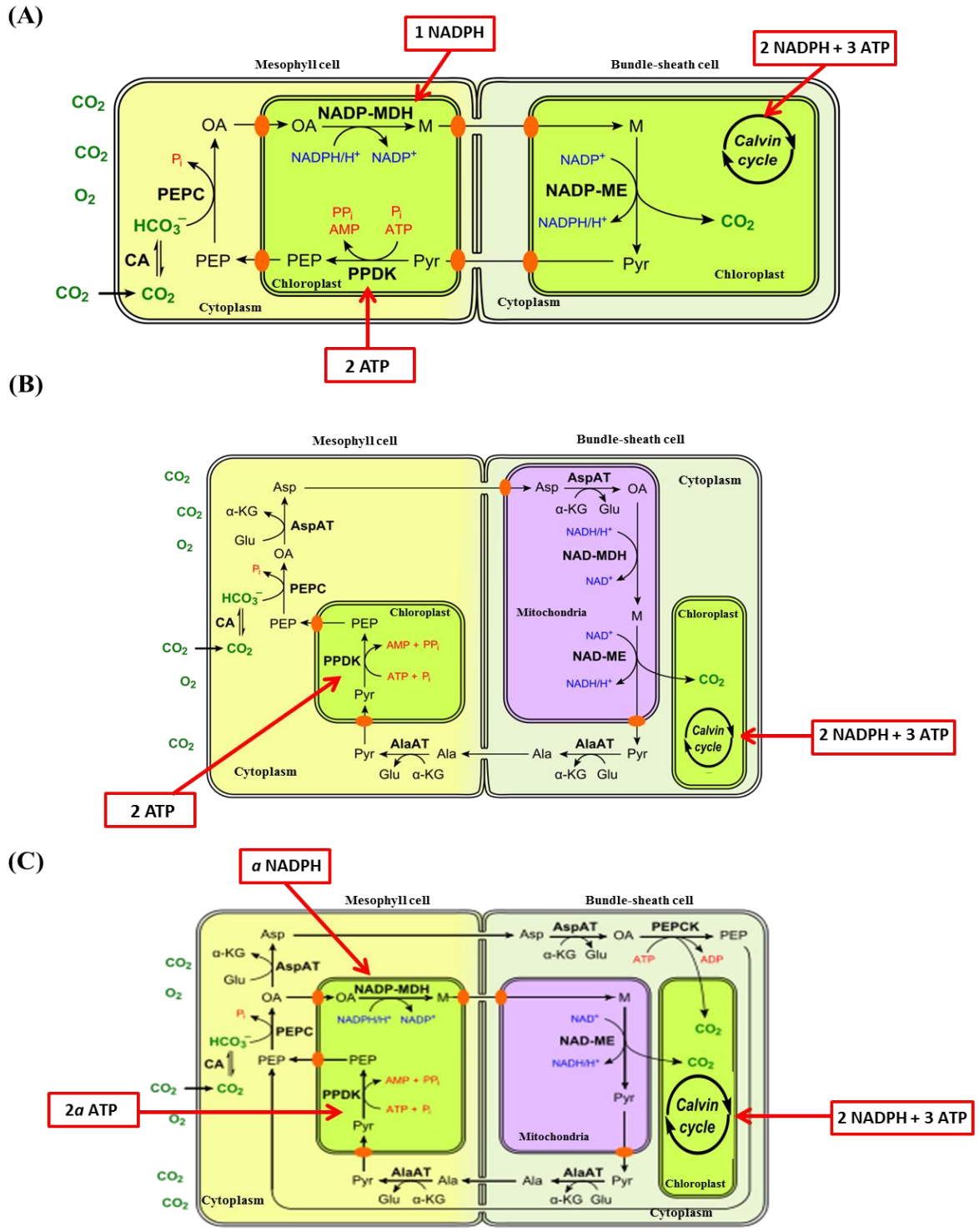

Figure 1. 11 Minimum requirements for ATP and NADPH in subtypes of C_4 photosynthesis

(A) NADP-malic enzyme (NADP-ME) type; **(B)** NAD-malic enzyme (NAD-ME) type; and **(C)** phosphoenolpyruvate carboxykinase (PEPCK or PCK) type. ''*a*'' in the PCK type indicates the ratio of malate to aspartate that is derived from OAA in mesophyll cells (0< *a* <1). A previous study estimated *a* = 0.286 at minimum (Kanai & Edwards, 1999). However, a consensus has not been established on the ratio (Koteyeva *et al.*, 2015).

1.6 Alternative electron flows

1.6.1 Cyclic electron flow around PSI

CEF is an alternative pathway of photosynthetic electron transport. It has long been suggested that CEF plays a role in supplying extra ATP which is required in C_4 photosynthesis because the ratio of ATP to NADPH produced in LEF is fixed and it would be difficult to produce only ATP via this pathway (Edwards & Walker, 1983; Hatch, 1987; Kanai & Edwards, 1999; Kramer & Evans, 2011; Rumeau *et al.*, 2007; Takabayashi *et al.*, 2005). During LEF, NADPH is produced by the electron transport from water to $NADP^+$ via PSII and PSI. Concomitantly, a proton gradient across thylakoid membranes (ΔpH) is generated and ATP is produced (**Figure 1. 12)**.

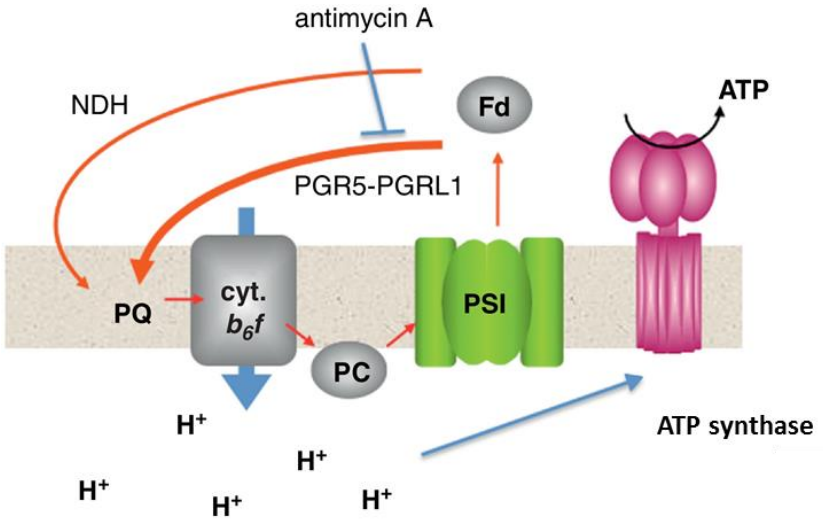

Figure 1. 12 Cyclic electron flow around PSI

Electrons flowing into a plastoquinone pool from PSII reduce cytochrome b_6f complexes (cyt b_6f) in the appressed regions of the thylakoid membrane. These flow via plastocyanin (PC) to PSI and from there to ferredoxin (Fd). Reduced Fd can feed electrons to a plastoquinone pool (PQ) in the stromal lamellae via either a PGR5 dependent pathway or an NDH dependent pathway. Reduced PQ then reduces cyt b_6f in non-appressed membrane regions. This in turn reduces PC and PSI Antimycin A inhibits the route of cyclic electron flow (Shikanai, 2014).

Since the electron transport and the generation of ΔpH are coupled, it is difficult for LEF to produce ATP without producing NADPH. By contrast, in CEF, electrons are transported from the acceptor side of PSI to PQ in a cyclic manner. During this process, NADPH is not produced as the terminal product of electron transport, but ΔpH is generated, which can induce ATP synthesis (**Figure 1. 12)**. Thus, CEF is proposed to play a role in the production

of ATP without producing NADPH, and consequently adjusts the ATP/ NADPH ratio produced during light reactions (Johnson, 2011; Kramer & Evans, 2011; Shikanai, 2007).

1.6.2 Mehler reaction

The Mehler reaction represents the photoreduction of O_2 at PSI (**Figure 1. 13)**. This photoreduction produces superoxide radicals ($O_2^{-\bullet}$), which are disproportionate to H_2O_2 and O_2 with the aid of superoxide dismutase. The H_2O_2 is rapidly detoxified to water by the ascorbate peroxidase pathway. Since the electron flow from water in PSII to water in PSI occurs in this process, it has been termed also as the water–water cycle (Asada, 1999; Makino *et al.*, 2002; Mehler, 1951). Mehler reaction not only scavenges $O_2^{-\bullet}$ and H_2O_2, but also generates a pH gradient (ΔpH) across the thylakoid membranes when little electron transport acceptors are available in PSI. This ΔpH enhances non-radiative dissipation of light energy as observed by non-photochemical quenching (NPQ). Therefore, the Mehler reaction is considered to function to dissipate the energy of excess photons (Asada, 1999, 2000; Foyer & Noctor, 2000; Osmond *et al.*, 1997; Osmond & Grace, 1995). Several studies suggested that Mehler reaction may also contribute to the production of additional ATP for C_4 photosynthesis (Badger *et al.*, 2000; Laisk & Edwards, 1998; Ruuska *et al.*, 2000; Katharina Siebke *et al.*, 2003).

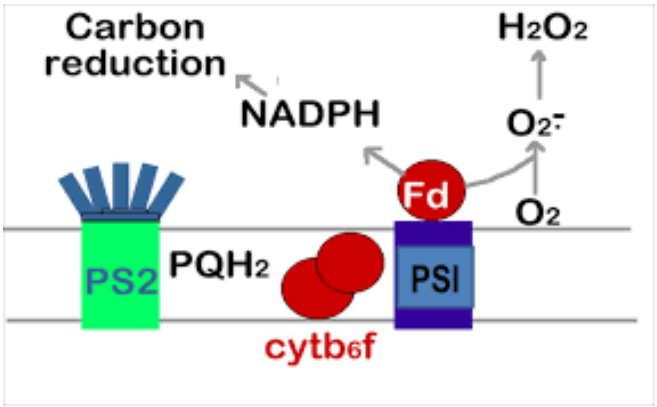

Figure 1. 13 The Mehler reaction

The Mehler reaction reduces oxygen O_2 to superoxide anion $O_2^{\cdot-}$ by donation of an electron in PSI. Superoxide anion can then be converted to hydrogen peroxide (H_2O_2) and can be further converted to water. This reaction leads to the rapid formation of pH gradient across the thylakoid membranes just after illumination (Asada, 2000).

It has been suggested by Munekage *et al.* (2004) that without the aid of CEF and Mehler reaction, LEF cannot maintain the correct ratio of ATP/NADPH production. All these three modes of electron transport (CEF, LEF and Mehler) are coupled to ATP synthesis and can

readily be demonstrated *in vitro*, in isolated chloroplasts (Ivanov *et al.*, 2007; Laisk *et al.*, 2007; Miyake, 2010; Roberty *et al.*, 2014; Romanowska & Drożak, 2006).

1.6.3 Quantification of the magnitudes of CEF and Mehler reaction

The variation in QY among subtypes indicates that there are differences in energy costs as determined by whether the decarboxylating enzyme is NAD-ME, NADP-ME or PCK (Ehleringer & Pearcy, 1983). This may also be attributed to the differences in the efficiency of photochemical activities between MC and BSC that influence light energy conversion among subtypes.

A prerequisite to understanding the efficiency of light energy conversion is the knowledge of the magnitude of the various electron fluxes (LEF, CEF and Mehler) under physiological conditions. The rate of LEF can be easily monitored by O_2 evolution or reduction of artificial electron acceptors from PSI (Chow *et al.*, 1989; Chow & Anderson, 1987; Romanowska *et al.*, 2008). However, quantification of CEF in physiological conditions is very difficult due to the absence of its net products (Shikanai, 2014). It is also important to consider that *in vitro* CEF measurements can also give estimations that are considerably lower than estimations under natural conditions. For example, Strand *et al.* (2016) found that CEF rate is very low when measured *in vitro*, but considerably higher when measured *in vivo* which can be explained by the alteration of the *in vitro* redox poise of CEF components. These alterations can come from the isolation of thylakoids which can disrupt granal stacking. Some isolation and rupture procedures used for *in vitro* assays may perturb the highly conserved, functionally significant fine structure of chloroplasts (Kirchhoff *et al.*, 2013), whilst structural integrity has been demonstrated to be associated with CEF (Johnson, 2011; Joliot & Joliot, 2002). The integrity of protein complexes involved in CEF within the thylakoid membrane may be altered during these procedures. Fan *et al.* (2016) grouped current methods for measuring/inferring CEF into two categories: 1) monitor CEF directly and 2) estimate CEF from the difference between LEF through PSII (ETR2) and total flux through PSI (ETR1) (**Figure 1. 14B**). They concluded that CEF quantification (in C_3 leaves) is best approximated through measurements of ETR1 and ETR2 under identical conditions according to category 2.

Measurement of the electron flux through PSI (ETR1) can be done via a Y(I)-based electron flux (Klughammer & Schreiber, 2008). ETR1, based on Y(I), is then calculated as ETR1 = Y(I) x I x 0.85 x f_I, where I is the irradiance, 0.85 is the assumed leaf absorptance and f_I is the fraction of the absorbed white light partitioned to PS I. It is worth noting that it is not easy to determine f_I experimentally under variable environmental conditions and calculation of ETR1

and CEF rate depends on an accurate estimation of f_I (**Figure 1. 14A)**. Value of f_I is usually assumed to be 0.5 which means that 50% of the absorbed light is portioned to PSI, but it has been hypothesized that this value could be higher in C_4 plants. Accurate measures of f_I can elucidate this question by assigning true values to f_I to C_4 species which have two photosynthetic tissues. This value can be experimentally determined under low irradiance and/or in the presence of CEF inhibitors such as antimycin A, where CEF is assumed to be zero, hence ETR2 is supposed to be approximately equal to ETR1 (**Figure 1. 14B)** (f_I values are in the range 0.4–0.5) (**Figure 1. 14A)** (Kou *et al.*, 2013).

On the other hand, measurement of ETR2 on whole-tissue can be better obtained by gross rate of oxygen evolution recorded by a gas-phase oxygen electrode compared to chlorophyll fluorescence technique (Fan *et al.*, 2016) if the latter is not optimized. Since four electrons are released for each oxygen molecule evolved, ETR2 (now LEF_{O2}) equals four times the gross rate of oxygen evolution (**Figure 1. 14B)** (Chow *et al.*, 1989; Kou *et al.*, 2013b). Membrane inlet mass spectrometry (MIMS), utilizing the stable $^{18}O_2$ isotope to differentially and simultaneously measure rates of O_2 uptake and evolution, provides a more precise method to accurately quantify ETR2 under near- natural conditions (**Figure 1. 14B)** (Beckmann *et al.*, 2009). It also allows the CO_2 concentration to be monitored in the cuvette to ensure photorespiration does not significantly contribute to the O_2 uptake signal.

Another parameter which is very difficult to quantify directly is the magnitude of Mehler reaction. It is commonly estimated from measurements of chlorophyll fluorescence and net CO_2 or O_2 exchange (Ort & Baker, 2002). It is also worth considering that O_2 uptake in plants is also associated with photorespiration or mitochondrial respiration which increases the complexity in interpreting the data. To elucidate the physiological significance of Mehler reaction, quantitative analysis and precise evaluation of the O_2 exchange *in vivo* are important. However, since it was previously demonstrated that O_2 uptakes from photorespiration, mitochondrial respiration and Mehler reaction have different isotope fractionation factors (Guy *et al.*, 2016), it is now possible to quantify the O_2 exchange rates using methods that use stable O_2 isotopes (**Figures 1. 15A** to **1. 15C**).

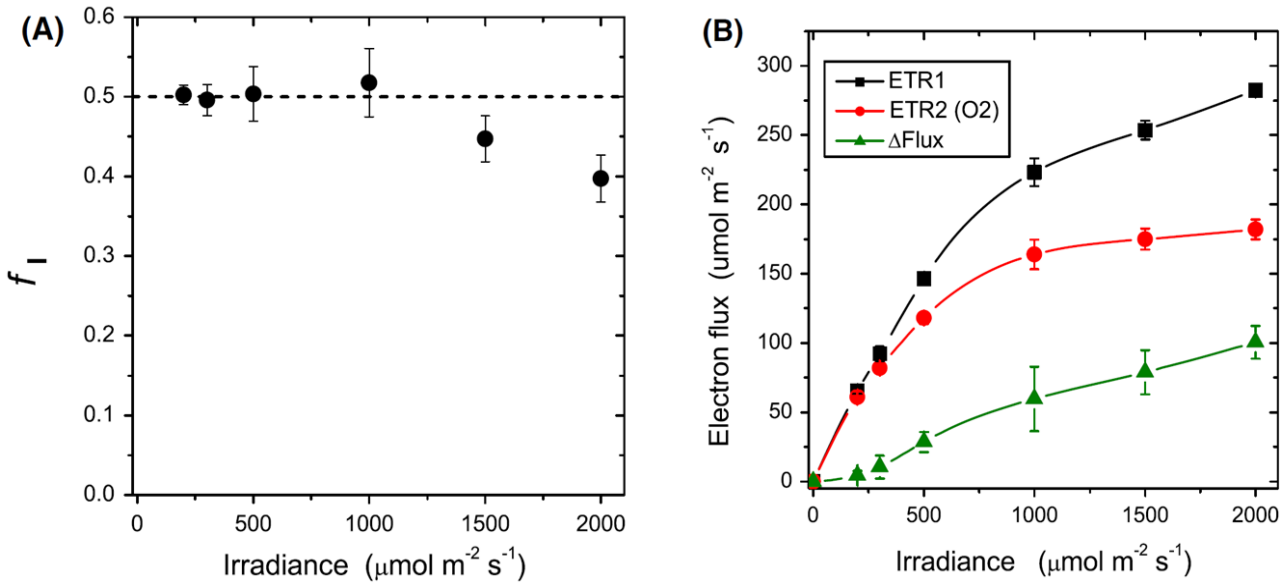

Figure 1. 14 Simultaneously collected values for ETR1 utilizing Y(I) obtained by the P700+ signal and ETR2(O2) based on gross oxygen fluxes measured with membrane inlet mass spectrometry (MIMS)

(A) The fraction of absorbed light partitioned to PSI (f_I), calculated from measurements of spinach leaf discs vacuum infiltrated with 200 μM antimycin A. Y(I) was obtained as described by Kou *et al.* (2013b). ETR1 was expressed as *Y(I) x I x 0.85 x* f_I. The gross oxygen evolution rate, ETR2(O_2), was obtained by adding the magnitude of the net $^{16}O_2$ evolution to that of $^{18}O_2$ uptake, corrected for changing concentrations of each gas in accordance with method described by Beckmann *et al.* (2009) at each irradiance, measured with a mass spectrometer. It was multiplied by 4 to convert the oxygen rate into a gross electron flux, ETR2(O_2). By equating ETR2 with ETR1 in the presence of antimycin A, f_I could be estimated. **(B)** Steady-state ETR2 and ETR1, obtained by MIMS and the $P700^+$ signal, respectively, are plotted as a function of irradiance. ETR1 was calculated by assuming f_I = 0.50 at all irradiances. The difference between them (ΔFlux) is shown as a function of irradiance (Fan *et al.*, 2016).

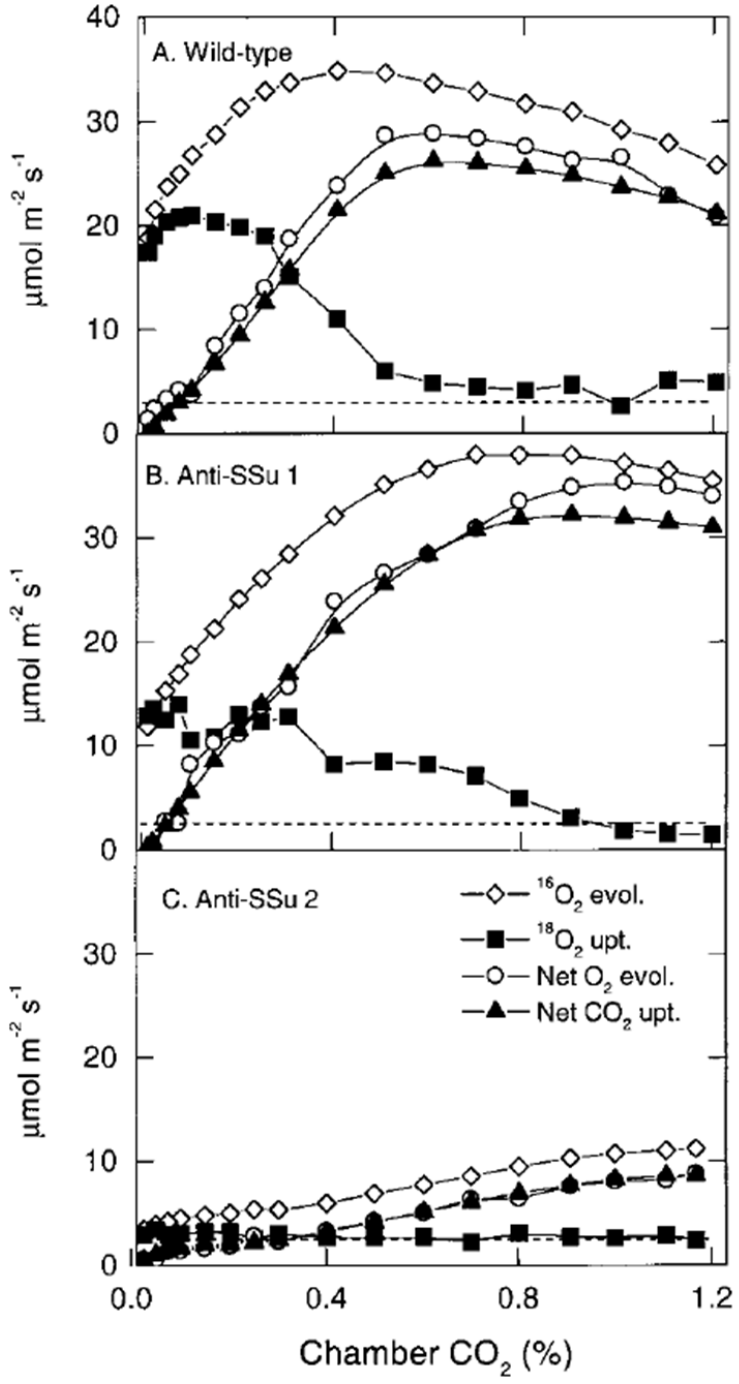

Figure 1. 15 Net CO_2 and O_2 exchange, $^{16}O_2$ evolution and $^{18}O_2$ uptake of wild-type and anti-SSu measured with MIMS

Net CO_2 and O_2 exchange, $^{16}O_2$ evolution and $^{18}O_2$ uptake of wild-type **(A)** and anti-SSu tobacco **(B, C)** measured with a mass spectrometer as a function of the prevailing CO_2 concentration. Leaf discs were in a closed chamber coupled to the mass spectrometer. Actinic light was provided via fibre optics through a transparent window. The starting CO_2 concentration was approximately 1–2% within the chamber, and the measurements were carried out during depletion as a result of the CO_2 assimilation. The measurements were conducted at 20% O_2, irradiance at the leaf surface of 970 µmol photons m^{-2} s^{-1}, and the chamber was thermostated to 25°C. The dashed line indicates the rate of $^{18}O_2$ uptake measured in the dark (Ruuska *et al.*, 2000).

1.7 Environmental responses of the light reactions of C_4 photosynthesis

1.7.1 Responses to shade

Plants experience continually changing light quality and quantity which varies from short sunflecks to long-lasting canopy gaps, and seasonal variations (Anderson & Osmond, 1987; Anderson *et al.*, 1988). Sudden and sustained light fluctuations during plant growth have a particular impact on the photosynthetic apparatus which can affect light-harvesting, energy conversion, electron transport, proton translocation and carbon fixation are also affected (Anderson *et al.*, 1995). Accordingly, plants have evolved many methods of responding to these changes such as alterations in the level of the whole plant or individual leaves (e.g. altered root/shoot ratios and leaf anatomy) or by adjustments in the functioning of individual proteins within the photosynthetic apparatus (Ballaré, 1999; Demmig-Adams & Adams, 1992; Weston *et al.*, 2000). These responses involving adjustments in the composition of the photosynthetic apparatus is known as photosynthetic acclimation (**Figures 1. 16A** to **1. 16B**) (Anderson & Osmond, 1987; Anderson *et al.*, 1988; Anderson *et al.*, 1995).

Acclimation also involves the coordinated reallocation of resources to achieve and maintain, not only optimal rates of photosynthesis, but also high QY under various light conditions and protective strategies under sustained environmental stress (Anderson & Osmond, 1987; Anderson *et al.*, 1988; Anderson *et al.*, 1995).

Extent and nature of acclimation vary between species. Most species show at least some variation in photosynthetic capacity, but the scale of observed changes in chloroplast composition varies dramatically. Initially this variation was believed to reflect whether plants were 'sun' or 'shade' species (Anderson & Osmond, 1987; Boardman, 1977). C_4 species are considered as 'sun' species which partly explain the rarity of C_4 species in shaded habitats and forests since it is usually assumed that C_4 species have less advanced adaptation to low-light environments, together with higher QY of C_4 photosynthesis (Horton & Neufeld, 1998; Sage & McKown, 2006; Smith & Martin, 1987). Plants that are adapted to high light environments such as C_4 species have shown to possess chloroplasts that have high rates of photosynthetic quantum conversion (Lichtenthaler *et al.*, 1981; Lichtenthaler *et al.*, 1984; Lichtenthaler *et al.*, 1982, 2007). They also have increased levels of PSII, cytochrome b_6f complex, ATP synthase, and components of the Calvin cycle, while there are reductions in the levels of the major chlorophyll a/*b*-binding light-harvesting complexes associated with PSII (LHCII). These are

reflected in increased capacities for oxygen evolution, electron transport and CO_2 consumption, and an increased ratio of chlorophyll *a* to chlorophyll *b* (chl *a/b*) (Bailey *et al.*, 2001; De la Torre & Burkey, 1990; Leong & Anderson, 1984; Mäenpää & Andersson, 1989).

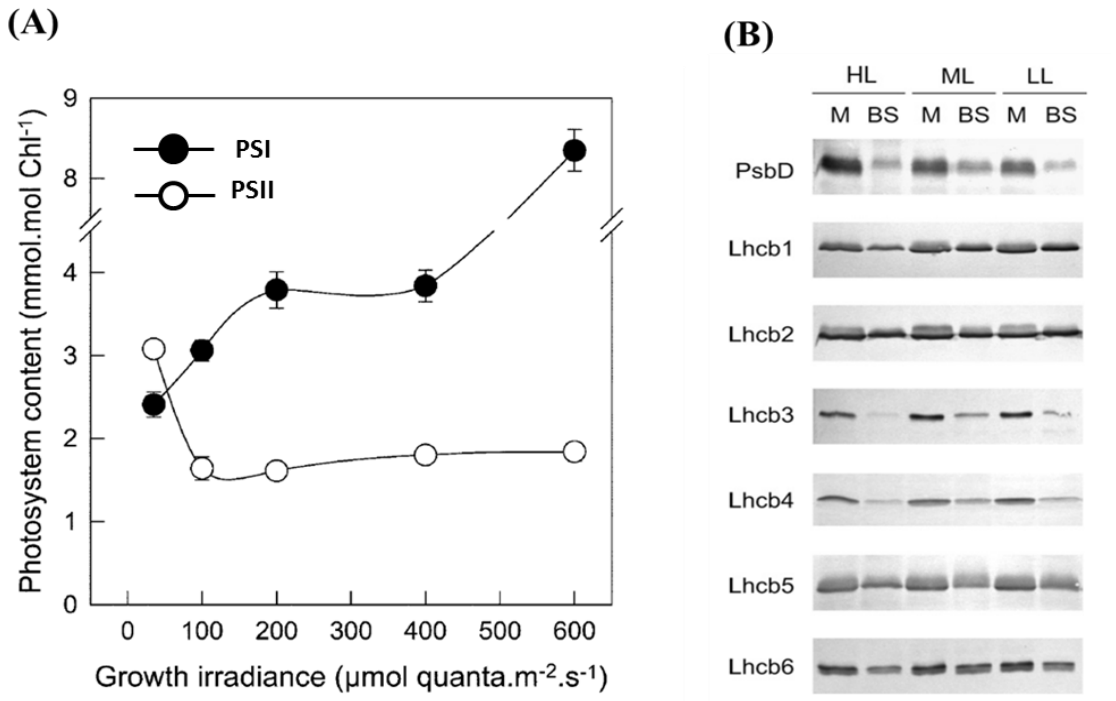

Figure 1. 16 Acclimation of the light-harvesting complexes in leaf to varying growth irradiance

(A) Changes in photosystem stoichiometry in leaf of *Arabidopsis* grown at different irradiance (Bailey *et al.*, 2001). **(B)** Immunodetection analysis of light-reaction centre polypeptide (PsbD) and light harvesting chlorophyll-protein complex **(**Lhcb) in mesophyll (M) and bundle sheath (BS) chloroplasts isolated from the leaves of high light (HL, 1000 µmol photons m^{-2} s^{-1}), moderate light (ML, 350 µmol photons m^{-2} s^{-1}) and low light (LL, 50 µmol photons m^{-2} s^{-1}) grown maize plants. (Drozak & Romanowska, 2006).

Under shade, there is a blend of very weak diffuse irradiance greatly enriched in far-red (PSI light), deficient in red and to a lesser extent in blue light. Thus, under this condition where light reaching the plant is enriched in far-red wavelengths preferentially absorbed by PSI, increases in the relative level of PSII which ensure that the supply of electrons from PSII is sufficient to keep pace with the rate of excitation of PSI so that light reaching PSI is used efficiently (Chow *et al.*, 1990; Walters & Horton, 1995).

Adjustments in photosystem stoichiometry in response to changes in light spectral quality have the effect of altering the proportion of incident light which is directed towards each photosystem (**Figure 1. 16A**). It was also reported that there is an increased light-harvesting chlorophyll proteins of PSII (LHCII) and PSI (LHCI) for maximal light capture (Chow *et al.*,

1990). This increase in light-harvesting components occurs at the expense of electron transport, photophosphorylation and carbon fixation components, particularly Rubisco, resulting in lower photosynthetic rates which saturate at lower irradiance (Anderson & Osmond, 1987; Anderson *et al.*, 1988).

These adjustments in photosystem stoichiometry and activities also serve to optimize electron transport, and maintain high QY thereby improving photosynthetic efficiency. In conditions where light is limiting, the resulting improved rate of photosynthesis may provide a competitive advantage for plants acclimating in this way (Chow *et al.*, 1990; Melis, 1991).

There exist several constraints upon C_4 photosynthesis under shade in comparison with C_3 species. C_4 plants may have lower QY under shade due to the additional energy requirement of the C_4 pump (Ehleringer & Björkman, 1977; Krall & Pearcy, 1993). The C_4 photosynthetic machinery lacks the capacity for maintaining a high state of photosynthetic induction during low-light periods (Horton & Neufeld, 1998; Sage & McKown, 2006). It has also been demonstrated that the CCM is less effective at low light due to increased relative photorespiration and rising percentage of BS CO_2 leakiness which increase additional ATP demand (Bellasio & Griffiths, 2014; Henderson *et al.*, 1992; Kromdijk *et al.*, 2014; Kromdijk *et al.*, 2010; Kubásek *et al.*, 2007; Tazoe, 2008).

It has also been shown that the three subtypes also acclimate differently under long-term exposure to shade. It was recently reported by Sonawane *et al.* (2018) that NAD-ME species and to a lesser extent PCK species were generally outperformed by NADP-ME species under shade (16% of full sunlight) conditions. Shade compromised the CCM efficiency to a greater extent in NAD-ME than in PCK or NADP-ME C_4 grasses by virtue of a greater increase in carbon isotope discrimination and BS CO_2 leakiness, and a greater reduction in QY. Together with other studies, it was also found that the QY and CCM of NADP-ME species were not significantly affected despite changes in the light environment (Bellasio & Griffiths, 2014a; Bellasio & Lundgren, 2016; Ghannoum *et al.*, 2005; Yin & Struik, 2015). It was also supported by a modelling approach by Wang *et al.* (2014) that the NADP-ME biochemical pathway is favoured at low light.

However, it is still unclear how these observed differences under shade relate to the changes in light reactions especially among C_4 subtypes. It is known that light intensity is likely to induce changes in the light reaction components which can alter relative light absorption and energy conversion efficiency by PSI and PSII. These changes might differ among subtypes.

1.7.2 Responses to low CO_2

The majority of studies on acclimation in higher plants have focused on the effects of different growth light conditions, yet despite a wealth of data describing acclimation in many different species, there remain significant unanswered questions concerning its nature, its purpose, and its regulation. For instance, does light acclimation reflect a single integrated response, or is it the result of a combination of processes? A single environmental stimulus can provoke changes in the levels of multiple proteins, all of which might be due to a single regulatory process or which could alternatively be separate responses to different signals. Acclimation not only occurs according to the characteristics of incident light, but also is observed to a greater or lesser extent in response to atmospheric CO_2 levels ($[CO_2]$).

The low $[CO_2]$ condition during the Cenozoic has long been considered the primary driver for the evolution of C_4 photosynthesis (Ehleringer *et al.,* 1991). This environment drove the evolution of the CCM of C_4 photosynthesis, which saturates the carboxylation reaction of Rubisco and almost eliminates photorespiration (Sharkey, 1988).

Due to the presence of the CCM, acclimation to low $[CO_2]$ of C_4 plants differs from C_3 plants. Growth at low $[CO_2]$ reduces growth and photosynthesis of C_3 plants because of the enhancement of oxygenase activity of Rubisco resulting to photorespiration (Anderson *et al.,* 2001; Gesch *et al.,* 2000; Tissue *et al.,* 1995). During low $[CO_2]$ or at CO_2 starvation, oxygen can serve as electron acceptor in Mehler reaction (Mehler, 1951; Schreiber & Neubauer, 1990). The products of the Mehler reaction such as superoxide, hydroxyl radicals and hydrogen peroxide are toxic, and can cause the inhibition of photosynthetic processes due to photooxidative damage of the photosynthetic electron chain (Aro *et al.,* 1993). Photoinhibition was also shown to be enhanced under low $[CO_2]$ condition in *Phaseolus vulgaris* (Daniel, 1997). It was also demonstrated by Durchan *et al.* (2001) in tobacco plants kept in CO_2 free air for several days had resulted in a dramatic decrease in photosynthetic activity (**Figures 1. 17A** to **1. 17D**) (Durchan *et al.,* 2001). Measurements of the electron transport activity in thylakoid membranes showed that a loss of PSII activity was mainly responsible for the observed decrease in photosynthetic activity (Durchan *et al.,* 2001). C_3 plants also commonly acclimate to low $[CO_2]$ by increasing the activities of Rubisco and other Calvin cycle enzymes (Anderson *et al.,* 2001; Pinto *et al.,* 2014), but this represents a significant cost in terms of leaf nitrogen (Gesch *et al.,* 2000).

In contrast, C_4 photosynthesis remains CO_2-saturated even when [CO_2] is reduced substantially below the current ambient level due to the CCM (Byrd & Brown, 2008; Tissue *et al.*, 1995), and hence photosynthetic acclimation is usually less pronounced (Anderson *et al.*, 2001; Edwards & Ogburn, 2012; Li *et al.*, 2014; Maherali *et al.*, 2002; Ward *et al.*, 2008). Within the C_4 CCM, low [CO_2] has been shown to facilitate some acclimations, particularly the upregulation of the carboxylases (Rubisco and PEPC). However, decarboxylase activity has largely been found to remain unchanged, reflecting the high control exerted by the carboxylases relative to the decarboxylases on the efficiency of C_4 metabolism (Pinto *et al.*, 2014). Various degrees of acclimation such as increased foliar N and g_s have also been recorded for C_4 species in response to long- term growth at low [CO_2] (Anderson *et al.*, 2001; Gill *et al.*, 2002; Pinto *et al.*, 2011).

The efficiency of CCM comes with the caveat of requiring additional energy, mainly associated with the regeneration of phosphoenolpyruvate (PEP) and the over-cycling of CO_2. C_4 plants overcome this limitation through a higher light use efficiency (LUE) under high light (HL) compared to C_3 plants. Aside from the linear electron flow (LEF), the additional can come from the enhancement of CEF and from Mehler's reaction which are commonly stimulated under high irradiances (Asada, 1999; Munekage *et al.*, 2004; Takabayashi *et al.*, 2005).

However, the high energy cost of C_4 photosynthesis may limit the productivity and distribution of C_4 plants in low light (LL) environments. In contrast to acclimation under low [CO_2], long-term exposure to LL causes large acclimations in both the CCM and light harvesting complexes of C_4 species (Drozak & Romanowska, 2006; Romanowska *et al.*, 2006; Sonawane *et al.*, 2018). It has also been reported that acclimations under long-term exposure to LL involve changes in photosystem activity and stoichiometry in chloroplasts (Anderson, 1986).

It is known that several processes such as CO_2 assimilation require the energy generated during light reactions of photosynthesis. The rate of energy generated during these reactions mainly depends on the intensity of light and efficiency of light energy conversion complexes; however, the effect of [CO_2] is still unknown.

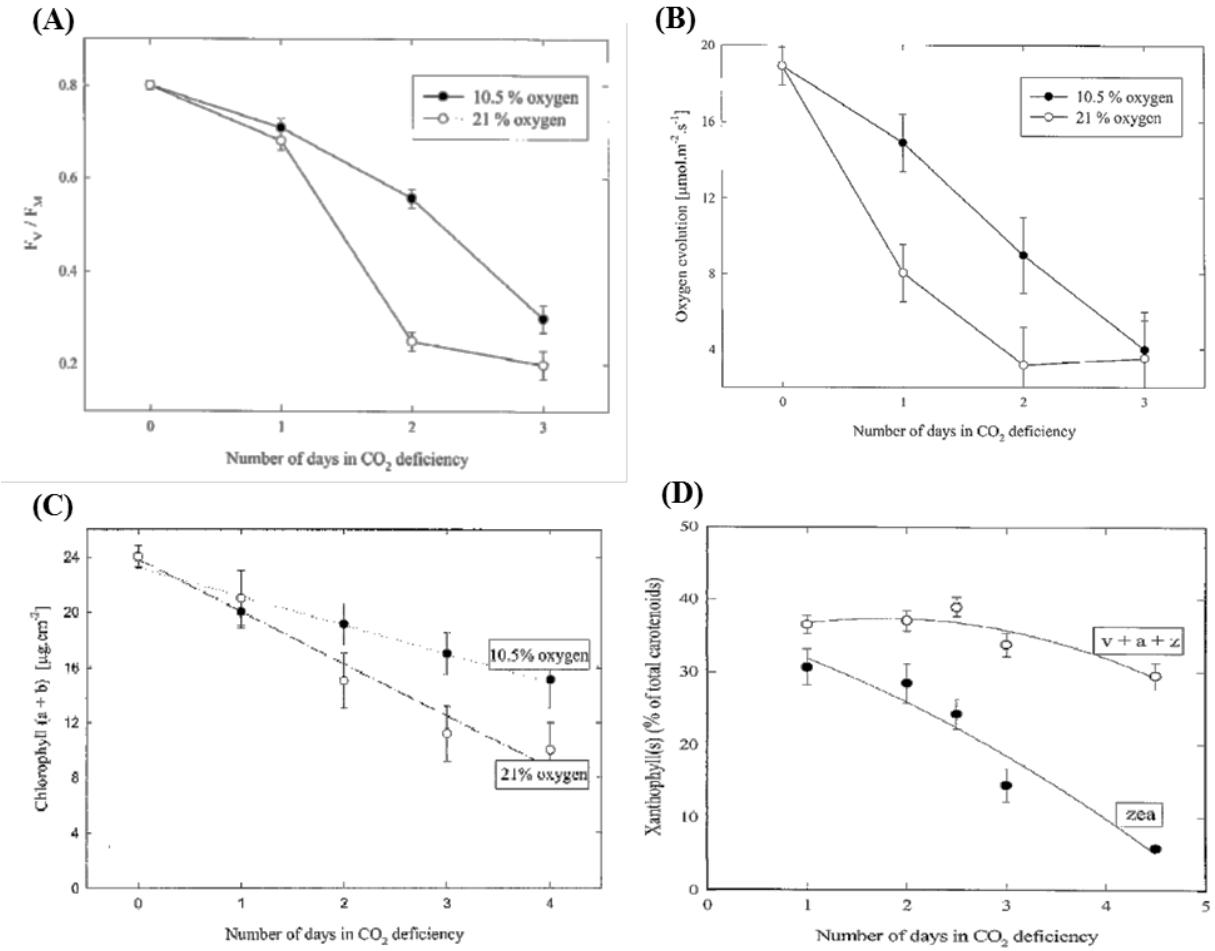

Figure 1. 17 Decrease of photosynthetic activity and alterations in pigment composition the course of CO_2 starvation in tobacco

Tobacco grown into an atmosphere without CO_2 with 21% or 10.5% of oxygen. **(A)** Photochemical efficiency of PSII assessed by the chlorophyll fluorescence ratio, F_V/F_m, in intact leaves; **(B)** oxygen evolution of intact leaves measured at saturating CO_2; **(C)** the decrease in chlorophyll (*a* + *b*); and **(D)** Content of xanthophylls and capacity of zeaxanthin formation during CO_2 starvation (Durchan *et al.*, 2001).

1.8 Knowledge gaps

As discussed earlier, a prerequisite to understanding the efficiency of light energy conversion among C_4 subtypes is the knowledge of the magnitude of the various electron fluxes which are the LEF, CEF and Mehler reaction under physiological conditions. However, quantifications of CEF and Mehler reaction in physiological conditions are very difficult due to the absence of net products. It has also been suggested by Fan *et al.* (2016) that a more reliable method to calculate CEF is by estimating ETR2 based on membrane-inlet mass spectrometry (MIMS) which utilises the stable $^{18}O_2$ isotope, and ETR1 based on the

chlorophyll fluorescence-derived Y(II)-method. By concurrently measuring these two parameters, it will be also be possible to experimentally determine f_I and use it to calculate CEF rate. It will also be possible to estimate Mehler reaction since the method allows the monitoring of gross O_2 evolution and uptake concurrently with measurements of net CO_2 uptake at different irradiances. *The validity of these methods was established in Chapters 2 and 3.*

It has also been shown that the three subtypes also acclimate differently under long-term exposure to shade. It was recently reported by Sonawane *et al.* (2018) that shade compromised the CCM efficiency to a greater extent in NAD-ME than in PCK or NADP-ME C_4 grasses by virtue of a greater increase in carbon isotope discrimination and BS CO_2 leakiness, and a greater reduction in QY. Together with other studies, it was also found that the QY and CCM of NADP-ME species were not significantly affected despite changes in the light environment (Bellasio & Griffiths, 2014a; Bellasio & Lundgren, 2016; Ghannoum *et al.*, 2005; Wang *et al.*, 2014; Yin & Struik, 2015). It is known that light intensity is likely to induce changes in the light reaction components which can alter relative light absorption and energy conversion efficiency by PSI and PSII. However, the plasticity of the light reactions to long-term exposure to shade among subtypes is still unclear. *This was addressed in Chapter 4.*

To further understand the level of plasticity of light harvesting complexes among C_4 subtypes under varying environmental conditions, it is important to investigate acclimation as a result of combination of processes. Comparing the sensitivity of the light reactions to long-term exposure to low [CO_2] and low light may also provide critical insight into the physiology of C_4 plants under conditions that led to their evolution. It is known that several processes such as CO_2 assimilation require the energy generated during light reactions of photosynthesis. The rate of energy generated during these reactions mainly depends on the intensity of light and efficiency of light energy conversion complexes; however, the effect of [CO_2] is still unknown. *This was addressed in Chapter 5.*

1.9 Aims and objectives

The overall aim of this PhD project was to investigate the plasticity of the components and activities of the light reactions of photosynthesis in representative species of C_3, C_3-C_4, and the three subtypes of C_4 species under environmental conditions that may affect the photosynthetic quantum yield such as low light and low CO_2.

The outcomes of this study will contribute significant insights towards understanding the underpinning causes of the differences in QY between the three C_4 biochemical subtypes.

The specific objectives of Chapter 2 were:

I. to develop a new *in planta* method which can give a more reliable estimation of ETR2 based on (a) MIMS, and (b) the chlorophyll fluorescence-derived Y(II)-method using a Dual-PAM/F in leaf discs;
II. to determine f_I experimentally and use it to calculate CEF rate in chloroplasts; and
III. to determine the effect of shade condition on light partitioning between the two photosystems in leaf of plants with different functional types.

The specific objectives of Chapter 3 were:

I. to quantify the magnitude of Mehler reaction *in vivo* using MIMS which uses $^{16}O/^{18}O$ isotopes to monitor O_2 exchange rates in the dark and in high irradiance with very high CO_2 partial pressures and at compensation point; and
II. to estimate both leaf day respiration (R_l) and dark respiration (R_d) rates from the spectrometric $^{16}O_2$ and $^{18}O_2$ exchange under dark and at high irradiances in leaf of plants with different functional types.

The specific objectives of Chapter 4 were:

I. to investigate the acclimation of the light reactions of photosynthesis under long-term exposure to low-light as measured by the rates of various electron fluxes, stoichiometry of photosystems and composition of pigments in C_3 and C_3-C_4 species and among C_4 species with different biochemical subtypes; and
II. to measure the stoichiometry of the two photosystems and relative electron fluxes *in vivo* in order to reflect functionality *in situ*, using several custom-built equipment in comparison with the commercial equipment (Dual-PAM) in C_3 and C_3-C_4 species and among C_4 species with different biochemical subtypes.

The specific objectives of Chapter 5 were:

I. to determine the influence of low [CO_2] in light use efficiency as measured by the rates of various electron fluxes, CO_2 assimilation, and composition of pigments; and

II. to investigate the acclimation of the light reactions of photosynthesis to long-term exposure to low light combined with low [CO_2] in C_3 and C_3-C_4 species and among C_4 species with different biochemical subtypes.

1.10 Thesis outline and structure

This thesis is categorized into six chapters, including four experimental chapters prepared for submission to peer-reviewed journals, as detailed below.

Chapters	Title
Chapter 1	General introduction and literature review
Chapter 2 (Experiment 1)	Cyclic electron flow and light partitioning between the two photosystems in leaves of plants with different functional types (Published in *Photosynthesis Research*)
Chapter 3 (Experiment 2)	Oxygen exchange and Mehler reaction in leaves of C_3 and C_4 plants (Ready for submission to *Photosynthesis Research*)
Chapter 4 (Experiment 3)	Effects of low light intensity on the energetics of closely related C_3, C_3-C_4 and C_4 grasses (Ready for submission to a special issue of *Journal of Experimental Botany*)
Chapter 5 (Experiment 4)	Acclimation of C_4 photosynthetic light reactions to low light and low CO_2
Chapter 6	General discussions and future outlooks
References	

CHAPTER 2

CYCLIC ELECTRON FLOW AND LIGHT PARTITIONING BETWEEN THE TWO PHOTOSYSTEMS IN LEAVES OF PLANTS WITH DIFFERENT FUNCTIONAL TYPES

This chapter formed the basis of the following published manuscript:

Sagun, J. V., Badger, M.R., Chow, W.S. & Ghannoum, O. (2019). Cyclic electron flow and light partitioning between the two photosystems in leaves of plants with different functional types. *Photosynthesis Research*. https://doi.org/10.1007/s11120-019-00666-1

ABSTRACT

Cyclic electron flow (CEF) around photosystem I (PSI) is essential for generating additional ATP and enhancing efficient photosynthesis. Accurate estimation of CEF requires knowledge of the fractions of absorbed light by PSI (f_I) and PSII (f_{II}), which are only known for a few model species such as spinach. No measures of f_I are available for C_4 grasses under different irradiances. We developed a new method to estimate (1) f_{II} *in vivo* by concurrently measuring linear electron flux (LEF_{O2}) through both photosystems in leaf discs using membrane inlet mass spectrometry, and total electron flux through PSII (ETR2) using chlorophyll fluorescence by a Dual-PAM at low light, and (2) CEF as ETR1 – ETR2. For spinach, f_I averaged 0.5 under control (high light), similar to what has previously been found, and widely used in photosynthetic calculations. For a C_3 grass, f_I was 0.5 and 0.4 under control and shade conditions, respectively. C_4 grasses belonging to NADP-ME, NAD-ME and PCK subtypes had f_I of 0.6 under control and shade conditions. Under control conditions, f_I ranged between 0.3 and 0.5 for gymnosperm, liverwort and fern species. CEF increased with irradiance and was induced at lower irradiances in C_4 grasses and fern relative to other species. CEF was greater in shade relative to control plants except for C_4 NADP-ME species. Our study reveals a range of CEF and f_I values in different plant functional groups. This variation must be taken into account for improved photosynthetic calculations and modelling.

Key words: C_4 photosynthesis, chlorophyll fluorescence, cyclic electron flux, electron transport rate, oxygen exchange rate, photosystem

2.1 INTRODUCTION

Photosynthetic electron transport in the thylakoid membrane of chloroplasts is highly regulated to cope with fluctuating light intensity and variable demand for ATP and NADPH. Photon energy absorbed by pigments and the light harvesting complexes drives electron transport through the thylakoid membranes. Electrons produced from the splitting of water molecule in photosystem II (PSII) are ultimately transferred via the cytochrome Cyt b_6f complex and photosystem I (PSI) to $NADP^+$, resulting in the production of reducing equivalents in the form of NADPH. These two processes, known as linear electron flow (LEF), generate a proton gradient across the thylakoid membrane (ΔpH). The ΔpH together with a membrane potential formed across the thylakoid membrane (Δψ) drives the production of ATP via ATP synthase (Allen, 2003).

During cyclic electron flow (CEF), NADPH or ferredoxin (Fd) is photoreduced at PSI and donates electrons to the Cyt b_6f complex via the plastoquinone (PQ) pool. There, the Q-cycle transfers 1 H^+ from the stroma to the lumen for each electron donated, resulting in a ΔpH, which can drive ATP synthesis without producing NADPH in chloroplasts (Allen, 2003). This process is not only key to photo-protection, but also essential for increasing the ATP/NADPH ratio. Depending on the environmental and/or physiological conditions, this ratio can be adjusted to the required levels by tuning the ratio of LEF to CEF (Miyake, 2010; Shikanai, 2007; Takahashi & Badger, 2010).

In angiosperms, CEF operates through two known pathways (Yamori & Shikanai, 2016). The major pathway depends on two additional proteins, PROTONGRADIENT REGULATION 5 (PGR5) (Munekage *et al.,* 2002) and PGR5-LIKE PHOTOSYNTHETIC PHENOTYPE 1 (PGRL1) (DalCorso *et al.,* 2008), whereas the minor activity pathway is mediated by a chloroplast NADH dehydrogenase-like (NDH) complex (Burrows *et al.,* 1998; Horváth *et al.,* 2000; Shikanai *et al.*, 1998). Antimycin A is an inhibitor of PGR5/PGRL1-dependent CEF, but the site of inhibition has long been unclear in chloroplasts (Munekage *et al.,* 2002).

In the absence of PGR5/PGRL1-dependent pathway, the chloroplast NDH-dependent pathway compensates for the loss of the important pathway to some extent (Munekage *et al.,* 2004; Shikanai, 2014). The chloroplast NDH complex, which is insensitive to antimycin A, recycles electrons from ferredoxin to plastoquinone and subsequently to PSI through the Cyt b_6f complex (Shikanai, 2016). In contrast to higher plants, Godde (1982) showed that the green alga *Chlamydomonas reinhardtii* CW-15 is able to use NADH as electron donor for its

photosynthetic electron flow. They also showed that NDH is sensitive to rotenone and thenoyltrifluoroacetone (TTFA). This finding is important because it was recently shown that the NDH system is the main pathway for CEF in Paniceae C_3 and C_4 grasses (Hernández-Prieto *et al.*, 2019).

A prerequisite to understanding the role of CEF is the ability to quantify CEF under physiological conditions, which has been difficult due to the absence of a net product of CEF (Shikanai, 2014). Unlike LEF, the rate of CEF cannot be monitored by O_2 evolution or reduction of artificial electron acceptors from PSI. Fan *et al.* (2016) grouped current methods for measuring and inferring CEF into two categories: 1) monitor CEF directly and 2) estimate CEF from the difference between LEF through PSII (ETR2) and total flux through PSI (ETR1). They concluded that CEF quantification in C_3 leaves is best approximated through measurements of ETR1 and ETR2 under identical conditions according to category 2.

Measurement of the electron flux through PSI (ETR1) can be done via a Y(I)-based electron flux (Klughammer & Schreiber, 2008). ETR1, based on Y(I), is then calculated as

$$ETR1 = Y(I) \times I \times 0.85 \times f_I$$

where I is the irradiance, 0.85 is the assumed leaf absorptance and f_I is the fraction of the absorbed white light partitioned to PSI. It is worth noting that it is not easy to determine f_I experimentally under variable environmental conditions; yet, calculations of ETR1 and CEF rate depend on an accurate estimation of f_I. This value can be experimentally determined under low irradiance and/or in the presence of CEF inhibitors such as antimycin A, where CEF is assumed to be zero, hence ETR2 is supposed to be approximately equal to ETR1 (f_I values are in the range 0.4–0.5) (Kou *et al.,* 2013). However, the validity of these methods needs further evaluation.

On the other hand, measurement of ETR2 on whole-tissue can be better obtained by gross rate of O_2 evolution recorded by a gas-phase oxygen electrode compared to chlorophyll fluorescence technique (Fan *et al.,* 2016) if the latter is not optimized. Since four electrons are released for each O_2 molecule evolved, ETR2 (now LEF_{O2}) equals four times the gross rate of O_2 evolution (Chow *et al.*, 1989; Kou *et al.,* 2013). Membrane inlet mass spectrometry (MIMS), utilizing the stable $^{18}O_2$ isotope to differentially and simultaneously measure rates of O_2 uptake and evolution, provides a more precise method to accurately quantify ETR2 under near-natural conditions (Beckmann *et al.*, 2009). It also allows the CO_2 concentration to be

monitored in the cuvette to ensure photorespiration does not significantly contribute to the O_2 uptake signal.

The overall aim of our study was to determine to what extent CEF and f_I vary between C_3 and C_4 plants, and in response to variation in light intensity. f_I and f_{II} are only known for a few species, commonly C_3, and f_I is always assumed to be 0.5 in untested species. It is also unknown in ferns, liverwort, gymnosperms or among the various C_4 species. In particular, C_4 photosynthesis possesses a CO_2 concentrating mechanisms (CCM) which operates across two photosynthetic cell types (mesophyll and bundle sheath) and serves to supercharge photosynthesis and minimize photorespiration in air. C_4 plants are broadly grouped into three biochemical subtypes according to the primary C_4 acid decarboxylase (NADP-ME, NAD-ME and PCK) operating in the bundle sheath (Hatch, 1987). Consequently, we developed a new method which can give a more reliable estimation of ETR2 based on (a) MIMS, and (b) the chlorophyll fluorescence-derived Y(II)-method using a Dual-PAM/F. This can concurrently measure Y(II) and LEF_{O2} in leaf discs in CO_2-enriched air applied to leaf discs of C_3 and C_4 plants. Leaf discs from representative species of liverwort, fern and angiosperms were also measured. This method also allowed us to experimentally determine f_I and use it to calculate CEF rate in chloroplasts of all species. Measurements were done in presence of CEF inhibitors (Antimycin A and TTFA) and/or in low irradiance where CEF is assumed to be zero. In addition, this study determined the effect of low light (shade) condition on light partitioning between the two photosystems.

2.2 MATERIALS AND METHODS

2.2.1 Plant culture

Representative grass species of C_3 (*Panicum bisulcatum*); C_4 NADP-ME subtype (*Panicum antidotale*); C_4 NAD-ME subtype (*Panicum miliaceum*); and C_4 PCK subtype (*Megathyrsus maximus*) and *Zea mays* (model C_4 NADP-ME species) were grown in vermiculite in a naturally-lit greenhouse made of polycarbonate at the Australian National University. The greenhouse temperature was maintained at 28/24^oC for day/night via an in-built greenhouse temperature control system. Within the greenhouse, a steel structure was placed and covered with shade cloth. The average ambient photosynthetic photon flux densities (PPFD) and temperature during the mid-day were 800 and 300 µmol photons m^{-2} s^{-1} and 30 ^oC and 29 ^oC for control and shade treatments, respectively. Representative C_3 species of gymnosperms (*Ginkgo biloba* and *Wollemi nobilis*), liverwort (*Marchantia polymorpha*), fern (*Polypodium* sp.) and spinach were grown under full sunlight (control condition). All plants were watered regularly and fertilized with Osmocote® (Scotts Australia). Leaves were harvested from 4–5 week-old plants.

2.2.2 Membrane inlet mass spectrometry (MIMS)

Gas exchange was measured in a closed cuvette coupled to a mass spectrometer (as described by Maxwell *et al.* (1998) and Dual-PAM/F (Heinz Walz) (**Figure 2. S 1**). Leaf discs (1.89 cm^2 area) were punched from the leaf and immediately placed within the chamber together with the wet filter paper supported on a mesh of equal area. The cuvette was first calibrated for oxygen and then flushed with nitrogen gas. Then, a known volume of CO_2 was added to create an atmosphere of approximately 4% CO_2 within the chamber; $^{18}O_2$ was injected to give an atmosphere of 18 – 21% O_2 and the signals were allowed to stabilise for 10 minutes. Gas consumption and leakage from the cuvette were negligible. The leaf was then illuminated at increasing irradiance from 50 to 2000 µmol photons m^{-2} s^{-1}. The chamber temperature was maintained at 28^oC.

2.2.3 Measurement of ETR1

Measurement of the electron flux through PSI (ETR1) was done via a Y(I)-based electron flux in leaf discs at 28^oC using the FIBER version of Dual-PAM (Dual-PAM/F) with a dual wavelength (830/875 nm) unit (Walz, Effeltrich, Germany) connected to the gas exchange system via a light guide to permit simultaneous measurements. The fibre optic cable was positioned within the Perspex lid at a distance of 1.0 cm from the leaf surface. The Perspex lid

weakened the light intensity coming from Dual-PAM/F by ~87% so we added external white actinic (AL, from a halogen lamp), strong far-red (sFR), weak far-red (wFR) and saturating light sources through various branches of the multifurcated light guide.

The photochemical yield of PSI, Y(I), in AL at a given irradiance was obtained by the percentage of the photo-oxidisable P700. The P700 redox state was measured following the method of Klughammer & Schreiber (1994). A saturation pulse (SP) (~10,000 µmol photons m^{-2} s^{-1}), which was introduced primarily for PAM fluorescence measurement, was applied for assessment of P700 parameters. The P700 single channel in SP-Analysis mode of the Dual-PAM software was used for this purpose.

The maximum photo-oxidisable P700 content (P_m) was first recorded as a prerequisite for the calculation of Y(I), non-photochemical quantum yield of PSI due to donor side limitation Y(ND) and non-photochemical quantum yield of PSI due to acceptor side limitation Y(NA). This was done by first determining a steady-state by illuminating the leaf disc with weak continuous far-red light (wFR) (~50 µmol photons m^{-2} s^{-1}, 723 nm) for >10 s (**Figure 2. S 2A**) coming from an external light source which was manually controlled. Then a 200 ms SP (~10,000 µmol photons $m^{-2}s^{-1}$) coming from Dual-PAM/F and external light source was superimposed. This additional external saturating light source was connected to the TRIGGER OUT socket of Dual-PAM/F. Both pulses were triggered at the same time through the Dual-PAM software in "Trigger out" mode.

The leaf disc was light-adapted (1000 µmol photons m^{-2} s^{-1}) for at least 10 minutes with AL to reach steady-state photosynthesis before measurements of light response curves. Light-adapted photosynthetic parameters were recorded after 8 to 10 min exposure to each AL intensity (50, 100, 200, 300, 400, 500, 750, 1000, 1500 and 2000 µmol photons m^{-2} s^{-1}) and when the rate of gross oxygen evolution was stable.

Fast kinetic recording in "External trigger" mode by the Dual-PAM was first started. The leaf disc was re-illuminated with the same AL for 10 s to retain a steady-state for $P700^+$ measurements immediately after the photosynthetic induction step using an electronic shutter controlled by one terminal of a pulse/delay generator (Model 555, Berkeley Nucleonics, San Rafael, CA, USA) connected to Dual-PAM/F. During each 10 s illumination, at time T = 8.80 s (corresponding to the time point t= -200 ms in **Figure 2. S 2B**), data acquisition by the Dual-PAM was started by a trigger pulse from a second terminal of the pulse/delay generator. At T = 8.95 s, a strong far-red light (sFR) (~4000 µmol photons m^{-2} s^{-1}) from two external

light-emitting diode arrays (741 nm ± 13 nm, LED 735–66–60, Roithner LaserTechnik, Vienna, Austria) was triggered on for 250 ms using a third terminal of the pulse/delay generator. The sFR depleted electrons from the inter-system chain, so that the subsequent saturating pulse oxidised P700 maximally (Siebke *et al.*, 1997). While the sFR was on, at *T*= 9.0 s, SP (~10,000 µmol photons $m^{-2}s^{-1}$) was applied for 200 ms by a pulse from Dual-PAM/F and a fourth terminal of the pulse/ delay generator, yielding the maximally-oxidised P_m' signal (where P_m' is the maximum $P700^+$ signal in AL) in **Figure 2. S 2B**. Finally, AL was turned off by the electronic shutter (at T=9.016 s). Data acquisition continued for 1200 ms after cessation of AL to obtain the baseline corresponding to complete re-reduction of $P700^+$. Y(I) was then calculated by the Dual-PAM from the complimentary PSI quantum yields of non-photochemical energy dissipation Y(ND) and Y(NA):

$$Y(I) = 1 - Y(ND) - Y(NA) \tag{2.1}$$

Y(ND) and Y(NA) were directly determined by the Saturation Pulse method. Y(ND) represents the fraction of overall P700 that is oxidised in a given state. It is calculated as:

$$Y(ND) = 1 - P700\,red. \tag{2.2}$$

where $P700_{red}$. is the fraction of P700 in the reduced state. As determination of $P700_{red}$. by the Saturation Pulse method requires previous P_m determination, the same also holds for Y(ND) determination. Y(NA), on the other hand, represents the fraction of overall P700 that cannot be oxidised by a Saturation Pulse in a given state due to lack of available acceptors. It is calculated as:

$$Y(NA) = \frac{(P_m - P'_m)}{P_m} \tag{2.3}$$

ETR1 was then calculated as:

$$ETR1 = Y(I) \times I \times 0.85 \times f_I \tag{2.4}$$

where I is the irradiance, 0.85 is the assumed absorptance and f_I is the assumed fraction of absorbed white light partitioned to PSI.

2.2.4 Determination of f_I and calculation of CEF

Two techniques were compared in this study to determine f_I: (1) the use of CEF inhibitors and (2) simultaneous measurement of linear electron flux by Chl fluorescence and gross oxygen evolution rate under white actinic light of low irradiances. In the first technique CEF

is assumed to be zero; thus ETR2 is supposed to be approximately equal to ETR1. In the second technique, linear electron fluxes measured by Chl Fluorescence and oxygen evolution are assumed to be equal.

To obtain f_I using the first technique f_I was determined by inhibiting CEF with the use of antimycin A and TTFA. The cut end of the leaf petiole was dipped into 200 µM antimycin A: 200 µM TTFA: H_2O solution (with a trace of ethanol) and allowed to absorb the solution in darkness overnight before measurement. Inhibitor concentration taken up by the leaf was calculated as:

$$Inhibitor\ concentration = \frac{(volume\ of\ consumed\ solution \times 200\ \mu M)}{(leaf\ fresh\ weight\ x\ 0.9)} \quad (2.5)$$

where 0.9 represents the 90% water content of the leaf. Discs were collected and used for Y(I)-based measurement of ETR1 after absorbing ≥200 µM of each inhibitor. Assuming that:

$$ETR1 = LEF_{O2} \quad (2.6)$$

then,

$$LEF_{O2} = Y(I) \times I \times 0.85 \times f_I \quad (2.7)$$

f_I was then calculated as:

$$f_I = \frac{LEF_{O2}}{Y(I)\ x\ I\ x\ 0.85} \quad (2.8)$$

CEF in leaf in the absence of inhibitors was then calculated as:

$$CEF = ETR1 - LEF_{O2} \quad (2.9)$$

To obtain f_I using the second technique, the fraction of absorbed white light partitioned to PSII, f_{II}, was first estimated in leaf discs of different species by measuring the photochemical yield of PS II, Y(II), by Chl fluorescence and the gross oxygen evolution rate simultaneously at low irradiance (50, 100, 200, 300, 400 µmol photons m^{-2} s^{-1}) and high CO_2 concentration. Chl fluorescence was measured with the Fluorescence single channel in SP-Analysis mode of the Dual-PAM software when the gas exchange signals were all stable. The steady-state fluorescence yield (F_s) was first monitored continuously under low irradiances and a 300 ms pulse of saturating light (~10,000 µmol photons m^{-2} s^{-1}) was supplied to determine maximum

variable fluorescence (F_m'). Y(II) at the steady state was defined as $(F_m' - F_s)/F_m'$, as proposed by Genty *et al.* (1989). ETR2 was then calculated as:

$$ETR2 = Y(II) \times I \times 0.85 \times f_{II} \quad (2.10)$$

Under low actinic irradiance (<500 µmol photons m^{-2} s^{-1}), Kou *et al.* (2013) showed that ETR2 can be equated to the linear electron flux (LEF_{O2}); further, at low actinic irradiance, the matching of ETR2 with LEF_{O2} is independent of the spectral distribution of the excitation light (Zhang *et al.*, 2018). LEF_{O2} in the present study is the gross oxygen evolution rate during illumination recorded by MIMS multiplied by four (since four electrons are released for each oxygen molecule evolved). Assuming that:

$$ETR2 = LEF_{O2} \quad (2.11)$$

then,

$$LEF_{O2} = Y(II) \times I \times 0.85 \times f_{II} \quad (2.12)$$

allowing f_{II} to be evaluated.

f_I was then calculated as:

$$f_I = 1 - f_{II} \quad (2.13)$$

The ETR2 obtained by the gross oxygen evolution rate is based on whole-tissue measurement and can be validly compared with ETR1 obtained from Y(I). This is because the $P700^+$ signal is also a whole-tissue measurement, by virtue of the fact that the measuring beams at 820 and 870 nm are only weakly absorbed by the leaf tissue and are, therefore, multiply scattered in the tissue until they are finally absorbed; subtraction of LEF_{O2} from ETR1 is then valid, as both refer to the same leaf tissue (Fan *et al.*, 2016).

2.2.5 Data analysis

For each variable, four replicates (independent samples) were obtained for the two light treatments. The results were subjected to analysis of variance and the means were compared by the Tukey test at 5% probability.

2.3 RESULTS

2.3.1 Comparing two methods for estimating the fraction of absorbed light partitioned to PSI (f_I)

Estimation of CEF from ETR1 requires prior information on f_I, which, in turn requires a situation where CEF is small or negligible. This can be achieved by: 1) using inhibitors of CEF such as antimycin A and TTFA, or 2) using low irradiance to drive LEF to produce minimal CEF. The efficiency of these two methods was evaluated by concurrently measuring fluorescence and P700 signals with mass spectrometric measurements of gross O_2 evolution in a closed leaf chamber (**Figures 2. S 1** and **2. S 2**).

Using the first method, leaf discs of C_4 grasses *P. miliaceum* and *M. maximus* were infiltrated with ~200 µM solution of each inhibitor and Y(I) was measured using Dual-PAM/F under increasing irradiance from 100 to 2000 µmol photons m^{-2} s^{-1}. Assuming that CEF was completely inhibited, ETR1 would approximately equal LEF_{O2} as in equation **(**2.6**)**. Then, f_I can be estimated by equating ETR1 with LEF_{O2} and using measured Y(I) as in equation **(**2.7**)** and equation **(**2.8**)**. If CEF was inhibited in this method, f_I would be independent of irradiance. However, f_I decreased with increasing irradiance for both species (**Table 2. S 1**). In addition, LEF_{O2} of treated leaf discs was lower compared to untreated discs; perhaps due to inhibition of carbon assimilation caused by impairment of CEF. This could affect ETR1 calculation and underestimate f_I due to the side effects of high concentration of CEF inhibitors on photosynthesis. Consequently, we considered that this method was unreliable for f_I estimation.

The second method used Y(II) obtained by simultaneously measuring Chl fluorescence and gross O_2 evolution rate at low irradiance and high pCO_2. At less than ~300-500 µmol photons m^{-2} s^{-1}, CEF was assumed to be negligible in CO_2-enriched air. Under these conditions, Kou *et al.* (2013) showed that $ETR2_{Fl}$ roughly matched LEF_{O2} in spinach. We equated LEF_{O2} to ETR2 as in equation (2.11). Then using Y(II) obtained from Dual-PAM/F, f_{II} was obtained according to equation (2.12), and subtracted from 1 to give f_I. The estimated f_{II} derived from Y(II) measurement was used to calculate a new ETR2 and plotted against irradiance, as was LEF_{O2}. Results showed that ETR2 of control and shade-grown *Z. mays* (NADP-ME) (**Figures 2. 1A** and **2. 1C**) and *P. bisulcatum* (C_3 grass) (**Figures 2. 1B** and **2. 1D**) roughly matched LEF_{O2} at irradiance <300-500 µmol photons m^{-2} s^{-1}. Hence, this method was considered more reliable compared to the first at low irradiance, and was subsequently used for f_I estimation of other species.

Utilising our second more reliable method, we calculated f_I for the species used in this study (**Table 2. 1**). All control C_4 species had estimated f_I of 0.6 except for PCK grass species (*M. maximus*) which had f_I of 0.5. On the other hand, f_I of shade-grown C_4 species remained constant except for NADP-ME grass species (*P. antidotale*) which had f_I of 0.7. Control C_3 grass species (*P. bisulcatum*) had f_I of 0.4 which is lower compared to spinach, which is also a C_3 species, having f_I of 0.5. However, shade-grown C_3 grass had f_I of 0.5. Other species such as liverwort (*Marchantia polymorpha*) and fern (*Polypodium* sp.) had f_I of 0.5 similar to C_3 species, while the two species of gymnosperms had lower f_I which was equal to 0.4 for ginkgo (*Ginkgo biloba*) and 0.3 for Wollemi pine (*Wollemi nobilis*) (**Table 2. 1**). Overall, there was a significant species x treatment effect on both f_I and f_{II} (**Table 2. 2**).

2.3.2 The response of ETR1 and CEF in C_3 and C_4 grass species to shade

Using our estimated f_I values, corrected ETR1 was calculated using equation (2.4). Corrected ETR1 was higher in control NADP-ME (**Figure 2. 2B**) and NAD-ME grasses (**Figure 2. 2C**) by ~20% and lower in control PCK (~9%) (**Figure 2. 2D**) and C_3 (~16%) (**Figure 2. 2A**) grasses when compared to uncorrected ETR1. Using corrected ETR1, CEF rates were then corrected using equation (2.9). At ≥500 µmol photons m^{-2} s^{-1}, CEF increased by ~32% and 38% in control NADP-ME (**Figure 2. 2B**) and NAD-ME (**Figure 2. 2C**) grass species and decreased by ~14% and ~28% in control PCK (**Figure 2. 2D**) and C_3 grass (**Figure 2. 2A**) species, respectively**.** Overall, there was no significant species x treatment effect on ETR1, CEF and LEF_{O2} measured at saturating irradiance (2000 µmol photons m^{-2} s^{-1}) (**Table 2. 2**). However, when measured at low, medium and saturating irradiance (200, 1000 and 2000 µmol photons m^{-2} s^{-1}), leaf discs of all shade-grown grass species had significantly higher CEF rates compared to control species (**Figures 2. 3A** to **2. 3D**), except for the NADP-ME grass species which had no significant difference to the control (**Figure 2. 3B**).

When measured at low irradiance, CEF rates increased the most in shade-grown C_3 grass species (+1900%) (**Figure 2. 3A**) followed by PCK grass (+1395%) (**Figure 2. 3D**), NADP-ME grass (+86%) (**Figure 2. 3B**) and NAD-ME grass (+75%) (**Figure 2. 3C**) species relative to control counterparts. Highest increase in CEF rate measured under saturating light was again observed in shade-grown C_3 grass (+58%) (**Figure 2. 3A**) followed by PCK grass (+32%) (**Figure 2. 3D**), NAD-ME grass (+29%) (**Figure 2. 3C**) and NADP-ME grass (+3%) (**Figure 2. 3B**) species relative to control plants.

Under shade conditions, CEF rates measured at 1000 µmol photons m^{-2} s^{-1} were ~35% higher in *P. miliaceum* (NAD-ME), *M. maximus* (PCK) and *Z. mays* (NADP-ME) relative to *P. bisulcatum* (C_3) and *P. antidotale* (NADP-ME) (**Tables 2. 2 and 2. S 2**).

When measured at 1000 µmol photons m^{-2} s^{-1}, LEF_{O2} was significantly lower in all shade-grown species relative to the control treatment (**Tables 2. 2 and 2. S 2**). However, ETR1 was not affected by the shade treatment in any of the species except for *P. antidotale*, where ETR1 decreased by 28% under shade (**Tables 2. 2 and 2. S 2**).

2.3.3 Rates of CEF of other species in response to irradiance

LEF_{O2}, ETR1 and CEF rates of all control species increased approximately linearly with irradiance (**Tables 2. 2 and 2. S 2**). Operation of CEF under low irradiance (200 µmol photons m^{-2} s^{-1}) was almost negligible in control C_3 grass and gymnosperm species (**Tables 2. 2 and 2. S 2**). This is because of the rate of LEF_{O2} almost equalled ETR1 (**Table 2. S 2**), suggesting that all electrons from PSII were transferred to acceptors in PSI in these species without cycling around PSI. CEF started to operate between 400-750 µmol photons m^{-2} s^{-1} in C_3 grass and gymnosperm species while operation of CEF in other species started at much lower irradiances (**Table 2. S 2**). Among all control C_4 species, rapid stimulation of CEF under low irradiance (<400 µmol photons m^{-2} s^{-1}) was observed in NADP-ME and NAD-ME species while CEF of PCK grass species was stimulated at much higher irradiance (**Table 2. S 2**). Among all control species measured at irradiance of 1000 µmol photons m^{-2} s^{-1}, all grass species including *Z. mays* had higher LEF_{O2} compared to the gymnosperms, liverwort and fern (**Figure 2. 4B**; **Tables 2. 2 and 2. S 2**). NADP-ME and NAD-ME grass species had the highest rates of CEF, which was not significantly different among the other species (**Figure 2. 4A**; **Tables 2. 2 and 2. S 2**). When measured at low irradiance of 200 µmol photons m^{-2} s^{-1}, all shade-grown plants had lower rates of CEF and LEF_{O2} compared to control plants under measured at medium irradiance of 1000 µmol photons m^{-2} s^{-1} (**Figure 2. 4A**; **Figure 2. 4B**; **Tables 2. 2 and 2. S 2**). This suggests that electron fluxes of shade-grown plants operate at a slower rate under their growing light conditions in comparison to control plants. The ratio of CEF to LEF_{O2} was generally higher in C_4 relative to C_3 grass under both control and shade conditions (**Figure 2. 4C**). In addition, the CEF to LEF_{O2} ratio was not significantly different among the C_4 grasses under either control or shade conditions (**Figure 2. 4C**). Liverwort and fern species had higher CEF to LEF_{O2} ratio relative to all other species under control conditions (**Figure 2. 4C**). Overall, no significant species x treatment effect on CEF to LEF_{O2} ratio under low, medium and saturating light (**Table 2. 2**).

2.4 DISCUSSIONS

In this study, we tested two methods to calculate the light partitioning between PSI and PSII (f_I and f_{II}, respectively) in several plant species by combining P700 using dual PAM and LEF using MIMS measurements. Given that our species of interest are not widely studied, we included spinach and maize in our study to compare our values with the literature. One method was more reliable and we adopted it to determine CEF around PSI.

2.4.1 The use of CEF inhibitors is unreliable for f_I estimation in leaves of C_4 grasses

The concentration of the CEF inhibitors that should infiltrate the leaf must be ≥200 μM. At this concentration, Kou *et al.* (2013) observed that antimycin A had no effect on LEF_{O2} assayed by O_2 evolution and largely abolished CEF in spinach leaf discs. However, the same was not observed in some C_4 grass leaves examined. After allowing the leaf to take up the inhibitor solution overnight, the leaf started to dry out and LEF_{O2} values were lower compared to the control (**Table 2. S 1**), possibly due to downstream inhibition of the Calvin-Benson Cycle in bundle sheath chloroplasts. The combination of these two potent CEF inhibitors might have multiple effects on photosynthesis. An example is from the study of Horton *et al.* (1991) where they found that antimycin A prevents LHCII aggregation which inhibits the process of excess excitation energy dissipation as heat (qE). It was also observed that TTFA can inhibit photosynthetic electron transport in and around PSII complex in spinach as measured from chlorophyll fluorescence parameters (Ikezawa *et al.,* 2014).

Aside from these reasons, it was also decided not to measure f_I under high irradiance for C_4 plants because of the amount of charge recombination occurring in both mesophyll and bundle-sheath chloroplasts (Takahashi *et al.,* 2013; Kou *et al.*, 2015). Even though it was expected that antimycin A and TTFA inhibited CEF, there was still some direct charge recombination occurring in both mesophyll and bundle-sheath chloroplasts, which kept P700 more reduced, because of the amount of PSI in bundle-sheath chloroplasts in C_4 leaves. In this case, Y(I) would be greater than in the absence of direct charge recombination and smaller f_I values under increasing irradiance (**Table 2. S 1**). This phenomenon was also observed in low-light-grown *Arabidopsis* that lacks NDH which still exhibited a substantial ΔFlux at high irradiance even in the presence of antimycin A, attributable to charge recombination in PSI and/or the Mehler reaction (Kou *et al.*, 2015).

2.4.2 Advantages of simultaneous measurement of Chl fluorescence and gas exchange rate under low irradiances for f_I determination

Several methods to experimentally quantify f_I and f_{II} have been proposed in earlier studies but the method which was utilised in this study estimates light partitioning through simultaneous measurements of O_2 evolution and the quantum yield of the photochemical reaction at PSII or PSI. This method is considered to be non-destructive, mechanistic and quantitative which assumes a linear relationship between the gas exchange and photochemical yields (**Figures 2. 1A** to **2. 1D**). This method was adopted in a number of studies (Fan *et al.*, 2016; Kono *et al.*, 2014.; Kou *et al.*, 2015; Kou *et al.*, 2013; Laisk *et al.*, 2014; Laisk & Loreto, 1996; Loreto *et al.*, 2009; Miyake & Yokota, 2000; Miyake *et al.*, 2004, 2005).

2.4.3 Comparison of f_I across a wide range of species and in response to shade

Higher value of f_I in C_4 species compared to C_3 species (**Tables 2. 1** and **2. 2**) validated the hypothesis that more excitation energy is distributed to PSI compared to PSII in C_4 species. This was expected because leaves of C_4 plants contain two types of photosynthetic cells, mesophyll and bundle sheath cells, which are quite distinctly organized, both structurally and functionally having varying PSI/PSII ratio depending on subtypes (Drozak & Romanowska, 2006; Ghannoum *et al.*, 2005; Romanowska & Albertsson, 1994; Romanowska *et al.*, 2008; Romanowska & Drożak, 2006). For the representative species of gymnosperm, liverwort and fern, the higher values of f_{II} compared to f_I suggests the greater amount of PSII components relative to PSI in mesophyll chloroplasts. However, further experiments involving morphological and biochemical examinations of the leaf should be done to quantify functional PSI and PSII contents as well as the antenna size of each photosystem.

Growth irradiance is believed to affect the distribution of excitation energy by modulating the composition of light-harvesting antennas of PSI and PSII (Anderson, 1986; Huner *et al.*, 2003; Tanaka & Melis, 1997). Growth under low light promotes large PSI and PSII antenna size whereas growth under high light generates a small photosynthetic unit (Akoumianaki-Ioannidou *et al.*, 2004.; Huner *et al.*, 2003; Leong & Anderson, 1984). In C_3 plants, the value of f_{II} was expected to be greater than that of f_I because PSII absorbs more light than PSI and this proportion increases with adaptation to shade based on the study of Evans (1986). But the result of this study showed that in the C_3 model species spinach, almost 50% of the absorbed light was partitioned to PSII and the other 50% to PSI (**Table 2. 1**) which is consistent to the study of Fan *et al.* (2016) and Kou *et al.* (2013), thus validating the reliability of this method. This partitioning is different in the leaf of control C_3 grass (*P. bisulcatum*) examined where

almost 60% of light was partitioned to PSII and this partitioning decreased when grown under shade. In the case of C_4 plants, a large fraction of the absorbed light energy (~60%) was partitioned to PSI in the leaf of control plants and slightly increased in shade-grown plants. Several studies showed that adaptation to shade can increase f_{II} because of the lowering of the chlorophyll a/b ratio which will increase the amount of chlorophyll associated with PSII relative to chlorophyll associated with PSI (Walters & Horton, 1995; Hogewoning *et al.*, 2012; Murakami *et al.*, 2016, 2017; Chow *et al.*, 1990). However, the results obtained here were different from these findings for both shade-grown C_3 and C_4 grasses. An increase in PSI content has previously been observed by Bailey *et al.* (2001), but this change occurred only under very low irradiance with light intensities below 100 µmol photons m^{-2} s^{-1}. The slight decrease in f_{II} values of shade-grown plants (**Table 2. 1**) can also be attributed to the light consumption brought about by the accessory pigment content of the photosynthetic complexes which were altered during shade acclimation (Laisk *et al.*, 2014).

2.4.4 CEF at increasing irradiance

The very low CEF rate observed at ≤300 µmol photons m^{-2} s^{-1} (**Figures 2. 2A** to **2. 2D**; **Figures 2. 3A** to **2. 3D**; **Tables 2. 2** and **2. S 2**) is because Calvin cycle was able to use the majority of NADPH at low irradiance, leaving little spare reduced ferredoxin for poising CEF. At maximum LEF_{O2}, however, more reduced ferredoxin would be available for competition between $NADP^+$ reduction and poising of CEF (Kou *et al.*, 2013; Okegawa *et al.*, 2008) and CEF was larger than LEF_{O2} (**Figures 2. 2A** to **2. 2D**; **Table 2. S 2**). This can be attributed to spectral distribution of the actinic light used in this study which favoured CEF over LEF. The actinic light from the halogen lamp used induced CEF above 500 µmol photons m^{-2} s^{-1} in control C_3 grass and above 300 µmol photons m^{-2} s^{-1} in control C_4 grass species. However, CEF was induced at lower irradiance (200 µmol photons m^{-2} s^{-1}) in shade-grown C_3 and C_4 grasses (**Figures 2. 3A** to **2. 3D**; **Table 2. S 2**) suggesting the formation of more reduced ferredoxin under low-light and that the Calvin-Benson cycle started to get saturated with NADPH. This demonstrates the significant effect of the spectral distribution of actinic light on the CEF being investigated.

2.4.5 Induction of CEF among different species (C_3 and C_4 grasses, gymnosperms, ferns, and liverwort) under high light

Although no significant difference was observed between the CEF of control species measured at 1000 µmol photons m^{-2} s^{-1} (**Figure 2. 4C**; **Table 2. S 2**), CEF started to operate between 400-750 µmol photons m^{-2} s^{-1} in C_3 grass and gymnosperm species while operation

of CEF in other species started at much lower irradiance, suggesting the greater capacity for CEF in C_4 and fern species (**Table 2. S 2**). Since it is widely known that CEF is crucial for a proper balance of NADPH and ATP in the thylakoid stroma of photosynthetic organisms (Golding & Johnson, 2003; Hatch, 1987; Huang *et al.*, 2012; Johnson, 2011; Kramer & Evans, 2011; Miyake, 2010; Munekage *et al.*, 2004; Rumeau *et al.*, 2007; Shikanai, 2007; Takabayashi *et al.*, 2005), differences in the capacity for CEF can be due to differences in the energy requirement among species. In C_4 plants, both C_3 and C_4 cycles are functional, thereby increasing the energetic cost of assimilating CO_2 relative to that in C_3 plants under varying irradiances.

Little is known about the energy requirements of ferns and liverworts and their capacities for CEF under varying irradiances. However, early onset of CEF under low irradiance in these species (**Table 2. S 2**) suggests that it served as a mechanism to protect the photosynthetic apparatus from photodamage since CEF can generate a ΔpH across the thylakoid membrane through increased electron transfer from PSI back to plastoquinone thus activating NPQ under intense radiation (Carlquist & Schneider, 2001; Watkins *et al.*, 2007). Induction of CEF in gymnosperms at higher irradiance in comparison to other species (**Table 2. S 2**) might be due to the ecophysiological traits of these species. Gymnosperms commonly grow in the mid- to high-latitude regions of the Northern Hemisphere where severe climatic conditions such as chilling temperatures are often experienced. As a result, they may be required to be more flexible than angiosperms to control photosynthesis according to surrounding environmental conditions (Shirao *et al.*, 2013).

2.4.6 Capacity for CEF among the C_4 subtypes

Much rapid stimulation of CEF at low irradiance (<400 µmol photons m^{-2} s^{-1}) in NADP-ME and NAD-ME species in comparison to PCK grass (**Table 2. S 2**) can be due to differences in the energy requirements among subtypes. For example, in NADP-ME species, BSC require more ATP than MC. This assumption is supported by the findings that the BS chloroplasts of most NADP-ME species either completely lack or have less grana with little activity of PSII, which is indispensable for the production of ATP and NADPH in LEF (Chapman *et al.*, 1980; Gutierrez *et al.*, 1974; Hatch, 1987; Kanai *et al.*, 1999; Romanowska *et al.*, 2008; Woo *et al.*, 1970).

2.4.7 Induction of CEF in shade-grown C_3 and C_4 species

The intensity of light under which plants grow has a significant effect on CEF (Miyake *et al.*, 2005). Highest increase in CEF rate under low and high irradiances was observed in the

shade-grown C_3 grass (**Figure 2. 3A**; **Table 2. S 2**) suggesting that C_3 grass species is more efficient in maintaining a balance in the ATP/NADPH ratio under low light conditions and can dissipate excess light energy harmlessly as heat under saturating light condition. This result also suggests that the induction of CEF in these shade-grown plants may serve as a photoprotective mechanism or to generate additional ATP switching from LEF to CEF as part of the acclimation strategy since it was shown that shade down-regulated LEF_{O2} in all species (**Figure 2. 4B**; **Table 2. S 2**). It has been shown that shade-grown *Arabidopsis* developed high PSI/PSII ratio in leaves which is preferentially involved in CEF to generate ATP suggesting that this maybe a way in which cells make the best use of the light available under such conditions (Joliot & Joliot, 2006). However, it was shown by Miyake *et al.* (2005) that tobacco plants exposed to high light have greater capacity for both CEF and NPQ when compared with plants grown under low light. They have suggested that the main role of CEF in plants acclimated to high light is to dissipate excess light energy through NPQ when illuminated at high irradiance. Under low light, the rate of photosynthesis of high light acclimated plants tends to be limited by the rate of ATP production rather than by the rate of NADPH production. Therefore, it was assumed that CEF assisted with ATP synthesis under weaker light in control plants (Yamori *et al.*, 2011). By contrast, for plants acclimated to low light, the rates of photosynthesis and photorespiration are expected to be low. Consequently, they should have reduced demand for CEF-dependent ATP regeneration. Thus, Yamori *et al.* (2011) speculated that, in plants exposed to low levels of light, the relatively low CEF activity corresponds to the ATP demand by primary metabolisms. Their results indicate that, CEF primarily assists in maintaining a balance in the ATP/NADPH ratio under sub-saturating light conditions but tends to mainly participate in photoprotection for PSI and PSII under saturating light conditions which can be true for the species of grasses used in our experiment.

No significant difference was observed in the capacity for CEF between control and shade-grown NADP-ME grass under low, medium and saturating irradiance (**Figure 2. 3B**; **Table 2. 2** and **2. S 2**) suggesting that CEF-dependent generation of ΔpH mainly contributed to ATP synthesis under those levels of irradiance in control and shade-grown plants. This result somehow confirmed the findings of Sonawane *et al.* (2018) using several species of C_4 grasses across subtypes. They showed that NAD-ME and to a lesser extent PCK species were generally outperformed by NADP-ME species. This response was underpinned by a more efficient CCM and quantum yield in NADP-ME.

2.5 CONCLUSIONS

In this study, we developed a reliable method to calculate the light partitioning between PSI and PSII (f_I and f_{II}, respectively) by combining P700 using dual PAM and LEF using MIMS measurements. We applied this method to estimate f_I for several plant species to determine if f_I deviates from what is widely assumed (f_I = 0.5) in the literature. C_4 grasses had f_I of 0.6 which is higher than what is usually assumed. C_3 grass had f_I of 0.4 which is lower compared to the model C_3 species. Other species such as liverwort and fern had f_I of 0.5 while gymnosperms had lower. However, it was also shown that these values can change depending on the growing conditions such as irradiance. Cyclic electron flow was negligible at low irradiance; it was generally higher in C_4 grasses and lower in gymnosperms. The values obtained here can be used to correctly quantify CEF and further used for photosynthesis modelling.

Table 2. 1 The fraction of absorbed light partitioned to PSI (f_I)

An estimation of the fraction of absorbed light partitioned to PSI (f_I) obtained by Chl fluorescence method measured under low irradiances, high CO_2 conditions (3-4%) and temperature of 28°C in leaf of control and shade-grown C_3, C_4, gymnosperm, fern, and liverwort species. Values are means ± s.e.

	Irradiance (µmol photons m^{-2} s^{-1})	f_I Control	f_I Shade
	50	0.40 ± 0.02	0.51 ± 0.01
Panicum bisulcatum (*n* = 4)	100	0.40 ± 0.01	0.47 ± 0.02
(C_3)	200	0.43 ± 0.01	0.59 ± 0.02
	300	0.45 ± 0.02	0.61 ± 0.03
	50	0.60 ± 0.01	0.58 ± 0.02
Panicum miliaceum (*n* = 4)	100	0.58 ± 0.01	0.59 ± 0.01
(NAD-ME)	200	0.62 ± 0.02	0.64 ± 0.02
	300	0.67 ± 0.03	0.69 ± 0.02
	50	0.43 ± 0.01	0.54 ± 0.03
Megathyrsus maximus (*n* = 4)	100	0.42 ± 0.00	0.56 ± 0.02
(PCK)	200	0.47 ± 0.01	0.63 ± 0.03
	300	0.50 ± 0.01	0.68 ± 0.03
	50	0.60 ± 0.02	0.62 ± 0.02
Panicum antidotale (*n* = 4)	100	0.57 ± 0.02	0.65 ± 0.01
(NADP-ME)	200	0.57 ± 0.02	0.68 ± 0.02
	300	0.62 ± 0.01	0.73 ± 0.02
Zea mays (*n* = 8)	50	0.58 ± 0.02	0.60 ± 0.01
(NADP-ME)	100	0.57 ± 0.02	0.59 ± 0.02
	200	0.58 ± 0.02	0.61 ± 0.03
	300	0.60 ± 0.02	0.65 ± 0.03
	50	0.49 ± 0.01	
Spinach (*n* = 5)	100	0.51 ± 0.00	
(C_3)	200	0.50 ± 0.00	
	300	0.50 ± 0.00	
	50	0.37 ± 0.01	
Ginkgo biloba (*n* = 4)	100	0.38 ± 0.01	
(Gymnosperm)	200	0.43 ± 0.00	
	300	0.46 ± 0.01	

	50	0.22 ± 0.03
Wollemi nobilis (*n* = 4)	100	0.31 ± 0.04
(Gymnosperm)	200	0.49 ± 0.07
	300	0.49 ± 0.08
	50	0.48 ± 0.01
Polypodium sp. (*n* = 4)	100	0.54 ± 0.01
(Fern)	200	0.61 ± 0.02
	300	0.59 ± 0.01
	50	0.44 ± 0.01
Marchantia polymorpha (*n* = 4)	100	0.49 ± 0.02
(Liverwort)	200	0.57 ± 0.03
	300	0.61 ± 0.04

Table 2. 2 Statistical summary

Summary of statistical analysis using two-way ANOVA for the effects of shade and species on various parameters collected for 9 plants grown under natural light (~800 µmol photons m^{-2} s^{-1}) and shaded (~300 µmol photons m^{-2} s^{-1}) conditions. Measurements were made at low light (200 µmol photons m^{-2} s^{-1}), medium light (1000 µmol photons m^{-2} s^{-1}) and saturating light (2000 µmol photons m^{-2} s^{-1}) under the temperature of 28°C and high CO_2 condition (3-4%).

Parameter	Main effects (P)		Interactions (P)
	Species	Treatment	Species x Treatment
Y(II)	0.021	0.000	0.014
Y(I) at low light	0.001	0.080	0.240
Y(I) at medium light	0.023	0.216	0.180
Y(I) at saurating light	0.084	0.704	0.184
f_I	0.000	0.000	0.003
f_{II}	0.000	0.000	0.003
LEF_{O2} at low light (µmol e^- m^{-2} s^{-1})	0.000	0.000	0.098
LEF_{O2} at medium light (µmol e^- m^{-2} s^{-1})	0.000	0.000	0.014
LEF_{O2} at saturating light (µmol e^- m^{-2} s^{-1})	0.000	0.000	0.140
ETR1 at low light (µmol e^- m^{-2} s^{-1})	0.000	0.002	0.011
ETR1 at medium light (µmol e^- m^{-2} s^{-1})	0.000	0.779	0.039
ETR1 at saturating light (µmol e^- m^{-2} s^{-1})	0.000	0.210	0.122
CEF at low light (µmol e^- m^{-2} s^{-1})	0.000	0.000	0.000
CEF at medium light (µmol e^- m^{-2} s^{-1})	0.000	0.000	0.266
CEF at saturating light (µmol e^- m^{-2} s^{-1})	0.000	0.000	0.341
CEF/LEF_{O2} at low light	0.000	0.000	0.544
CEF/LEF_{O2} at medium light	0.000	0.000	0.052
CEF/LEF_{O2} at saturating light	0.001	0.000	0.294

Table 2. S 1 Fraction of absorbed light partitioned to PSI (f_I) under increasing irradiances.

An estimation of the fraction of absorbed light partitioned to PSI (f_I) under increasing irradiances obtained by inhibiting CEF in leaf of control *Panicum miliaceum* (NAD-ME grass) and *Megathyrsus maximus* (PCK grass) by infiltration with 200 µM antimycin A: thenoyltrifluoroacetone (TTFA) solution. LEF_{O2} is the linear electron flux determined by the gross rate O_2 evolution measured under the temperature of 28°C and high CO_2 condition (3-4%), Y(I) is the photochemical yield of PSI, Y(ND) is a measure of PSI donor side limitation and Y(NA) is a measure of PSI acceptor side limitation. Values are means ± s.e. (n = 4 leaves).

	Irradiance (µmol photons m^{-2} s^{-1})	Control				Treated				
		LEF_{O2} (µmol e^- m^{-2} s^{-1})	Y(I)	Y(ND)	Y(NA)	LEF_{O2} (µmol e^- m^{-2} s^{-1})	Y(I)	Y(ND)	Y(NA)	f_I
Panicum miliaceum (NAD-ME)	100	26.4 ± 1.3	0.68 ± 0.04	0.22 ± 0.02	0.10 ± 0.06	24.2 ± 1.4	0.68 ± 0.02	0.2 ± 0.02	0.11 ± 0.03	0.42 ± 0.01
	200	43.0 ± 1.6	0.67 ± 0.05	0.21 ± 0.02	0.06 ± 0.01	34.7 ± 2.7	0.69 ± 0.02	0.22 ± 0.02	0.08 ± 0.02	0.3 ± 0.02
	400	64.0 ± 1.8	0.65 ± 0.04	0.26 ± 0.02	0.09 ± 0.06	49.4 ± 2.5	0.68 ± 0.02	0.25 ± 0.01	0.07 ± 0.02	0.21 ± 0.01
	750	92.1 ± 2.2	0.64 ± 0.04	0.27 ± 0.02	0.09 ± 0.05	65.9 ± 6.7	0.64 ± 0.01	0.28 ± 0.02	0.08 ± 0.03	0.16 ± 0.02
	1000	117.3 ± 6.2	0.60 ± 0.02	0.29 ± 0.02	0.12 ± 0.04	98.6 ± 6.6	0.62 ± 0.00	0.28 ± 0.01	0.1 ± 0.01	0.19 ± 0.01
	1500	150.9 ± 4.7	0.55 ± 0.03	0.28 ± 0.02	0.18 ± 0.05	120.1 ± 7.8	0.56 ± 0.01	0.31 ± 0.01	0.13 ± 0.01	0.17 ± 0.01
	2000	165.7 ± 5.9	0.51 ± 0.03	0.27 ± 0.02	0.22 ± 0.05	123.7 ± 12.2	0.54 ± 0.02	0.31 ± 0.02	0.15 ± 0.03	0.14 ± 0.01
Megathyrsus maximus (PCK)	100	25.9 ± 0.25	0.45 ± 0.03	0.06 ± 0.01	0.49 ± 0.03	21.1 ± 2.1	0.66 ± 0.02	0.14 ± 0.02	0.21 ± 0.02	0.38 ± 0.05
	200	35.9 ± 0.46	0.51 ± 0.03	0.10 ± 0.01	0.40 ± 0.03	28.9 ± 3.2	0.67 ± 0.03	0.18 ± 0.02	0.15 ± 0.03	0.26 ± 0.04
	400	46.9 ± 1.04	0.53 ± 0.03	0.15 ± 0.01	0.32 ± 0.04	40.4 ± 3.4	0.64 ± 0.05	0.18 ± 0.01	0.18 ± 0.05	0.19 ± 0.01
	750	62.0 ± 2.52	0.50 ± 0.02	0.17 ± 0.01	0.34 ± 0.03	59.3 ± 10.6	0.61 ± 0.06	0.18 ± 0.02	0.21 ± 0.07	0.15 ± 0.01
	1000	72.9 ± 5.65	0.46 ± 0.03	0.17 ± 0.02	0.38 ± 0.04	77.5 ± 18.9	0.58 ± 0.06	0.16 ± 0.02	0.26 ± 0.08	0.15 ± 0.02
	1500	94.9 ± 5.65	0.42 ± 0.03	0.18 ± 0.02	0.40 ± 0.03	86.9 ± 24.6	0.54 ± 0.05	0.15 ± 0.03	0.31 ± 0.09	0.12 ± 0.02
	2000	97.6 ± 6.88	0.41 ± 0.03	0.14 ± 0.01	0.45 ± 0.03	82.9 ± 24.9	0.53 ± 0.04	0.14 ± 0.03	0.33 ± 0.08	0.09 ± 0.02

Table 2. S 2 Responses of various electron fluxes to increasing irradiance

Responses of various electron fluxes to increasing irradiance in leaf of control and shade-grown C_3, C_4, gymnosperm, fern, and liverwort species measured under the temperature of 28°C and high CO_2 condition (3-4%). LEF_{O2} is the linear electron flux determined by the gross rate O_2 evolution, ETR1 is the total electron flux through PSI calculated using experimentally derived *f*, CEF is the cyclic electron flux around PSI. Values are means ± s.e.

		Control			Shade		
		LEF_{O2} (μmol e^- m^{-2} s^{-1})	ETR1 (μmol e^- m^{-2} s^{-1})	CEF (μmol e^- m^{-2} s^{-1})	LEF_{O2} (μmol e^- m^{-2} s^{-1})	ETR1 (μmol e^- m^{-2} s^{-1})	CEF (μmol e^- m^{-2} s^{-1})
Panicum bisulcatum (*n* = 4) (C_3)	100	33.0 ± 1.2	24.8 ± 1.9	-10.9 ± 3.0	30.1 ± 1.0	28.6 ± 2.2	2.1 ± 2.9
	200	63.0 ± 1.7	50.5 ± 3.3	-12.5 ± 4.3	41.9 ± 3.3	60.2 ± 4.2	19.7 ± 7.8
	400	102.3 ± 5.5	100.1 ± 3.3	5.8 ± 3.9	59.5 ± 4.1	121.3 ± 4.6	63.9 ± 7.3
	750	131.2 ± 2.6	196.3 ± 3.9	65.1 ± 6.0	71.2 ± 4.3	216.7 ± 13.9	145.5 ± 16.6
	1000	152.9 ± 4.1	285.5 ± 5.3	132.6 ± 7.2	77.3 ± 6.3	284.2 ± 9.8	206.9 ± 15.1
	1500	177.8 ± 4.0	396.8 ± 3.8	219.0 ± 5.9	81.3 ± 6.5	399.1 ± 18.5	317.8 ± 23.6
	2000	188.8 ± 6.1	489.8 ± 6.2	301.0 ± 12.2	83.2 ± 6.0	557.9 ± 40.6	474.7 ± 45.8
Panicum miliaceum (*n* = 4) (NAD-ME)	100	20.4 ± 0.7	34.2 ± 3.7	8.8 ± 4.0	20.2 ± 0.8	40.5 ± 0.8	17.9 ± 1.7
	200	42.7 ± 2.6	69.3 ± 7.1	26.6 ± 7.3	30.1 ± 2.2	81.6 ± 2.5	46.7 ± 3.8
	400	48.6 ± 7.5	136.5 ± 13.5	71.4 ± 15.8	40.5 ± 3.6	159.0 ± 6.0	110.3 ± 8.1
	750	89.0 ± 9.2	246.2 ± 24.0	157.2 ± 25.6	56.1 ± 5.0	280.3 ± 11.0	224.2 ± 10.7
	1000	108.0 ± 10.8	322.4 ± 31.8	214.4 ± 32.2	58.2 ± 4.7	345.4 ± 14.9	287.2 ± 12.0
	1500	117.7 ± 13.5	445.1 ± 42.2	327.4 ± 41.3	62.3 ± 5.0	545.8 ± 10.9	483.5 ± 12.2
	2000	126.1 ± 14.8	589.6 ± 62.0	463.5 ± 61.5	63.1 ± 5.8	662.8 ± 10.9	599.7 ± 14.6
Megathyrsus maximus (*n* = 4) (PCK)	100	28.0 ± 0.6	24.8 ± 1.1	-5.1 ± 1.4	26.7 ± 0.9	39.4 ± 3.5	12.7 ± 6.6
	200	51.1 ± 2.0	54.3 ± 2.3	3.2 ± 3.9	40.1 ± 0.8	83.4 ± 2.5	47.4 ± 4.9

	400	69.0 ± 1.4	116.5 ± 7.3	35 ± 7.7	50.0 ± 2.0	170.1 ± 3.9	127.1 ± 6.7
	750	106.9 ± 3.5	230.7 ± 12.3	123.8 ± 14.8	53.3 ± 5.4	282.0 ± 14.3	228.7 ± 14.9
	1000	126.8 ± 4.7	305.3 ± 18.2	178.5 ± 22.3	58.5 ± 4.7	338.0 ± 5.7	279.5 ± 7.3
	1500	142.5 ± 5.0	413.2 ± 16.0	270.7 ± 19.9	73.1 ± 6.1	494.6 ± 18.4	421.5 ± 23.0
	2000	152.4 ± 5.5	527.7 ± 38.4	375.3 ± 43.4	73.0 ± 5.7	568.7 ± 21.6	495.7 ± 25.7
Panicum antidotale (*n* = 4) (NADP-ME)	100	23.0 ± 1.4	30.6 ± 3.0	3.0 ± 3.7	14.8 ± 1.0	29.3 ± 0.5	14.9 ± 1.5
	200	45.5 ± 2.4	67.9 ± 6.3	22.4 ± 5.8	21.6 ± 1.9	59.1 ± 2.4	41.5 ± 2.6
	400	61.5 ± 2.7	138.6 ± 12.4	61.2 ± 10.2	30.2 ± 3.4	114.3 ± 8.4	93.0 ± 9.8
	750	110.1 ± 5.6	252.7 ± 19.7	142.6 ± 15.0	26.0 ± 1.5	200.3 ± 9.3	174.3 ± 10.3
	1000	133.4 ± 7.1	332.1 ± 29.4	198.7 ± 23.8	29.7 ± 2.6	238.6 ± 10.7	208.9 ± 13.2
	1500	153.0 ± 9.9	460.4 ± 38.9	307.4 ± 32.8	34.9 ± 4.2	355.6 ± 16.5	320.7 ± 19.7
	2000	159.4 ± 15.8	583.2 ± 48.7	423.8 ± 46.0	42.7 ± 3.5	479.2 ± 31.4	436.5 ± 31.1
Zea mays (*n* = 8) (NADP-ME)	100	22.7 ± 0.5	23.8 ± 4.3	0.8 ± 5.0	18.5 ± 1.3	33.8 ± 2.8	10.8 ± 4.0
	200	40.8 ± 1.1	50.9 ± 9.8	10.1 ± 10.7	34.3 ± 3.4	70.1 ± 3.9	33.6 ± 9.0
	400	69.9 ± 2.9	113.3 ± 21.0	46.1 ± 21.7	49.2 ± 7.1	146.6 ± 11.7	93.6 ± 16.9
	750	102.7 ± 5.9	225.1 ± 41.6	122.4 ± 42.9	80.0 ± 17.3	272.2 ± 23	192.2 ± 17.5
	1000	127.4 ± 10.0	294.3 ± 53.7	166.9 ± 59.7	89.4 ± 15.5	347.9 ± 29.9	258.5 ± 25.3
	1500	143.1 ± 10.1	413.2 ± 65.8	270.1 ± 72.6	94.0 ± 20.1	507.7 ± 41.1	413.7 ± 41.7
	2000	148.5 ± 19.1	531.7 ± 95.0	383.2 ± 107.4	97.6 ± 21.0	647.1 ± 46.3	549.5 ± 37.9
Ginkgo biloba (*n* = 4) (Gymnosperm)	100	35.8 ± 0.2	28.4 ± 0.7	-5.8 ± 1.6			
	200	55.7 ± 2.7	55.4 ± 1.6	-0.3 ± 4.1			
	400	90.5 ± 8.2	103.4 ± 1.7	24.2 ± 5.2			
	750	92.0 ± 6.8	176.3 ± 2.0	84.3 ± 6.9			
	1000	96.8 ± 7.8	207.4 ± 2.4	110.6 ± 8.9			

	1500	100.0 ± 8.8	283.6 ± 4.7	183.6 ± 9.4
	2000	105.5 ± 8.6	358.9 ± 7.4	253.4 ± 10.5
Wollemi nobilis (*n* = 5) (Gymnosperm)	100	33.9 ± 3.0	16.3 ± 1.9	-21.7 ± 4.4
	200	47.6 ± 7.2	36.6 ± 3.9	-11.0 ± 7.3
	400	56.9 ± 7.6	62.4 ± 8.1	0.4 ± 9.4
	750	74.4 ± 7.9	103.5 ± 14.6	29.2 ± 10.9
	1000	86.4 ± 9.9	149.1 ± 21.7	62.7 ± 18.1
	1500	85.2 ± 7.1	179.4 ± 32.3	94.2 ± 29.2
	2000	98.2 ± 7.2	252.9 ± 14.3	154.7 ± 8.0
Polypodium sp. (*n* = 5) (Fern)	100	25.0 ± 0.5	33.5 ± 1.4	7.4 ± 1.1
	200	31.6 ± 0.9	48.7 ± 13.2	17.1 ± 13.1
	400	33.3 ± 1.2	88.3 ± 22.7	52.5 ± 22.7
	750	37.0 ± 2.2	161.3 ± 42.2	124.3 ± 42.2
	1000	36.3 ± 1.3	201.3 ± 47.2	165.0 ± 48.4
	1500	39.2 ± 1.4	300.7 ± 66.8	261.5 ± 67.1
	2000	42.3 ± 2.8	399.8 ± 106.4	357.5 ± 107.7
Marchantia polymorpha (*n* = 5) (Liverwort)	100	29.8 ± 2.8	38.1 ± 1.3	3.8 ± 3.3
	200	49.3 ± 7.4	74.6 ± 3.2	25.3 ± 5.2
	400	48.7 ± 9.2	115.7 ± 26.7	55.5 ± 28.4
	750	65.4 ± 12.1	203.5 ± 36.6	138.1 ± 39.1
	1000	70.5 ± 15.0	263.5 ± 43.9	193.0 ± 43.7
	1500	70.3 ± 12.6	385.6 ± 54.5	315.3 ± 55.3
	2000	76.7 ± 15.8	513.5 ± 67.5	436.8 ± 63.6

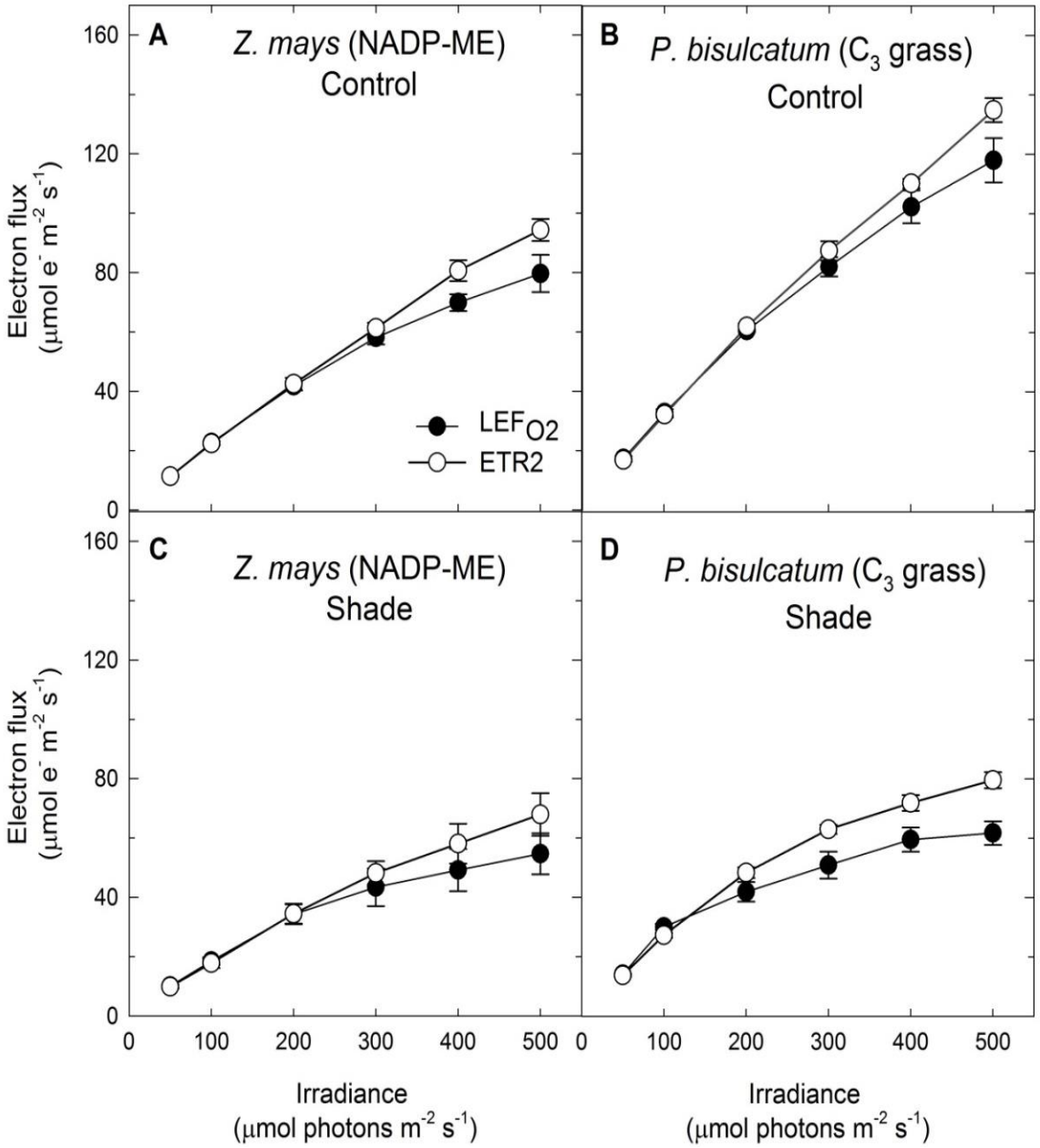

Figure 2. 1 Electron fluxes through PSII in response to measurement irradiance

Electron fluxes through PSII in response to measurement irradiance calculated in 2 different ways in leaf discs of **(A)** control and **(C)** shade-grown *Zea mays* (NADP-ME) and **(B)** control and **(D)** shade-grown *Panicum bisulcatum* (C_3 grass). LEF_{O2} (the gross oxygen evolution rate multiplied by four) represents the linear electron flux through both photosystems; ETR2 is the measure of electron flux through PSII based on Chl fluorescence emitted from a certain depth in leaf tissue calculated using experimentally derived f_{II}. Measurements were made under the temperature of 28^{o}C and high CO_2 condition (3-4%). Values are means ± s.e. (n = 4 leaf discs).

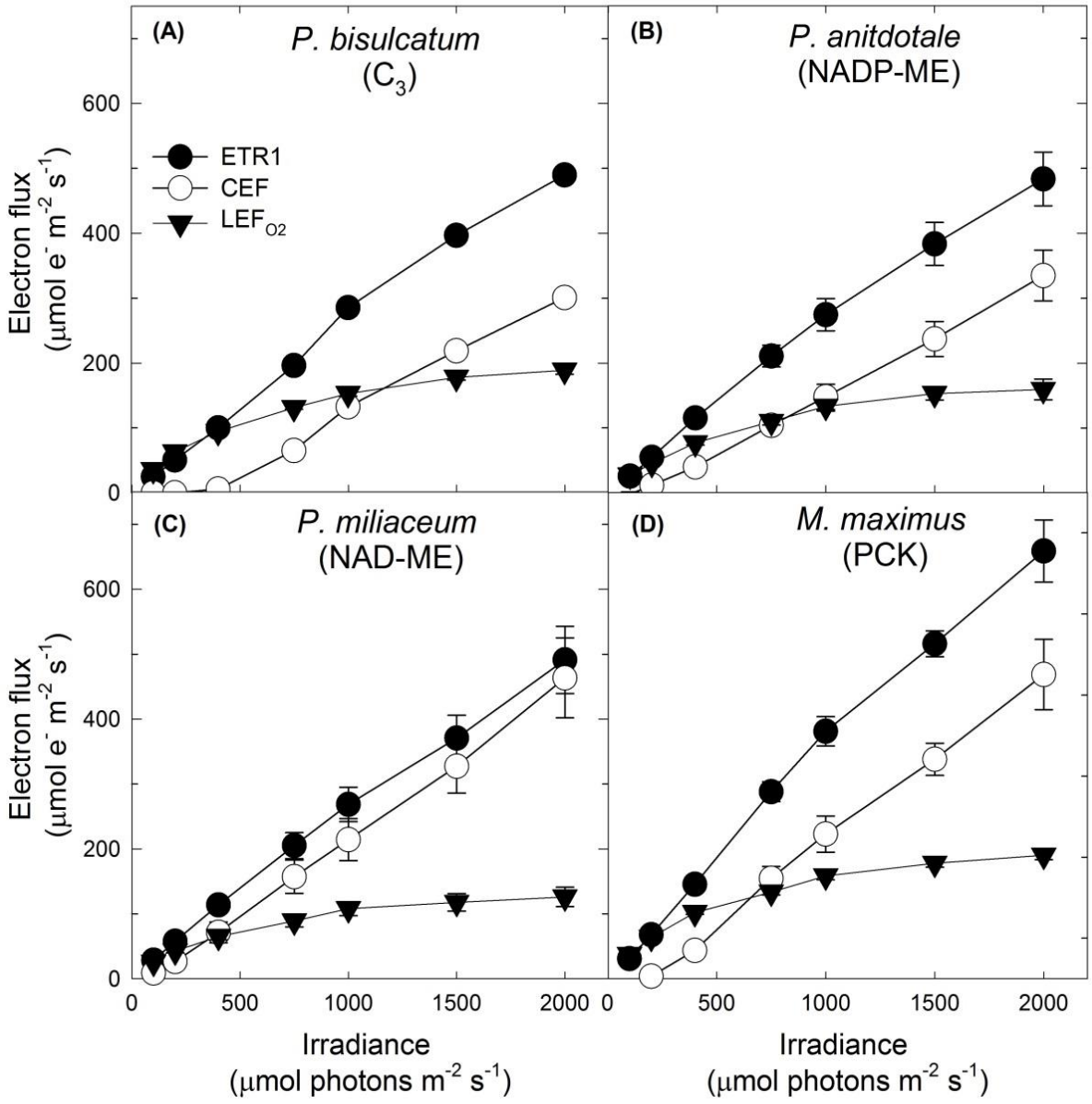

Figure 2. 2 Corrected electron fluxes using experimentally derived f_I

Corrected electron fluxes in response to irradiance in leaf discs of control **(A)** *Panicum bisulcatum* (C_3), **(B)** *Panicum antidotale* (NADP-ME), **(C)** *Panicum miliaceum* (NAD-ME), and **(D)** *Megathyrsus maximus* (PCK). LEF_{O2} (the gross oxygen evolution rate multiplied by four) represents the linear electron flux through both photosystems. ETR1 is the measure of electron flux through PSI calculated using experimentally derived f_I. CEF represents the cyclic electron flux around PSI calculated by subtracting LEF_{O2} from ETR1. Measurements were made under the temperature of 28^{o}C and high CO_2 condition (3-4%). Values are means ± s.e. (n = 4 leaf discs).

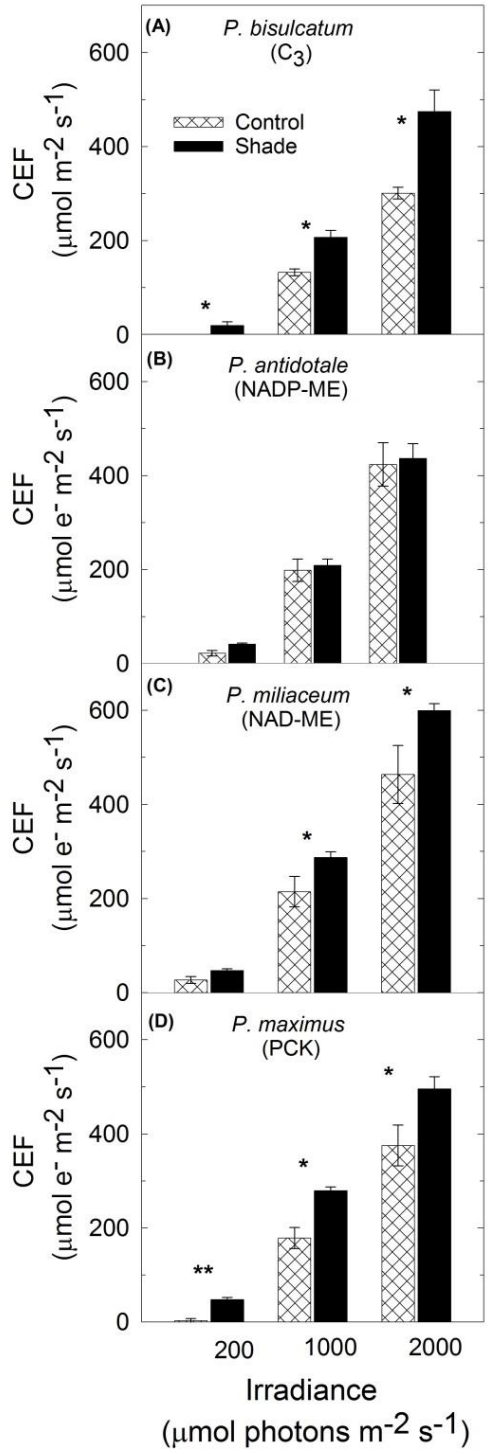

Figure 2. 3 Cyclic electron flux around PSI (CEF) in response to irradiance

Cyclic electron flux around PSI (CEF) in response to low, medium and saturating irradiance (200, 1000, 2000 μmol photons m^{-2} s^{-1}) measured under the temperature of 28^{o}C and high CO_2 condition (3-4%) in leaf discs of control and shade-grown **(A)** *Panicum bisulcatum* (C_3), **(B)** *Panicum antidotale* (NADP-ME), **(C)** *Panicum miliaceum* (NAD-ME), and **(D)** *Megathyrsus maximus* (PCK). Each column represents the mean ± s.e. of species (n = 4 leaf discs) at each light intensity. Statistical significance levels (t-test) for the growth condition within each species and measurement light intensity are shown and they are: * ≡ $p < 0.05$; ** ≡ $p < 0.01$; *** ≡ $p < 0.001$.

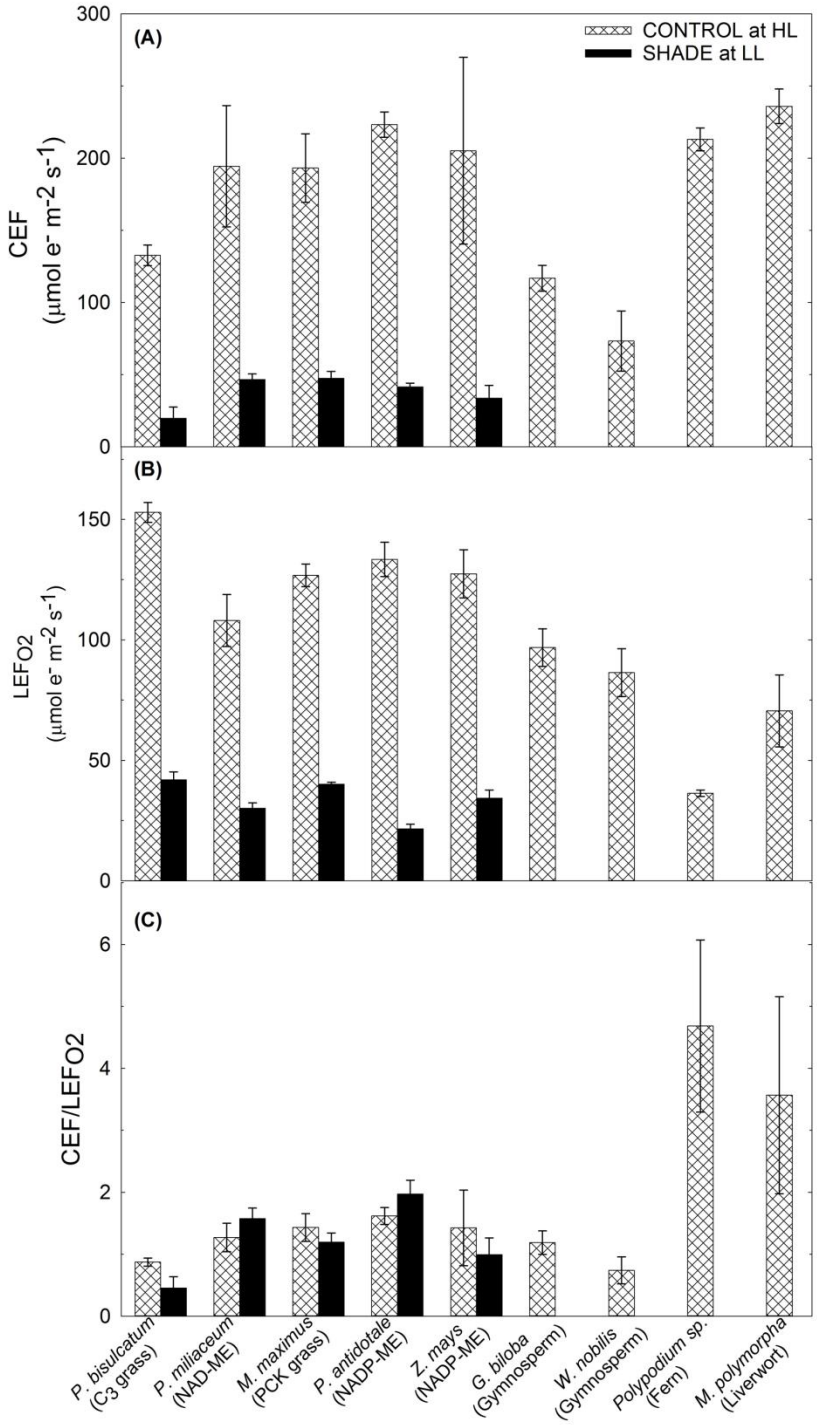

Figure 2. 4 Various electron fluxes of control plants measured at 1000 µmol photons m^{-2} s^{-1} (HL) and shade-grown plants measured at 200 µmol photons m^{-2} s^{-1} (LL)

Measurements were done under the temperature of 28^{o}C and high CO_2 condition (3-4%) in leaf discs of *Panicum bisulcatum* (C_3), *Panicum miliaceum* (NAD-ME), *Megathyrsus maximus* (PCK), *Panicum antidotale* (NADP-ME), *Zea mays* (NADP-ME), *Ginkgo biloba* (gymnosperm), *Wollemi nobilis* (gymnosperm), *Polypodium* sp. (fern), and *Marchantia polymorpha* (liverwort). Each column represents the mean ± s.e. of each species (n = 4 leaf discs).

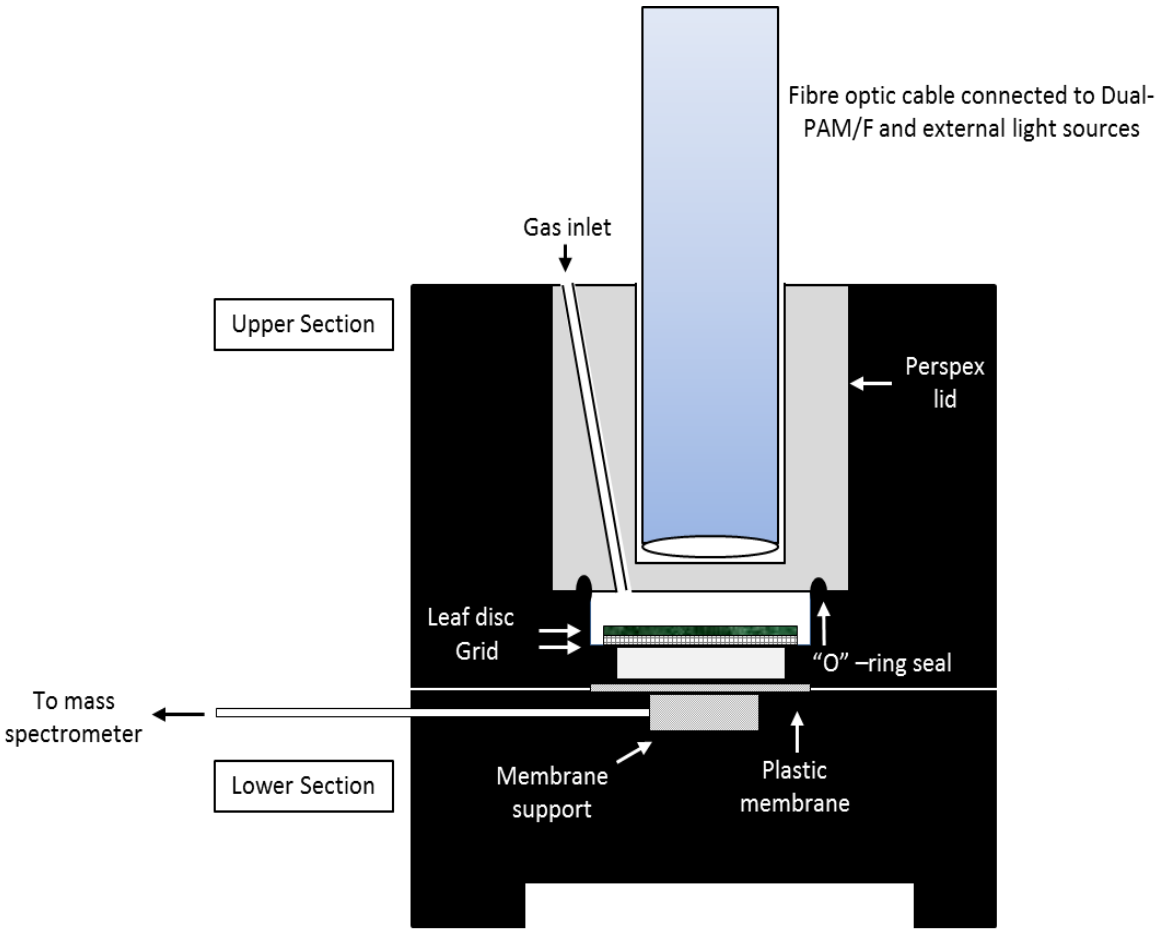

Figure 2. S 1 Cross sectional diagram of the gas exchange cuvette

The chamber was coupled to a mass spectrometer, Dual-PAM/F, and actinic, strong and weak far-red and saturating light sources as described in the text. The fibre optic cable was housed within the Perspex lid, which together with 2 rubber O-rings created a gas-tight seal. The chamber was linked to the mass spectrometer through a thin, gas-permeable plastic membrane and an ethanol/dry ice water trap. The mass spectrometer (micromass ISOPRIME; Micromass Ltd, Manchester, UK) was operated in peak switching mode for $^{18}O_2$ (mass 36), $^{16}O_2$ (mass 32) and CO_2 (mass 44). Net CO_2 assimilation was calculated from the reduction of CO_2 concentration, while gross oxygen evolution, gross oxygen uptake and net oxygen evolution were calculated from changes in $^{16}O_2$ and $^{18}O_2$ respectively, as previously described by Canvin *et al.* (1980).

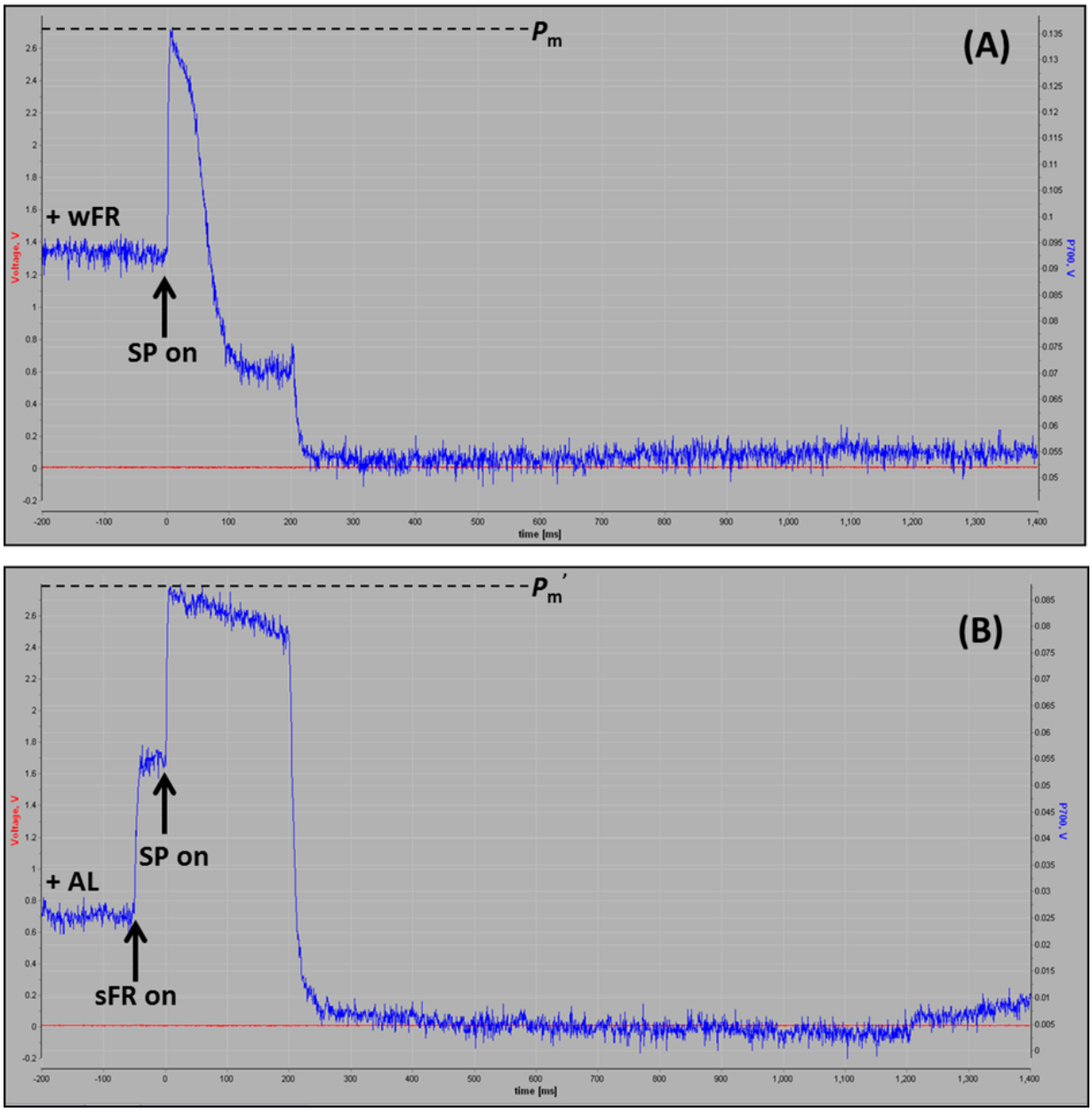

Figure 2. S 2 An example of the determination of energy conversion efficiency in PSI by Saturating Pulse method of Dual-PAM (Klughammer & Schreiber, 2008)

(A) The maximum amount of photo- oxidisable P700 obtained through P_m determination with continuous far-red light (wFR) background. **(B)** Determination of the maximum $P700^+$ (P_m') under actinic white light (AL, 1000 µmol photons m^{-2} s^{-1}). The signal relaxed to a baseline corresponding to fully reduced P700.

CHAPTER 3

OXYGEN EXCHANGE AND MEHLER REACTION IN LEAVES OF C_3 AND C_4 PLANTS

ABSTRACT

Alternative electron fluxes such as the cyclic electron flux around photosystem I (PSI) (CEF) and Mehler reaction are essential for efficient photosynthesis because they generate additional ATP and protect both photosystems against photoinhibition. The capacity for Mehler reaction can be estimated by measuring O_2 exchange rate under varying irradiance and CO_2 concentration. In this study, mass spectrometric measurements of O_2 exchange were made using leaves of the representative species of C_3 and C_4 grasses, gymnosperm, liverwort and fern grown under natural light (control) and shade. For all control plants, O_2 uptake was similar when measured in the dark or under high light and high CO_2, which suggests little potential for Mehler reaction, and that O_2 uptake was mainly due to photorespiration or mitochondrial respiration. For shade-grown C_4 plants, O_2 uptake measured under high irradiance was significantly higher than in the dark, suggesting that Mehler reaction may contribute 20-50% of the maximum electron flow under low light.

Key words: C_4 photosynthesis, chlorophyll fluorescence, electron transport rate, Mehler reaction, oxygen exchange rate, photosystem, respiration.

3.1. INTRODUCTION

Photosynthetic electron transport in the thylakoid membrane is highly regulated to cope with fluctuating light intensity and variable demand for ATP and NADPH. Processes such as the Calvin-Benson cycle, photorespiration, nitrate assimilation and sulphate assimilation constitute additional electron sinks using NADPH, while excess light energy will result in the accumulation of NADPH. If the supply of the reducing equivalents in the chloroplasts exceeds what is consumed by these major electron sinks, photoinhibition can occur which involves damage to PSII in the thylakoid membranes (Asada, 1999; Miyake & Okamura, 2003).

To minimize photoinhibition, plant chloroplasts dissipate excess photon energy as heat, a protective mechanism called non-photochemical quenching (NPQ) of chlorophyll (Chl) fluorescence (Demmig-Adams & Adams, 1996; Müller *et al.,* 2001; Niyogi, 1999; Niyogi *et al.,* 1998). The induction of NPQ requires pH gradient (ΔpH) across the thylakoid membranes and two pathways are proposed for these inductions which also serve as alternative electron sinks. The first pathway is known as the Mehler reaction, which utilises an O_2-dependent electron flow within the chloroplasts (Asada, 1999). This process contributes to ΔpH across the thylakoid membranes and no ATP is consumed (Shikanai *et al.,* 1998).The second proposed pathway is cyclic electron flow around PSI (CEF) (Gerst, 1995; Heber & Walker, 1992; Makino *et al.,* 2002). CEF is key to photo-protection and essential for increasing the ATP/NADPH ratio. A related previous study focussed on the role of CEF, while this study focusses on the role of the Mehler reaction in C_3 and C_4 leaves.

The Mehler reaction is the electron flow from water via PSII, cyt b_6f and PSI to molecular oxygen. Since the redox potentials of the electron acceptors on the acceptor side of the PSI complex are sufficiently low to reduce O_2, electron flow to O_2 occurs, particularly when $NADP^+$ is not available. This results in the formation of reactive oxygen species (ROS), such as O_2^- and H_2O_2 (Asada, 1999). Superoxide dismutase and ascorbate peroxidase scavenge O_2^- and H_2O_2 and NADPH is used to regenerate ascorbate. Summing up these reactions, electrons are transferred from water to H_2O_2 to form water. Thus, this reaction acts as a large electron sink (Asada, 2000).

The Mehler reaction may also contribute to production of additional ATP because the Q-cycle is active in photosynthesis and $4H^+$ per ATP are required in ATP synthase (Cramer *et al.,* 2002; Rumberg *et al.,* 2013). In C_3 plants, a ratio of 3ATP/2NADPH is needed to meet the

requirements for carbon reduction via the reductive pentose-phosphate cycle, generated in linear electron transport. Extra electron transport is required only to create and maintain the regulatory proton gradient. Its steady-state rate must be low, because it only has to compensate for slow proton leakage through the thylakoid membrane (Hormann *et al.*, 1994). In addition to the requirement of 3ATP/2NADPH per CO_2 fixed in the C_3 cycle, C_4 plants require an additional 2 ATP per CO_2 for the regeneration of phosphoenolpyruvate in the mesophyll during the C_4 cycle. Additional energy is also consumed during the leakage of CO_2 out of the bundle sheath, and the leakiness fraction may vary between species and environmental conditions (von Caemmerer, 2000; Furbank *et al.*, 1990; Henderson *et al.*, 1992). If this ATP is provided by electron transport supported by the Mehler reaction, this would make a considerable contribution to O_2 uptake and PSII activity in the light.

To elucidate the physiological significance of Mehler reaction, quantitative analysis and precise evaluation of the O_2 exchange *in vivo* are important. However, the Mehler reaction is difficult to measure directly. It is commonly estimated from measurements of chlorophyll fluorescence and net CO_2 or O_2 exchange. Since it was previously demonstrated that O_2 uptakes from photorespiration, mitochondrial respiration and Mehler reaction have different isotope fractionation factors (Guy *et al.*, 2016), it is now possible to quantify the O_2 exchange rates by membrane inlet mass spectrometry (MIMS) which uses $^{16}O/^{18}O$ isotopes to monitor O_2 exchange rates.

Using the same set-up, Siebke *et al.* (2003) compared O_2 exchange characteristics between C_4 species under different conditions. Their study investigated the role of O_2 as an electron acceptor during C_4 photosynthesis using representative species from NAD-ME and NADP-ME type grasses measured at different irradiances and leaf temperatures. Their results suggested that the significant amount of O_2 uptake of these species may be associated with the Mehler reaction, and that the Mehler reaction varies with irradiance and O_2 concentration. However, their study did not include C_4 PCK or C_3 species and did not consider the impact of growth irradiance.

In addition to these gaps, the current study also discusses the possibility of direct estimation of both leaf day (light) respiration (R_l) and dark respiration (R_d) rates from the spectrometric $^{16}O_2$ and $^{18}O_2$ exchange at high irradiances and in the dark, respectively. Leaf day respiration is the rate of non-photorespiratory CO_2 evolution in the light (Azcón-Bieto *et al.*, 1981) which is an important parameter in modelling net rate of photosynthesis. Measurement of R_l is also important to assess its magnitude as an electron sink in plants under light stress. It has been

shown that excess NADPH can be transported to mitochondria via shuttle machineries where it is oxidised in metabolic pathways under photoinhibitory conditions (Hoefnagel *et al.,* 1998; Raghavendra & Padmasree, 2003; Scheibe, 2004; van Lis, 2004; Bartoli *et al.,* 2005; Raghavendra, 2003; Yoshida *et al.,* 2006, 2007, 2008; Yoshida *et al.,* 2011).

Measurements of R_d are relatively straight forward, but not R_l *in vivo* because of the CO_2 evolution from photorespiration (**Figure 3.S 1**). Estimations of R_l by gas exchange technique are commonly done using two methods. The first was described by Kok (1948) which analyses the response of photosynthetic rate (A) to light at low intensities and the second method, described by Laisk (1977), analyses the response curves of A to low intercellular CO_2 concentration (C_i) that are obtained at several light intensities. The Laisk method has been widely used as a standard method to estimate R_l (e.g. Atkin *et al.,* 2000; Brooks & Farquhar, 1985; Flexas *et al.,* 2007; Peisker & Apel, 2001; Priault *et al.,* 2006; von Caemmerer *et al.,* 1994). However, this method cannot be applied in C_4 plants because the CO_2 concentrating mechanism (CCM) leads to a high CO_2 concentration at Rubisco active sites in bundle sheath cells (BSC) even at low C_i. Hence, higher irradiances are required to obtain linear A–C_i relationships, yielding high values of A at low C_i and giving negative R_l values which is very unlikely. Recently, Yin *et al.* (2011) proposed a new method to estimate R_l indirectly from combined gas exchange and chlorophyll fluorescence measurements across a range of low irradiances which can be applied in both C_3 and C_4 species. This new method, like the Kok method, works best for non-photorespiratory conditions. However, all of these three methods are based on the assumption that R_l varies little with light intensity, which is still subject to debate.

However, R_l cannot be simply predicted from A, and must instead be experimentally determined. Some other methods were proposed recently involving CO_2 labelling to calculate CO_2 evolution rates under photorespiratory and non-respiratory conditions. According to Tcherkez *et al.* (2017), the method that exploits respiratory $^{12}CO_2$ release in a $^{13}CO_2$ atmosphere provides a more 'natural' way to measure R_l because it does not require changing either the CO_2 mole fraction or light. Although CO_2 exchange represents the prevalent way in which leaf respiration is considered in the current literature, respiration is also an exchange of oxygen. Oxygen fluxes can also be specifically monitored using $^{16}O/^{18}O$ isotopes which requires mass spectrometry such as MIMS (Maxwell *et al.,* 1998; Peltier & Thibault, 1985; Siebke *et al.,* 2003).

In the current study, we used the MIMS setup to measure the rates of O_2 uptake, O_2 evolution and CO_2 uptake in the dark and in high irradiance with very high CO_2 partial pressures and at the compensation point. We compared C_3 and C_4 grasses grown under high light (control) and low light (shade) conditions, as well as control grown representative species of gymnosperm, liverwort and fern. Our overall aim was to investigate the role of Mehler reaction and respiration in plants with different functional groups.

3.2. MATERIALS AND METHODS

3.2.1 Plant culture

From the Paniceae grass tribe, representative species of C_3 (*Panicum bisulcatum*); C_4 NADP-ME subtype (*Panicum antidotale*); C_4 NAD-ME subtype (*Panicum miliaceum*); and C_4 PCK subtype (*Megathyrsus maximus*) were grown in vermiculite in a naturally lit greenhouse at the Australian National University. *Zea mays* was also used as a model C_4 NADP-ME species. The greenhouse temperature was maintained at 28/24^{o}C for day/night via an in-built glasshouse temperature control system. Within the greenhouse, a steel structure was placed and covered with shade cloth. The average ambient photosynthetic photon flux densities (PPFD) and temperature during the mid-day were 800 and 300 µmol photons m^{-2} s^{-1} and 30 ^{o}C and 29 ^{o}C, respectively for control and shade treatments. Plants were watered regularly and fertilized with Osmocote® (Scotts Australia). Leaves were harvested from 4–5 week-old plants. Representative species of gymnosperms (*Ginkgo biloba* and *Wollemi nobilis*), liverwort (*Marchantia polymorpha*), fern (*Polypodium* sp.) and C_3 (spinach) were grown under full sunlight (control conditions), and were also used for measurements.

3.2.2 Membrane inlet mass spectrometry

Gas exchange was measured in a closed cuvette coupled to a membrane inlet mass spectrometer (MIMS) as described by Maxwell *et al.* (1998) (**Figure 3.S 2**). Leaf discs (1.89 cm^2 area) were punched from the leaf and immediately placed within the chamber together with the wet filter paper supported on a mesh of equal area. The cuvette was first calibrated for oxygen and then flushed with nitrogen gas. Then, a known volume of CO_2 was added to create an atmosphere of approximately 4% CO_2 within the chamber; $^{18}O_2$ was injected to give an atmosphere of 18 – 21% O_2 and the signals were allowed to stabilise for 10 minutes. Gas consumption and leakage from the cuvette were negligible. The chamber temperature was maintained at 28^{o}C.

For steady state measurements, leaf discs were illuminated with actinic light at an irradiance of 2000 µmol photons m^{-2} s^{-1}. Measurements began at high CO_2 concentration and proceeded until the CO_2 reached the compensation point (Γ). Then the light was turned off and dark rates were measured (**Figure 3.S 3**). This chamber has no fan and therefore a high boundary layer resistance surrounds the leaf disc. This means that unusually high CO_2 pressure is required to saturate O_2 exchange and CO_2 assimilation rates (Ruuska *et al.*, 2000).

To perform light-response curves, each leaf disc was light-adapted (1000 µmol photons m^{-2} s^{-1}) for at least 10 minutes with actinic light to reach steady-state photosynthesis before measurements of light response curves. Light-adapted photosynthetic parameters were recorded after 8 to 10 min exposure to each irradiance (50, 100, 200, 300, 400, 500, 750, 1000, 1500 and 2000 µmol photons m^{-2} s^{-1}) and when the rate of gross oxygen evolution was stable.

3.2.3 Definitions

In the present study, LEF_{O2} is the gross oxygen evolution rate during illumination recorded by MIMS multiplied by four (since four electrons are released for each oxygen molecule evolved).

At high pCO_2, rates of gross O_2 evolution reflect mainly photosynthesis and residual photorespiration; rates of net CO_2 uptake reflect photosynthetic uptake and respiratory and photorespiratory evolution; and rates of gross O_2 uptake reflect mainly respiration, Mehler reaction and residual photorespiration. At Γ, O_2 uptake rates reflect mainly respiration and photorespiration.

3.2.4 Calculation of assimilation quotient (*AQ*), rates of Rubisco carboxylation (V_c) and oxygenation (V_o), and Mehler reaction (*Me*)

The assimilation quotient (*AQ*) was taken as the ratio of the net CO_2 uptake to net O_2 evolution.

Rubisco oxygenase activity is a major component of the leaf's oxygen uptake processes. One mol of O_2 is consumed per mol of RuBP oxygenated and a further ½ mol of O_2 is consumed in the photorespiratory carbon oxidation (PCO) cycle by glycolate oxidase in the peroxisomes (Badger, 1985). In these calculations, no O_2 uptake was assumed at PSI via the Mehler reaction and it was assumed that the respiratory O_2 uptake by mitochondria in the light (R_l) was half of the rate of respiratory O_2 uptake in the dark (R_d). Modifying the equation from Renou *et al.* (1990) gives:

$$Vo = \frac{2}{3}\,(^{18}O_2\ uptake\ in\ light) - (^{18}O_2\ uptake\ in\ dark/2) \qquad (3.1)$$

$$Vc = (net\ CO_2\ uptake\ in\ light) + \frac{1}{3}\,(^{18}O_2\ uptake\ in\ light) + \frac{2}{3}\,(^{18}O_2\ uptake\ in\ dark/2) \qquad (3.2)$$

The capacity of Mehler reaction (*Me*) was then calculated using the equation from Biehler & Fock (1996):

$$Me = (^{18}O_2\ uptake\ in\ light) - (Vo + \frac{Rd}{2}) \quad (3.3)$$

assuming that the rate of CO_2 evolution equals the rate of O_2 uptake.

These three parameters were also calculated under Γ using the $^{18}O_2$ uptake rate at this condition.

3.2.5 Data analysis

For each variable, four replicates (independent samples) were obtained for the two light treatments. The results were subjected to analysis of variance and the means were compared by the Tukey test at 5% probability.

3.3 RESULTS

3.3.1 Light dependence of oxygen exchange

At high pCO_2, rates of gross O_2 evolution and net CO_2 uptake were constant over a range of saturating pCO_2, after which they declined until Γ was reached (**Figure 3.S 3**). Net O_2 evolution roughly equalled net CO_2 exchange. At Γ, gross O_2 evolution roughly equalled gross O_2 uptake (**Figure 3.S 3**; **Tables 3.S 1** and **3.S 2).** Given that measurements at high pCO_2 and Γ represent steady state values, we focused on exploring results at these two points. Hence, O_2 and CO_2 exchanges were calculated at high pCO_2, Γ and different irradiances for all species grown under high-light (control) and for shade grown C_3 and C_4 grasses (**Figure 3. 1**; **Tables 3.S 1** and **3.S 2**). At high pCO_2, gross O_2 evolution rates increased steeply with irradiance in control C_3 and C_4 grasses, and increased slightly in gymnosperms, fern and liverwort, saturating at ~750 µmol photons m^{-2} s^{-1} (**Figure 3. 1A**; **Tables 3. 1**; **3.S 1** and **3.S 2).** At high irradiance, the C_3 grass had the highest gross O_2 evolution rate among all species. Among the C_4 grasses, NADP-ME and PCK grasses had similar gross O_2 evolution rates while the NAD-ME grass had the lowest rate (**Figure 3. 1A**; **Tables 3. 1** and **3.S 1**). The gymnosperms, fern and liverwort species had lower gross O_2 evolution rates at high irradiance compared to the grasses (**Figure 3. 1A**; **Tables 3. 1**; **3.S 1** and **3.S 2**). At high pCO_2, rates of gross O_2 uptake increased with irradiance only slightly in control species except for maize which showed a decreasing trend (**Figure 3. 1B**; **Tables 3. 1** and **3.S 1**). At Γ, gross O_2 evolution rate increased with increasing irradiance mostly in control C_3 grass, followed by the gymnosperms and liverwort. Lowest rates of gross O_2 evolution at Γ were observed in all control C_4 grasses and the fern species (**Figure 3. 1C**; **Tables 3. 1**; **3.S 1** and **3.S 2**).

Oxygen uptake rates are shown in detail for the four control and shade-grown Panicea grasses (**Figures 3. 2A** to **3. 2H**; **Table 3.S 1**). At Γ, O_2 uptake rates were significantly lower in shade-grown grasses at all irradiances except for the PCK grass (**Figures 3. 2C** to **3. 2G**; **Tables 3. 1** and **3.S 1**). The shade-grown C_3 grass showed the highest decrease (71% at high irradiance) in O_2 uptake rate at Γ relative to the control (**Figure 3. 2E**; **Tables 3. 1** and **3.S 1**), while NADP-ME grass (**Figure 3. 2H**; **Tables 3. 1** and **3.S 1**) and NAD-ME grass (**Figure 3. 2F**; **Tables 3. 1** and **3.S 1**) decreased by 30-60% at high irradiance. O_2 uptake rate was not affected by measurement irradiance in either control or shade-grown PCK grass (**Figure 3. 2C**; **Tables 3. 1** and **3.S 1**). At Γ, gross O_2 uptake and gross O_2 evolution were also roughly equal in control and shade-grown species. The rates were generally higher in C_3 grass and gymnosperms than in other species at high irradiance (**Tables 3. 1**; **3.S 1** and **3.S 2**).

At high pCO_2, there were no significant differences between the rate of gross O_2 uptake at high light and dark respiratory O_2 uptake in control species (**Figure 3. 3A**; **Tables 3. 1** and **3.S 1**). In contrast, shade-grown C_4 species had significantly higher rates of gross O_2 uptake at high light compared to the dark (**Figure 3. 3B**; **Tables 3. 1** and **3.S 1**). In addition, gross O_2 uptake at Γ was always greater than at high pCO_2 in control and shade plants, except for shaded NAD-ME and NADP-ME grasses (**Figure 3. 3**; **Tables 3. 1**; **3.S 1** and **3.S 2**).

O_2 uptake of shade-grown C_3 grass at high pCO_2 was ~18% of gross O_2 evolution measured under high irradiance which is lower compared to the control. Shade-grown C_4 grasses had O_2 uptake at high pCO_2 ~40-50% of gross O_2 evolution which is higher compared to the control (**Tables 3.S 1** and **3.S 2**). In *Wollemi nobilis*, O_2 uptake was ~40% of gross O_2 evolution. For control C_3 grass, C_4 species and *Ginkgo biloba*, O_2 uptake was ~10-20% of gross O_2 evolution. In liverwort and fern species, O_2 uptake at high pCO_2 was ~30% of gross O_2 evolution. These ratios did not vary greatly with irradiance above 400 µmol photons m^{-2} s^{-1} (**Tables 3. 1**; **3.S 1** and **3.S 2**)..

3.3.2 Estimates of V_o, V_c, V_o/V_c, *Me* and *AQ* under high pCO_2

At high pCO_2, all control species showed slightly increasing trends in V_o under increasing irradiance except for maize which reached negative rates starting from 1000 µmol photons m^{-2} s^{-1} (**Figure 3. 4A**; **Table 3. 1**). However, no significant differences were observed in rates at each irradiance step. Highest V_o were observed in *Wollemi nobilis* and the C_3 grass followed by C_4 grasses, liverwort, ginkgo and maize (**Figure 3. 4A**; **Table 3. 1**). V_o of shade-grown C_4 species were slightly higher than in the control, but also showed no significant differences at each irradiance step. Shade-grown C_3 grass had lower V_o compared to control with 73% decrease in rate under high irradiances (**Figure 3. 4B**; **Table 3. 1**).

V_c increased in response to irradiance in all species except for liverwort and fern (**Figure 3. 4C**; **Table 3. 1**). Highest V_c in control species were observed among C_4 followed by C_3 and the two gymnosperm species (**Figure 3. 4C**; **Table 3. 1**). Lower V_c was observed in all shade-grown species relative to the control treatment, wherein NADP-ME grass had the greatest decrease in rate (-72%) followed by PCK grass (-54%), NAD-ME grass (-31%), and C_3 grass (-30%). Maize was the least affected by shade with only 16% decrease in V_c measured under high irradiance (**Figure 3. 4D**; **Table 3. 1**).

The ratios of V_o/V_c in control plants were higher in fern, *Wollemi nobilis*, liverwort and C_3 species compared to the C_4 species and ginkgo which may reflect the amount of Rubisco in

these species (**Figure 3. 4E**; **Table 3. 1**). This ratio increased in all shade-grown species except for the C_3 grass which showed a ~60% decrease (**Figure 3. 4F**).

The capacity for Mehler reaction under high pCO_2 (*Me*) was calculated by subtracting V_o and R_l from the O_2 uptake under high-light and high pCO_2, assuming that R_l is $R_d/2$. This equation gave roughly stable *Me* under increasing irradiance in all control and shade-grown species (**Figures 3. 4G** to **3. 4H**; **Table 3. 1**). Highest *Me* rates were observed in control C_3 grass, *Wollemi nobilis* followed by control C_4 grasses, liverwort, fern and ginkgo. Negative rates were observed in maize under high irradiances suggesting a very low or negligible capacity of *Me* in this species (**Figure 3. 4G**; **Table 3. 1**). Calculated *Me* rates increased in all shade-grown C_4 species relative to the to control, except for the C_3 grass which had ~70% lower Me (**Figure 3. 4H**; **Table 3. 1**).

At high pCO_2, the *AQ* showed a decreasing trend under increasing irradiance for both the control and shade-grown species (**Figures 3. 5A** to **3. 5F**; **Tables 3. 1**; **3.S 1** and **3.S 2)**. Higher *AQ* was observed in shade-grown species in comparison with the control (**Figures 3. 5A** to **3. 5E**; **Tables 3. 1**; **3.S 1** and **3.S 2)**. The *AQ* was verified as a non-destructive measure of *in vivo* NO_3^- assimilation over 50 years ago for algae (Myers, 1949) and over a decade ago for higher plants by using barley mutants deficient in NO_3^- reductase activity (Bloom *et al.*, 1989). Transfer of electrons to NO_3^- and NO_2^- during photoassimilation increases O_2 evolution from the light-dependent reactions of photosynthesis, while CO_2 consumption by the Calvin cycle continues at similar rates (Bloom *et al.*, 2002). Therefore, plants that are photoassimilating NO_3- exhibit a lower *AQ*. According to Bloom *et al.* (1989); and Bloom *et al.* (2002), the *AQ* may also respond to other processes, principally photorespiration and Mehler reaction.

3.3.3 Estimates of V_o, V_c, V_o/V_c, and *Me* at Γ

Rates of Rubisco oxygenation and carboxylation were also calculated at Γ (V_o* and V_c*). It was observed that V_o* of all species are higher compared to V_o suggesting the occurrence of high photorespiration under Γ even in C_4 species. Higher V_o* with increasing trend were observed in control C_3 grass and in ginkgo followed by *Wollemi nobilis* and liverwort. Lower rates were observed in all C_4 species and fern (**Figure 3. 6A**). Significant decrease in V_o* was observed in all shade-grown plants with C_3 grass having the greatest decrease in rate (-75%) (**Figure 3. 6B**; **Table 3. 1**). The calculated V_c* were very low for both control and shade-grown species measured under increasing irradiance in comparison to V_c (**Figures 3. 6C** to **3. 6D**; **Table 3. 1**).

It was also observed that ratios of V_o*/V_c* in all species were higher compared to V_o/V_c ratios suggesting the higher rate of Rubisco oxygenation under Γ. Highest ratio with increasing trend was observed in control C_3 grass and in the two gymnosperm species under increasing irradiances. Lowest ratio was observed in all control C_4 species and in fern (**Figure 3. 6E**; **Table 3. 1**). No significant difference form the controls were observed in the ratio of V_o*/V_c* in all shade-grown species **Figure 3. 6F**; **Table 3. 1**).

The capacity for Mehler reaction under Γ (*Me**) was also calculated using O_2 uptake rate and V_o* taken under this condition. Highest rates were observed in control C_3 grass and ginkgo, followed by *Wollemi nobilis* and liverwort. Lowest rates were observed in all control C_4 species including fern (**Figure 3. 6G**; **Table 3. 1**). Shade significantly lowered *Me** in all species wherein C_3 grass had the greatest decrease in rate (-75%) (**Figure 3. 6H**; **Table 3. 1**). The *Me** for control and shade-grown species were higher compared to Me suggesting that the calculated rates under Γ are mainly from photorespiration.

3.4 DISCUSSIONS

3.4.1 O_2 exchange of control-grown C_3 and C_4 grasses at high pCO_2

In C_3 species, the occurrence of the Mehler reaction was previously studied by Ruuska *et al.* (2000) in transgenic tobacco lines with an antisense gene directed against the mRNA of the small subunit of Rubisco. It was expected that a reduced activity of the Calvin-Benson cycle will promote the Mehler reaction. However, in the transgenic tobacco with 10% Rubisco of the wild-type level, gross O_2 uptake at high light and high pCO_2 (970 μmol photons m^{-2} s^{-1}, 1–2% CO_2 and 20% O_2) was roughly similar to that in the dark which is the same as the results obtained in the current study (**Figure 3. 3**; **Tables 3. 1** and **3.S 1**). This result was interpreted as a low or virtually no potential for the Mehler reaction and that the O_2 uptake was mainly due to photorespiration at high light and pCO_2. In this study, we also observed that the gross O_2 uptake of control C_3 grass was higher compared to control C_4 plants. This result was similar to previous studies (Canvin *et al.,* 1980; Maroco, 1997; Maroco *et al.,* 1998), suggesting that higher O_2 uptake in C_3 species is mainly due to V_o (**Figure 3. 4A**). However, Mehler reaction still occurs in C_3 species in varying magnitude depending on species, conditions and instruments used, making it difficult to generalize about its occurrence or magnitude. The potential Mehler rate can range from being negligibly small (Laisk *et al.,* 2006; Ruuska *et al.,* 2000) to almost 30% of whole-chain electron transport (**Figures 3. 4G** to **3. 4H**) (Asada, 2000; Badger *et al.,* 2000).

Mitochondrial respiration under light (R_l) can be one of the reasons for the O_2 uptake at high light in photosynthetic cells. Mitochondria provide the cell with TCA cycle carbon skeletons for light-dependent NH_4^+ assimilation in the chloroplast and ATP and NADH for other biosynthetic reactions in the light. Mitochondria were also shown to oxidise excess photosynthetic reducing equivalents during light stress (Raghavendra & Padmasree, 2003). In control-grown C_4 species, O_2 uptake at high pCO_2 was not significantly different between the light and the dark (**Figure 3. 3A**; **Tables 3. 1** and **3.S 1**), suggesting that this can be mainly due to R_l, given that photorespiration in C_4 plants is negligible under very high pCO_2. However, estimation of R_d or R_l using MIMS and stable $^{16}O_2$ and $^{18}O_2$ isotopes is not very conclusive because it is difficult to separate the contributions of other O_2 uptake components. Estimation of R_d from O_2 consumption was also shown to yield conflicting results and have indicated it to be unaffected, inhibited or even stimulated (Avelange *et al.*, 1991; Peltier & Thibault, 1985; Turpin *et al.*, 1988; Xue *et al.*, 1996). Tcherkez *et al.* (2017) suggested that the best way to measure R_d or R_l is to monitor the $^{12}CO_2/^{13}CO_2$ disequilibrium in an enclosed

chamber. Using the same experimental set-up, Siebke *et al.* (2003) also measured O_2 uptake in C_4 grasses. However, their result showed that gross O_2 uptake at high light and high pCO_2 was between two and seven times greater than O_2 uptake in the dark. But they still suggested that this is from either elevated R_l or a significant contribution of the Mehler reaction. Chlororespiration is another oxygen-related process in thylakoids which is the electron transport from the stromal reductant NADPH to oxygen via the plastoquinone (PQ) pool (McDonald *et al.*, 2011; Peltier & Cournac, 2002; Rumeau *et al.*, 2007). This mechanism is assumed to be mediated the NDH complex and plastid terminal oxidase (PTOX). Several studies have shown that PTOX and thylakoidal NDH complex were upregulated in leaves incubated under high light intensity (Casano *et al.*, 2000; Quiles, 2006).

However, if it will be argued that the O_2 uptake at high light in C_4 species was mainly due to Mehler reaction, this could be linked to the photosynthetic electron transport rate and could be of physiological relevance in balancing the ATP to NADPH requirements of C_4 mesophyll chloroplasts (Furbank *et al.*, 1990; Furbank *et al.*, 1983; Laisk & Edwards, 1998). It was observed that the light-stimulated O_2 uptake in control C_4 species was around 6-18% of the maximum O_2 evolution (**Table 3.S 1**). It was suggested by von Caemmerer & Furbank (1999) that the ATP consumption of the C_4 cycle is at least 40% of the total ATP consumption. Our results suggest that electron transport to O_2 at 6-18% of total electron transport could meet part of this requirement.

3.4.2 O_2 exchange of gymnosperms, liverwort and fern at high pCO_2

Gross O_2 uptake at high pCO_2 measured at high light was also not significantly different to dark O_2 uptake in leaves of the representative gymnosperm, liverwort and fern species (**Figure 3. 3A**). This result does not agree with the findings of Shirao *et al.* (2013) where they showed that rates of O_2 uptake also measured by MIMS in the absence of photorespiration were significantly promoted by illumination in leaves of gymnosperms and ferns. They also showed that light-stimulated O_2 uptake was around 10% of the maximum O_2 evolution in gymnosperms and only 1% in angiosperms. The same percentage was obtained in the present study with *Ginkgo biloba* (**Tables 3. 1** and **3.S 1**). However, *Wollemi nobilis*, which is a conifer, had O_2 uptake of around 40% of O_2 evolution. Liverwort and fern had roughly the same O_2 uptake to O_2 evolution ratio which is approximately 30% (**Tables 3. 1** and **3.S 1**). These results also suggest that this is mainly due to R_l or to V_o because of the absence of CCM in these species. However, light dependence of O_2 uptake other than R_l and photorespiration should also be considered such as the mechanisms involving flavodiiron (FLV) proteins or

chloroprespiration. These also drive O_2-dependent alternative electron flow in these basal land plants and protects PSI from oxidative damages (Ducruet *et al.*,2005; Gerotto *et al.*, 2016; Hanawa *et al.*, 2017; Shimakawa *et al.*, 2017; Shirao *et al.*, 2013; Streb *et al.*, 2005; Takagi *et al.*, 2017).

3.4.3 O_2 exchange of shade-grown grasses at high pCO_2

A decrease of 67% in O_2 uptake rate under high light and high pCO_2 was observed in shade-grown C_3 grass from the control (**Figure 3. 2A**; **Tables 3. 1** and **3.S 1**). Shade-grown C_3 grass also showed no significant difference of O_2 uptake at high pCO_2 measured under high light or in the dark (**Figure 3. 3B**; **Tables 3. 1** and **3.S 1**). These results suggest that shade might have affected the mechanisms involved in O_2 uptake in the leaf of this C_3 grass species by down-regulation of proteins needed for O_2 uptake such as Rubisco as shown by the decrease in V_o (**Figure 3. 4B)**. It was reported by Evans (1988) that large reductions in Rubisco content and activity (>55%) was observed in several C_3 species when grown under shade.

There was also no significant decrease in the ratio of O_2 uptake to O_2 evolution under high pCO_2 and high light in control-grown C_3 grass, suggesting that the C_3 grass has a good acclimation property under shade and might have very low operation of Mehler reaction (**Figure 3. 4H**).

Shade-grown C_4 plants only slightly increased O_2 uptake at high pCO_2 measured under high light compared to control but the difference was not significant (**Figure 3. 3B**; **Tables 3. 1** and **3.S 1**). However, O_2 uptake of shade-grown C_4 plants under high light was significantly higher compared to dark O_2 uptake suggesting enhanced operation of Mehler reaction up to 20-50% of the maximum electron flow (**Figures 3. 4B** and **3. 4H**; **Tables 3. 1**and **3.S 1**).

It was demonstrated by Sonawane *et al.* (2018) that shade compromised the carbon-concentrating mechanism (CCM) efficiency and photosynthetic quantum yield in C_4 grasses with different biochemical subtypes by affecting the activity of the C_3 cycle (e.g. Rubisco) more significantly than that of the C_4 cycle (e.g. PEPC). Since both the C_3 and C_4 cycles are compromised under shade, electron flow in the thylakoid will be limited at the reducing side of PSI upon exposure to high irradiance, owing to inactivation of ferredoxin-NADP reductase (FNR) and enzymes of the Calvin cycle. Following illumination, the limiting site might shift from the acceptor to the donor side of PSI where the electron flow to PSI will be suppressed by increasing the counter-pressure to proton release during PQH_2 oxidation at cyt b_6f (Harbinson & Hedley, 1993; Laisk *et al.*, 2005; Tsuyama & Kobayashi, 2009). Thus, electron

drain from PSI in the Mehler reaction is important in shade-grown plants for the rapid P700/PC oxidation. On the other hand, Shirao *et al.* (2013) suggested that PTOX also plays important role in the rapid P700/PC oxidation simply by draining electrons from the PQ pool without generating ΔpH across the membrane unlike the Mehler reaction. These processes may serve more as photo-protective mechanisms against photo-oxidative stress to the photosynthetic machinery under high irradiance than as support for additional ATP production in shade-grown plants.

3.4.4 O_2 exchange at the CO_2 compensation point

At the CO_2 compensation point (Γ), almost all of the electron flux in the photosynthetic electron transport system is going to photorespiration (Hanawa *et al.*, 2017; Sejima *et al.*, 2016). Under this condition, photosynthetic organisms have electron sinks alternative to CO_2 assimilation, which contribute to the consumption of excess photon energy and thereby suppress the accumulation of electrons in the photosynthetic electron transport system. At least two large electron sinks, FLV-dependent and photorespiration were found to operate in photosynthetic organisms which facilitate O_2 uptake. Photosynthetic organisms in aquatic environments prefer the FLV-dependent electron sink to photorespiration, while higher plants use mainly photorespiration (Shimakawa *et al.*, 2017). Many researchers reported that photorespiration functions as electron sink under steady state at Γ (Badger *et al.*, 2000; Hanawa *et al.*, 2017; Kozaki & Takeba, 1996; Lovelock & Winter, 1996; Takahashi *et al.*, 2007). It was also found that FLV-dependent alternative electron flow decreased its activity as photorespiration started to function (Shimakawa *et al.*, 2017).

Photorespiration has been estimated by Hanawa *et al.* (2017) in representative species of C_3, C_4, gymnosperms and liverworts at Γ using chlorophyll fluorescence and O_2-exchange measurements. They found that photorespiration in gymnosperms was the main driver of photosynthetic linear electron flow, and alternative electron flow activity other than photorespiration was negligible (84% capacity for photorespiration). They also examined *Ginkgo biloba* which showed alternative electron flows other than photorespiration only played minor role. As in gymnosperms, high activities of photorespiration were also found in C_3 species in their study. In *Phlebodium aureum*, a fern species closest to the species used in our present study, their calculated electron fluxes in both photosynthesis and photorespiration accounted for approximately 90% of electron flux in PSII, which indicated that photorespiration mainly drove photosynthetic linear electron flow, whereas alternative electron flow activity other than photorespiration accounted for approximately 10% of

electron-sink capacity. Liverwort *Marchantia polymorpha* was also examined which showed that there was a 73% capacity for photorespiration which was roughly the same with C_4 species, suggesting that alternative electron flows other than photorespiration appear to function at Γ.

These observations might explain why O_2 uptake at Γ was always greater than O_2 uptake at high pCO_2 in all control plants (**Figure 3. 3A**; **Tables 3. 1**; **3.S 1** and **3.S 2**), suggesting that photorespiration forms a greater fraction of total O_2 uptake at Γ (**Figure 3. 6A**). However, in C_4 species Siebke *et al.* (2003) observed that the difference in O_2 uptake between high pCO_2 and Γ is smaller than their calculated photorespiratory O_2 uptake. They noted that going from high pCO_2 to Γ, O_2 uptake does not increase simply by an amount equivalent to photorespiration but rather complex adjustments in mitochondrial respiration and Mehler reaction also take place. However, a varying result was obtained from shade-grown C_4 species where NAP-ME grass, NAD-ME grass and maize had lower O_2 uptake at Γ than O_2 uptake at high pCO_2 (**Figure 3. 3B**; **Tables 3. 1**and **3.S 1**), suggesting that photorespiratory O_2 uptake was the main reason for the total O_2 uptake at Γ in these shade-grown plants (**Figure 3. 6B**). It is also worth noting that at Γ, the O_2 concentration in the bundle sheath of C_4 leaves is at least equal to ambient O_2 concentration and hence photorespiration is always likely, especially at low light and low CCM activity, due to increased O_2/CO_2 ratio in the bundle sheath.

Several studies also suggested that the rate of O_2 consumption at Γ is due largely to Rubisco content and activity (Kiirats, 2002; von Caemmerer & Quick, 2006). This might explain why O_2 uptake of C_4 species at Γ is less than that observed in other species (except for fern) probably because C_4 species have lower amounts of Rubisco in their leaves compared to other species examined (**Figures 3. 3A** and **3. 6B**; **Tables 3. 1**; **3.S 1** and **3.S 2**). Decrease in O_2 uptake rates at Γ in shade-grown plants compared to control plants may also be due to the decrease in the amount of Rubisco as affected by the growing condition as previously discussed (**Figures 3. 3A** and **3. 6B**; **Tables 3. 1**and **3.S 1**).

3.5 CONCLUSIONS

We examined the capacity for Mehler reaction in several plant species grown under natural light (control) and shade by measuring the O_2 exchange rates using MIMS. We found that O_2 uptake of all control C_3 and C_4 species, including the gymnosperms, liverwort and fern measured under high light and high pCO_2 had no significant difference with the dark O_2 uptake (R_d). This suggests that these species have low or virtually no potential for the Mehler reaction and that the O_2 uptake was mainly due to photorespiration. There is also a high probability that the observed O_2 uptake under high light and high pCO_2 was from mitochondrial respiration (R_l) since several studies have shown that mitochondrial activity continues in light, oxidising excess photosynthetic reducing equivalents and providing the cell with TCA cycle carbon skeleton. However, O_2 uptake of shade-grown C_4 plants under high light was significantly higher compared to dark O_2 uptake, suggesting enhanced operation of Mehler reaction or R_l having 20-50% of the maximum electron flow.

Table 3. 1 Statistical summary

Summary of statistical analysis using two-way ANOVA for the effects of shade and species on various parameters collected for 9 plants grown under natural light (~800 µmol photons m^{-2} s^{-1}) and shaded (~200 µmol photons m^{-2} s^{-1}) conditions. Measurements were made at low light (LL) (200 µmol photons m^{-2} s^{-1}), medium light (ML) (1000 µmol photons m^{-2} s^{-1}) and saturating light (SL) (2000 µmol photons m^{-2} s^{-1}) under the temperature of 28^{o}C.

Parameter	Main effects (P)		Interactions (P)
	Species	Treatment	Species x Treatment
V_o at LL (µmol e^- m^{-2} s^{-1})	0.004	0.011	0.056
V_o at ML (µmol e^- m^{-2} s^{-1})	0.000	0.006	0.000
V_o at SL (µmol e^- m^{-2} s^{-1})	0.008	0.004	0.000
V_o * at LL (µmol e^- m^{-2} s^{-1})	0.000	0.000	0.000
V_o * at ML (µmol e^- m^{-2} s^{-1})	0.000	0.000	0.000
V_o * at SL (µmol e^- m^{-2} s^{-1})	0.000	0.000	0.000
V_c at LL (µmol e^- m^{-2} s^{-1})	0.000	0.000	0.000
V_c at ML (µmol e^- m^{-2} s^{-1})	0.000	0.000	0.000
V_c at SL (µmol e^- m^{-2} s^{-1})	0.000	0.000	0.045
V_c * at LL (µmol e^- m^{-2} s^{-1})	0.000	0.000	0.001
V_c * at ML (µmol e^- m^{-2} s^{-1})	0.000	0.000	0.000
V_c * at SL (µmol e^- m^{-2} s^{-1})	0.000	0.000	0.000
Me at LL (µmol e^- m^{-2} s^{-1})	0.004	0.011	0.057
Me at ML (µmol e^- m^{-2} s^{-1})	0.000	0.006	0.000
Me at SL (µmol e^- m^{-2} s^{-1})	0.008	0.004	0.000
*Me** at LL (µmol e^- m^{-2} s^{-1})	0.000	0.000	0.000
*Me** at ML (µmol e^- m^{-2} s^{-1})	0.000	0.000	0.000
*Me** at SL (µmol e^- m^{-2} s^{-1})	0.000	0.000	0.000
V_o/V_c at LL	0.157	0.000	0.544
V_o/V_c at ML	0.000	0.000	0.000
V_o/V_c at SL	0.004	0.000	0.000
V_o*/V_c* at LL	0.000	0.134	0.164
V_o*/V_c* at ML	0.000	0.004	0.038
V_o*/V_c* at SL	0.000	0.002	0.055

CO_2 uptake under high pCO_2 and dark (µmol m^{-2} s^{-1})	0.000	0.000	0.017
O_2 uptake under high pCO_2 and dark (µmol m^{-2} s^{-1})	0.000	0.000	0.362
O_2 uptake at high pCO_2 and LL (µmol m^{-2} s^{-1})	0.000	0.815	0.048
O_2 uptake at high pCO_2 and ML (µmol m^{-2} s^{-1})	0.000	0.133	0.000
O_2 uptake at high pCO_2 and SL (µmol m^{-2} s^{-1})	0.001	0.111	0.000
Gross O_2 evolution at high pCO_2 and LL (µmol m^{-2} s^{-1})	0.000	0.000	0.098
Gross O_2 evolution at high pCO_2 and ML (µmol m^{-2} s^{-1})	0.000	0.000	0.014
Gross O_2 evolution at high pCO_2 and SL (µmol m^{-2} s^{-1})	0.000	0.000	0.140
Net O_2 evolution at high pCO_2 and LL (µmol m^{-2} s^{-1}))	0.000	0.000	0.525
Net O_2 evolution at high pCO_2 and ML (µmol m^{-2} s^{-1})	0.000	0.000	0.010
Net O_2 evolution at high pCO_2 and SL (µmol m^{-2} s^{-1})	0.000	0.000	0.232
Net CO_2 uptake at high pCO_2 and LL (µmol m^{-2} s^{-1})	0.004	0.001	0.003
Net CO_2 uptake at high pCO_2 and ML (µmol m^{-2} s^{-1})	0.000	0.000	0.000
Net CO_2 uptake at high pCO_2 and SL (µmol m^{-2} s^{-1})	0.000	0.179	0.179
AQ at LL	0.000	0.004	0.048
AQ at ML	0.000	0.000	0.000
AQ at SL	0.000	0.000	0.001
Gross O_2 evolution at Γ and LL (µmol m^{-2} s^{-1})	0.000	0.000	0.000
Gross O_2 evolution at Γ and ML (µmol m^{-2} s^{-1})	0.000	0.000	0.000
Gross O_2 evolution at Γ and SL (µmol m^{-2} s^{-1})	0.000	0.000	0.000
O_2 uptake at Γ and (µmol m^{-2} s^{-1})	0.000	0.000	0.000
O_2 uptake at Γ and ML (µmol m^{-2} s^{-1})	0.000	0.000	0.000
O_2 uptake at Γ and SL (µmol m^{-2} s^{-1})	0.000	0.000	0.000
O_2 uptake/O_2 evolution at high pCO_2 and LL	0.000	0.004	0.048
O_2 uptake/O_2 evolution at high pCO_2 and ML	0.000	0.000	0.000
O_2 uptake/O_2 evolution at high pCO_2 and SL	0.000	0.000	0.001
O_2 uptake at Γ/O_2 evolution at high pCO_2 at LL	0.000	0.011	0.139
O_2 uptake at Γ/O_2 evolution at high pCO_2 at ML	0.000	0.937	0.037
O_2 uptake at Γ/O_2 evolution at high pCO_2 at SL	0.000	0.746	0.071

Table 3.S 1 Summary of CO_2 and O_2 exchange data of C_3 and C_4 species grown at high light (CONTROL) and SHADE

CO_2 and O_2 exchange data of C_3 and C_4 species grown at high light (CONTROL) and SHADE measured with a mass spectrometer described in **Figure 3.S 2**. Measurements were made at increasing irradiance from 200 to 2000 µmol photons m^{-2} s^{-1} and temperature of 28°C. Values are means ± s.e. (*n* = 4 leaf discs).

Species	Irradiance (µmol photons m^{-2} s^{-1})	Rates in darkness (µmol m^{-2} s^{-1})		Rates at high pCO_2 (µmol m^{-2} s^{-1})					Rates at the compensation point, Γ (µmol m^{-2} s^{-1})		O_2 uptake rate/O_2 evolution at high pCO_2	O_2 uptake at Γ/O_2 evolution at high pCO_2
		CO_2 uptake	O_2 uptake	O_2 uptake	Gross O_2 evolution	Net O_2 evolution	Net CO_2 uptake	*AQ*	Gross O_2 evolution	O_2 uptake		
C_3 *Panicum bisulcatum* (CONTROL)	200	-1.3 ± 0.2	3.9 ± 0.6	3.2 ± 0.7	15.8 ± 0.4	11.8 ± 0.6	10.7 ± 0.6	0.91 ± 0.01	13.4 ± 0.2	12.9 ± 0.2	0.2 ± 0.1	0.8 ± 0
	750	-1 ± 0.2	3.8 ± 0.5	4.4 ± 0.3	32.8 ± 0.6	21.4 ± 2.3	17.5 ± 1.7	0.82 ± 0.01	28.1 ± 0.2	27.6 ± 0.2	0.1 ± 0	0.8 ± 0
	1500	-1.4 ± 0.6	3.7 ± 0.6	6.6 ± 0.8	44.5 ± 1	26 ± 2.6	21.2 ± 2.2	0.81 ± 0.01	34.9 ± 1	33.9 ± 0.5	0.2 ± 0	0.8 ± 0
	2000	-2.2 ± 0.3	3.6 ± 0.7	6.8 ± 1.1	47.2 ± 1.5	29.6 ± 2.3	23.7 ± 2.1	0.8 ± 0.01	36 ± 0.4	34.6 ± 0.1	0.2 ± 0	0.7 ± 0
C_3 *Panicum bisulcatum* (SHADE)	200	-0.4 ± 0.1	1.9 ± 0.3	2.5 ± 0.4	10.1 ± 1	7.8 ± 1.2	6.9 ± 0.6	0.9 ± 0.07	8 ± 0.1	7.6 ± 0.3	0.3 ± 0.1	0.8 ± 0.1
	750	-0.7 ± 0.2	2 ± 0.4	2.9 ± 0.7	17.8 ± 0.9	15 ± 0.4	13.1 ± 0.4	0.87 ± 0.02	10.2 ± 0	10.2 ± 0.2	0.2 ± 0	0.6 ± 0
	1500	-0.7 ± 0.1	2.4 ± 0.3	2.2 ± 0.3	20.3 ± 1.4	18.2 ± 1.3	15.4 ± 0.8	0.85 ± 0.02	10.2 ± 0.1	9.5 ± 0.1	0.1 ± 0	0.5 ± 0
	2000	-0.9 ± 0.1	2.3 ± 0.5	3.1 ± 0.7	20.8 ± 1.3	17.9 ± 1.1	14.3 ± 0.5	0.81 ± 0.04	10.3 ± 0.1	9.3 ± 0.1	0.2 ± 0	0.5 ± 0
NAD-ME *Panicum miliaceum* (CONTROL)	200	-1.7 ± 0.3	3.6 ± 0.6	3.3 ± 0.6	10.7 ± 0.7	7.2 ± 1	7 ± 0.8	1 ± 0.04	6.9 ± 0.6	6.5 ± 0.7	0.3 ± 0.1	0.6 ± 0
	750	-1.6 ± 0.3	3.1 ± 0.3	4.1 ± 0.6	22.3 ± 2.3	18.3 ± 2.1	16.2 ± 1.9	0.87 ± 0.02	9 ± 0.5	7.6 ± 0.3	0.2 ± 0	0.3 ± 0
	1500	-1.6 ± 0.3	3.5 ± 0.5	4.6 ± 1	29.4 ± 3.4	25.3 ± 3.8	20.8 ± 2.6	0.82 ± 0.03	10.9 ± 0.4	10.4 ± 0.6	0.2 ± 0.1	0.3 ± 0
	2000	-2 ± 0.2	3.3 ± 0.5	4.8 ± 1.2	31.5 ± 3.7	27.2 ± 4.1	21.8 ± 2.7	0.8 ± 0.02	11.4 ± 0.3	9.6 ± 0.2	0.2 ± 0.1	0.3 ± 0
NAD-ME *Panicum miliaceum* (SHADE)	200	-0.4 ± 0.1	3.5 ± 0.8	6.1 ± 0.6	8.7 ± 0.4	2.0 ± 0.4	3.8 ± 0.3	1.9 ± 0.13	4.2 ± 0.2	2.9 ± 0.2	0.7 ± 0	0.3 ± 0
	750	-0.8 ± 0.4	3.7 ± 0.6	7.4 ± 1.3	14 ± 1.3	6.6 ± 0.7	11.9 ± 0.9	1.84 ± 0.19	5.5 ± 0.2	4.5 ± 0.1	0.5 ± 0.1	0.3 ± 0
	1500	-0.4 ± 0.2	3.5 ± 0.5	7.9 ± 1.3	15.6 ± 1.3	7.3 ± 0.7	13.2 ± 0.7	1.85 ± 0.19	5.9 ± 0.2	4.9 ± 0.1	0.5 ± 0.1	0.3 ± 0
	2000	-0.8 ± 0	3.7 ± 0.5	7.4 ± 0.9	15.8 ± 1.4	8.5 ± 1	13 ± 1.1	1.55 ± 0.1	7.1 ± 0.4	5.7 ± 0.2	0.5 ± 0	0.4 ± 0

PCK *Megathyrus maximus* (CONTROL)	200	-1.3 ± 0.3	3.1 ± 0.4	2.7 ± 0.3	12.8 ± 0.5	10.1 ± 0.6	9.6 ± 0.4	0.95 ± 0.03	6 ± 0.1	5.7 ± 0.3	0.2 ± 0	0.5 ± 0
	750	-1 ± 0.3	3 ± 0.5	3.2 ± 0.5	26.7 ± 0.9	23.7 ± 1	20.3 ± 0.9	0.85 ± 0.02	7.1 ± 0.3	6 ± 0.3	0.1 ± 0	0.2 ± 0
	1500	-1.8 ± 0.4	3.4 ± 0.2	4.4 ± 1	35.6 ± 1.3	31.3 ± 1.6	28.1 ± 2.4	0.9 ± 0.08	8.4 ± 0.4	7.2 ± 0.5	0.1 ± 0	0.2 ± 0
	2000	-2.1 ± 0.1	3 ± 0.5	5.3 ± 0.5	38.1 ± 1.4	33.1 ± 1.7	26.4 ± 1.3	0.8 ± 0.01	9.5 ± 0.1	8.1 ± 0.4	0.1 ± 0	0.2 ± 0
PCK *Megathyrus maximus* (SHADE)	200	-0.7 ± 0.1	2.6 ± 0.3	3.2 ± 0.3	9 ± 0.9	5.9 ± 1.1	6.4 ± 0.7	1.13 ± 0.07	4.1 ± 0.3	4.8 ± 0.3	0.4 ± 0.1	0.6 ± 0.1
	750	-0.8 ± 0.1	2.8 ± 0.2	3.9 ± 0.4	13.3 ± 1.4	10.4 ± 1.8	10.1 ± 1.5	0.99 ± 0.05	5.2 ± 0	5.7 ± 0.1	0.3 ± 0.1	0.5 ± 0.1
	1500	-0.7 ± 0.2	3 ± 0.5	4.1 ± 0.5	18.3 ± 1.5	14.2 ± 2	13.2 ± 1.6	0.94 ± 0.02	5.9 ± 0.4	7.1 ± 0.5	0.2 ± 0.1	0.4 ± 0.1
	2000	-1.1 ± 0.2	2.4 ± 0.5	5.1 ± 0.4	18.3 ± 1.4	12.9 ± 1.7	11.7 ± 1.3	0.92 ± 0.04	6.4 ± 0.2	6.8 ± 0.2	0.3 ± 0	0.4 ± 0
NADP-ME *Panicum antidotale* (CONTROL)	200	-1.9 ± 0.3	3.9 ± 0.4	3.3 ± 0.4	11.4 ± 0.6	8.1 ± 0.7	8.1 ± 0.5	0.99 ± 0.05	6 ± 0.1	5.8 ± 0.7	0.3 ± 0	0.5 ± 0.1
	750	-2.5 ± 0.6	4.3 ± 0.4	4 ± 0.8	27.5 ± 1.4	23.7 ± 1.4	19.3 ± 1.1	0.83 ± 0.04	7.7 ± 0.2	7.9 ± 0.7	0.2 ± 0	0.3 ± 0
	1500	-2.9 ± 0.6	5.2 ± 0.6	4.7 ± 1.1	38.3 ± 2.5	34.1 ± 3.2	27.6 ± 2.3	0.82 ± 0.04	9.6 ± 0.1	8.7 ± 0.2	0.1 ± 0	0.2 ± 0
	2000	-3.4 ± 0.4	5.2 ± 0.4	4.4 ± 1.2	39.9 ± 4	35 ± 4.3	28.1 ± 3.2	0.83 ± 0.03	11 ± 0.2	9.8 ± 0.3	0.2 ± 0	0.3 ± 0
NADP-ME *Panicum antidotale* (SHADE)	200	-0.3 ± 0.1	1.3 ± 0.1	1.9 ± 0.1	4.4 ± 0.3	2.6 ± 0.4	3.5 ± 0.3	1.41 ± 0.1	2.1 ± 0	1.6 ± 0.1	0.4 ± 0	0.4 ± 0.1
	750	-0.3 ± 0.1	1.6 ± 0.3	2.7 ± 0.2	6.5 ± 0.4	3.8 ± 0.3	5.2 ± 0.3	1.39 ± 0.06	2.7 ± 0.1	2 ± 0.1	0.4 ± 0	0.3 ± 0
	1500	-0.5 ± 0.1	1.7 ± 0.1	3.5 ± 0.3	8.7 ± 1	5.5 ± 0.9	6.7 ± 0.8	1.29 ± 0.12	3.6 ± 0.2	2.6 ± 0.1	0.4 ± 0	0.3 ± 0.1
	2000	-0.4 ± 0.1	2.1 ± 0.1	4.8 ± 0.5	10.7 ± 0.9	6.3 ± 1.2	7.8 ± 1.2	1.2 ± 0.19	3.8 ± 0.3	2.5 ± 0.1	0.5 ± 0.1	0.2 ± 0
NADP-ME *Zea mays* (CONTROL)	200	-1.5 ± 0.4	4.1 ± 0.5	3.9 ± 0.6	10.2 ± 0.3	7.4 ± 0.9	6.6 ± 0.3	0.91 ± 0.08	5.7 ± 0.1	4.9 ± 0.1	0.4 ± 0.1	0.5 ± 0
	750	-1.7 ± 0.3	3.4 ± 0.2	3 ± 0.4	25.7 ± 1.5	25.1 ± 1.8	19.9 ± 1.4	0.79 ± 0.02	7 ± 0.2	5.8 ± 0.2	0.1 ± 0	0.2 ± 0
	1500	-2.4 ± 0.8	4.8 ± 0.5	2.1 ± 0.7	35.8 ± 2.5	36.3 ± 3	27.8 ± 2.1	0.77 ± 0.01	7.7 ± 0.2	6.5 ± 0.2	0.1 ± 0	0.2 ± 0
	2000	-2.4 ± 0.7	4.2 ± 0.5	1.4 ± 0.4	37.1 ± 4.8	37.7 ± 5.5	28.7 ± 4.1	0.77 ± 0.01	8.9 ± 0.2	7.2 ± 0.2	0 ± 0	0.2 ± 0
NADP-ME *Zea mays* (SHADE)	200	0 ± 0.1	2.5 ± 0.4	3.8 ± 0.1	9.1 ± 1.7	5.3 ± 1.8	8.1 ± 1.9	1.74 ± 0.22	3.1 ± 0.2	4.1 ± 0.1	0.5 ± 0.1	0.5 ± 0.1
	750	-0.5 ± 0.3	2.6 ± 0.2	7.5 ± 0.4	20 ± 3.7	12.7 ± 3.9	18 ± 4	1.54 ± 0.15	3.7 ± 0.1	4.5 ± 0.1	0.4 ± 0.1	0.3 ± 0
	1500	-0.8 ± 0.4	3.3 ± 0.5	9.3 ± 0.6	23.5 ± 4.3	14.4 ± 4.2	20.9 ± 4.6	1.58 ± 0.19	4.4 ± 0.2	3.8 ± 0.1	0.4 ± 0.1	0.2 ± 0
	2000	-0.8 ± 0.3	3 ± 0.3	9.4 ± 0.2	24.4 ± 4.6	15.2 ± 4.5	21.3 ± 3.9	1.54 ± 0.17	5 ± 0.3	3.9 ± 0.1	0.4 ± 0.1	0.2 ± 0

Table 3.S 2 Summary of CO_2 and O_2 exchange data of gymnosperms, liverwort and fern species

CO_2 and O_2 exchange data of gymnosperms, liverwort and fern species measured with a mass spectrometer described in **Figure 3.S 2** were made at increasing irradiance from 200 to 2000 µmol photons m^{-2} s^{-1} and temperature of 28°C. Values are means ± s.e. (n = 4 leaf discs).

Species	Irradiance (µmol photons m^{-2} s^{-1})	Rates in darkness (µmol m^{-2} s^{-1})		Rates at high pCO_2 (µmol m^{-2} s^{-1})					Rates at the compensation point, Γ (µmol m^{-2} s^{-1})		O_2 uptake rate/O_2 evolution at high pCO_2	O_2 uptake at Γ/O_2 evolution at high pCO_2
		CO_2 uptake	O_2 uptake	O_2 uptake	Gross O_2 evolution	Net O_2 evolution	Net CO_2 uptake	*AQ*	Gross O_2 evolution	O_2 uptake		
Ginkgo biloba (Gymnosperm)	200	-0.2 ± 0.2	1.6 ± 0.4	3 ± 1	13.9 ± 0.7	11.7 ± 1.7	9.3 ± 1.1	0.81 ± 0.03	13 ± 0.2	11.7 ± 0.7	0.2 ± 0.1	0.8 ± 0
	750	-0.3 ± 0.2	1.8 ± 0.5	1.6 ± 0.5	23 ± 1.7	21.7 ± 2	17.4 ± 1.4	0.8 ± 0.01	21.4 ± 0.1	23.3 ± 0.7	0.1 ± 0	1 ± 0.1
	1500	-1.4 ± 0.2	2.8 ± 0.2	2.1 ± 0.8	25 ± 2.2	23.2 ± 2.6	18 ± 1.9	0.8 ± 0.01	25.2 ± 0	24.3 ± 0.4	0.1 ± 0	1 ± 0.1
	2000	-1.2 ± 0.1	2.6 ± 0.5	2.3 ± 1	26.4 ± 2.2	24.2 ± 2.2	18.6 ± 1.8	0.8 ± 0.01	26.4 ± 0	25.5 ± 0.6	0.1 ± 0	1 ± 0.1
Wollemi nobilis (Gymnosperm)	200	-2.5 ± 0.5	7.2 ± 1	7.5 ± 1.3	11.9 ± 1.8	4.9 ± 1.3	7.5 ± 1	2 ± 0.6	13.6 ± 0.6	14 ± 0.4	0.7 ± 0.1	1.3 ± 0.2
	750	-2.8 ± 0.6	6.9 ± 0.8	8.9 ± 1.4	18.6 ± 2	9.3 ± 1.7	11.1 ± 1.1	1.28 ± 0.16	16.5 ± 0.6	17.9 ± 1.4	0.5 ± 0.1	1 ± 0.2
	1500	-2.3 ± 0.6	8.7 ± 1.3	8.7 ± 1.7	21.3 ± 1.8	12.8 ± 2	13.2 ± 0.6	1.09 ± 0.12	18.1 ± 0.7	16.5 ± 0.6	0.4 ± 0.1	0.8 ± 0.1
	2000	-2.1 ± 0.5	7.1 ± 1.8	9.5 ± 2	24.6 ± 1.8	14.8 ± 1.7	14.7 ± 0.9	1.02 ± 0.08	19.1 ± 0.1	17.8 ± 0.1	0.4 ± 0.1	0.7 ± 0.1
Marchantia polymorpha (Liverwort)	200	-1.9 ± 0.1	3.6 ± 1	3.6 ± 0.8	12.3 ± 1.8	7.9 ± 1.8	8 ± 1.3	1.07 ± 0.12	12.4 ± 0.6	10.6 ± 0.6	0.3 ± 0.1	0.9 ± 0.2
	750	-1.8 ± 0.1	4 ± 0.7	4 ± 1.1	16.4 ± 3	9.5 ± 3.1	7.4 ± 1.7	0.88 ± 0.14	14.1 ± 0.2	12.6 ± 0.1	0.3 ± 0.1	0.9 ± 0.3
	1500	-1.9 ± 0.2	4.3 ± 0.5	4.2 ± 1	17.6 ± 3.1	10.9 ± 3.1	8.7 ± 2	0.85 ± 0.12	15.8 ± 0.2	13.6 ± 0.1	0.2 ± 0	0.9 ± 0.2
	2000	-1.6 ± 0.4	3.6 ± 0.6	4.5 ± 0.2	19.2 ± 4	11 ± 2.8	8 ± 1.7	0.76 ± 0.04	15.6 ± 0.5	14.1 ± 0.3	0.3 ± 0.1	0.9 ± 0.3
Polypodium sp. (Fern)	200	-0.7 ± 0.1	2 ± 0.4	2.6 ± 0.4	7.9 ± 0.2	4.7 ± 0.2	4.8 ± 0.2	1.03 ± 0.06	5.5 ± 0.1	4.8 ± 0.4	0.3 ± 0.1	0.6 ± 0.1
	750	-0.8 ± 0.2	2.1 ± 0.3	3.1 ± 0.1	9.3 ± 0.6	5.9 ± 0.4	5.6 ± 0.1	0.95 ± 0.08	5.8 ± 0.1	5.3 ± 0.1	0.3 ± 0	0.6 ± 0
	1500	-0.8 ± 0.1	2.2 ± 0.4	2.8 ± 0.1	9.8 ± 0.4	6.4 ± 0.2	5.8 ± 0.3	0.91 ± 0.04	6.5 ± 0	5.5 ± 0.1	0.3 ± 0	0.6 ± 0
	2000	-0.9 ± 0.1	2.1 ± 0.2	3.2 ± 0.1	10.6 ± 0.7	6.6 ± 0.3	5.7 ± 0.3	0.86 ± 0.04	6.6 ± 0.1	5.6 ± 0.1	0.3 ± 0	0.5 ± 0.1

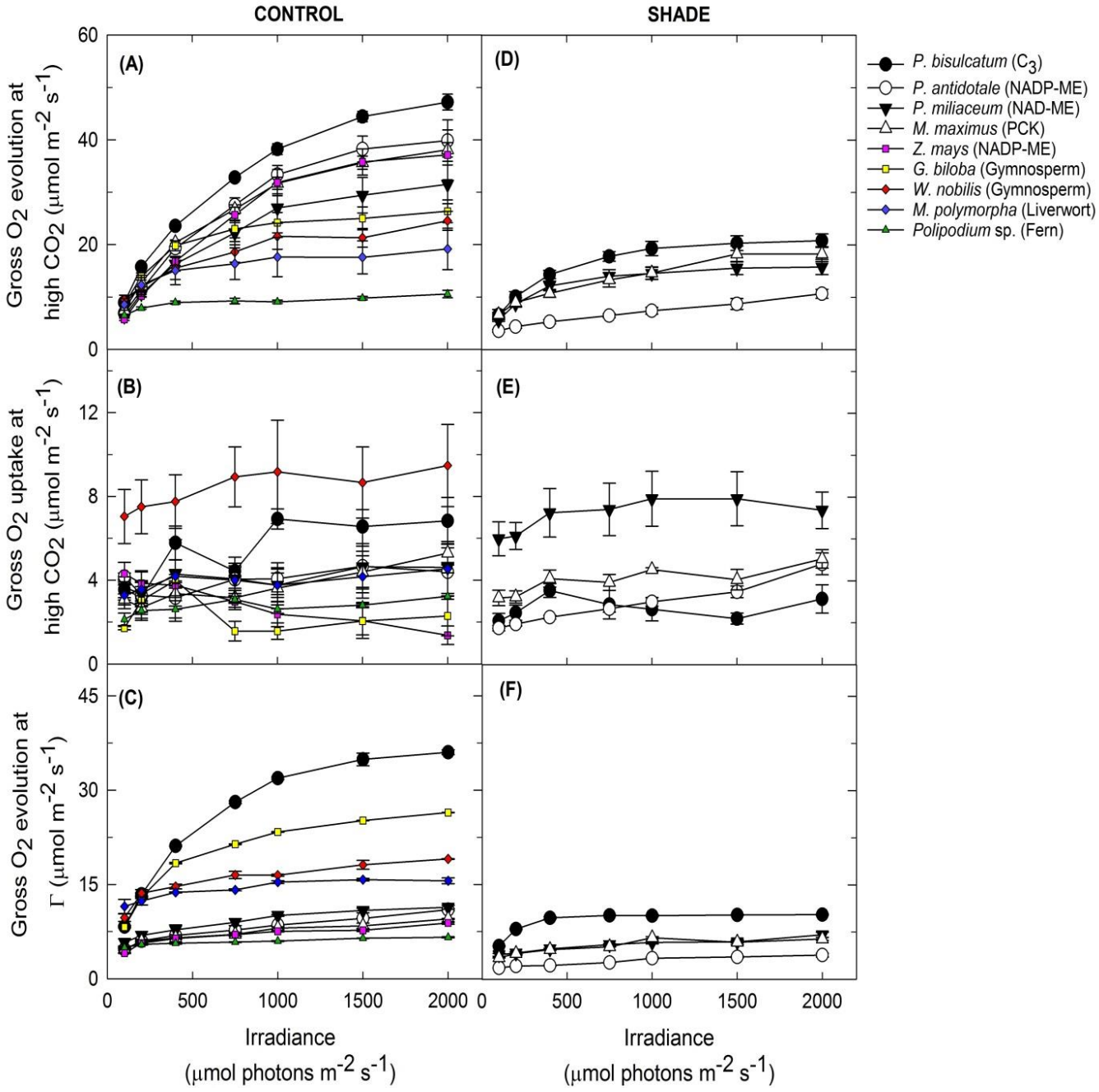

Figure 3. 1 Light dependence of O_2 exchange in leaf discs of control and shade-grown plant species.

Light dependence of O_2 exchange in leaf discs of control and shade-grown *Panicum bisulcatum* (C_3), *Panicum antidotale* (NADP-ME), *Panicum miliaceum* (NAD-ME), *Megathyrsus maximus* (PCK), *Zea mays* (NADP-ME), *Ginkgo biloba* (gymnosperm), *Wollemi nobilis* (gymnosperm), *Marchantia polymorpha* (liverwort) and *Polypodium* sp. (fern). **(A, D)** Gross O_2 evolution at high pCO_2; **(B, E)** gross O_2 uptake at high pCO_2; **(C, F)** gross O_2 evolution at Γ. Measurements were made at 28°C and 21% O_2. Values are means ± s.e. (n = 4 leaf discs).

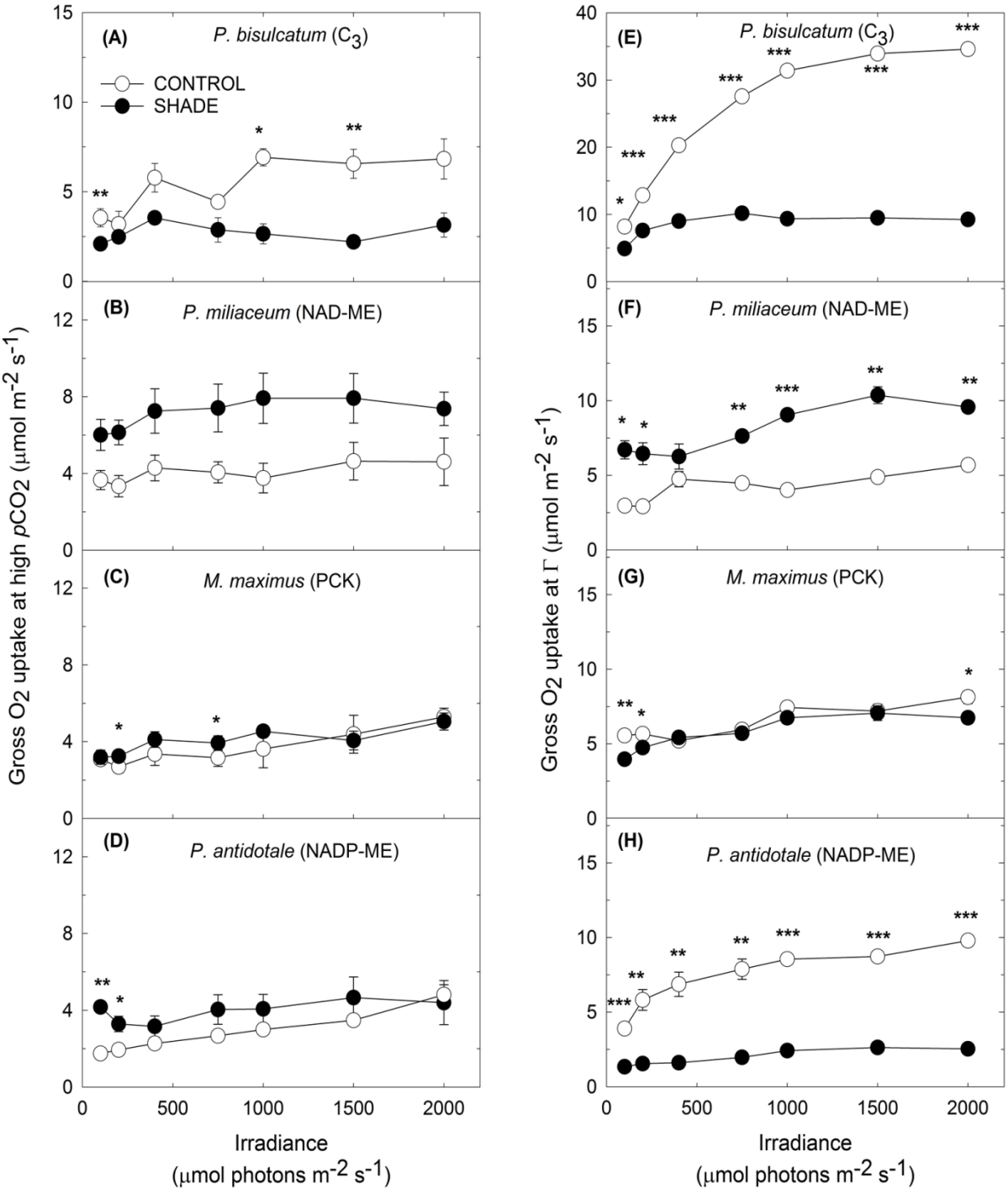

Figure 3. 2 Rate of gross O_2 uptake at high pCO_2 and at compensation point

Rate of gross O_2 uptake at high pCO_2 and at compensation point in leaf discs of control (open symbols) and shade-grown (closed symbols) **(A, E)** *Panicum bisulcatum* (C_3); **(B, F)** *Panicum miliaceum* (NAD-ME); **(C, G)** *Megathyrsus maximus* (PCK) and **(D, H)** *Panicum antidotale* (NADP-ME). Measurements were made at 28°C and 21% O_2. Values are means ± s.e. (n = 4 leaf discs). Statistical significance levels (t-test) for the growth condition within each species or subtype are shown and they are: * ≡ $p < 0.05$; ** ≡ $p < 0.01$; *** ≡ $p < 0.001$.

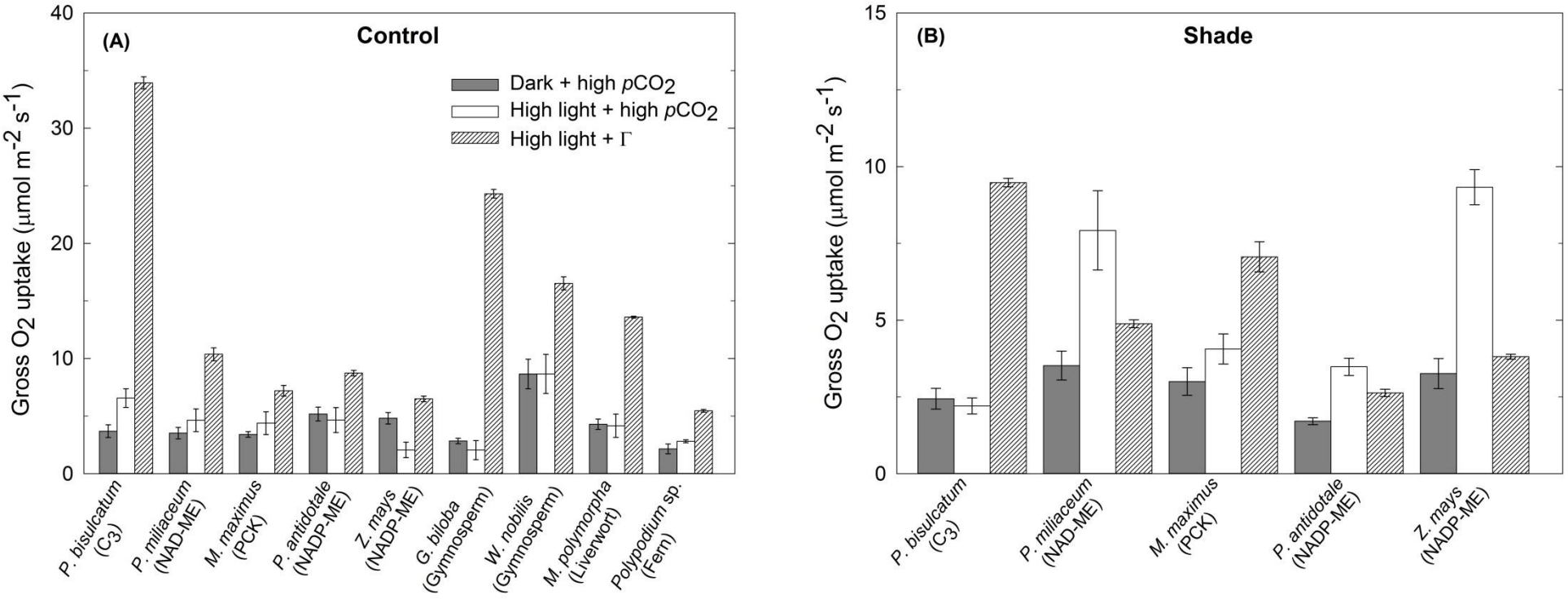

Figure 3. 3 Gross O_2 uptake rate at high pCO_2 and corresponding O_2 uptake in the dark

Gross O_2 uptake rate at high pCO_2 and corresponding O_2 uptake in the dark (solid bar) or 2000 µmol photons m^{-2} s^{-1} (open bar) in leaf discs of **(A)** control and **(B)** shade-grown *Panicum bisulcatum* (C_3), *Panicum miliaceum* (NAD-ME), *Megathyrsus maximus* (PCK), *Panicum antidotale* (NADP-ME), *Zea mays* (NADP-ME), *Ginkgo biloba* (gymnosperm), *Wollemi nobilis* (gymnosperm), *Marchantia polymorpha* (liverwort) and *Polypodium* sp. (fern). Each column represents the mean ± s.e. of species or subtype (n = 4 leaf discs).

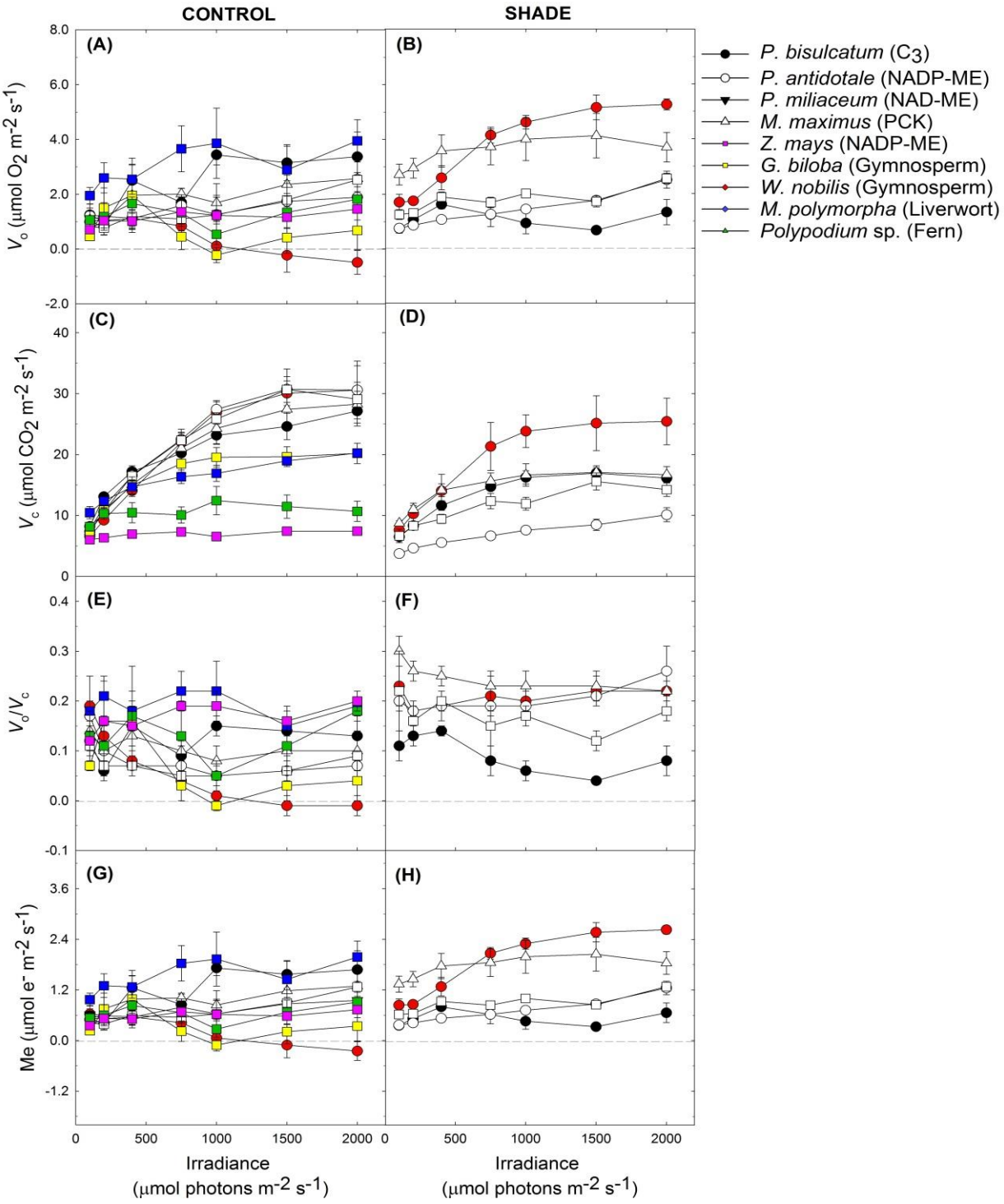

Figure 3. 4 Rates of Rubisco oxygenation (V_o) and carboxylation (V_c), and capacity for Mehler reaction (Me) at high pCO_2 and under increasing irradiance

Rates of Rubisco oxygenation (V_o) and carboxylation (V_c), and capacity for Mehler reaction (*Me*) at high pCO_2 and under increasing irradiance in leaf discs of control **(A, C, E, G)** and shade-grown **(B, D, F, H)** *Panicum bisulcatum* (C_3), *Panicum antidotale* (NADP-ME), *Panicum miliaceum* (NAD-ME), *Megathyrsus maximus* (PCK), *Zea mays* (NADP-ME), *Ginkgo biloba* (gymnosperm), *Wollemi nobilis* (gymnosperm), *Marchantia polymorpha* (liverwort) and *Polypodium* sp. (fern). Measurements were made at 28°C and 21% O_2. Values are means ± s.e. (n = 4 leaf discs).

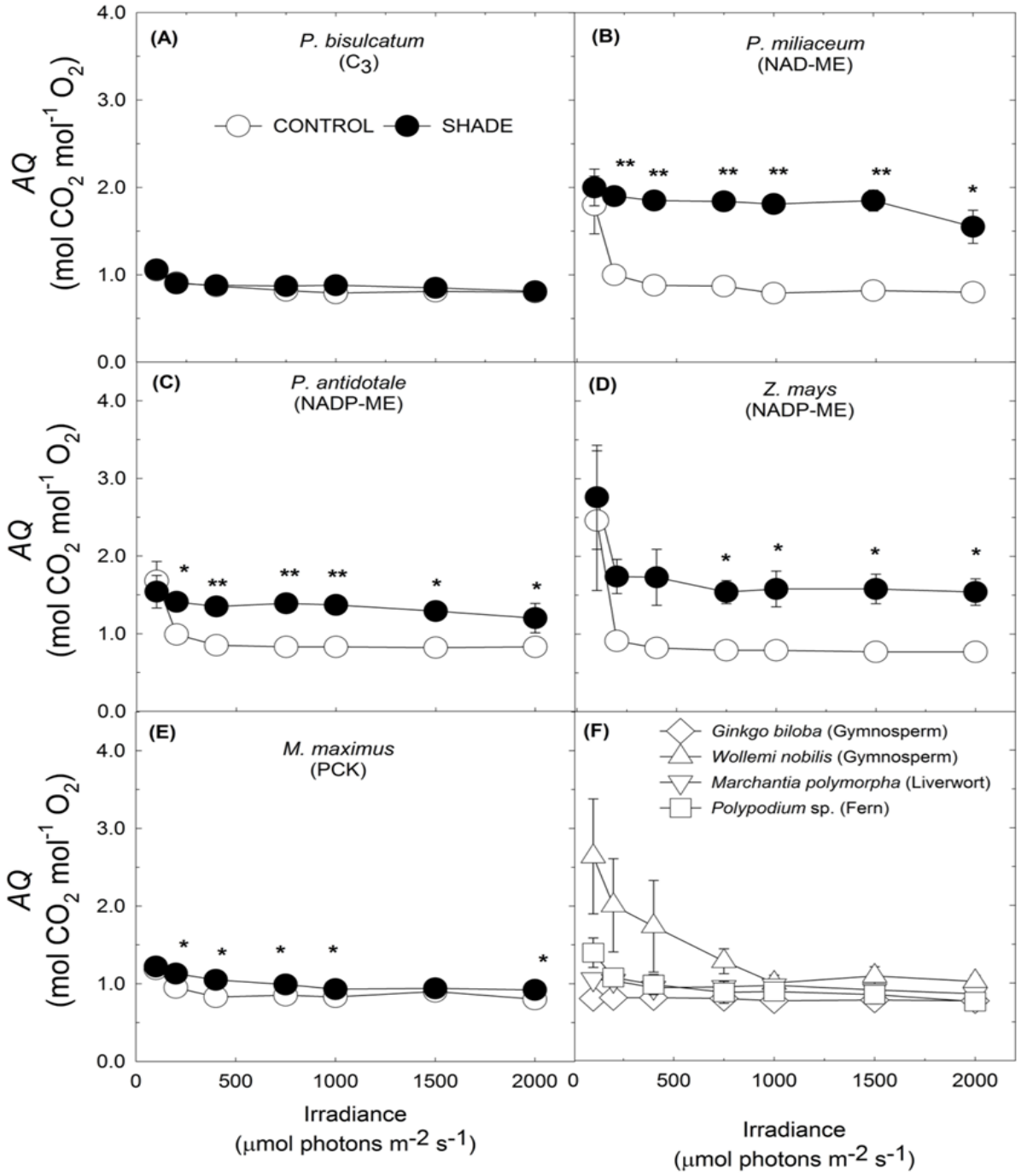

Figure 3. 5 Assimilation quotient (*AQ*) at high pCO_2 and under increasing irradiance

The assimilation quotient calculated as the ratio of the net CO_2 uptake to net O_2 evolution at high pCO_2 and under increasing irradiance in leaf discs of control (open symbol) and shade-grown (closed symbol) *Panicum bisulcatum* (C_3) **(A)**; *Panicum miliaceum* (NAD-ME) **(B)**; *Panicum antidotale* (NADP-ME) **(C)**; *Zea mays* (NADP-ME) **(D)**; *Megathyrsus maximus* (PCK) **(E)**; *Ginkgo biloba* (gymnosperm) **(F)**; *Wollemi nobilis* (gymnosperm) **(F)**; *Marchantia polymorpha* (liverwort) **(F)**; and *Polypodium* sp. (fern) **(F)**. Measurements were made at 28°C and 21% O_2. Values are means ± s.e. (n = 4 leaf discs). Statistical significance levels (t-test) for the growth condition within each species or subtype are shown and they are: * ≡ $p < 0.05$; ** ≡ $p < 0.01$; *** ≡ $p < 0.001$.

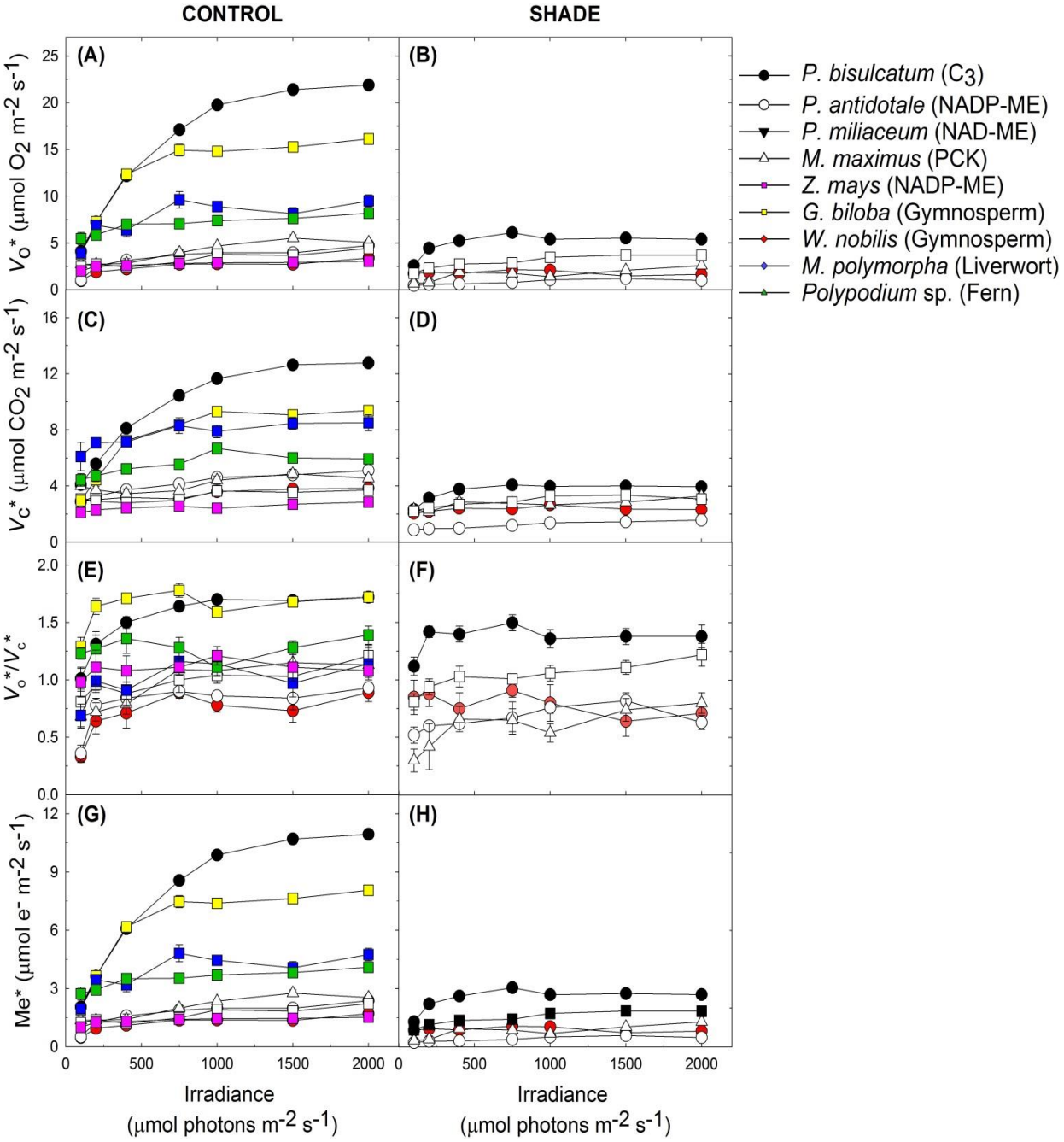

Figure 3. 6 Rates of Rubisco oxygenation (V_o*) and carboxylation (V_c*), and capacity for Mehler reaction (*Me) at compensation point (Γ) and under increasing irradiance**

Rates of Rubisco oxygenation (V_o*) and carboxylation (V_c*), and capacity for Mehler reaction (*Me**) at compensation point (Γ) and under increasing irradiance in leaf discs of control **(A, C, E, G)** and shade-grown **(B, D, F, H)** *Panicum bisulcatum* (C_3), *Panicum antidotale* (NADP-ME), *Panicum miliaceum* (NAD-ME), *Megathyrsus maximus* (PCK), *Zea mays* (NADP-ME), *Ginkgo biloba* (gymnosperm), *Wollemi nobilis* (gymnosperm), *Marchantia polymorpha* (liverwort) and *Polypodium* sp. (fern). Measurements were made at 28°C and 21% O_2. Values are means ± s.e. (n = 4 leaf discs).

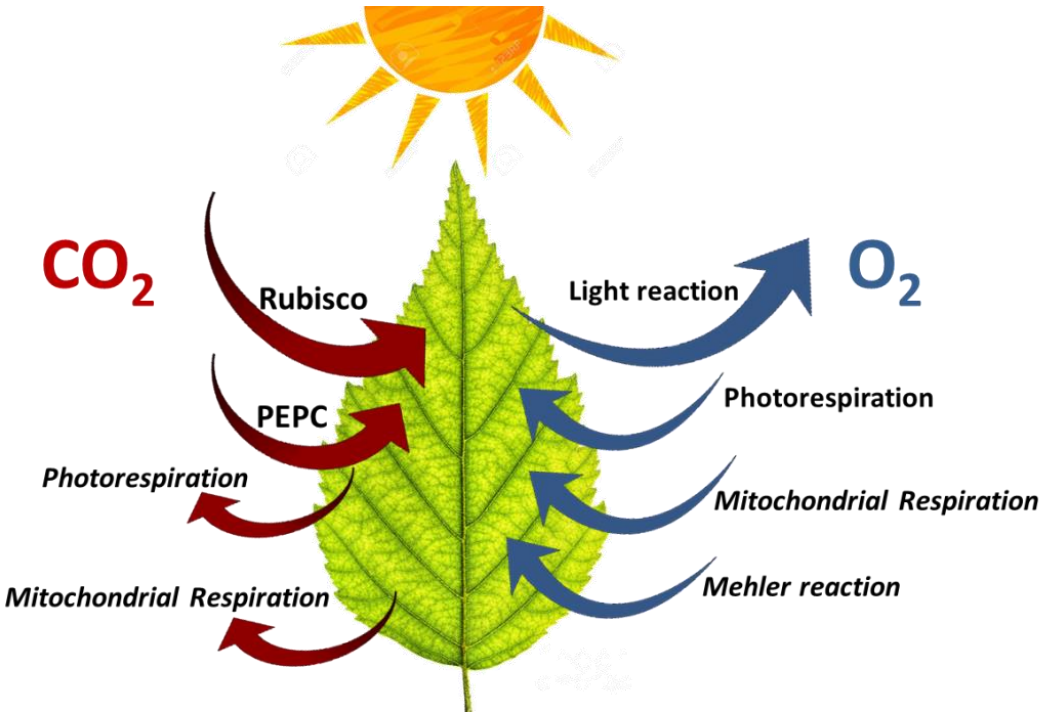

Figure 3.S 1 Summary of the differences in main gas fluxes occurring in an illuminated leaf.

Photorespiration and mitochondrial respiration in the light (R_l) both release CO_2 in the mitochondria, and these two processes are the main pathways for CO_2 evolution in the light. To be able to determine R_l, these components must be separated.

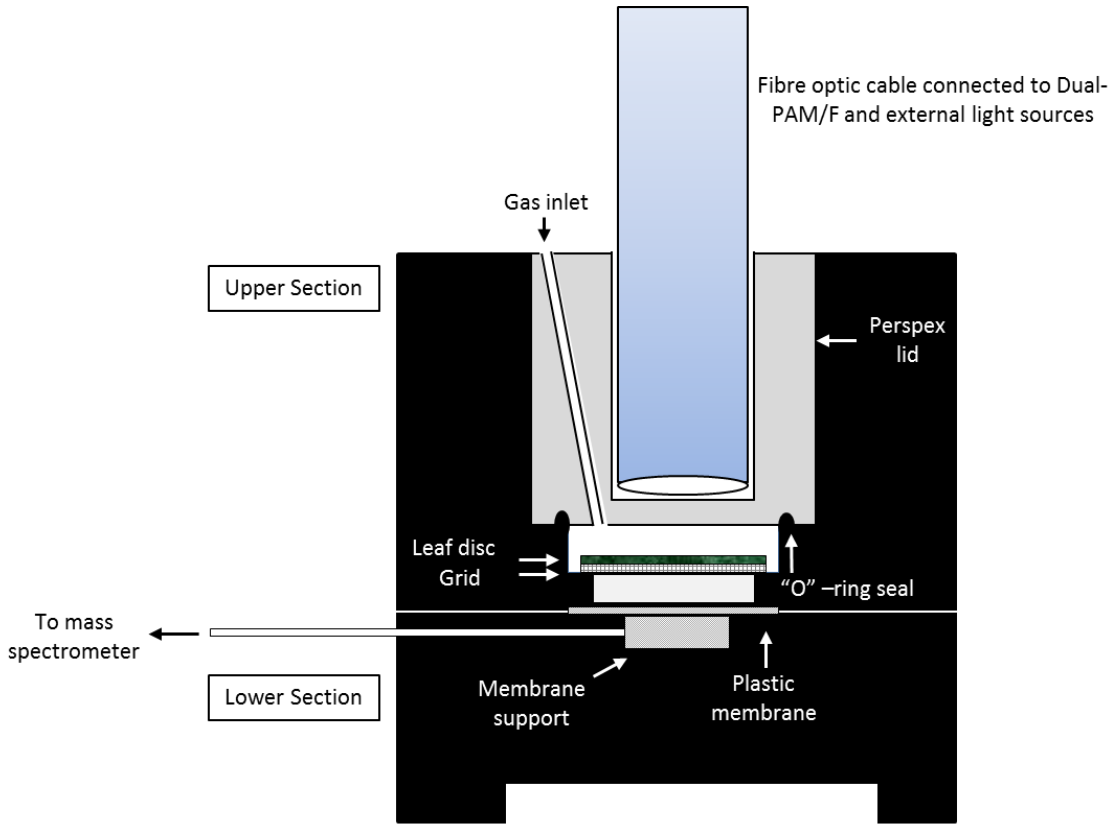

Figure 3.S 2 Cross-sectional diagram of the gas exchange cuvette.

The chamber was coupled to a mass spectrometer, Dual-PAM/F, and actinic, strong and weak far-red and saturating light sources as described in the text. The fibre optic cable was housed within the Perspex lid, which together with 2 rubber O-rings created a gas-tight seal. The chamber was linked to the mass spectrometer through a thin, gas-permeable plastic membrane and an ethanol/dry ice water trap. The mass spectrometer (micromass ISOPRIME; Micromass Ltd, Manchester, UK) was operated in peak switching mode for $^{18}O_2$ (mass 36), $^{16}O_2$ (mass 32) and CO_2 (mass 44). Net CO_2 assimilation was calculated from the reduction of CO_2 concentration, while gross oxygen evolution, gross oxygen uptake and net oxygen evolution were calculated from changes in $^{16}O_2$ and $^{18}O_2$ respectively, as previously described by Canvin *et al.* (1980).

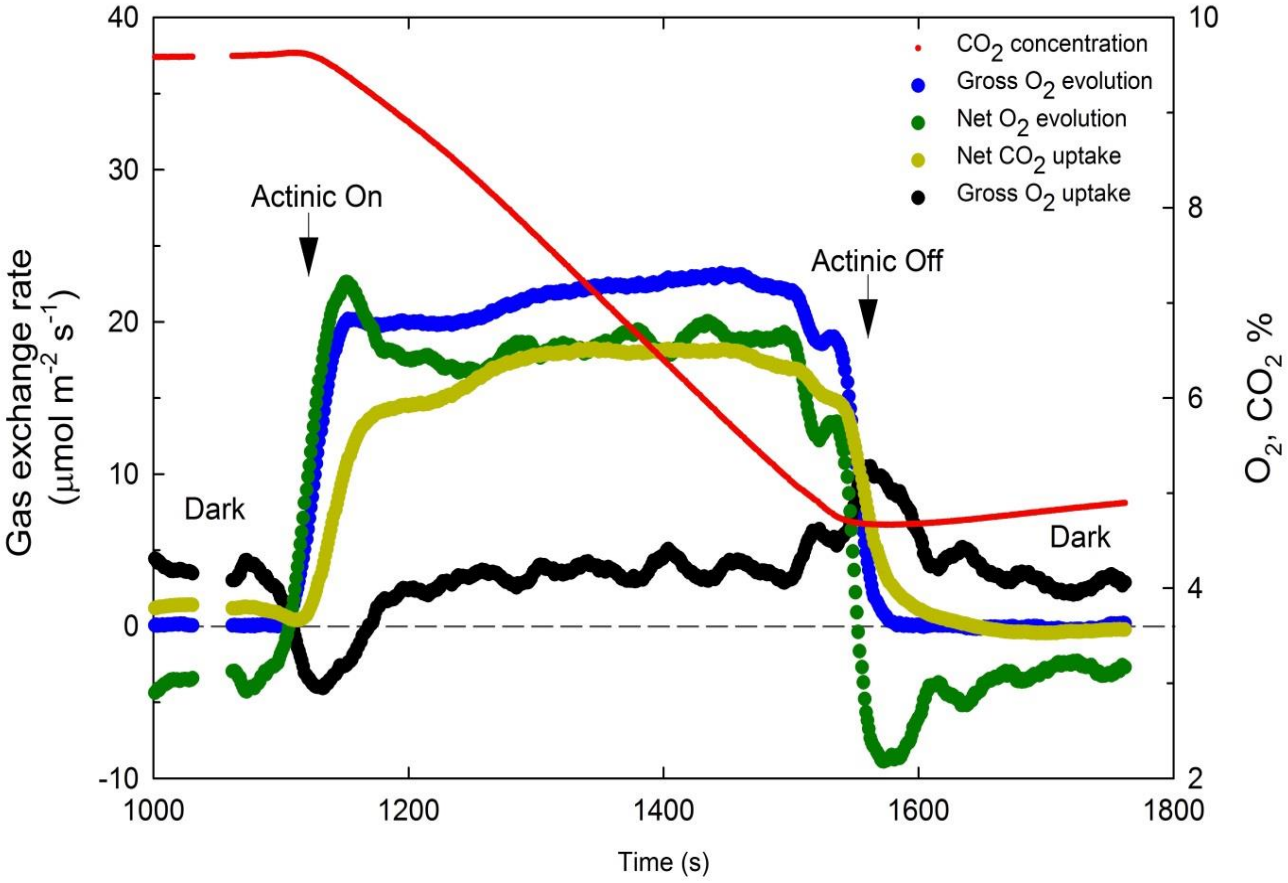

Figure 3.S 3 Typical gas exchange traces of gross O_2 evolution, gross O_2 uptake and net CO_2 uptake measured using MIMS.

Typical gas exchange traces of gross O_2 evolution, gross O_2 uptake and net CO_2 uptake of a *Panicum miliaceum* (NAD-ME) leaf at irradiance of 2000 µmol photons m^{-2} s^{-1}. Measurements were made in a closed system, beginning at high CO_2 concentration and proceeding until the CO_2 reached the compensation point (Γ). Then the light was turned off and dark rates were measured. This chamber, which was first described by Maxwell *et al.* (1998), has no fan and therefore a high boundary layer resistance surrounds the leaf disc. This means that unusually high CO_2 pressure is required to saturate O_2 exchange and CO_2 assimilation rate (Ruuska *et al.*, 2000).

CHAPTER 4

EFFECTS OF LOW LIGHT INTENSITY ON THE ENERGETICS OF CLOSELY RELATED C_3, C_3-C_4 AND C_4 GRASSES

ABSTRACT

The quantum yield of CO_2 assimilation (*QY*) has been widely used for evaluating photosynthetic efficiency. It is known that *QY* is generally lower in C_3 relative to C_4 plants at warm temperatures and differs among the C_4 subtypes; *QY* tends to be higher in NADP-ME and lower in NAD-ME species. The cause of the *QY* differences between the C_4 subtypes is not yet clear. Hence, the plasticity of light energy conversion efficiency was investigated among the C_4 subtypes. We grew representative grass species of C_3, C_3-C_4 and C_4 photosynthesis, encompassing all three biochemical subtypes (NADP-ME, NAD-ME, PCK) under shade (20% sunlight) or full sunlight (control) conditions. We measured *in situ* activity and stoichiometry of PSI and PSII, photosynthetic rates at high-light and low light and leaf spectral properties. We also measured *in vitro* activities and contents of photosynthetic enzymes and leaf pigment contents. Light-harvesting properties and photosynthetic rate of NAD-ME species were more negatively affected under shade compared with NADP-ME and PCK species, and even with C_3 and C_3-C_4 species. I suggest that high *QY* in NADP-ME species is partially related to the greater ability of light harvesting components of the leaf to adjust under varying light intensities. This is a very important plant characteristic for maximising light energy absorption while preventing photo-inhibition under sudden exposure to high light. This also ensures that the light reactions provide the right ATP/NADPH ratio even under limited supply of light energy. These findings progress our understanding of the light harvesting complexes, and provide information that could aid in the pursuit of enhanced photosynthetic capacity.

Key words: C_3, C_3-C_4, C_4 grasses, chlorophyll fluorescence, photosynthesis, quantum yield, biochemical subtypes

4.1. INTRODUCTION

Higher growing season temperatures and light levels primarily explain the dominance of C_4 plants in warm-climate grasslands and savannas (Sage *et al.*, 1999). The main physiological trait predicting the dependence of C_3/C_4 distribution on temperature is photosynthetic quantum yield (*QY*) (Collatz *et al.*, 1998; Ehleringer, 1978; Ehleringer *et al.*, 1997). *QY* is the ratio of moles of CO_2 assimilated to moles of quanta of photosynthetic active radiation (PAR) absorbed by a leaf (Ehleringer & Björkman, 1977). Under normal atmospheric conditions and at a leaf temperature >30^{o}C, *QY* is generally higher in C_4 compared to C_3 and intermediate C_3-C_4 species (Ehleringer & Björkman, 1977; Ludlow & Wilson, 1971; Maroco *et al.*, 1997). At warm temperatures, lower *QY* of C_3 relative to C_4 species is due to the higher energy cost of photorespiration relative to the cost of operating the CO_2 concentrating mechanism (CCM) in C_4 plants (Hatch, 1987). In addition, *QY* differs among the C_4 subtypes, with NADP-ME grasses generally having a higher *QY*, followed by PCK then NAD-ME grasses (Ehleringer & Pearcy, 1983). *QY* partly reflects the energy-conversion efficiency in response to ATP/NADPH demand during CO_2 fixation (Furbank *et al.*, 1990; Hatch *et al.*, 1995).

Energy-conversion efficiency in plants partly depends on the ratios of photosystem I (PSI), photosystem II (PSII) and associated light-harvesting and electron transport components in the chloroplasts (Anderson *et al.*, 1988; Chow *et al.*, 2012; Ghannoum *et al.*, 2005; Pfundel *et al.*, 1996; Romanowska *et al.*, 2008; Romanowska & Drożak, 2006). The PSI/PSII ratios differ between mesophyll cells (MC) and bundle sheath cells (BSC) of the C_4 subtypes (Ghannoum *et al.*, 2005; Hatch, 1987; Hernández-Prieto *et al.*, 2019; Romanowska & Drożak, 2006). Studies showing the dependence of energy-conversion efficiency on the PSII/PSI ratio were done in C_3 plants (Chow *et al.*, 1990; Evans, 1987, 2006a) and in isolated MC and BSC chloroplasts in the three C_4 subtypes (Romanowska & Drożak, 2006). These studies suggested that the *QY* reflects the distribution of quanta between PSI and PSII, and the balance between these two photosystems in chloroplasts is a compensation strategy designed to correct unbalanced absorption of light. Such adjustments allow the plant to maintain high light use efficiency under diverse light quality conditions and constitute acclimation that confers to plants a significant evolutionary advantage over that of a fixed photosystem stoichiometry in thylakoid membranes.

Light intensity during plant development is also a key factor responsible for adjustments of the photosystems activity and stoichiometry (Anderson, 1986). In response to long-term shading, the photosynthetic apparatus acclimates to maximize light use efficiency (Boardman,

2003; Sage & McKown, 2006). This acclimation varies depending on plant species and ecotype (Ward & Woolhouse, 1986). This partly explain the rarity of C_4 species in shaded habitats and forests since it is usually assumed that C_4 species have less advanced adaptation to low-light environments, together with higher *QY* of C_4 photosynthesis (Horton & Neufeld, 1998; Sage & McKown, 2006; Smith & Martin, 1987). Plants that are adapted to high light environments such as C_4 species have shown to possess chloroplasts that have high rates of photosynthetic quantum conversion (Lichtenthaler *et al.*, 1981; Lichtenthaler *et al.*, 1984; Lichtenthaler *et al.*, 1982, 2007).

There exist several constraints upon C_4 photosynthesis under shade in comparison with C_3 species. C_4 plants may have lower *QY* under shade due to the additional energy requirement of the C_4 pump (Ehleringer & Björkman, 1977; Krall & Pearcy, 1993). The C_4 photosynthetic machinery lacks the capacity for maintaining a high state of photosynthetic induction during low-light periods (Horton & Neufeld, 1998; Sage & McKown, 2006). It has also been demonstrated that the CCM is less effective at low light due to increased relative photorespiration and rising percentage of BS CO_2 leakiness which increase additional ATP demand (Bellasio & Griffiths, 2014; Henderson *et al.*, 1992; Kromdijk *et al.*, 2014; Kromdijk *et al.*, 2010; Kubásek *et al.*, 2007; Tazoe, 2008).

It has also been shown that the three subtypes also acclimate differently under long-term exposure to shade. It was recently reported by Sonawane *et al.* (2018) that NAD-ME species and to a lesser extent PCK species were generally outperformed by NADP-ME species under shade (16% of full sunlight) conditions. Shade compromised the CCM efficiency to a greater extent in NAD-ME than in PCK or NADP-ME C_4 grasses by virtue of a greater increase in carbon isotope discrimination and BS CO_2 leakiness, and a greater reduction in *QY*. Together with other studies, it was also found that the *QY* and CCM of NADP-ME species were not significantly affected despite changes in the light environment (Bellasio & Griffiths, 2014a; Bellasio & Lundgren, 2016; Ghannoum *et al.*, 2005; Yin & Struik, 2015). It was also supported by a modelling approach by Wang *et al.* (2014) that the NADP-ME biochemical pathway is favoured at low light.

However, it is still unclear how these observed differences under shade relate to the changes in light reactions especially among C_4 subtypes. It is known that light intensity is likely to induce changes in the light reaction components which can alter relative light absorption and energy conversion efficiency by PSI and PSII. These changes might differ among subtypes.

In this study, representative species of C_3, C_3-C_4 and the three subtypes of C_4 photosynthesis were grown under high-light (control) and shade (20% sunlight) to determine the differences in plasticity of the light reactions to long-term exposure to shade. We sought to determine if the high photosynthetic *QY* observed in C_4 grasses and the variations in *QY* among the subtypes are associated with differences in the activity and stoichiometry of the photosystems and/or pigment composition. In particular, the stoichiometry of the two photosystems and relative electron fluxes were measured *in vivo* in order to reflect functionality *in situ*, without any potential complication associated with isolation of thylakoids. Measurements involved the use of commercial equipment (Dual-PAM) which can simultaneously assess P700 and chlorophyll fluorescence and several custom–built equipment developed by Chow *et al.* (1989), Chow & Hope (2004) and Kou *et al.* (2013a) which can measure the total electron flux through PSI (ETR1), as well as the linear electron flux through PSII and PSI (LEF_{O2}) in series and cyclic electron flow around PSI (CEF). We also measured activities of Rubisco and other enzymes involved in C_4 photosynthesis to relate the observed *QY* to CCM efficiency under variable growth light conditions. Finally, we compared the results obtained using the commercial and custom-built systems.

.

4.2. MATERIALS AND METHODS

4.2.1. Plant culture

Representative species of Paniceae grasses belonging to C_3 (*Panicum bisulcatum*); C_3-C_4 intermediate (*Panicum milioides*); and C_4 photosynthesis with NADP-ME subtype (*Panicum antidotale* and *Zea mays*); NAD-ME subtype (*Panicum miliaceum*); and PCK subtype (*Megathyrsus maximus*) plants were grown in vermiculite in a naturally lit greenhouse chamber at the Australian National University. The chamber temperature was maintained at 24/21^{o}C for day/night by in-built greenhouse temperature control system. Within the chamber, a steel structure was erected and covered with shade cloth. The average ambient photosynthetic photon flux density, PPFD and temperature during the mid-day were 800 and 200 µmol photons m^{-2} s^{-1} and 30 and 29^{o}C for the sun/control and shade treatments, respectively. Plants were watered regularly and fertilized with Osmocote® (Scotts Australia). Leaves were analysed from 4–5 week-old plants.

4.2.2. Leaf gas exchange and chlorophyll fluorescence measurements

Leaf gas exchange was measured using an open gas exchange system (LI-6400; LICOR, Inc., Lincoln, NE, USA). Measurements were made at photosynthetic photon flux densities (PPFD) of 1000 (high-light) and 200 µmol photons $m^{-2}s^{-1}$ (shade) and 28^{o}C leaf temperature about 7-8 weeks after transplanting on an attached, youngest fully expanded leaf on the main stem. CO_2 levels were held fixed at 400 ppm within the leaf chamber, corresponding to the ambient level.

4.2.3. Electrochromic signal to determine the photosystem stoichiometry

The electrochromic shift (ECS) signal from leaf segments (30 mm x 30 mm) was measured as described by Chow & Hope (2004). A measuring beam at 520 nm, selected by an interference filter (full width at half peak height = 2 nm), was admitted by an electronic shutter shortly before each measurement. The measuring beam was transmitted to the end window of a photomultiplier, through a leaf segment oriented at 45° to the light path. Shortly afterwards, data acquisition commenced before the triggering of a xenon single-turnover flash. The xenon flash was directed at 45° to the leaf segment, but at 90° to the measuring beam. Data acquisition continued for 50 ms in total, followed by closing of the electronic shutter to keep the leaf segment in darkness until the next measurement. Timing of these events was controlled by a pulse/delay generator (Model 555, Berkeley Nucleonics Corporation, USA). The xenon flash was filtered by a red Perspex long-pass filter (transmitted wavelengths >590

nm) and a heat-reflection filter that did not transmit wavelengths >700 nm. The elimination of the far-red component of the xenon flash by the heat-reflection filter was meant to avoid unbalanced excitation of both photosystems, since a far-red component, if present, would reach further into the leaf tissue where it would excite predominantly PSI. It is desirable to excite both photosystems in the same tissue, particularly if the flash is only sub-saturating. Xenon flashes were given at 0.2 Hz; typically 25 signals were averaged to improve the signal-to-noise ratio. The ECS signal was also measured in leaf segments during suppression of PSI by moderately strong far-red light (**Figure 4. S 1**).

Leaf segments were illuminated for 10 s to steady-state by an array of far-red, light-emitting diodes in conjunction with a Schott RG9 filter (~695 μmol photons m^{-2} s^{-1}, peak wavelength 741 nm, range 700–780 nm). The direction of the moderately strong far-red light made an angle of ~45° with the leaf segment. The P700 molecules in PSI reaction centres were not all photo-oxidized, however, necessitating correction for a small fraction of P700 in the reduced state. The small fraction of reduced P700 was determined from the redox state of P700 during illumination with the same far-red light as described by Chow & Hope (2004) (**Figure 4. S 2**).

The complementary fraction *r* of reduced P700 was then obtained and taken into account when evaluating the contribution of PSII reaction centres to the ECS signal in the presence of moderately strong far-red light. Let the contents of PSII and PSI reaction centres be n_{PSII} and n_{PSI}, respectively. The amplitude of the fast ECS rise, either in the absence [$E_{f(-FR)}$] or the presence [$E_{f(+FR)}$] of far-red light is directly proportional to the sum of the contributing reaction centres, with *k* as the inverse of the constant of proportionality:

$$kE_{f(-FR)} = n_{psII} + n_{PSI} \tag{4.1}$$

and

$$kE_{f(-FR)} = n_{psII} + rn_{PSI} \tag{4.2}$$

Manipulation of these two equations gives the stoichiometry of the two photosystems:

$$\frac{n_{PSII}}{n_{PSI}} = \frac{[E_{f(+FR)} - rE_{f(-FR)}]}{[E_{f(-FR)} - rE_{f(+FR)}} \tag{4.3}$$

4.2.4. Quantification of functional PSII by the oxygen yield per single turn-over flash

The same leaf disc was used for quantification of the functional PSII centres, by measuring the amount of oxygen evolution per single turn-over flash in a leaf-disc oxygen electrode, with continuous background far-red light (Chow *et al.*, 1989). These estimations are based on the assumption that for every four flashes (at 10 Hz), four electrons are transferred through each functional PSII, resulting in the evolution of one O_2 molecule.

4.2.5. Estimation of steady-state cyclic electron flux (CEF) around PSI using custom-built equipment

The rate of CEF was determined using the following equation:

$$CEF = ETR1 - LEF_{O2} \tag{4.4}$$

where ETR1 is the total electron flux through PSI and LEF_{O2} is linear electron flux through both photosystems. LEF_{O2} and ETR1 were measured as described below.

4.2.5.1. LEF_{O2} measurement

LEF_{O2} was estimated by measuring O_2 evolution in a gas-phase oxygen electrode (Hansatech, King's Lynn, UK) chamber, thermostat-controlled at 25^{o}C and with a multifurcated light guide, containing 1% CO_2 supplied by fabric matting moistened with 1 M $NaHCO_3/Na_2CO_3$ (pH 9). White incandescent light from a projector halogen lamp filtered by a Calflex C heat-reflecting filter (Linos Photonics, Göttingen, Germany) and neutral-density filters was used to illuminate a leaf disk. O_2 evolution was measured over several minutes until it reached a steady state. The post-illumination drift was subtracted algebraically from the steady-state net oxygen evolution rate, and the gross O_2 evolution rate obtained was multiplied by four to give LEF_{O2}. For calibration of the oxygen signals, 1 mL of air at 25°C (taken to contain 8.05 µmol O_2) was injected into the gas-phase O_2 electrode chamber.

4.2.5.2. ETR1 measurement from redox kinetics of P700

Redox changes of P700 were observed with a dual wavelength (820/870 nm) unit (ED-P700DW) attached to a pulse amplitude modulation (PAM) fluorometer (Walz, Effeltrich, Germany) in the reflectance mode (response time constant = 95 ms) as described by Kou *et al.* (2013). A leaf disc was brought to steady-state photosynthesis by illuminating it with white actinic light for about 10 minutes before simultaneous measurement of O_2 evolution and Chl fluorescence yields. To retain steady-state for $P700^{+}$ measurements, immediately after these simultaneous measurements, each leaf disc was re- illuminated with the same

actinic light for 9.016 s, using an electronic shutter controlled by one terminal of a pulse/delay generator (Model 555, Berkeley Nucleonics, San Rafael, CA, USA).

During each 9.016-s illumination, at time T= 8.80 s (corresponding to the time point t =-50 ms), data acquisition (using software written by the late AB Hope) was started by a second terminal of the pulse/delay generator. At T= 8.85 s, a strong far-red light (FR, ~2000 µmol photons m^{-2} s^{-1}) from a Roithner LaserTechnik, Vienna, Austria) was triggered on for light-emitting diode array (741 nm ± 13 nm, LED735–66–60, 100 ms using a third terminal of the pulse/delay generator. The strong FR light depleted electrons from the inter-system chain, so that the subsequent saturating pulse maximally oxidised P700 (Siebke *et al.*, 1997). While the strong FR light was on, at T= 8.90 s, a saturating light pulse (~9000 µmol photons m^{-2} s^{-1}) was applied for 10 ms by a pulse from a fourth terminal of the pulse/ delay generator, yielding the maximally-oxidised P_m' signal (where P_m' is the maximum $P700^+$ signal in actinic light). Finally, the white actinic light was turned off by the electronic shutter (at T= 9.016 s). Data acquisition continued for 85 ms after cessation of actinic illumination to obtain the baseline corresponding to complete reduction of P700. Immediately after completion of one cycle of illumination and data acquisition (at T= 9.101 s), another 9.016-s illumination was restarted, thereby maintaining steady-state photosynthesis. Nine traces were averaged automatically to improve the signal-to-noise ratio. Next, the maximum photo-oxidisable P700 content, P_m was determined (**Figure 4. S 2**). A steady-state by illumination with weak continuous far-red light (~12 µmol photons m^{-2} s^{-1}, 723 nm) for >10 s was then established. A single saturating turnover flash was then superimposed. Flashes were given at 0.2 Hz; nine consecutive signals were automatically averaged. The maximum $P700^+$ signal (P_m) immediately after the flash was used to normalise the signal interval *d*. The photochemical yield of PSI [Y(I)] is then given by:

$$Y(I) = \frac{d}{P_m} \tag{4.5}$$

where P_m is the maximum signal, and *d* is the signal interval (Klughammer & Schreiber, 2008).

ETR1 was then calculated as:

$$ETR1 = Y(I)\ x\ I\ x\ 0.85\ x\ f_I \tag{4.6}$$

where *I* is the irradiance, 0.85 is the assumed absorptance and f_I is the fraction of absorbed white light partitioned to PSI which was experimentally derived.

4.2.6. Measurements of leaf reflectance, transmittance and absorptance

Leaf reflectance, transmittance and absorptance to solar radiation over the 400 – 700 nm wavelength were measured with a Li-Cor 1800-12 Integrating Sphere (Li-Cor, Inc., Lincoln, NE, USA), coupled by a 200 µm diameter single mode fibre to an Ocean Optics model USB2000 spectrometer (Ocean Optics Inc., Dunedin, FL, USA), with a 2048 element detector array, 0.5 nm sampling interval, and 7.3 nm spectral resolution in the 350–1000 nm range. The Ocean Optics software is designed for signal verification, adjustment of integration time, and data acquisition. An integration time of 13 ms was used for all sample measurements. Single leaf reflectance and transmittance measurements were acquired following the methodology described in the product manual for the LiCor 1800-12 system (Li-Cor Inc., 1984). Reflectance of the sample (R_s) is the amount of flux reflected by the leaf, normalized by the amount of flux incident on it and calculated as:

$$R_s = \frac{(I_s - I_d)R_r}{(I_r - I_d)} \tag{4.7}$$

where I_s is the measured sphere output when the sample is illuminated, I_r is that measured when the reference material (barium sulfate) is illuminated and I_d is measured by illuminating the sample port with no sample in place. For equation (4.6), it was assumed that the reflectance of the reference material (R_r) is 1. Transmittance of the sample (T_s) is the amount of flux transmitted by the leaf, normalized by the amount of flux incident on it and calculated as:

$$T_s = \frac{I_s R_r}{I_r} \tag{4.8}$$

Any flux not reflected or transmitted is absorbed (*Abs*) and obtained using this equation based on conservation of energy:

$$R_s + T_s + Abs = 1 \tag{4.9}$$

4.2.7. Chlorophyll fluorescence using Dual-PAM

The chlorophyll fluorescence and P700 redox state measurement were also determined in vivo with the same leaves using a Dual-PAM-100 (Heinz Walz). The F_v/F_m and P_m were determined after dark adaptation for 20 minutes. Light responses of leaf chlorophyll fluorescence and P700 were also measured after 15 min light adaptation under PPFD of 1000 µmol photons m^{-2} s^{-1}. Light-adapted fluorescence parameters were recorded after 3 min

exposure to each of the PPFDs (30, 37, 46, 61, 77, 94, 119, 150, 190, 240, 297, 363, 454, 555, 684, 849, 1052, 1311, 1618 and 1976 µmol photons m^{-2} s^{-1}).

The fluorescence parameters were calculated as follows:

$$F_v/F_m = (F_m - F_o)/F_m \quad (4.10)$$

$$Y(II) = (F_m' - F_s')/F_m' \quad (4.11)$$

where F_o represents the minimum fluorescence in the dark-adapted state and light-adapted state, respectively, and F_m and F_m' represent the maximum fluorescence upon illumination with a pulse (600 ms) of saturating light (10000 µmol photons m^{-2} s^{-1}) in the dark-adapted state and light-adapted state, respectively (Kramer *et al.*, 2004). F_s' is the light steady-state fluorescence. F_v/F_m represents the maximum quantum yield of PSII. Y(II) is the effective quantum yield of PSII.

The parameters related to PSI are calculated as follows:

$$Y(ND) = 1 - P700\,red. \quad (4.12)$$

$$Y(I) = P700\,red. - Y(NA) \quad (4.13)$$

$$Y(NA) = (P_m - P_m')/P_m \quad (4.16)$$

After far-red pre-illumination for 10 s, P_m was determined through the application of a saturation pulse. P_m' was determined similarly to P_m but without far-red pre-illumination. This method was taken from Klughammer & Schreiber (2008). Y(ND) represents the fraction of overall P700 that is oxidized in a given state due to a lack of donors which is enhanced by a trans-thylakoid proton gradient (photosynthetic control at the cytochrome b_6f complex as well as down-regulation of PSII) and photodamage to PSII. Y(NA) represents the fraction of overall P700 that cannot be oxidized by a saturation pulse in a given state due to a lack of acceptors; it is enhanced by dark adaptation (deactivation of key enzymes of the Calvin–Benson cycle) and damage at the site of CO_2 fixation. The saturating pulse used for P700 measurements was 10000 µmol photons m^{-2} s^{-1}. CEF was also calculated using equation (4.4).

4.2.8. Quantum yield for CO_2 uptake and assimilation quotient calculations

The apparent quantum yield for CO_2 uptake was calculated as the ratio of CO_2 assimilation rates measured at HL (QY_{1000}) or at growth irradiance (QY_{growth}) to absorbed irradiance as follows:

$$QY_{1000}\ or\ QY_{growth} = \frac{A_{1000}\ or\ A_{growth}}{I\ x\ (Abs_{ave})} \quad (4.17)$$

where A_{1000} and A_{growth} are the CO_2 assimilation rates at 1000 µmol photons m^{-2} s^{-1} and at growth irradiance, I is the measurement irradiance, and Abs_{ave} is the average leaf absorptance for each species and light treatment in the blue (470 nm) and red (660 nm) wavelength regions (**Figures 4. 3A** to **4. 3F**), which correspond to the LED light source of the LiCOR equipment.

The assimilation quotient (AQ_{1000}) was calculated using CO_2 assimilation (measured at 1000 photons µmol m^{-2} s^{-1} and ambient CO_2 400 ppm) and O_2 evolution rates (measured at saturating light (2000 µmol m^{-2} s^{-1}) and saturating CO_2 (>1000 µl L^{-1}). Given A and LEF_{O2} were not measured under the same conditions, these values should be considered with caution.

$$AQ_{1000} = \frac{Net\ CO_2\ uptake}{Net\ O_2\ evolution} = \frac{A_{1000}\ (at\ ambient\ CO_2 \text{ and } 1000\ \mu mol\ photon\ m^{-2}s^{-1})}{LEF_{O2}\ (at\ high\ CO_2 \text{ and } 2000\ \mu mol\ photon\ m^{-2}s^{-1})/4\ (4e^{-}per\ 1O_2)} \quad (4.18)$$

4.2.9. Carotenoid and chlorophyll analysis and quantification by HPLC

Carotenoids and chlorophyll analysis through HPLC was done following the modified protocol from Pogson *et al.* (1996). Approximately 50 mg fresh leaves were extracted in a microcentrifuge tube by grinding using a tissue lyser (Qiagen) (25 Hz for 3 minutes). Pigments were extracted by adding 1 mL of extraction buffer, comprising of acetone:ethyl acetate (60:40) with 0.1% Butylated hydroxytoluene (BHT) and then vortexed for 1 minute or until the tissue loose its green colour. The organic component of the extract was separated by gently adding 900 µL of water and inverting the tube 4 – 5 times. The solution was then centrifuged for 5 minutes at 15000 rpm at 4^{o}C. The upper phase was collected and transferred in a new microcentrifuge tube (a little of the lower phase was still obvious at this point). This extract was then centrifuged for 5 minutes at 15000 rpm at 4^{o}C and 200 µL was transferred to another tube. A final volume of 20 µL was used for injection into HPLC system (Agilent 1260 Infinity) equipped with YMC-C30 (250 x 4.6mm, S-5µm) column and Diode Array Detector (DAD) detector. A newly optimized 17 minutes elution method was used to separate

pigments using reverse phase solvent gradient comprised of mobile phase A (methanol:water:triethylamine, 98:2:0.1 v/v) and B (methyl tert-butyl ether). The initial solvent composition was 85% and 15% of the solvent A and B respectively for one minute, followed by 35% of B up to minute 11. The ratio of B increased to 65% at 11.1 minutes followed by a gradient up to 70% at 15 minutes and stabilized at this ratio through to 17 minutes. The solvent flow rate was 1 ml/min until 17 minutes from the beginning. Solvent composition was returned to the initial state (15% of B) at 17.1 minutes and the column was equilibrated up to 25 minutes with the flow rate of 2.0ml/minutes. The column temperature was maintained at 23^{o}C and auto-sampler temperature was set to 8^{o}C and illumination turned off. Carotenoid and chlorophyll peak signals were analysed at 440 nm based on Pogson *et al.* (1996) and Cuttriss *et al.* (2007). **Figure 4. S 3** shows the typical HPLC profiles of leaf pigments absorbing at 440 nm, with peaks corresponding to different carotenoids and chlorophylls.

4.2.10. Activity of Rubisco, PEPC, NADP-ME, NAD-ME and PCK

Following gas exchange measurements, leaf discs (0.6 cm^2) were taken and rapidly frozen in liquid nitrogen. Activities of photosynthetic enzymes were measured at 25°C using an NADH-coupled enzyme assay with the rate of NADH oxidation or reduction monitored at 340 nm using a diode array spectrophotometer (Agilent model 8453) as described by Sharwood *et al.* (2016). For assays of Rubisco, PEPC and NADP-ME, leaf discs were extracted using ice-cold mortar and pestle into 1 ml of ice cold, extraction buffer [50 mM EPPS-NaOH, pH 7.8, 1 mM EDTA, 5 mM DTT, 5 mM $MgCl_2$, 1% (v/v) plant protease inhibitor cocktail (Sigma-Aldrich), and 1% (w/v) polyvinylpolypyrrolidone (PVPP). The extract was rapidly centrifuged for 30 seconds at 15,000 g at 4 °C. Protein content was measured against BSA standards using Pierce Coomasie Plus (Bradford) protein assay kit (Thermoscientific, Rockford, USA). Fifty µl of the soluble leaf protein was used to measure Rubisco content by [^{14}C]CABP (2-C-carboxyarabinitol 1,5-bisphosphate) binding as described by Sharwood *et al.* (2016). Rubisco activity was measured in assay buffer [100 mM EPPS-NaOH, pH 8.0, 10 mM $MgCl_2$, 0.2 mM NADH, 20 mM $NaHCO_3$, 1 mM ATP (pH 7.0), 5 mM phosphocreatine (pH 7.0), 50 U creatine phosphokinase, 0.2 mg carbonic anhydrase, 50 U 3-phosphoglycerate kinase, 40 U glyceraldehyde-3-phosphate dehydrogenase, 113 U triose-phosphate isomerase, 39 U glycerol-3-phosphate dehydrogenase]. Ribulose-1, 5-bisphosphate (RuBP) (0.26 mM) was included in the cuvettes, with 10 µl of soluble leaf protein extract added to start the assays. Maximal PEPC activity was measured in assay buffer containing [50 mM EPPS-NaOH (pH 8.0), 0.5 mM EDTA, 10

mM $MgCl_2$, 0.2 mM NADH, 5 mM glucose-6-phosphate, 1 mM $NaHCO_3$, 1 U/mL MDH] after the addition of 8 mM of PEP. NADP-ME activity was measured in assay buffer containing [50 mM Tricine buffer (pH 8.3), 0.5 mM NADP, 5 mM malate, 0.1 mM EDTA] after addition of 10 mM $MgCl_2$.

The maximal activity of PCK was measured in the carboxylase direction using a method described by Sharwood *et al.* (2016) in an NADH-coupled assay. Leaf discs (0.6 cm^2) were extracted in 50 mM HEPES pH 7.0, 5 mM DTT, 1% (w/v) PVPP, 2 mM EDTA, 2 mM $MnCl_2$, and 0.05% Triton using ice-cold mortar and pestle. PCK activity from leaf extracts was measured in assay buffer [50 mM HEPES, pH 7.0, 4% mercaptoethanol (w/v), 100 mM KCl, 90 mM $NaHCO_3$, 1 mM ADP, 2 mM $MnCl_2$, 0.14 mM NADH, and malate dehydrogenase (MDH; 6 U; 3.7 µl)] after the addition of 15 mM PEP. The activity of NAD-ME was measured using a method described by Setién *et al.* (2014). Leaf discs (0.6 cm^2) were extracted in [50 mM HEPES-KOH (pH 8.0), 2 mM EDTA, 0.05% Triton, 2 mM $MnCl_2$, 10 mM DTT, 1% PVPP and 1% (v/v) plant protease inhibitor cocktail in ice-cold mortar and pestle. NAD-ME activity was measured at 25^oC in a reaction buffer containing [50 mM HEPES-KOH (pH 8.0), 5 mM NAD, 5 mM DTT, 0.1 mM coenzyme-A, 5 mM malate, 0.2 mM EDTA] after the addition of 4 mM $MnCl_2$.

4.2.11. Data analysis

Leaf parameters were measured on area, Chl, and/or Rubisco basis. For each variable, four replicates (independent samples) were obtained for the two light treatments. The results were subjected to analysis of variance and the means were compared by the Tukey test at 5% probability.

4.3. RESULTS

4.3.1 Photosynthetic rate and PSII content

The control C_4 species generally had higher CO_2 assimilation rate (A_{growth}) measured at growth light (HL, 1000 µmol photons m^{-2} s^{-1}) followed by the C_3-C_4 then C_3 species (**Figure 4. 1A**; **Tables 4. 1** and **4. 2**). Shade reduced A_{growth} measured at growth light (LL, 200 µmol photons m^{-2} s^{-1}) to a greater extent in the C_4 and C_3-C_4 (-50% to -60%) relative to the C_3 species (-20%). Yet, A_{growth} remained slightly higher in the C_4 species relative to non-C_4 shade-grown plants (**Figure 4. 1A**; **Tables 4. 1** and **4. 2**).

The leaf content of functional PSII was quantified by flash-induced O_2 evolution. Under control conditions, the NAD-ME C_4 species had the lowest amount of PSII and the C_3 and C_3-C_4 species had the highest amount relative to the remaining species (**Figure 4. 1B**; **Tables 4. 1** and **4. 2**). Shade reduced the amount of leaf PSII in all species; this reduction was largest in *P. miliaceum* and smallest in *M. maximus* (**Figure 4. 1B**; **Tables 4. 1** and **4. 2**).

4.3.2 Using electrochromic signal to determine the photosystem stoichiometry

Having determined the percentage of unreduced P700 in PSI during illumination with moderately strong far-red light, and available for charge separation, we obtained the xenon flash-induced EC signal in the absence or presence of the far-red light (**Figure 4. S 1**). The amplitude of the fast rise decreased in the presence of moderately strong far-red light, being now contributed to by all the PSII and the small fraction *r* of the PSI reaction centres (**Figure 4. S 2**). The ratio of the PSII/PSI reaction centres was then calculated (**Figure 4. 1C**; **Table 4. 2**).The leaf PSII/PSI ratio was highest in *P. bisulcatum* (C_3) relative to other control species. Shade significantly lowered leaf PSII/PSI ratio of all species except for *P. miliaceum* and *Z. mays* (**Figure 4. 1C**; **Tables 4. 1** and **4. 2**).

4.3.3 Leaf electron fluxes

Leaf LEF_{O2}, measured using a gas-phase O_2 electrode under saturating irradiance varied among species independently of the photosynthetic type (**Figure 4. 2A**; **Tables 4. 1** and **4. 2**). LEF_{O2} was highest in *Z. mays* relative to other control species, and lowest in *M. maximus* and *P. antidolate* under control and shade conditions. Shade substantially reduced (- 40% to -60%) LEF_{O2} in all species (**Figure 4. 2A**; **Tables 4. 1** and **4. 2**).

Total electron flux through PSI (ETR1) was derived from Y(I) using a custom-built equipment for measuring redox kinetics of P700. ETR1 measured at saturating irradiance

varied amongst the grass species. In control plants, ETR1 was highest in the two NADP-ME grasses and lowest in *M. maximus* (PCK) relative to the other species (**Tables 4. 1** and **4. 2**). Shade substantially reduced ETR1 (-55% to -80%) in all species, but ETR1 remained higher in maize relative to other shaded species (**Figure 4. 2B**; **Tables 4. 1** and **4. 2**).

Cyclic electron flow (CEF), was calculated from LEF_{O2} and ETR1 (equation 4.4) measured at saturating irradiance (2000 µmol photons m^{-2} s^{-1}). CEF showed similar trends to ETR1. In control plants, CEF was highest in the two NADP-ME species, and similar amongst the other species (**Figure 4. 2C**; **Tables 4. 1** and **4. 2**). Shade significantly down-regulated CEF in all species; the reduction was most pronouncedly in the C_3 (-94%) and least in the NAD-ME species (-60%) relative to the other species, with the NADP-ME and NAD-ME species generally maintaining higher CEF under shade relative to PCK and the non-C_4 species (**Figure 4. 2C**; **Tables 4. 1** and **4. 2**).

Overall, there were good linear relationships between *A* measured at high irradiance and CEF or LEF_{O2} for individual species: however, there was no strong common relationship across the various species even within C_4 plants (**Figures 4. S 4A** and **4. S 4B**).

4.3.4 Custom-built unit versus commercial equipment for measuring leaf electron fluxes

Electron flux data from leaves measured using custom-built equipment was compared with data gathered using the commercial Dual-PAM (**Figures 4. 2A** to **4. 2C**; **Tables 4. 1**; **4. 2**; and **4. S 1**). In control plants, values of ETR2 -derived from Y(II)- measured using Dual-PAM were significantly lower compared to LEF_{O2} measured using the oxygen electrode (**Figures 4. 2A** and **4. S 4C**; **Tables 4. 1**; **4. 2**; and **4. S 1**). There was also a discrepancy between ETR1 measured using the custom-built unit for estimating P700 kinetics compared to ETR1 measured using Dual PAM (**Figures 4. 2B**; and **4. S 4D**; **Tables 4. 1**; **4. 2**; and **4. S 1**). Both relationships markedly deviated from 1:1, and showed distinct relationships for certain species such as *Z. mays* and *P. milioides* (**Figures 4. S 4C** and **4. S 4D**). Accordingly, CEF rates of control species were severely under-estimated by using Dual-PAM relative to the custom-built equipment (**Figure 4. 2C**). For the remainder of the Results and Discussion sections we only consider data collected using custom-built equipment.

4.3.5 Leaf optical properties

Absorptance spectra for all grass species were typical of vascular plants (Olle Björkman & Demmig, 1987; Knapp & Carter, 1998). The highest total leaf-specific absorptance (up to 80% of incident irradiance) was observed in the blue region (400–500 nm) and red region (600-680) around the chlorophyll *a* peak of 660–670 nm (**Figures 4. 3A** to **4. 3F** and **Figures 4. S 5A** to **4. S 5B**). The lowest total leaf-specific absorptance (less than 50% of incident irradiance) occurred around the green wavelengths (500-580 nm), the spectral region with the highest transmittance and reflectance (**Figures 4. 3A** to **4. 3F** and **Figures 4. S 5A** to **4. S 5B**).

Shade-reduced leaf absorptance of all species in the visible region of the spectrum (400 – 700 nm). This reduction was more pronounced in the green region (-3% to -18%) and around chl *a* region (660-670 nm) with 0% to -11% reduction, in comparison to the blue region (+2% to -8%) (**Figures 4. 3A** to **4. 3F**). Among the shade-grown species, *P. bisulcatum* (**Figure 4. 3A**; **Table 4. 1**) and *P. antidotale* (**Figure 4. 3E**; **Table 4. 1**) had the least reductions in total absorptance (-2% and -10%, respectively), while and *P. miliaceum* had the greatest reduction (-37%) (**Figure 4. 3C**; **Table 4. 1**). The remaining grasses showed reductions of -20% (**Figure 4. 3D**), -25% (**Figure 4. 3F**) and -26% (**Figure 4. 3B**) in total absorptance.

4.3.1. Leaf pigment content and composition

Lutein was the predominant carotenoid in all samples; the other carotenoids that accumulated, in order of abundance, were β-carotene, violaxanthin, neoxanthin, antheraxanthin and zeaxanthin (**Table 4. 3**). All species contained the same pigments, but the ratios of the individual pigments (expressed as a percentage of total carotenoid) differed between species (**Tables 4. 1** and **4. 3**).

Shade reduced the total leaf carotenoid and chlorophyll contents of *P. milioides*, *P. miliaceum* and *P. antidotale*, while chlorophyll content increased in *Z. mays* (**Figures 4. 4A** and **4. 4B**; **Table 4. 1)**. The greatest decrease was observed in *P. miliaceum* with 45% and 38% decrease in leaf carotenoid and chlorophyll content, respectively (**Figures 4. 4A** and **4. 4B**; **Table 4. 1)**. Shade also reduced the ratios of chlorophyll *a/b* and carotenoids/chlorophyll in all species; i.e. carotenoids became less abundant relative to chlorophylls under shade (**Figure 4. 4D**; **Table 4. 1)**. These results are generally consistent with the literature whereby shade/low light plants have lower chlorophyll a/b and carotenoids/chlorophyll ratios relative to sun/high light plants (Anderson, 1986). Overall, there was an excellent linear relationship between total

chlorophyll and total carotenoid contents in the leaves of all species under both light treatments (**Figure 4. S 6**).

4.3.6 Activity of photosynthetic enzymes

Among all control species, *P. milioides* had the highest leaf content of Rubisco sites and Rubisco activity. Among the control C_4 species, *P. miliaceum* had the highest Rubisco content while *Z. mays* had the highest Rubisco activity (**Tables 4. 1** and **4. 4**). Shade reduced soluble protein content and Rubisco content and activity in all plants (**Tables 4. 1** and **4. 4**). In control C_4 species, PEPC activity was highest in *Z. mays* and lowest in *P. miliaceum*. Shade reduced PEPC activity by 62–76% in all C_4 species (**Tables 4. 1** and **4. 4**).

Activities of NADP-ME, PCK, and NAD-ME enzymes were dominant in the species with the respective subtype. In addition, substantial PCK activity (16–32 µmol m^{-2} s^{-1}) and NAD-ME activity (42–58 µmol m^{-2} s^{-1}) operated as secondary decarboxylases in the control species (**Figure 4. 5B**; **Tables 4. 1** and **4. 4**). Shade reduced the activity of NADP-ME (-31% to -48%), PCK (-65%) and NAD-ME (-62%), as well as the total decarboxylases (-36% to -59%) (**Figure 4. 5A**; **Tables 4. 1** and **4. 4**). The percentage contribution of the secondary decarboxylases increased (NAD-ME) or decreased under shade except in *P. miliaceum* where the opposite occurred (**Figure 4. 5B**; **Tables 4. 1** and **4. 4**).

4.3.7 Quantum yield and assimilation quotient

Quantum yield (*QY*) was calculated as the ratio between CO_2 assimilation rates measured at ambient CO_2 and high (A_{1000}) or growth irradiance (A_{growth}) to absorbed irradiance (**Figure 4. 1D**). In control plants, QY_{1000} and QY_{growth} were generally lowest in C_3, intermediate in C_3-C_4 and highest in C_4 species. Under shade, QY_{1000} was lowest in C_3 relative to C_3-C_4 and C_4 species, while QY_{growth} was similar amongst all species (**Figure 4. 1D**; **Tables 4. 1** and **4. 2**). Within the C_4 species, there was a consistent but non-significant trend for *QY* to be highest in NADP-ME, intermediate in PCK and lowest in NAD-ME species confirming previous observations (Ehleringer & Pearcy, 1983; Sonawane *et al.*, 2018).

The assimilation quotient (AQ_{1000}) was calculated as the ratio between A_{1000} and LEF_{O2}. AQ_{1000} was highest in the PCK and NADP-ME species (although lower in *Z. mays* than *P. antidotale*) relative to the NAD-ME and the two non-C_4 species (**Tables 4. 1** and **4. 2**). Lower AQ_{1000} in *Z. mays* relative to the other NADP-ME species may reflect the high photosynthetic capacity of maize which would normally require above ambient CO_2 for

saturation (e.g. **Chapter 3**). In turn, lower AQ_{1000} and QY_{1000} in C_3 and C_3-C_4 species reflect their high photorespiration rates at ambient CO_2 relative to C_4 species.

4.4 DISCUSSIONS

The overall aim of this study was to determine how photosynthetic types and subtypes influence the variations in energy conversion efficiency and susceptibility to low light. Accordingly, we grew related C_3, C_3-C_4 and C_4 Paniceae grasses, including all three C_4 biochemical subtypes, under control (high light) and shade conditions and measured leaf chlorophyll fluorescence, photosynthesis, electron transport rates, absorptance and pigment contents.

4.4.1 Photosynthetic characteristics and responses to shade in the C_3 and C_3-C_4 species

Photosynthetic rates were lowest under control conditions and least affected by shade in the C_3 relative to the other species. The C_3-C_4 species had intermediate photosynthetic rates, while its shade responses of photosynthesis, leaf absorptance and pigments were more pronounced than the C_3 and more similar to the C_4 species. In contrast, leaf absorptance and total chlorophyll and carotenoid contents were unaffected in the C_3 species under shade. Both *QY* and *AQ* were lowest in the C_3 and intermediate in the C_3-C_4 relative to the C_4 species (**Tables 4. 1** and **4. 2**) reflecting the higher photorespiration in the non-C_4 species. Higher QY under control conditions in the C_3-C_4 relative to C_3 species reflects the reduced photorespiration rates due to the operation of the glycine shuttle in C_3-C_4 plants (Sage *et al.*, 2012) . However, this advantage disappeared under shade. Hence, a pattern is emerging of a greater energy efficiency of the C_3-C_4 species under control conditions in return for greater sensitivity under shade relative to the C_3 species. While CEF was virtually suppressed in the C_3 species under shade, C_3-C_4 plants required higher CEF, possibly to cover the costs of the C_3-C_4 shuttle and the operation of photosynthetic light and dark reactions in two cell types (Pinto *et al.*, 2011; Sage *et al.*, 2012).

The C_3 and C_3-C_4 species had higher leaf PSII contents, partially reflecting the higher Rubisco contents in these species, and partially the importance of PSII in balancing energy in these plants through photochemical and non-photochemical quenching (Ruban *et al.,* 2012). Shade significantly lowered PSII/PSI ratio in the C_3-C_4 and C_3 species (**Figure 4. 1C**; **Table 4. 1**), suggesting increased PSI content over PSII in shade grown leaves, in line with what has been observed in *Arabidopsis* grown under low light (Bailey *et al.,* 2001). It is possible that

more PSI is required to support more CEF to increase the ratio of ATP to NADPH under shade. However, this hypothesis did not reflect the low level of CEF in shade-grown C_3 and C_3-C_4 plants relative to the control (**Figure 4. 2C**; **Table 4. 1**). If the amount of PSI has increased under shade, its efficiency was severely compromised as indicated by the lower Y(I) (**Tables 4. 1** and **4. 2**). Alternatively, the decrease in PSII/PSI ratio may be explained by fewer PSII units with a larger light-harvesting antenna, relative to PSI (Anderson *et al.,* 1988; Chow *et al.,* 1990; Hihara & Sonoike, 2001; Melis, 1991; Leong & Anderson 1984; Chow *et al.* 1988). Our results support this explanation for all species (**Figure 4. 1B**).

4.4.2 Overall comparison among C_4 species

In a previous study, Sonawane *et al.* (2018) demonstrated that long-term exposure to low light (119 μmol photons m^{-2} s^{-1}) compromised the photosynthetic efficiency most in NAD-ME followed by PCK, but not in NADP-ME grasses. They observed that NAD-ME species had increased bundle sheath CO_2 leakiness, greater reduction in *QY* and greater increase in carbon isotope discrimination which was interpreted as reduced CCM efficiency and imbalance between the C_3 and C_4 cycles. This study investigates whether increased efficiency of NADP-ME (and conversely, reduced efficiency of NAD-ME) species under shade was also contributed by the light reactions and their energy conversion efficiency. Results obtained here reconfirm what Sonawane *et al.* (2018) found and reveal new insight about the energetics of the C_4 subtypes.

4.4.3 The two NADP-ME species had higher CEF and *QY* relative to other C_4 species

Amongst the C_4 species, the two NADP-ME species tended to have higher photosynthesis rates and energy efficiency, including higher Y(I), CEF, *QY* and *AQ* (**Tables 4. 1** and **4. 2**). It is well known that NADP-ME species have very low PSII content in BS chloroplasts (Anderson *et al.,* 1971; Dengler *et al.,* 1994; Drozak & Romanowska, 2006; Ghannoum *et al.,* 2005; Hernández-Prieto *et al.,* 2019; Romanowska *et al.,* 2008). As such, it has long been hypothesised that NADP-ME species require higher PSI efficiency (Furbank *et al.,* 1990). Here, higher efficiency of PSI in the two NADP-ME species was reflected in their higher operation of ETR1 and CEF under saturating light compared to other species (**Figure 4. 2B**; **Tables 4. 1** and **4. 2**). These observations support the findings that NADP-ME species have high PSI content in BS chloroplasts (Ku *et al.,* 1974; Romanowska *et al.,* 2006, 2008; Schuster *et al.,* 1985; Woo *et al.,* 1970), and hence view that BS chloroplasts of NADP-ME species generate ATP through CEF. Accordingly, we observed a strong correlation between CEF and photosynthetic rate of C_4 species under high irradiance (**Figure 4. S 4A**). High

operation of CEF around PSI might partially explain the high QY among NADP-ME species. Recently, Yin & Struik (2018) suggested that extra ATP required in C_4 photosynthesis for the CCM comes from CEF, and that ~50% of electron flux in NADP-ME species is CEF which predominantly occurs in BSCs. Shade reduced ETR1 and CEF the greatest in the two NADP-ME species (**Figure 4. 2B**; **Tables 4. 1** and **4. 2**), which highlights the dependence of photosynthetic rates on CEF in this subtype.

In the NADP-ME maize, Bellasio & Griffiths (2014b) suggested that the operation of two decarboxylase systems (NADP-ME and PCK) in the BSC increase the flexibility of energy, particularly NADPH, supply. This may be generally true (Wang *et al.,* 2014), but no appreciable changes in the decarboxylase contribution between control and shade condition was observed in any of the C_4 species (**Figures 4. 5A** and **4. 5B**). Nevertheless, based on modelling considerations, the flexibility of C_4 subtypes may be advantageous under varying environmental conditions (Wang *et al.,* 2014). For example, employing mixed C_4 pathways, either the NADP-ME type with the PCK type or the NAD-ME type with the PCK type, effectively decreases the need to maintain high concentration gradients of transport metabolites and affords high photosynthetic efficiency under a broad range of light regimes (Wang *et al.,* 2014). This may partially explain the high energy efficiency in NADP-ME and PCK relative to NAD-ME species (**Tables 4. 1** and **4. 2**). Higher *AQ* and *QY* support the view that these NADP-ME and PCK subtypes have reduced leakiness (Sonawane *et al.,* 2018), even though differences in leakiness amongst the C_4 subtypes have been difficult to detect using stable isotopic techniques (Cousins *et al.,* 2008; Henderson *et al.,* 1992).

Maize was the only C_4 species to increase leaf pigment contents and suffer no reduced absorptance under shade (**Figures 4. 3A** to **4. 3F** and **Figures 4. 4A** to **4. 4D**), indicating that shade acclimation involved optimal nitrogen allocation to chloroplast pigment-proteins in order to balance energy capture and energy transfer as previously suggested (Evans, 1989; Hikosaka & Terashima, 1995). Such adjustments are advantageous for leaves which developed under shade and, hence are more susceptible to photosystem damage than control leaves. These plants cannot dissipate excess light energy due to reduced photosynthesis, so NPQ involving carotenoids was needed. Increased chl content is also an adaptive and common response to shade, since they can provide a higher light harvesting capacity in low-light environments (Lei & Lechowicz, 1997; Lei *et al.,* 1996).

4.4.4 The NAD-ME species had the lowest energy efficiency and sensitivity to LL relative to other C_4 species

Whilst leaf PSII/PSI ratio was similar among the C_4 grasses, PSII content was lowest and most reduced by shade in the NAD-ME species. Lower PSII content in the NAD-ME species may seem surprising given that PSII activity is generally highest in isolated M and BS chloroplasts of PCK *M. maximus*, followed by NAD-ME *P. miliaceum* then NADP-ME *Z. mays* (Drozak & Romanowska, 2006). CEF was least reduced while leaf absorptance and pigment composition were most reduced in the NAD-ME species. *P. miliaceum also showed* the greatest decrease in the activity of Rubisco and decarboxylases, similar to what has previously been reported (Sonawane *et al.,* 2018). In addition, the NAD-ME species had lower *AQ* than PCK and NADP-ME species and lower *QY* than NADP-ME species. The greater sensitivity of NAD-ME species to shade was previously observed by Sonawane *et al.* (2018). Reduced leaf Y(II), F_v/F_m, LEF_{O2} and PSII content (**Tables 4. 1** and **4. 2**) under shade reflects the greater photosynthetic inhibition of NAD-ME species to low light relative to the other C_4 subtypes (Sonawane *et al.,* 2018), and might also be an acclimation response to prevent photo-inhibition (Park *et al.,* 2016). The greater shade sensitivity of *P. miliaceum* may be attributed to the inefficiency of the CCM and light harvesting components of NAD-ME subtype and inability to adjust under shade (limited plasticity) since this subtype is more adapted to open and arid habitats relative to the other two C_4 subtypes (Liu *et al.,* 2012; Schulze *et al.,* 1996; Vogel *et al.,* 1986). It also has two fully fledged linear electron transport systems in both MC and BSC which also need to adjust under shade. This is not the case for the NADP-ME subtype, and somewhat intermediate for the PCK subtype (Ghannoum *et al.,* 2005; Pinto *et al.,* 2011). The relatively greater decrease in total pigment in shaded *P. miliaceum* suggests a low capacity to acclimate under shade in comparison to other C_4 subtypes and C_3 and C_3-C_4 species (**Figures 4. 4A** to **4. 4D**). This finding again supports the study of Sonawane *et al.* (2018) demonstrating that NADP-ME and PCK species are more efficient under shade compared to NAD-ME species.

4.4.5 Changes in leaf pigments and absorptance under shade reflect composition of light harvesting complexes rather than increased photoprotection

Photosynthetic pigments might play an important role behind the *QY* variations observed among plant species because they can balance the absorption of light energy. Strong correlations have been observed between total chlorophyll and total carotenoid contents (**Figure 4. S 4B**) suggesting the related functions of these pigments in leaves. Results from HPLC showed that all control species had the same pigment composition in leaf samples, and

there were no significant differences observed in the quantity of total carotenoids or chlorophylls (**Tables 4. 1** and **4. 3**). Lutein was the most abundant leaf carotenoid with C_4 species having the highest content (**Tables 4. 1** and **4. 3**). Lutein often accounts for >50% of the total carotenoid pool in plants. It is localized in LHCs and is the only carotenoid detected in the PSII core (Bassi *et al.,* 1993; Kühlbrandt *et al.*, 1994). In addition, lutein is required for the *in vitro* reconstitution of LHCs (Cammarata *et al.,* 2013; Plumley & Schmidt, 2006). Since lutein was more abundant in C_4 compared to C_3 and C_3-C_4 leaves, it can be suggested that C_4 leaves have more LHCII and are more efficient in protecting PSII cores against photo-inhibition. This was expected because C_4 plants are more dominant in open and high light environments (Edwards *et al.,* 2010; Ehleringer *et al.*, 1997).

Another abundant pigment detected in the leaf of all species is violaxanthin (**Tables 4. 1** and **4. 3**). Violaxanthin plays an important role in the dissipation of excessive energy in the antenna chlorophyll via the xanthophyll cycle (Demmig-Adams, 1998; Demmig & Bjorkman, 1987). This mechanism which involves the light-dependent interconversions of three xanthophylls (zeaxanthin, antheraxanthin, and violaxanthin) maintains the energy balance under very high irradiance. Excess light energy can be transferred to xanthophylls for harmless thermal dissipation (Jin, 2003; Yamamoto, 1979). Low amounts of zeaxanthin in leaves of C_3 and C_4 species in comparison to C_3-C_4 grass might indicate that these plants were not experiencing light stress under their growing conditions (**Tables 4. 1** and **4. 3**). Zeaxanthin is generally not formed in leaves at low irradiance, but as the amount of energy captured begins to exceed that which can be used in photosynthesis, more zeaxanthin is formed from violaxanthin (Demmig-Adams & Adams, 1992).

The ratios of leaf chl *a/b* were not significantly different among control species. However, shade decreased chl *a/b* ratios in all species (**Figure 4. 4C**). Chl *a* is the most commonly used photosynthetic pigment and absorbs blue, red and violet wavelengths in the visible spectrum. Chl *b* primarily absorbs blue light and is used to complement the absorption spectrum of chl *a* by extending the range of absorbed light wavelengths. The chl-protein complex of both photosystems is composed of a core complex (reaction centre) and a light-harvesting complex (Thornber, 1986). The chl *a/b* ratios are greater in the core complex than the light-harvesting complex in both photosystems. A low chl *a/b* ratio could imply an increased proportion of light-harvesting complexes relative to reaction centres (Green & Durnford, 1996; Hikosaka & Terashima, 1995). This might be the case for the lower leaf chl *a/b* ratios and lower carotenoids/chl ratios observed in all shade-grown plants (**Figures 4. 4C** and **4. 4D**) which might reflect the strategy of these plants to prioritise light harvesting (through chl) more than

photoprotection (through carotenoids). This decrease in ratios might also reflect increased PSI units (size or number) which are also detected in decreased leaf PSII/PSI ratios of shade-grown plants measured using ECS (**Tables 4. 1** and **4. 2**). This result also suggests that nitrogen might have been allocated more to increase light-harvesting complexes rather than reaction centres as part of acclimation to balance energy absorption under shade. Hikosaka & Terashima (1995) suggested that chl *a/b* ratio can be a useful indicator of nitrogen partitioning within a leaf, because this ratio should be positively correlated with the ratio of PSII cores to light harvesting chlorophyll-protein complex (LHCII). It was also showed by Evans (1989) and Green & Durnford, (1996) that LHCII contains the majority of chl *b*, and consequently has a lower chl *a/b* ratio than other chlorophyll binding proteins associated with PSII. The increase in light-harvesting complexes relative to reaction centres might be an adaptation to broaden the spectral range over which PSI and PSII absorb light (Yamazaki *et al.*, 2005).

Lower absorptance under shade can, at least partially, be explained by lower chlorophyll and carotenoids contents (**Figures 4. 3A** to **4. 3F**). Chlorophyll content is a sensitive indicator of plant stress (Evans, 1993; Lin & Ehleringer, 1983; Vogelmann, 1993). Increased leaf reflectance (decreased absorptance) within the PAR wavebands, specifically 535–640 nm (green) and 685–700 nm (red) in response to environmental conditions was a result of decreased chlorophyll content. Leaf spectral properties are more consistently altered in response to stress in the visible wavelengths than in the remainder of the incident solar spectrum (Carter, 1993; Carter *et al.*, 1992). Similarly, leaf absorptance in the current study noticeably decreased in the green region (500-580 nm), where non-photosynthetic pigments such as anthocyanins also absorb (Gould *et al.*, 1995; Paradiso *et al.*, 2011; Smillie & Hetherington, 1999), and in the chl *a* region (660-670 nm), which reflects the lower chl *a/b* ratio in shaded plants. These changes can also be due to alterations in leaf structure under shade. Reduced leaf thickness and changes in arrangement of cells within a leaf which can increase transmitted light, thus preventing photo-inhibition (Vogelmann, 2003).

4.4.6 Comparison between custom-built and commercial equipment

The common approach to calculate CEF is to determine ETR2 and then subtracting it from ETR1 using chl fluorescence. However, Fan *et al.* (2016) pointed out that there are some uncertainties for using chl fluorescence in estimating ETR2. One of these is an underestimation of the signal detected from the leaf because this signal comes from an unspecified depth in the leaf tissue and that depth may vary during the course of an experiment, for example, due to chloroplast movement (Sato & Kadota, 2006), leading to

underestimation of CEF (**Figure 4. 2C**). To avoid this, we calculated ETR2 based on whole-tissue measurement of the gross rate of oxygen evolution (LEF_{O2}). According to Fan *et al.* (2016), this can be validly compared with ETR1 obtained from Y(I) because the $P700^+$ signal is also a whole-tissue measurement, since 820 and 870 nm measuring beams are only weakly absorbed by the leaf tissue and are, therefore, multiply scattered in the tissue until they are finally absorbed; subtraction of LEF_{O2} from ETR1 is then valid, as both refer to the same leaf tissue. Estimation of ETR1 by two different equipment used the same principle of the Y(I)-based electron flux. However, the source of actinic light and saturating pulse is different between the two pieces of equipment. Dual-PAM uses the red light as a source of actinic and saturating light while the custom-built equipment uses white light from a halogen lamp. ETR1 is directly estimated by Dual-PAM using equation 6, utilising 0.5 as a default value for f_I. The custom-built unit separately measures the components of Y(I) (see **Methods**) and the f_I values were experimentally determined (Sagun *et al.,* 2019). These factors gave different values of ETR1 which then affected CEF calculations (**Figure 4. S 4D**)

The ratio of PSII/PSI was independently measured using electrochromic signal (ECS) which reflects trans-membrane charge transfer through the thylakoid membrane (Witt, 1979). The reliability of this method was evaluated by Fan *et al.* (2007) using spinach leaves by comparing the calculated values with two other methods, namely electron paramagnetic resonance (EPR) (Danielsson *et al.,* 2004) and by separately determining the content of functional PSII and PSI in leaf segments by the O_2 yield per single turnover-flash and by photo-oxidation of P700 in thylakoids isolated from the same leaf. They found that the ratios obtained using ECS were comparable to the values obtained using the two other approaches. The ECS offers a similar advantage, being a "voltmeter reading" determined by the number of reaction centres of either photosystem present, and corresponding to a change in delocalized electric potential difference generated across the thylakoid membrane upon charge separation in the reaction centres. Further, it can also be applied to leaf segments without the need to isolate thylakoid membranes, thus avoiding any loss of PSI complexes via breakage of stromal lamellae from the membrane system, or decline of PSII activity during isolation of thylakoids.

4.5 CONCLUSIONS

Variations in quantum yield among C_4 subtypes can be attributed to several factors such as the efficiency of light harvesting components under changing environmental conditions. This study was undertaken to investigate differences in the efficiency of light energy conversion in leaves of representative species of C_4 plants from three biochemical subtypes, together with C_3 and C_3-C_4 grasses grown under full sunlight and shade (20% of full sunlight). Measurements of the activity and stoichiometry of the light harvesting components in leaves and BS were done using methods which maintained the integrity of the chloroplast structure. Results showed that NAD-ME species were generally outperformed by NADP-ME and PCK species under shade, while C_4 species were generally more efficient than C_3 and C_3-C_4 species under sun and shade conditions. In general, the observed high *QY* of NADP-ME species by Ehleringer & Pearcy (1983) might be associated with the comparatively greater plasticity adjustments in the light harvesting components of leaf under varying environmental conditions. This is very important acclimation characteristic as it maximises light energy absorption while preventing photo-inhibition under stress conditions such as long-term shade. This ensures the light reactions can still provide the right ATP/NADPH ratio even under limited supply of light energy. This study elucidates the characteristics and low light acclimation of light energy conversion in grasses with different photosynthetic types.

Table 4. 1 Statistical summary

Summary of statistical analysis using two-way ANOVA for the effects of shade and species on various leaf parameters collected from 10 plants grown under full sunlight (~800 µmol photons m^{-2} s^{-1}) or shaded (~200 µmol photons m^{-2} s^{-1}) conditions and measured at 200 µmol photons m^{-2} s^{-1} (LL), 1000 µmol photons m^{-2} s^{-1} (HL) or 2000 µmol photons m^{-2} s^{-1} (SL).

Parameter	Main effects (P)		Interactions (P)
	Species	Treatment	Species x Treatment
PSII content (µmol m^{-2})	0.000	0.000	0.037
PSII/PSI ratio	0.000	0.000	0.000
Absorptance at 470 nm	0.000	0.000	0.046
Absorptance at 550 nm	0.000	0.000	0.026
Absorptance at 665 nm	0.000	0.000	0.004
Neoxanthin (%)	0.000	0.020	0.249
Violaxanthin (%)	0.000	0.000	0.000
Antheraxanthin (%)	0.046	0.341	0.176
Lutein (%)	0.000	0.000	0.342
Zeaxanthin (%)	0.000	0.132	0.000
β-carotene (%)	0.000	0.000	0.049
Chlorophyll *a/b*	0.000	0.000	0.580
Total carotenoids (mg m^{-2})	0.004	0.000	0.000
Total chlorophyll (mg m^{-2})	0.000	0.000	0.000
Total carotenoids/total chlorophyll	0.000	0.000	0.000
F_v/F_m	0.000	0.000	0.017
Dual-PAM Y(I) (µmol e^- m^{-2} s^{-1})	0.000	0.000	0.002
Dual-PAM Y(II) (µmol e^- m^{-2} s^{-1})	0.000	0.000	0.002
Dual-PAM ETR1 (µmol e^- m^{-2} s^{-1})	0.003	0.000	0.002
Dual- PAM ETR2 (µmol e^- m^{-2} s^{-1})	0.000	0.000	0.003
Dual-PAM CEF (µmol e^- m^{-2} s^{-1})	0.000	0.001	0.023
Y(I)	0.000	0.000	0.000
ETR1 (µmol e^- m^{-2} s^{-1})	0.000	0.000	0.000
LEF_{O2} (µmol e^- m^{-2} s^{-1})	0.000	0.000	0.000
CEF (µmol e^- m^{-2} s^{-1})	0.000	0.000	0.000
A_{1000} (µmol CO_2 m^{-2} s^{-1})	0.000	0.000	0.001
A_{growth} (µmol CO_2 m^{-2} s^{-1})	0.000	0.000	0.000
AQ_{1000} (mol CO_2 mol^{-1} O_2)	0.000	0.0878	0.216
QY_{1000} (mol CO_2 mol^{-1} photons)	0.000	0.000	0.000
QY_{growth} (mol CO_2 mol^{-1} photons)	0.000	0.000	0.000
Leaf Rubisco activity (µmol CO_2 m^{-2} s^{-1})	0.000	0.000	0.000
K_{cat} (s^{-1})	0.000	0.000	0.025
Rubisco content (µmol LSU sites m^{-2})	0.000	0.000	0.000
Protein content (g m^{-2})	0.001	0.009	0.167
PEPC activity (µmol CO_2 m^{-2} s^{-1})	0.000	0.000	0.660
NADP-ME activity (µmol CO_2 m^{-2} s^{-1})	0.000	0.000	0.000
PCK activity (µmol CO_2 m^{-2} s^{-1})	0.000	0.000	0.001
NAD-ME activity (µmol CO_2 m^{-2} s^{-1})	0.000	0.000	0.000
Total decarboxylase activity (µmol CO_2 m^{-2} s^{-1})	0.000	0.000	0.000

Table 4. 2 Parameters measured using Licor and custom-built equipment (as described in MM) in representative species of C_3, C_3-C_4, and C_4 plants

Photosynthetic rate measured at growth irradiance, A_{growth} (1000 or 200 µmol photons m^{-2} s^{-1}) and other electron transport parameters measured under saturating light (2000 µmol m^{-2} s^{-1}) using custom-built equipment (as described in MM) in representative species of C_3, C_3-C_4, and C_4 plants grown under control (~800 µmol photons m^{-2} s^{-1}) and shaded (~200 µmol photons m^{-2} s^{-1}) conditions. Y(I) is the effective quantum yield of PSI, LEF_{O2} is the total electron flux, ETR1 is the electron transport rate through PSI, CEF is the cyclic electron flux around PSI, AQ_{1000} is the assimilation quotient (ratio of A_{1000} to LEF_{O2}), and QY is the ration of A (A_{growth} or A_{1000}) to absorbed light. Letters indicate the ranking (highest = a) within each treatment using multiple-comparison Tukey's post-hoc test. Values are means ± s.e. of species (n = 4 plants).

Parameter	Light	*Panicum bisulcatum*	*Panicum milioides*	*Panicum miliaceum*	*Megathyrsus maximus*	*Panicum antidotale*	*Zea mays*
		C_3	**C_3-C_4**	**NAD-ME**	**PCK**	**NADP-ME**	**NADP-ME**
A_{growth} (µmol $m^{-2}s^{-1}$)	CONTROL	15.1 ± 1.2 d	22.7 ± 1.2 c	25.7 ± 1.0 bc	28.5 ± 1.0 b	29.01 ± 2.35 ab	34.06 ± 1.86 a
	SHADE	8.33 ± 0.33 ab	8.3 ± 0.75 b	12.42 ± 0.44 a	12.13 ± 0.29 ab	11.57 ± 0.52 ab	10.99 ± 0.49 ab
	Shade/Control	*0.8 ± 0.13 a*	*0.37 ± 0.07 b*	*0.5 ± 0.02 b*	*0.43 ± 0.02 b*	*0.41 ± 0.06 b*	*0.33 ± 0.04 b*
PSII content (µmol m^{-2})	CONTROL	2.85 ± 0.12 a	2.78 ± 0.09 a	1.99 ± 0.06 b	2.34 ± 0.06 ab	2.19 ± 0.11 b	2.33 ± 0.06 ab
	SHADE	1.65 ± 0.06 a	1.19 ± 0.05 ab	0.62 ± 0.23 c	1.56 ± 0.22 a	1.20 ± 0.10 ab	1.02 ± 0.16 bc
	Shade/Control	*0.58 ± 0.02 ab*	*0.43 ± 0.03 ab*	*0.31 ± 0.12 b*	*0.67 ± 0.1 a*	*0.55 ± 0.06 ab*	*0.43 ± 0.06 ab*
PSII/PSI	CONTROL	1.46 ± 0.08 a	1.09 ± 0.02 b	1.03 ± 0.07 b	1.00 ± 0.05 b	1.11 ± 0.05 b	0.97 ± 0.04 b
	SHADE	0.99 ± 0.01 a	0.53 ± 0.01 b	0.94 ± 0.02 a	0.63 ± 0.03 b	0.62 ± 0.02 b	0.91 ± 0.05 a
	Shade/Control	*0.68 ± 0.03 b*	*0.48 ± 0.01 b*	*0.93 ± 0.07 a*	*0.64 ± 0.05 b*	*0.56 ± 0.04 b*	*0.94 ± 0.06 a*
Y(I)	CONTROL	0.18 ± 0 e	0.24 ± 0.01 c	0.21 ± 0 d	0.15 ± 0 e	0.31 ± 0.01 b	0.37 ± 0.02 a
	SHADE	0.08 ± 0 bc	0.1 ± 0 ab	0.09 ± 0.01 b	0.05 ± 0.01 c	0.07 ± 0 bc	0.12 ± 0.01 a
	Shade/Control	*0.44 ± 0.02 a*	*0.39 ± 0.01 ab*	*0.41 ± 0.03 ab*	*0.35 ± 0.04 ab*	*0.22 ± 0.01 c*	*0.33 ± 0.01 b*

LEF_{O2} (µmol e^- m^{-2} s^{-1})	CONTROL	79.9 ± 5.1 c	124.3 ± 3 b	129.6 ± 2.2 b	67.6 ± 1.1 d	68.1 ± 2.1 d	142.5 ± 1.4 a
	SHADE	48.7 ± 0.2 bc	48.1 ± 3.7 bc	54.4 ± 2.6 b	31.1 ± 1.3 d	41.8 ± 1.2 c	66 ± 1 a
	Shade/Control	*0.62 ± 0.04 a*	*0.39 ± 0.03 b*	*0.42 ± 0.03 b*	*0.46 ± 0.01 b*	*0.61 ± 0.02 a*	*0.46 ± 0.01 b*
ETR1 (µmol e^- m^{-2} s^{-1})	CONTROL	152.2 ± 3.4 d	207.4 ± 8.7 c	218.1 ± 2.3 c	153 ± 3.1 d	320.8 ± 7.4 b	373.1 ± 16.9 a
	SHADE	53.7 ± 3.1 c	64.8 ± 1.8 bc	89.2 ± 4.9 b	53.6 ± 6.7 c	69.6 ± 1.2 bc	121 ± 4.9 a
	Shade/Control	*0.35 ± 0.01 a*	*0.31 ± 0.01 ab*	*0.41 ± 0.03 a*	*0.35 ± 0.04 a*	*0.22 ± 0.01 b*	*0.33 ± 0.01 a*
CEF (µmol e^- m^{-2} s^{-1})	CONTROL	72.3 ± 8.2 b	83.1 ± 7.6 b	88.5 ± 3.8 b	85.4 ± 4.1 b	252.7 ± 7.3 a	230.6 ± 17.3 a
	SHADE	4.9 ± 3 b	16.7 ± 2.7 b	34.9 ± 6.8 ab	22.6 ± 7.7 b	27.8 ± 1 ab	55 ± 4.9 a
	Shade/Control	*0.06 ± 0.04 b*	*0.21 ± 0.05 ab*	*0.41 ± 0.1 a*	*0.27 ± 0.09 ab*	*0.11 ± 0.01 b*	*0.24 ± 0.01 ab*
AQ_{1000} (mol CO_2 mol^{-1} O_2)	CONTROL	0.19 ± 0.01 b	0.18 ± 0.01 b	0.2 ± 0.01 b	0.42 ± 0.01 a	0.43 ± 0.04 a	0.24 ± 0.01 b
	SHADE	0.23 ± 0.02 b	0.22 ± 0.02 b	0.21 ± 0.01 b	0.47 ± 0.03 a	0.38 ± 0.03 a	0.28 ± 0.01 b
	Shade/Control	*1.05 ± 0.1 a*	*1.35 ± 0.13 a*	*1.23 ± 0.08 a*	*1.24 ± 0.1 a*	*0.86 ± 0.1 a*	*1.04 ± 0.07 a*
QY_{1000} (mol CO_2 mol^{-1} photons)	CONTROL	0.014 ± 0.002 c	0.025 ± 0.002 b	0.028 ± 0.001 ab	0.030 ± 0.001 ab	0.031 ± 0.003 ab	0.036 ± 0.002 a
	SHADE	0.012 ± 0.001 b	0.012 ± 0.002 ab	0.014 ± 0.001 ab	0.015 ± 0.001 ab	0.017 ± 0.001 a	0.020 ± 0.001 a
	Shade/Control	0.89 ± 0.11 a	0.51 ± 0.1 b	0.49 ± 0.02 b	0.52 ± 0.03 b	0.57 ± 0.06 b	0.57 ± 0.04 b
QY_{growth} (mol CO_2 mol^{-1} photons)	CONTROL	0.014 ± 0.002 c	0.025 ± 0.002 b	0.028 ± 0.001 ab	0.030 ± 0.001 ab	0.031 ± 0.003 ab	0.036 ± 0.002 a
	SHADE	0.012 ± 0.001 a	0.010 ± 0.002 a	0.015 ± 0.001 a	0.013 ± 0.001 a	0.013 ± 0.001 a	0.012 ± 0.001 a
	Shade/Control	0.92 ± 0.13 a	0.4 ± 0.09 b	0.55 ± 0.03 b	0.44 ± 0.02 b	0.42 ± 0.06 b	0.34 ± 0.04 b

Table 4. 3 Content of leaf pigments in representative C_3, C_3-C_4, and C_4 species

Leaf pigments in representative C_3, C_3-C_4, and C_4 species grown under control (~800 µmol photons m^{-2} s^{-1}) or shaded (~200 µmol photons m^{-2} s^{-1}) conditions. Letters indicate the ranking within each species using multiple-comparison Tukey's post-hoc test. Values are means ± s.e. of species (*n* = 4 plants).

Parameter	Light	*Panicum bisulcatum*	*Panicum milioides*	*Panicum miliaceum*	*Megathyrsus maximus*	*Panicum antidotale*	*Zea mays*
		C_3	**C_3-C_4**	**NAD-ME**	**PCK**	**NADP-ME**	**NADP-ME**
Neoxantin (%)	CONTROL	9.5 ± 0.2 ab	10 ± 0.2 a	8.4 ± 0.2 c	9.9 ± 0.3 a	8.6 ± 0.2 bc	8.0 ± 0.1 c
	SHADE	10.3 ± 0.0 a	10.6 ± 0.3 a	8.3 ± 0.2 b	10.7 ± 0.3 a	8.6 ± 0.4 b	8.1 ± 0.3
	Shade/Control	*1.09 ± 0.03 a*	*1.06 ± 0.04 a*	*1 ± 0.05 a*	*1.09 ± 0.06 a*	*1 ± 0.07 a*	*1.01 ± 0.03 a*
Violaxanthin (%)	CONTROL	20.5 ± 0.5 a	20.3 ± 0.8 ab	19.5 ± 0.6 ab	18.5 ± 0.5 ab	18.5 ± 0.5 ab	17.1 ± 0.5 b
	SHADE	15.9 ± 0.0 b	17.9 ± 0.3 a	15.9 ± 0.2 b	9.2 ± 0.2 e	14.0 ± 0.4 c	12.0 ± 0.2 d
	Shade/Control	*0.78 ± 0.02 ab*	*0.89 ± 0.05 a*	*0.82 ± 0.03 ab*	*0.5 ± 0.01 c*	*0.76 ± 0.04 ab*	*0.7 ± 0.02 b*
Antheraxanthin (%)	CONTROL	1.7 ± 0.0 ab	1.6 ± 0.0 ab	1.8 ± 0.1 ab	1.6 ± 0.1 b	1.7 ± 0.0 ab	1.8 ± 0.0 a
	SHADE	1.5 ± 0.0 a	1.6 ± 0.0 a	2.0 ± 0.0 a	1.8 ± 0.3 a	1.9 ± 0.1 a	1.7 ± 0.0 a
	Shade/Control	*0.87 ± 0.01 a*	*1.01 ± 0.03 a*	*1.11 ± 0.04 a*	*1.17 ± 0.22 a*	*1.11 ± 0.07 a*	*0.97 ± 0.03 a*
Lutein (%)	CONTROL	36.8 ± 0.7 c	37.3 ± 0.3 c	39.2 ± 0.8 bc	40.9 ± 0.9 ab	39.5 ± 0.4 abc	42.1 ± 0.4 a
	SHADE	42.4 ± 0.0 c	43.0 ± 0.2 c	43.7 ± 0.4 bc	47.8 ± 0.5 a	45.1 ± 0.4 b	48.0 ± 0.2 a
	Shade/Control	*1.15 ± 0.02 a*	*1.15 ± 0.01 a*	*1.12 ± 0.02 a*	*1.17 ± 0.04 a*	*1.14 ± 0.02 a*	*1.14 ± 0.01 a*

Zeaxanthin (%)	CONTROL	1.5 ± 0.1 b	3.1 ± 0.3 a	1.3 ± 0.3 b	0.9 ± 0.1 b	1.4 ± 0.4 b	1.6 ± 0.2 b
	SHADE	1.7 ± 0 b	0.6 ± 0.1 c	0.3 ± 0.0 c	4.5 ± 0.5 a	0.6 ± 0.1 c	0.6 ± 0.1 c
	Shade/Control	*1.16 ± 0.07 b*	*0.22 ± 0.05 b*	*0.28 ± 0.06 b*	*5.42 ± 0.86 a*	*0.68 ± 0.31 b*	*0.42 ± 0.07 b*
β-Carotene (%)	CONTROL	30 ± 0.2 ab	27.8 ± 0.2 b	29.9 ± 0.5 ab	28.3 ± 1.0 ab	30.3 ± 0.5 a	29.5 ± 0.4 ab
	SHADE	28.2 ± 0.0 b	26.3 ± 0.2 c	29.8 ± 0.5 a	25.9 ± 0.2 c	29.8 ± 0.4 a	29.6 ± 0.2 a
	Shade/Control	*0.94 ± 0.01 a*	*0.95 ± 0.01 a*	*1 ± 0.02 a*	*0.92 ± 0.04 a*	*0.98 ± 0.03 a*	*1 ± 0.01 a*
chlorophyll *a* (mg m^{-2})	CONTROL	382.9 ± 21.8 a	332.2 ± 36.2 a	366 ± 35 a	284.5 ± 33.7 a	378.1 ± 27.4 a	365.9 ± 6.0 a
	SHADE	355.6 ± 2.5 ab	175.8 ± 14.0 d	179.8 ± 28.4 d	301 ± 11.8 bc	212.6 ± 21.9 cd	450.7 ± 8.3 a
	Shade/Control	*0.94 ± 0.05 ab*	*0.55 ± 0.07 c*	*0.53 ± 0.15 c*	*0.75 ± 0.03 bc*	*0.81 ± 0.07 bc*	*1.23 ± 0.01 a*
chlorophyll *b* (mg m^{-2})	CONTROL	95.2 ± 6.4 a	82.3 ± 9.5 a	83.4 ± 8.7 a	73.3 ± 8.8 a	86.27 ± 5.95 a	85.6 ± 1.3 a
	SHADE	94.3 ± 0.6 ab	48.2 ± 4.0 c	44.4 ± 6.5 c	87 ± 3.7 b	53.74 ± 5.92 c	113.9 ± 1.6 a
	Shade/Control	*1 ± 0.07 abc*	*0.61 ± 0.08 cd*	*0.58 ± 0.17 d*	*0.74 ± 0.02 bcd*	*1.02 ± 0.09 ab*	*1.33 ± 0.01 a*

Table 4. 4 Activities of Rubisco, PEPC and decarboxylases and soluble protein content

Activities of Rubisco, PEPC and decarboxylases and soluble protein content measured in leaf of representative species of C_3, C_3-C_4, and C_4 plants grown under control (~800 µmol photons m^{-2} s^{-1}) and shaded (~200 µmol photons m^{-2} s^{-1}) conditions. Letters indicate the ranking (highest = a) within each species using multiple-comparison Tukey's post-hoc test. Values are means ± s.e. of species (*n* = 4 plants; NA = not applicable).

Parameter	**Light**	***Panicum bisulcatum***	***Panicum milioides***	***Panicum miliaceum***	***Megathyrsus maximus***	***Panicum antidotale***	***Zea mays***
		C_3	**C_3-C_4**	**NAD-ME**	**PCK**	**NADP-ME**	**NADP-ME**
Rubisco activity (µmol CO_2 $m^{-2}s^{-1}$)	CONTROL	21.9 ± 3.8 bc	45.4 ± 2.3 a	14.2 ± 0.4 cd	10.3 ± 0.2 d	15.0 ± 0.2 bcd	23.4 ± 0.8 b
	SHADE	5.8 ± 0.5 b	10.3 ± 0.5 a	2.8 ± 0.3 c	6.8 ± 0.5 b	6.7 ± 0.5 b	11.8 ± 0.2 a
	Shade/Control	*0.27 ± 0.05 c*	*0.23 ± 0.01 c*	*0.2 ± 0.03 c*	*0.66 ± 0.04 a*	*0.44 ± 0.03 b*	*0.51 ± 0.01 b*
Rubisco content (µmol LSU sites m^{-2})	CONTROL	10.6 ± 1.0 b	37.4 ± 5.6 a	8.8 ± 0.5 b	2.9 ± 0.1 b	5.4 ± 0.3 b	6.1 ± 0.3 b
	SHADE	6.0 ± 0.3 b	10.3 ± 0.4 a	2.3 ± 0.4 c	2.9 ± 0.1 c	2.7 ± 0.2 c	4.7 ± 0.5 c
	Shade/Control	*0.58 ± 0.02 bc*	*0.29 ± 0.04 d*	*0.26 ± 0.05 d*	*0.98 ± 0.03 a*	*0.49 ± 0.02 cd*	*0.78 ± 0.1 ab*
K_{cat} (s^{-1})	CONTROL	2.1 ± 0.4 cd	1.3 ± 0.2 d	1.6 ± 0.10 d	3.5 ± 0.1 ab	2.8 ± 0.2 bc	3.9 ± 0.2 a
	SHADE	1.0 ± 0.1 b	1.0 ± 0.1 b	1.3 ± 0.2 b	2.4 ± 0.10 a	2.5 ± 0.3 a	2.6 ± 0.3 a
	Shade/Control	*0.48 ± 0.09 a*	*0.82 ± 0.13 a*	*0.8 ± 0.15 a*	*0.68 ± 0.05 a*	*0.91 ± 0.07 a*	*0.67 ± 0.09 a*
PEPC activity (µmol $m^{-2}s^{-1}$)	CONTROL	NA	NA	82.4 ± 1.6 c	99.0 ± 6.6 ab	87.1 ± 6.0 bc	110.8 ± 8.2 a
	SHADE	NA	NA	20.1 ± 0.6 b	31.7 ± 1.5 ab	27.9 ± 0.8 ab	41.7 ± 0.7 a
	Shade/Control			*0.24 ± 0.01 b*	*0.32 ± 0.03 ab*	*0.32 ± 0.03 ab*	*0.38 ± 0.03 a*

NADP-ME activity ($\mu mol\ m^{-2}s^{-1}$)	CONTROL	NA	NA	3.3 ± 0.1 c	0.7 ± 0.0 d	44.3 ± 0.4 b	46.6 ± 0.4 a
	SHADE	NA	NA	0.4 ± 0.1 c	0.4 ± 0.0 c	23.2 ± 1.1 b	32.1 ± 1.4 a
	Shade/Control			*0.13 ± 0.03 c*	*0.62 ± 0.06 ab*	*0.52 ± 0.02 b*	*0.69 ± 0.04 a*
NAD-ME activity ($\mu mol\ m^{-2}s^{-1}$)	CONTROL	NA	NA	50.8 ± 12.4 a	14.9 ± 0.6 b	10.4 ± 0.6 b	11.4 ± 1.0 b
	SHADE	NA	NA	19.1 ± 2.2 a	12.9 ± 1.2 b	8.4 ± 0.4 b	10.5 ± 0.6 b
	Shade/Control			*0.34 ± 0.02 b*	*0.81 ± 0.08 a*	*0.84 ± 0.08 a*	*1.04 ± 0.09 a*
PCK activity ($\mu mol\ m^{-2}s^{-1}$)	CONTROL	NA	NA	20.9 ± 1.9 c	42.4 ± 3.7 a	32.1 ± 1.9 b	16.2 ± 1.0 c
	SHADE	NA	NA	11.5 ± 1.3 ab	14.9 ± 1.1 a	15.0 ± 0.7 a	5.0 ± 1.4 bc
	Shade/Control			*0.56 ± 0.08 a*	*0.36 ± 0.04 ab*	*0.47 ± 0.03 ab*	*0.3 ± 0.07 b*
Protein content ($g\ m^{-2}$)	CONTROL	38.9 ± 1.4 bc	66.1 ± 5.9 a	38.7 ± 4.6 ab	50.7 ± 4.5 c	25.5 ± 1.4 bc	37.7 ± 1.4 bc
	SHADE	22.2 ± 2.1 a	52.2 ± 12.5 b	21.0 ± 1.1 a	20.8 ± 2.7 a	21.0 ± 0.3 a	48.0 ± 19.9 b
	Shade/Control	*0.58 ± 0.07 a*	*0.71 ± 0.35 a*	*0.45 ± 0.04 a*	*0.82 ± 0.04 a*	*1.05 ± 0.44 a*	*0.74 ± 0.05 a*

Table 4. S 1 Dual-PAM parameters

Dual-PAM parameters measured at saturating light (2000 µmol m^{-2} s^{-1}) in representative C_3, C_3-C_4, and C_4 species grown under control (~800 µmol photons m^{-2} s^{-1}) or shaded (~200 µmol photons m^{-2} s^{-1}) conditions. F_v/F_m is the maximum quantum yield of PSII, Y(I) and Y(II) are the effective quantum yield of PSI and PSII, ETR1 and ETR2 are the electron transport rate through PSI and PSI, and CEF is the cyclic electron flux around PSI. Letters indicate the ranking (highest = a) within each species using multiple-comparison Tukey's post-hoc test. Values are means ± s.e. of species (*n* = 4 plants).

Parameter	Light	*Panicum bisulcatum*	*Panicum milioides*	*Panicum miliaceum*	*Megathyrsus maximus*	*Panicum antidotale*	*Zea mays*
		C_3	**C_3-C_4**	**NAD-ME**	**PCK**	**NADP-ME**	**NADP-ME**
F_v/F_m	CONTROL	0.79 ± 0 a	0.78 ± 0.01 ab	0.71 ± 0.01 c	0.78 ± 0 ab	0.76 ± 0 b	0.75 ± 0.01 b
	SHADE	0.74 ± 0.02 a	0.69 ± 0.01 b	0.68 ± 0.01 b	0.73 ± 0 a	0.71 ± 0.01 ab	0.7 ± 0.01 ab
	Shade/Control	*0.93 ± 0.03 ab*	*0.88 ± 0.01 b*	*0.95 ± 0 a*	*0.93 ± 0 ab*	*0.94 ± 0.01 a*	*0.94 ± 0 a*
Y(I)	CONTROL	0.14 ± 0.01 a	0.13 ± 0 ab	0.1 ± 0.01 bc	0.11 ± 0.01 ab	0.08 ± 0.01 c	0.12 ± 0 ab
	SHADE	0.09 ± 0.01 ab	0.09 ± 0.01 a	0.07 ± 0.01 ab	0.06 ± 0.01 b	0.09 ± 0.01 a	0.1 ± 0.01 a
	Shade/Control	*0.64 ± 0.05 ab*	*0.62 ± 0.12 b*	*0.49 ± 0.05 b*	*0.64 ± 0.13 ab*	*1.04 ± 0.04 a*	*0.83 ± 0.11 ab*
Y(II)	CONTROL	0.06 ± 0 a	0.03 ± 0 b	0.02 ± 0 c	0.03 ± 0 bc	0.02 ± 0 bc	0.02 ± 0 bc
	SHADE	0.03 ± 0 a	0.01 ± 0 b	0.01 ± 0 b	0.02 ± 0 b	0.02 ± 0 b	0.02 ± 0 b
	Shade/Control	*0.59 ± 0.03 ab*	*0.39 ± 0.09 b*	*0.43 ± 0.05 ab*	*0.51 ± 0.1 ab*	*0.84 ± 0.13 a*	*0.69 ± 0.15 ab*
ETR2 (µmol e^- m^{-2} s^{-1})	CONTROL	47.8 ± 2.3 a	27.3 ± 2 b	17.6 ± 1.9 c	25.3 ± 1.2 bc	20.1 ± 1.3 bc	18.9 ± 0.8 bc
	SHADE	28.3 ± 2.6 a	10.4 ± 2.2 bc	7.4 ± 1.5 c	13.3 ± 2.8 bc	16.4 ± 1.8 b	13.1 ± 2.9 bc
	Shade/Control	*0.59 ± 0.03 ab*	*0.39 ± 0.08 b*	*0.41 ± 0.06 ab*	*0.52 ± 0.1 ab*	*0.84 ± 0.14 a*	*0.69 ± 0.15 ab*
ETR1 (µmol e^- m^{-2} s^{-1})	CONTROL	67.4 ± 3.8 a	70.5 ± 0.8 a	67.4 ± 5.2 a	53 ± 4.1 ab	42.1 ± 1.6 b	57.8 ± 3 a
	SHADE	43.3 ± 4.3 a	43.9 ± 8.7 a	32.1 ± 0.9 a	30.4 ± 4.1 a	43.7 ± 3.3 a	47.7 ± 5.1 a
	Shade/Control	*0.64 ± 0.05 bc*	*0.62 ± 0.12 bc*	*0.49 ± 0.04 c*	*0.57 ± 0.06 bc*	*1.03 ± 0.04 a*	*0.84 ± 0.11 ab*
CEF (µmol e^- m^{-2} s^{-1})	CONTROL	19.6 ± 3.5 d	43.2 ± 2.6 ab	49.8 ± 3.5 a	27.7 ± 3.1 bcd	22.1 ± 0.8 cd	38.9 ± 2.6 abc
	SHADE	14.9 ± 3.1 a	33.5 ± 10 ab	24.6 ± 1.6 abc	17.1 ± 3.4 bc	27.3 ± 4.8 abc	34.6 ± 2.3 a
	Shade/Control	*0.82 ± 0.16 a*	*0.78 ± 0.22 a*	*0.51 ± 0.08 a*	*0.62 ± 0.1 a*	*1.23 ± 0.2 a*	*0.91 ± 0.11 a*

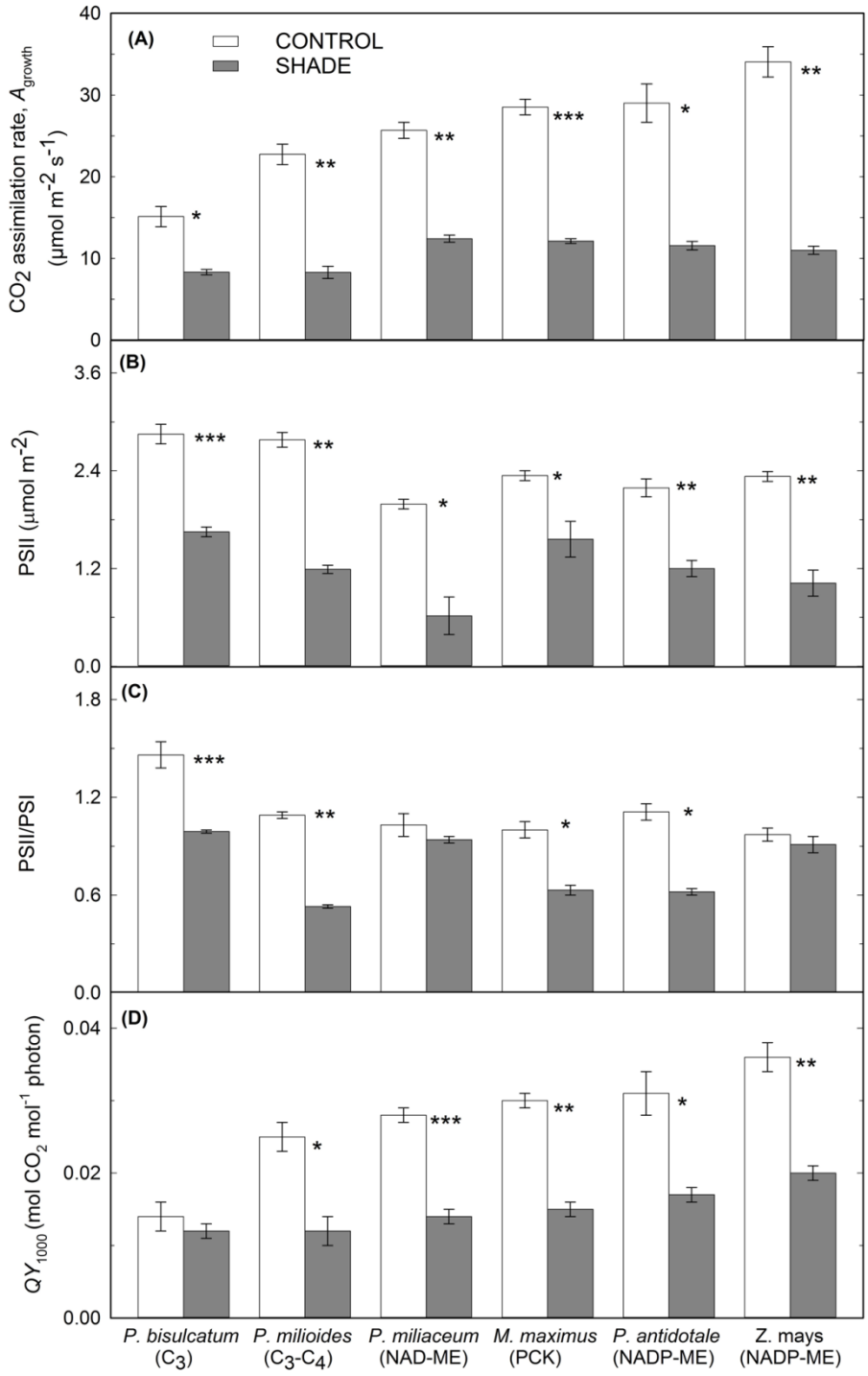

Figure 4. 1 CO_2 assimilation, functional PSII content, PSII/PSI ratio, and the quantum yield for CO_2 uptake

Leaf (**A**) CO_2 assimilation rate (A_{growth}) measured at ambient CO_2 and growth irradiance (1000 or 200 µmol photons m^{-2} s^{-1} for HL and LL plants, respectively); (**B**) functional PSII content (determined by the oxygen yield per single turnover); **(C)** PSII/PSI ratio (determined by electrochromic shift); and **(D)** photosynthetic quantum yield at HL (QY_{1000}) for control and shade-grown C_3, C_3-C_4 and C_4 grasses. Statistical significance levels (t-test) for the growth condition within each species are shown and they are: * ≡ p<0.05; ** ≡ p < 0.01; *** ≡ p < 0.001. Each column represents the mean ± s.e. of each species (n = 4 plants).

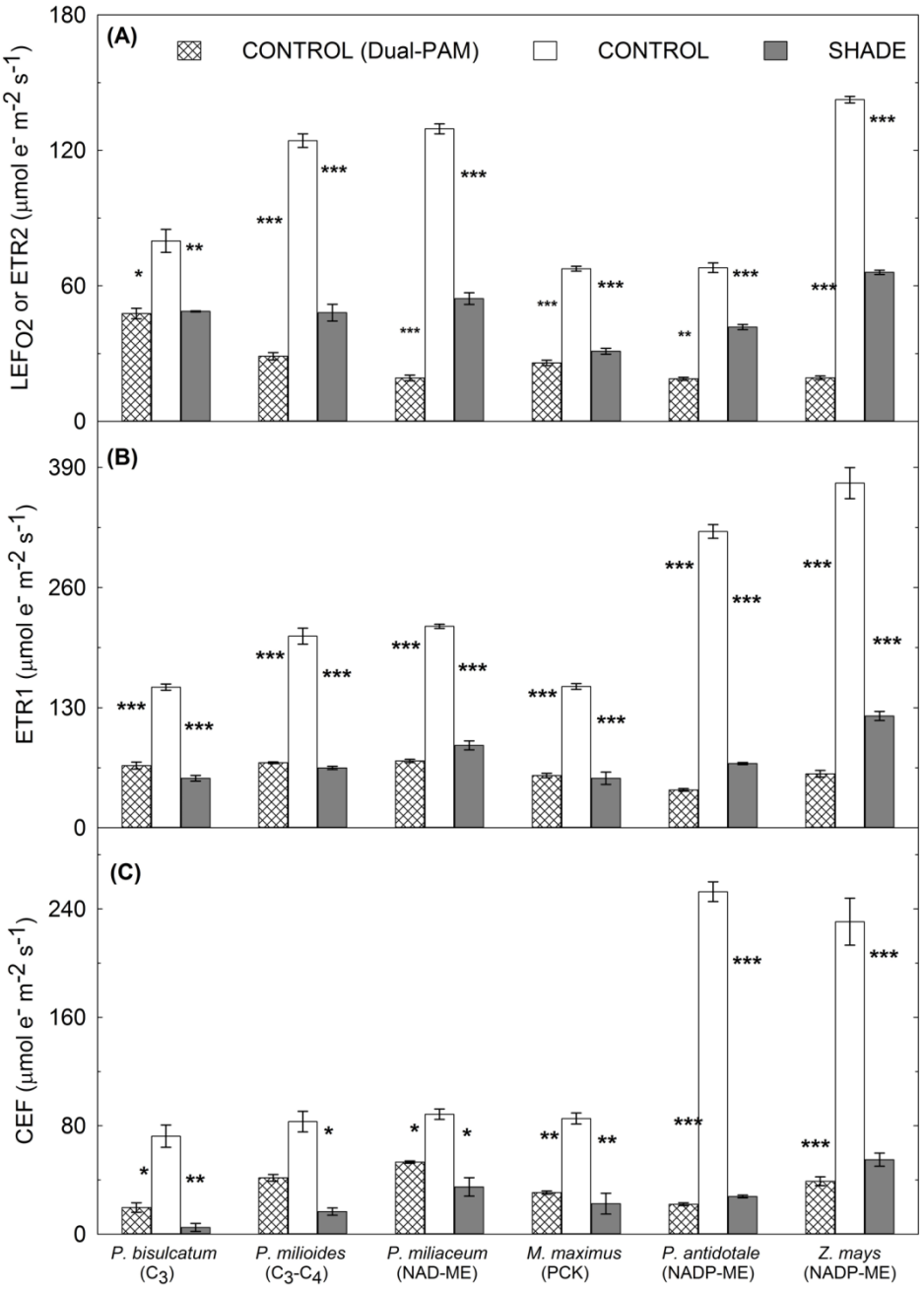

Figure 4. 2 Various electron fluxes in leaves of control and shade-grown C_3, C_3-C_4 and C_4 grasses

Measurements of **(A)** electron flux through both photosystems (LEF_{O2}) and ETR2 at saturating light (2000 µmol photons m^{-2} s^{-1}); **(B)** electron flux through PSI (ETR1); and **(C)** cyclic electron flux around PSI (CEF) at saturating light (2000 µmol photons m^{-2} s^{-1}) in leaves of control and shade-grown C_3, C_3-C_4 and C_4 grasses. Electron fluxes were measured using custom-built equipment for oxygen evolution (LEF_{O2}) and redox kinetics of P700 (ETR1) (clear and grey columns). For comparison, electron fluxes of control plants were also measured using Dual-PAM (checked columns). Each column represents the mean ± s.e. of species or subtype (n = 4 plants). Statistical significance levels (t-test) for the growth condition within each species are shown and they are: * ≡ p<0.05; ** ≡ p < 0.01; *** ≡ p < 0.001.

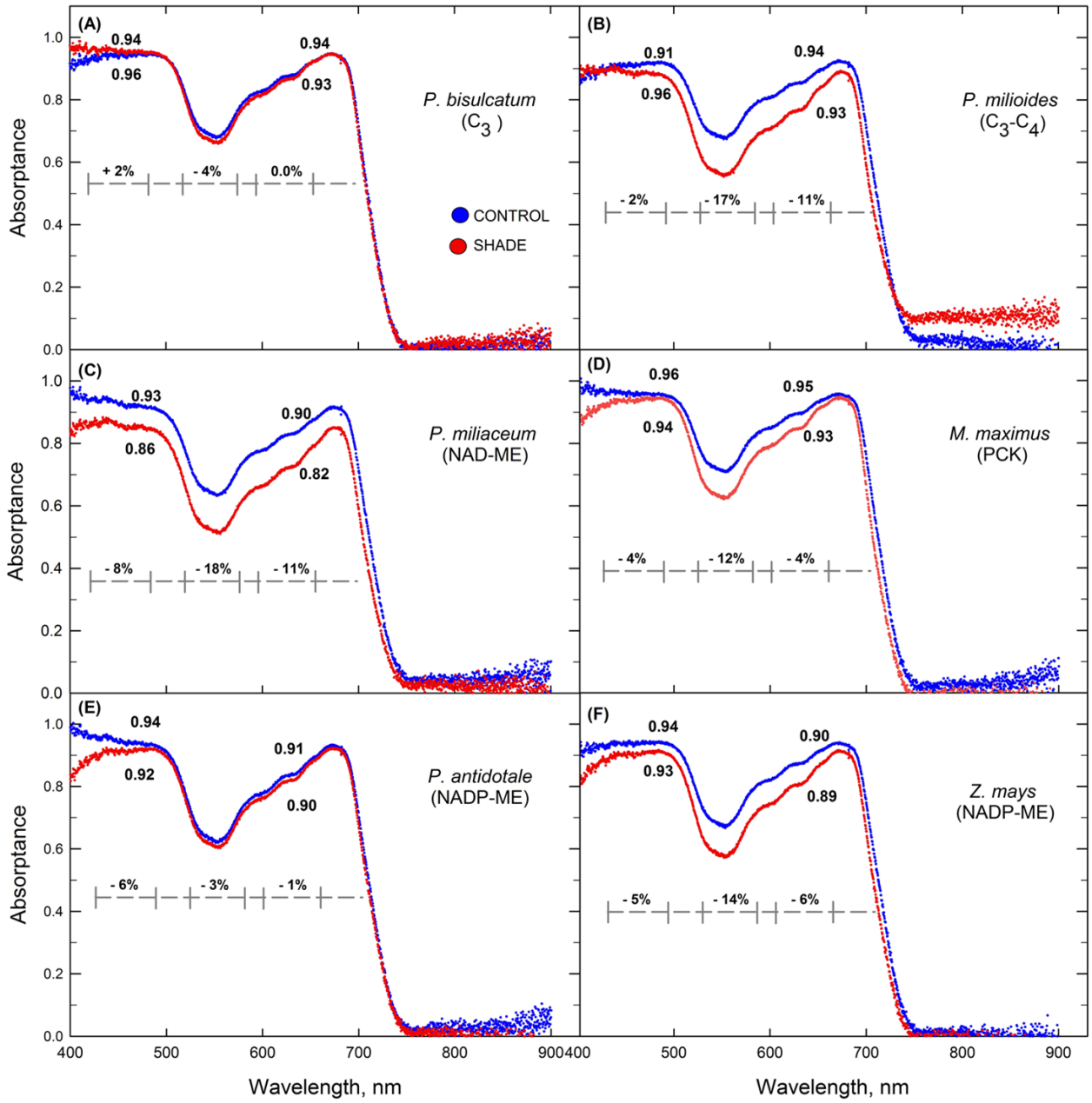

Figure 4. 3 Leaf average spectral absorptance

Average leaf spectral absorptance showing the percentage decrease in absorptance in the blue (430-453 nm), green (500-580 nm), and red (640-662 nm) regions for control (blue traces) and shade-(red traces) grown (**A**) *Panicum bisulcatum* (C_3); (**B**) *Panicum milioides* (C_3-C_4); (**C**) *Panicum miliaceum* (NAD-ME); (**D**) *Megathyrsus maximus* (PCK); (**E**) *Panicum antidotale* (NADP-ME); and (**F**) *Zea mays* (NADP-ME) (n = 4 plants). The numbers represent the specific absorptance for control and shaded leaves at 470 nm and 665 nm, corresponding to the blue and red LED light source used by the LICOR equipment during gas exchange.

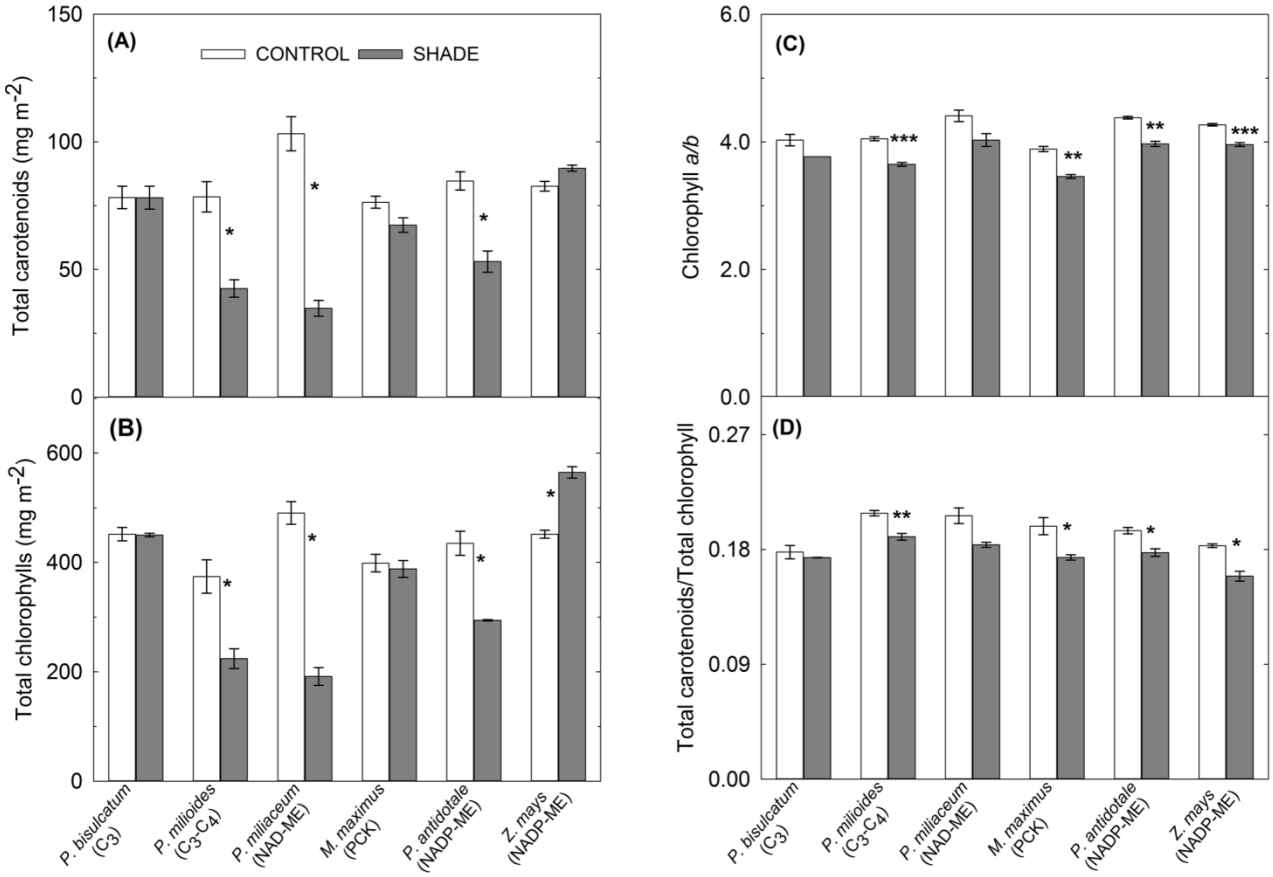

Figure 4. 4 Content of chlorophyll and carotenoids in leaf

Differences in leaf **(A)** total carotenoids; **(B)** total chlorophylls; **(C)** chlorophyll *a/b* ratio; and **(D)** total carotenoid/total chlorophyll ratio between control and shade-grown C_3, C_3-C_4 and C_4 grasses. Each column represents the mean ± s.e. of species (n = 4 plants). Statistical significance levels (t-test) for the growth condition within each species are shown and they are: * ≡ p<0.05; ** ≡ p < 0.01; *** ≡ p < 0.001.

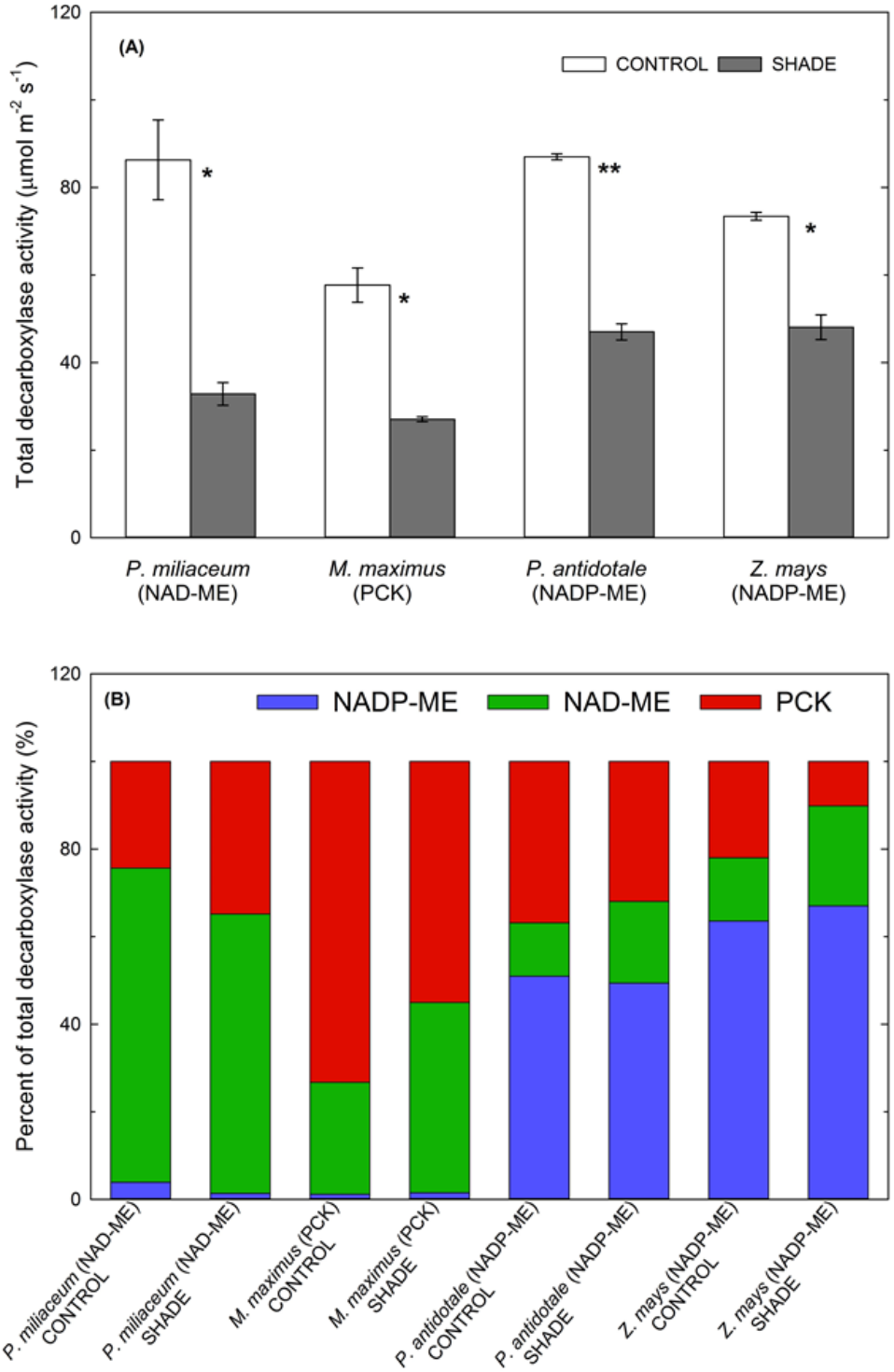

Figure 4. 5 Activities of the C_4 decarboxylases

Total activity of the C_4 decarboxylases **(A)** and percentage contribution of each C_4 decarboxylase to the total decarboxylase activity **(B)** in control and shade-grown C_4 grasses. Each column represents the mean ± s.e. of species (n = 4 plants). Statistical significance levels (t-test) for the growth condition within each species are shown and they are: * ≡ p<0.05; ** ≡ p < 0.01; *** ≡ p < 0.001.

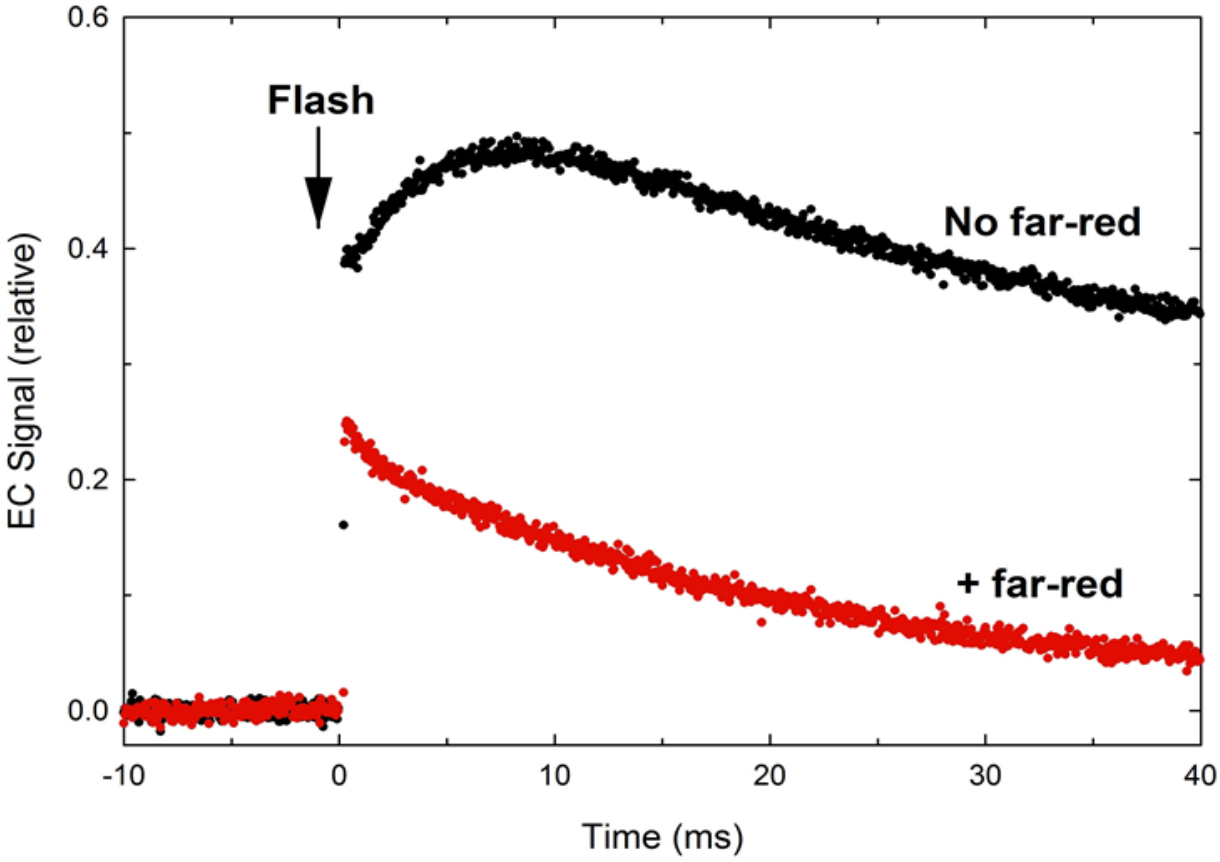

Figure 4. S 1 The amplitude of the fast rise in the EC signal

The amplitude of the fast rise in the EC signal, as varied by lowering the fraction of functional PSI by suppressing PSI activity with far-red light given to leaf segments of control *Zea mays* (NADP-ME). Moderately strong far-red light was used to photo-oxidize a large proportion (~0.92) of P700. Each trace is the average of four replicates, each given 50 scans at 0.2 Hz.

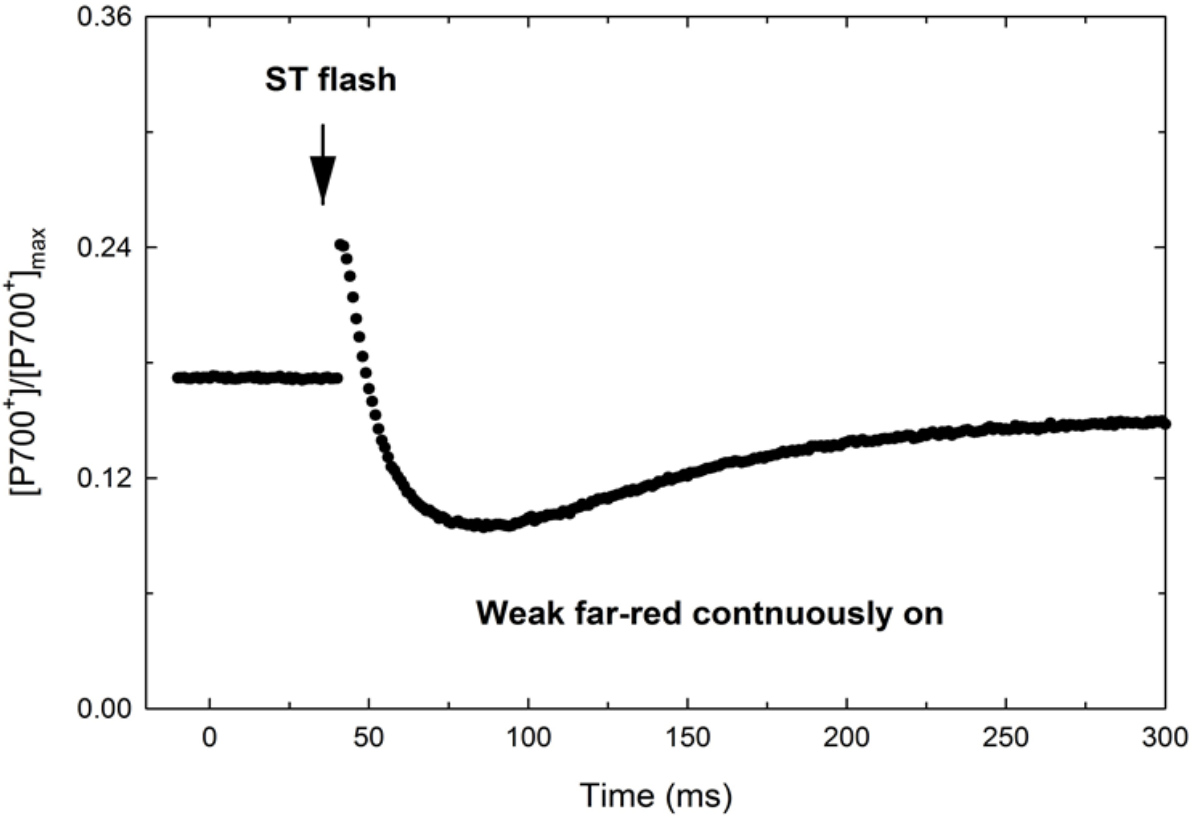

Figure 4. S 2 An example of changes in the oxidation state of P700 in leaf segments

An example of changes in the oxidation state of P700 in leaf segments of control *Zea mays* (NADP-ME) under continuous far-red light on which was superimposed a xenon flash (ST) at time t=0 (arrow). The fraction of oxidized P700 in continuous far-red light can be determined from the signal normalized to the maximum $P700^+$ immediately after the flash. The traces are averages of 16 scans.

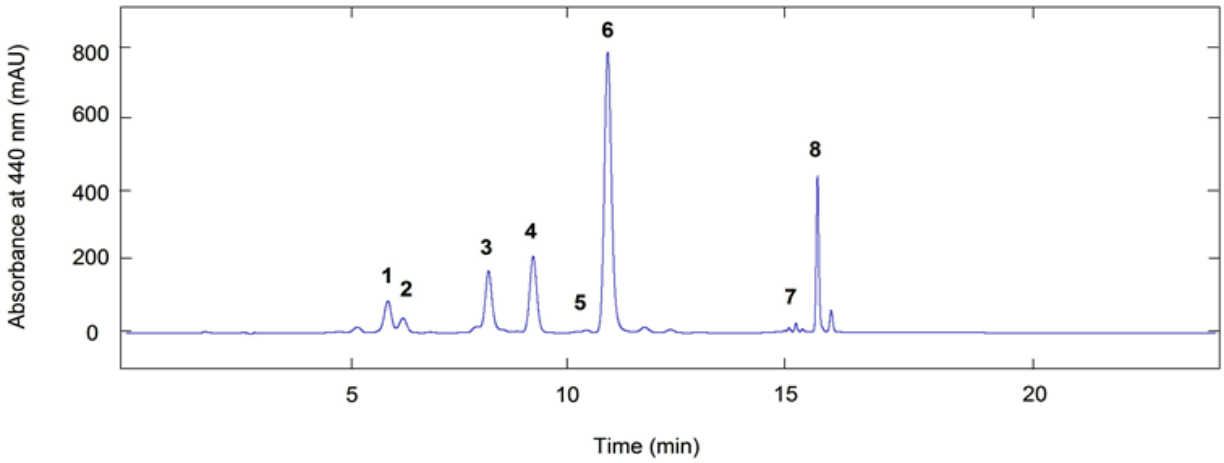

Figure 4. S 3 An example of HPLC chromatogram of leaf extract

An example of HPLC chromatogram of leaf extract of control *Panicum miliaceum* (NAD-ME grass) recorded at 440 nm. The compounds are **(1)** violaxanthin; **(2)** neoxanthin; **(3)** chlorophyll *b*; **(4)** lutein; (5) zeaxanthin; **(6)** chlorophyll *a*; **(7)** antheraxanthin; and **(8)** β-carotene.

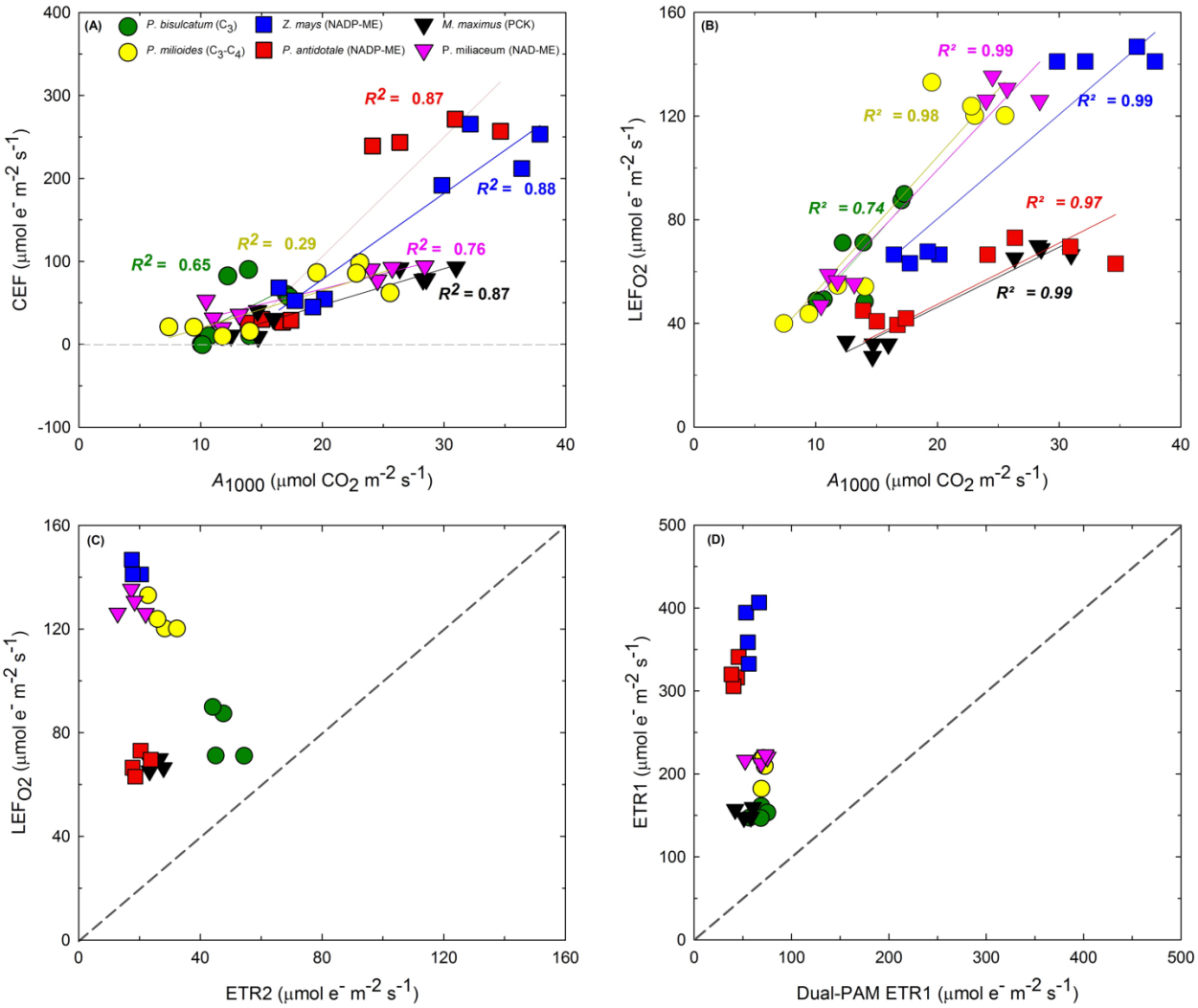

Figure 4. S 4 Relationships between photosynthetic rate at 1000 µmol photons m^{-2} s^{-1} (A_{1000}) and various electron transport fluxes using custom built equipment.

Relationships between photosynthetic rate at 1000 µmol photons m^{-2} s^{-1} (A_{1000}) and either (**A**) cyclic electron flow rate (CEF) around PSI at 2000 µmol photons m^{-2} s^{-1} or (**B**) linear electron flow rate through both photosystems (LEF_{O2}) both measured at saturating irradiance (2000 µmol photons m^{-2} s^{-1}) using custom built equipment. Also shown are the relationships between **(C)** electron transport rates through both photosystems measured using Dual-PAM (ETR2) or custom-built unit (LEF_{O2}); and **(D)** electron transport rates through PSI (ETR1) measured using Dual-PAM (Dual-PAM ETR1) or custom built unit (ETR1) in control and shade-grown C_3, C_3-C_4 and C_4 species. Dotted lines represent the 1:1 relationship to be used as a visual reference.

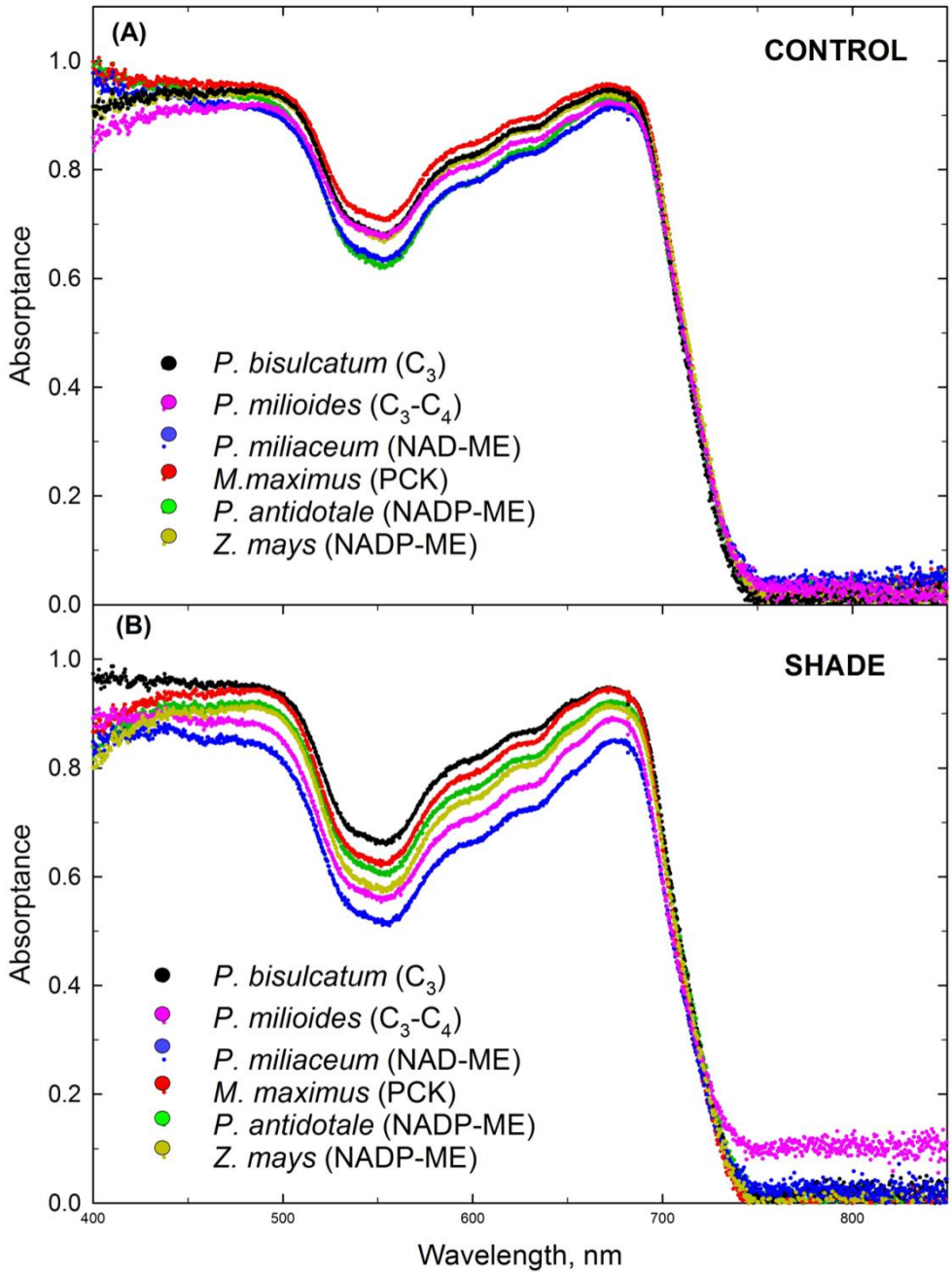

Figure 4. S 5 Average leaf spectral absorptance for control (A) and shade-(B) grown plants

Average leaf spectral absorptance for control (**A**) and shade-(**B**) grown *Panicum bisulcatum* (C_3); *Panicum milioides* (C_3-C_4); *Panicum miliaceum* (NAD-ME); *Megathyrsus maximus* (PCK); *Panicum antidotale* (NADP-ME grass); and *Zea mays* (NADP-ME) (*n* = 4 plants).

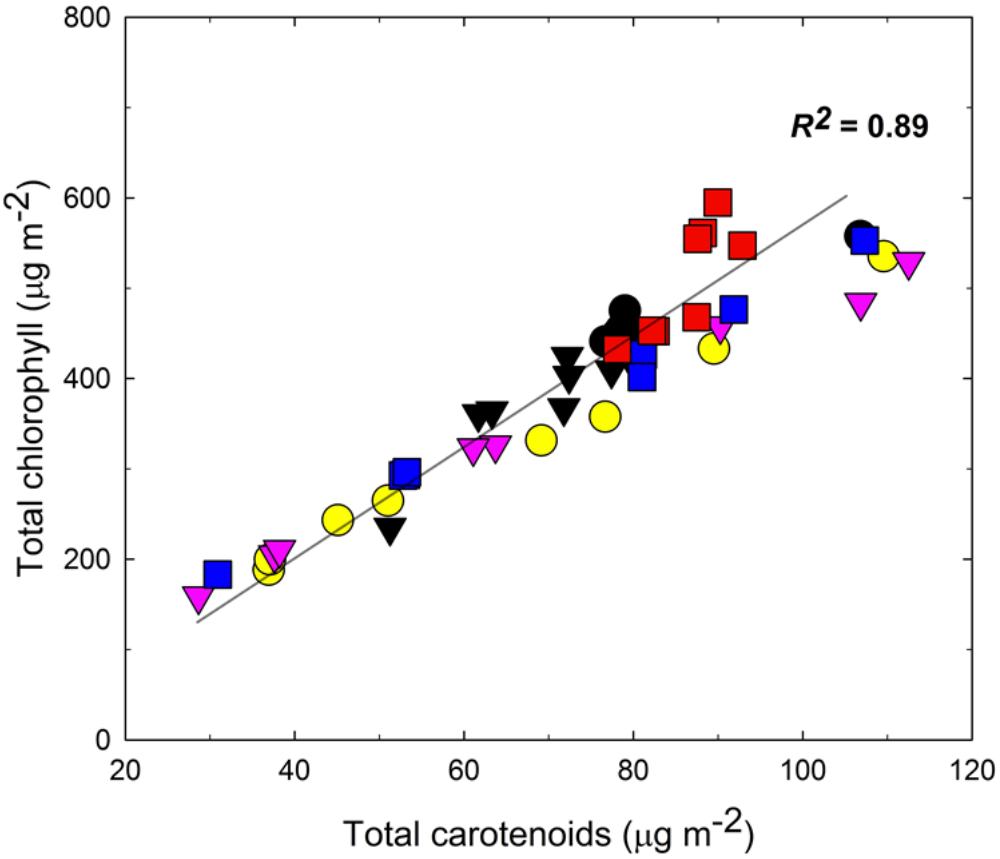

Figure 4. S 6 Relationship between total leaf chlorophylls and total leaf carotenoids

Relationship between total leaf chlorophylls and total leaf carotenoids in control and shade-grown C_3, C_3-C_4 and C_4 grass species. Other details as in **Figure 4. S 4**. Straight lines are linear regressions for all data points.

CHAPTER 5

ACCLIMATION OF C_4 PHOTOSYNTHETIC LIGHT REACTIONS TO LOW LIGHT AND LOW CO_2

ABSTRACT

Light intensity and CO_2 concentration are two environmental factors that distinctly affect the efficiency of photosynthesis. Recently, it has become possible to measure the activity of photosystems (PSI and PSII) under different light intensities from fluorescence analysis and relate it with the efficiency of carbon assimilation from conventional gas exchange measurements in C_4 plants. However, most physiology comparisons of C_3 and C_4 plants are made under current or elevated concentrations of atmospheric CO_2 which does not reflect the low CO_2 environment under which C_4 photosynthesis evolved. In this study, we examined the influence of low light and low CO_2 on the activity of photosynthetic light reactions in C_4 plants in comparison to C_3 and C_3-C_4 plants. Several grass species were grown (*Panicum bisulcatum* (C_3), *Panicum milioides* (C_3-C_4), *Panicum miliaceum* (C_4 NAD-ME), *Megathyrsus maximus* (C_4 PCK), *Panicum antidotale* (C_4 NADP-ME) and *Zea mays* (C_4 NADP-ME) under four experimental conditions: control (400 CO_2 ppm and 1000 µmol photons m^{-2} s^{-1}), low CO_2 (180 ppm and 1000 µmol m^{-2} s^{-1}), low light (400 ppm and 200 µmol m^{-2} s^{-1}) and low CO_2 with low light (180 ppm and 200 µmol m^{-2} s^{-1}). Acclimation brought abought by the four conditions was examined by analyses of leaf spectral properties, pigment content, excitation energy distribution and capacity through fluorescence spectroscopy, activity of photosynthetic enzymes, and rate of photosynthesis. We found that low light (LL) influenced the activities of photosystem complexes and the rate of photosynthesis to a greater extent than low CO_2 (LC) in C_3, C_3-C_4 and C_4 species. This was evident by heightened decreases in yield efficiency of PSI and PSII and down-regulation of various electron transport rates brought about by the decrease in the content of functional PSII, total leaf pigments and leaf absorptance. LL also caused a large reduction in Rubisco content in C_3 and C_3-C_4 species and in the activities of PEPC and the photosynthetic decarboxylases in C_4 species, whereas LC had a limited effect. Among all photosynthetic types, C_4 species exhibited less plasticity photosynthetic rates under low light compared to C_3 and C_3-C_4 species. While C_3 and C_3-C_4 species showed less plasticity of PSI and PSII efficiency under low light. Interestingly, the C_3 grass did not show any substantial acclimation under LC but greatly acclimated when LC was combined with LL.

Key words: C_4 photosynthesis, chlorophyll fluorescence, electron transport rate, low CO_2, quantum yield, biochemical subtypes, light reactions, acclimation

5.1 INTRODUCTION

The decline of atmospheric CO_2 concentration ($[CO_2]$) during the Cenozoic has long been considered the primary driver for the evolution of C_4 photosynthesis (Ehleringer *et al.*, 1991). This environment drove the evolution of the CO_2-concentrating mechanism (CCM) of C_4 photosynthesis, which saturates the carboxylation reaction of Rubisco (ribulose-1,5-bisphosphate carboxylase/oxygenase) and almost eliminates photorespiration, a pathway that becomes increasingly wasteful with declining $[CO_2]$ (Sharkey, 1988). The C_4 CCM functions by transiently fixing CO_2 within the mesophyll cell (MC) before transporting it to the bundle sheath cell (BSC) to be released. During this process, phosphoenolpyruvate carboxylase (PEPC) catalyses the initial carboxylation of CO_2 into organic C_4 acids in the MC. These C_4 acids are then transported through to the BSC before being decarboxylated to release the CO_2, which can then be fixed by Rubisco (Hatch, 1987). The C_4 photosynthetic pathway is classified into three biochemical subtypes based on the primary C_4 decarboxylase enzyme. These enzymes are NADP-malic enzyme (NADP-ME), NAD-malic enzyme (NAD-ME), and phosphoenolpyruvate carboxykinase (PCK) (Gutierrez *et al.*, 1974; Kanai & Edwards, 1999). There are strong anatomical and biochemical variations associated with these biochemical subtypes (Dengler *et al.*, 1994; Edwards, 2011; Prendergast *et al.*, 1987).

Due to the presence of the CCM, acclimation to low $[CO_2]$ also differs between C_3 and C_4 plants. C_3 plants commonly acclimate to low $[CO_2]$ by increasing the activities of Rubisco and other Calvin cycle enzymes (Anderson *et al.*, 2001; Pinto *et al.*, 2014), but this represents a significant cost in terms of leaf nitrogen (Gesch *et al.*, 2000). Other compensatory mechanisms include prolonged vegetative growth (Campbell *et al.*, 2005; Ward *et al.*, 2000), the production of cheap foliage with a high specific leaf area (Campbell *et al.*, 2005) and a shift in the partitioning of growth from roots to leaves (Ward *et al.*, 2000). In contrast, C_4 photosynthesis remains CO_2-saturated even when $[CO_2]$ is reduced substantially below the current ambient level due to the CCM (Byrd & Brown, 2008; Tissue *et al.*, 1995), and hence photosynthetic acclimation is usually less pronounced (Anderson *et al.*, 2001; Edwards & Ogburn, 2012; Li *et al.*, 2014; Maherali *et al.*, 2002; Ward *et al.*, 2008). Within the C_4 CCM, low $[CO_2]$ has been shown to facilitate some acclimation, particularly the upregulation of the carboxylases (Rubisco and PEPC). However, decarboxylase activity has largely been found to remain unchanged, reflecting the high control exerted by the carboxylases relative to the decarboxylases on the efficiency of C_4 metabolism (Pinto *et al.*, 2014). Various degrees of acclimation such as increased foliar N and stomatal conductance (g_s) have also been recorded

for C_4 species in response to long- term growth at low [CO_2] (Anderson *et al.,* 2001; Gill *et al.,* 2002; Pinto *et al.,* 2011).

The efficiency of CCM comes with the caveat of requiring additional energy, mainly associated with the regeneration of phosphoenolpyruvate (PEP) and the over-cycling of CO_2. C_4 plants overcome this limitation through a higher light use efficiency (LUE) under high light (HL) compared to C_3 plants. Aside from the linear electron flow (LEF), additional energy produced by C_4 species can come from the enhancement of cyclic electron flow (CEF) and from Mehler's reaction which are commonly stimulated under high irradiances (Asada, 1999; Munekage *et al.*, 2004; Takabayashi *et al.,* 2005a). High LUE is also one of the reasons for the ecological dominance of C_4 plants in open, high light (HL) environments and their disproportionately high global productivity relative to their small taxonomic representation (Edwards *et al.,* 2010; Ehleringer *et al.,* 1997). This also contributes to the observed higher quantum yield for CO_2 uptake (*QY*) of C_4 species compared to C_3 species under warm temperatures and normal atmospheric conditions (Ehleringer & Björkman, 1977; Ehleringer & Pearcy, 1983; Zhu *et al.,* 2008).

However, the high energy cost of C_4 photosynthesis may limit the productivity and distribution of C_4 plants in low light (LL) environments. In contrast to acclimation under low [CO_2], long-term exposure to low light (LL) causes large acclimations in both the CCM and light harvesting complexes of C_4 species (Drozak & Romanowska, 2006; Romanowska *et al.*, 2006; Sonawane *et al.*, 2018). It has also been reported that acclimation under long-term exposure to LL involves changes in photosystem activity and stoichiometry in chloroplasts (Anderson, 1986). The photosynthetic apparatus commonly acclimates to maximize light use efficiency following long-term exposure to shade (Boardman, 2003; Sage & McKown, 2006). This acclimation varies depending on plant species and ecotype (Sonawane *et al.,* 2018; Ward & Woolhouse, 1986). It has been shown by Romanowska & Drożak (2006) that during growth of the three C_4 subtypes under low light condition (180 µmol photons m^{-2} s^{-1}), each subtype developed a different photochemical pattern characteristic in the MC and BSC chloroplasts which could have important implications for the differences in *QY*.

It is known that several processes such as CO_2 assimilation require the energy generated during light reactions of photosynthesis. The rate of energy generated during these reactions mainly depends on the intensity of light and efficiency of light energy conversion complexes; however, the effect of [CO_2] is still unknown. That is why it is important to investigate how the combination of LL and low [CO_2] influence LUE of different photosynthetic types and

subtypes to have a clear understanding about the level of plasticity of light harvesting complexes under varying environmental conditions. Comparing the sensitivity to low [CO_2] and changes in growing light conditions of the different pathways of photosynthesis and subtypes of C_4 photosynthesis among closely related grass species may also provide critical insight into the physiology of C_4 plants under conditions that led to their evolution.

Consequently, this study compared the photosynthetic physiology (light energy conversion efficiency) and biochemistry (activity of the photosynthetic carboxylase and decarboxylase enzymes) of several closely related grass species *Panicum bisulcatum* (C_3), *Panicum milioides* (C_3-C_4), *Panicum miliaceum* (C_4 NAD-ME), *Megathyrsus maximus* (C_4 PCK), *Panicum antidotale* (C_4 NADP-ME) and *Zea mays* (C_4 NADP-ME)) grown under ambient (400 ppm) or low (180 ppm) [CO_2] combined with HL (1000 μmol photons m^{-2} s^{-1}) or LL (200 μmol photons m^{-2} s^{-1}). This gave a total of four experimental conditions; control (HL and ambient [CO_2]), LC (HL and low [CO_2]), LL (LL and ambient [CO_2]), and LL+LC (LL and low [CO_2]). We hypothesized that, when all the species are grown under LC, the C_3 and C_3-C_4 species will acclimate more than C_4 species. Acclimation will include lower photosynthetic rates, changes in photosystem stoichiometry, lower rates of electron transport, lower pigment contents, and lower photosynthetic enzyme activities. When grown at LL, C_4 species will have the greater acclimation and this will vary among subtypes. Finally, when grown under the combination of LL+LC, C_4 species will have the greatest acclimation and the effect of LC will be an additive effect to changes in the light energy conversion efficiency among the subtypes.

5.2 MATERIALS AND METHODS

5.2.1. Experimental set-up

An experiment was conducted in four walk-in growth chambers (Biochambers, Winnipeg, Manitoba) at Western Sydney University which are supplied with CO_2 additives and scrubbers and controlled by LI-820 CO_2 gas analysers (LI-COR Inc., Lincoln, NE, USA). The conditions inside the growth chambers were combinations of either high-light (HL) (1000 µmol photons m^{-2} s^{-1}) or low-light (LL) (200 µmol photons m^{-2} s^{-1}) of photosynthetic flux density (PPFD) at pot level with either ambient CO_2 concentration (AC) (400 ppm) or low CO_2 concentration (LC) (200 ppm). The average day/night temperature was 28/22^oC, with 60% relative humidity (RH), and a phoyoperiod of 16 hours. The four growth chambers were set-up in the following treatment combinations: Treatment 1: high light with ambient [CO_2] (control); Treatment 2: low light with low [CO_2] (LL+LC); Treatment 3: high light with low [CO_2] (LC); Treatment 4: low light with ambient [CO_2] (LL).

Representative grass species of C_3 (*Panicum bisulcatum*), C_3-C_4 (*Panicum milioides*) and C_4 photosynthesis with NADP-ME subtype (*Panicum antidotale* and *Zea mays*); NAD-ME subtype (*Panicum miliaceum*); and PCK subtype (*Megathyrsus maximus*) were germintated in 30 liter pots containing soil (Osmocote® Professional Seed Raising Mix) and fertilised with Osmocote® initially inside the control chamber. Two weeks after germination, some of the plants were transferred into three other chambers. Plants were watered to full capacity every 2 – 3 days and were randomized twice a week to reduce the effects of within-chamber variation and between chambers once every 12 days to reduce chamber variation. Leaves were measured and harvested from 4 – 5-week-old plants.

5.2.2. Photosynthesis measurement

Combined gas exchange and chlorophyll fluorescence measurements were made using a LI-6400XT open gas exchange system (LI-6400XT, LI-COR, Lincoln, NE, USA) with an integrated fluorescence chamber head, enclosing 2 cm^2 areas, using the youngest fully expanded leaves under 21% O_2 condition. Measurements were conducted at a leaf temperature of 28^oC between 10:00 and 15:00 h. Prior to measurements, the leaf was allowed (15 – 20 minutes) to reach a steady-state of CO_2 uptake at ambient CO_2 (400 ppm) with a saturating PPFD of 2000 µmol photons m^{-2} s^{-1} for C_4 species and 1500 µmol photons m^{-2} s^{-1} for C_3 and C_3-C_4 species. Once the steady state had been reached an initial ‘single’ measurement was taken. Consequently, the responses of CO_2 assimilation rates (*A*) to step

increase of intercellular CO_2 (C_i), *A*-C_i curve, were measured by raising the CO_2 concentration inside the LI-6400XT leaf chamber in 10 steps between 50 and 1500 ppm.

For each light response curve, the leaf was allowed to reach a steady-state of CO_2 uptake at saturating [CO_2] (800 ppm) before measuring the responses to PPFD. The light response curve was started from high light to low light (11 steps) followed by measurements of dark respiration (R_d) after 20 min dark adaptation.

5.2.3. Dual-PAM measurements

The chlorophyll fluorescence and P700 redox state were determined *in vivo* from the same leaf using a Dual-PAM-100 (Heinz Walz). The maximum quantum yield of PSII (F_v/F_m) and the maximum P700 signal (P_m) were first determined after dark adaptation for 20 minutes. Then, the steady-state of photosynthesis was achieved after 15 min of light adaptation under PPFD of 1000 µmol photons m^{-2} s^{-1}. Consequently, light responses of leaf chlorophyll fluorescence and P700 were then recorded after 3 minutes exposure to each of the PPFDs (30, 37, 46, 61, 77, 94, 119, 150, 190, 240, 297, 363, 454, 555, 684, 849, 1052, 1311, 1618 and 1976 µmol photons m^{-2} s^{-1}).

The fluorescence parameters were calculated as follows:

$$F_v/F_m = (F_m - F_o)/F_m \quad (5.1)$$

$$Y(II) = (F_m' - F_s')/F_m' \quad (5.2)$$

$$qP = (F_m' - F)/(F_m' - F_o) \quad (5.3)$$

where F_o represents the minimum fluorescence in the dark-adapted state and light-adapted state, respectively, and F_m and F_m' represent the maximum fluorescence upon illumination with a pulse (600 ms) of saturating light (10000 µmol photons m^{-2} s^{-1}) in the dark-adapted state and light-adapted state, respectively (Kramer *et al.*, 2004). F_s' is the light steady-state fluorescence. F_v/F_m represents the maximum quantum yield of PSII. Y(II) is the effective quantum yield of PSII. The coefficient of photochemical quenching (qP) is a measure of overall "openness" of PSII. qP can vary between 1 (defined for dark adapted state) to 0 (all PSII centres closed). The parameters related to PSI were calculated as follows:

$$Y(I) = P700\ red. - Y(NA) \quad (5.4)$$

After far-red pre-illumination for 10 s, P_m was determined through the application of a saturating pulse. This method was taken from Klughammer & Schreiber (2008). Y(NA) represents the fraction of overall P700 that cannot be oxidized by a saturation pulse in a given state due to a lack of acceptors; it is enhanced by dark adaptation (deactivation of key enzymes of the Calvin–Benson cycle) and damage at the site of CO_2 fixation. The saturating pulse used in P700 measurement is 10000 μmol m^{-2} s^{-1}.

The electron transport rates through PSI (ETR1) and PSII (ETRII) were calculated as:

$$ETR1 \; or \; ETR2 = YI \; or \; YII \; x \; I \; x \; 0.85 \; x \; 0.5 \tag{5.5}$$

where I is the irradiance, 0.85 is the assumed absorptance and 0.5 the assumed fraction of absorbed white light partitioned to PSI or PSII. Cyclic electron flow around PSI (CEF) was then calculated as:

$$CEF = ETR1 - ETR2 \tag{5.6}$$

5.2.4. Leaf reflectance, transmittance and absorptance measurements

Leaf reflectance, transmittance and absorptance to solar radiation over the 400 – 700 nm wavelength were measured with a LI-COR 1800-12 Integrating Sphere (LI-COR, Inc., Lincoln, NE, USA), coupled by a 200 μm diameter single mode fibre to an Ocean Optics model USB2000 spectrometer (Ocean Optics Inc., Dunedin, FL, USA), with a 2048 element detector array, 0.5 nm sampling interval, and 7.3 nm spectral resolution in the 350–1000 nm range. Software was designed for signal verification, adjustment of integration time, and data acquisition. An integration time of 13 ms was used for all sample measurements. Single leaf reflectance and transmittance measurements were acquired following the methodology described in the product manual for the LiCor 1800-12 system (Li-Cor Inc., 1984). Reflectance of the sample (R_s) is the amount of flux reflected by the leaf, normalized by the amount of flux incident on it and calculated as:

$$R_s = \frac{(I_s - I_d)R_r}{(I_r - I_d)} \tag{5.7}$$

where I_s is the measured sphere output when the sample is illuminated and I_r is that measured when the reference material (barium sulfate) is illuminated and I_d is measured by illuminating the sample port with no sample in place. For equation (5.6), it was assumed that the reflectance of the reference material (R_r) is 1. Transmittance of the sample (T_s) is the amount

of flux transmitted by the leaf, normalized by the amount of flux incident on it and calculated as:

$$T_s = \frac{I_s R_r}{I_r} \quad (5.8)$$

Any flux not reflected or transmitted is absorbed (*Abs*) and obtained using this equation based on conservation of energy:

$$R_s + T_s + Abs = 1 \quad (5.9)$$

5.2.5. Quantum yield for CO_2 uptake (QY)

The absorbed quantum yield for CO_2 uptake at saturating irradiance (QY_{sat}) and at growth irradiance (QY_{growth}) were calculated as follows:

$$QY_{sat} \text{ or } QY_{growth} = \frac{A_{1000} \text{ or } A_{growth}}{I \times (Abs_{ave})} \quad (5.10)$$

where A_{sat} and A_{growth} are the CO_2 assimilation rates at saturating irradiance and at growth irradiance, I is the irradiance during measurement of A and Abs_{ave} is the average leaf absorptance in blue (470 nm) and red (660 nm) wavelength regions (~0.9).

5.2.6. Quantification of functional PSII by the oxygen yield per single turn-over flash

The same leaf disc was used for quantification of the functional PSII centres, by measuring the amount of oxygen evolution per single turn-over flash in a leaf-disc oxygen electrode, with continuous background far-red light (Chow *et al.,* 1989). These estimations are based on the assumption that for every four flashes (at 10 Hz), four electrons are transferred through each functional PSII, resulting in the evolution of one O_2 molecule.

5.2.7. Carotenoid and chlorophyll analysis and quantification by HPLC

Carotenoids and chlorophyll analysis through HPLC was done following the modified protocol from Pogson *et al.* (1996). Approximately 50 mg fresh leaves were extracted in a microcentrifuge tube by grinding using a tissue lyser (Qiagen) (25 Hz for 3 minutes). Pigments were extracted by adding 1 mL of extraction buffer, comprising of acetone:ethyl acetate (60:40) with 0.1% Butylated hydroxytoluene (BHT) and then vortexed for 1 minute or until the tissue lost its green colour. The organic component of the extract was separated by gently adding 900 µL of water and inverting the tube 4 – 5 times. The solution was then centrifuged for 5 minutes at 15000 rpm at 4^{o}C. The upper phase was collected and transferred in a new microcentrifuge tube (a little of the lower phase was still obvious at this point). This

extract was then centrifuged for 5 minutes at 15000 rpm at 4^{o}C and 200 µL was transferred to another tube. A final volume of 20 µL was used for injection into HPLC system (Agilent 1260 Infinity) equipped with YMC-C30 (250 x 4.6mm, S-5µm) column and Diode Array Detector (DAD) detector. A newly optimized 17 minutes elution method was used to separate pigments using reverse phase solvent gradient comprised of mobile phase A (methanol:water:triethylamine, 98:2:0.1 v/v) and B (methyl tert-butyl ether). The initial solvent composition was 85% and 15% of the solvent A and B respectively until one minute followed by 35% of B at 11.0 minute. The ratio of B increased to 65% at 11.1 minutes followed by a gradient up to 70% at 15.0 minute and stabilized until 17.0 minute. The solvent flow rate was 1 ml/min until 17.0 minutes from the beginning. Solvent composition was returned to the initial state (15% of B) at 17.1 minutes and the column was equilibrated until 25.0 minutes with the flow rate of 2.0ml/minutes. The column temperature was maintained at 23^{o}C and autosampler temperature was set to 8^{o}C and illumination turned off. Carotenoid and chlorophyll peak signals were recorded at 440 nm, 340 nm, and 286 nm and individual pigments were identified by comparing their retention time and absorption spectra with the published literature. The pigment concentration was interpreted in terms of milligram per leaf area (mg m^{-2}) by integrating peak area with the standard curve as described by Pogson *et al.* (1996) and Cuttriss *et al.* (2007).

5.2.8. Content of Rubisco and activity of PEPC, NADP-ME, NAD-ME and PCK

Following gas exchange measurements, leaf discs (0.6 cm^2) were taken and rapidly frozen in liquid nitrogen. For assays of Rubisco content, as well as the activity of PEPC and NADP-ME, the soluble leaf protein was extracted using ice-cold mortar and pestle into 1 ml of ice cold, extraction buffer [50 mM EPPS-NaOH, pH 7.8, 1 mM EDTA, 5 mM DTT, 5 mM $MgCl_2$, 1% (v/v) plant protease inhibitor cocktail (Sigma-Aldrich), and 1% (w/v) polyvinylpolypyrrolidone (PVPP)]. Chlorophyll content was estimated according to Porra *et al.* (1989) by mixing 100 µL of total extract with 900 µL of acetone. The extract was rapidly centrifuged for 30 seconds at 15,000 g at 4 °C, and 50 µl of the soluble leaf protein was assayed for Rubisco content by [^{14}C]CABP (2-C-carboxyarabinitol 1,5-bisphosphate) binding as described by Whitney *et al.* (2001).

The activities of photosynthetic enzymes PEPC and NADP-ME were determined from the extracted soluble protein and measured at 25 °C using an NADH-coupled enzyme assay with the rate of NADH oxidation or reduction monitored at 340 nm using a diode array

spectrophotometer (Agilent model 8453). Assays were performed in 1 ml cuvettes containing 0.48 ml of assay buffer following Sharwood *et al.* (2016).

Maximal PEPC activity was measured in an assay buffer containing [50 mM EPPS-NaOH (pH 8.0), 0.5 mM EDTA, 10 mM $MgCl_2$, 0.2 mM NADH, 5 mM glucose-6-phosphate, 1 mM $NaHCO_3$, 1 U/mL MDH] after the addition of 8 mM of PEP. NADP-ME activity was measured in assay buffer containing [50 mM Tricine buffer (pH 8.3), 0.5 mM NADP, 5 mM malate, 0.1 mM EDTA] after addition of 10 mM $MgCl_2$.

The maximal activity of PCK was measured in the carboxylase direction using a method also described by Sharwood *et al.* (2016) in an NADH-coupled assay. Leaf discs (0.6 cm^2) were extracted in 50 mM HEPES pH 7.0, 5 mM DTT, 1% (w/v) PVPP, 2 mM EDTA, 2 mM $MnCl_2$, and 0.05% Triton using ice-cold mortar and petsle. PEPCK activity from leaf extracts was measured in assay buffer [50 mM HEPES, pH 7.0, 4% mercaptoethanol (w/v), 100 mM KCl, 90 mM $NaHCO_3$, 1 mM ADP, 2 mM $MnCl_2$, 0.14 mM NADH, and malate dehydrogenase (MDH; 6 U; 3.7 µl)] after the addition of 15 mM PEP.

The activity of NAD-malic enzyme was measured using a method described by Setién *et al.* (2014). Leaf discs (0.6 cm^2) were extracted in [50 mM HEPES-KOH (pH 8.0), 2 mM EDTA, 0.05% Triton, 2 mM $MnCl_2$, 10 mM DTT, 1% PVPP and 1% (v/v) plant protease inhibitor cocktail in ice-cold mortar and pestle. NAD-ME activity was measured at 25^oC in a reaction buffer containing [50 mM HEPES-KOH (pH 8.0), 5 mM NAD, 5 mM DTT, 0.1 mM coenzyme-A, 5 mM malate, 0.2 mM EDTA] after the addition of 4 mM $MnCl_2$.

5.2.9. Leaf dry mass

LMA of fully expanded leaf was calculated from leaf dry mass (oven-dried for 48 h at 65^oC) over the leaf area (g m^{-2}). Five leaves from each of the replicates were sampled.

5.2.10. Statistical analysis

In this study, one chamber was considered as the control chamber and the other three chambers were considered as separate treatments. Variables were analyzed separately and compared among species within each treatment and to the data from the control chamber (high light with ambient [CO_2]). The main effects (species and treatment) and the two-way effect (species x treatment) were analyzed using analysis of variance (ANOVA) at Statistical Tool for Agricultural Research (STAR 2.0.1) software (International Rice Research Institute 2013 – 2020) with the replicates in each species as sources of error. The effect of low light

treatment was obtained from comparing plants at low light + ambient [CO_2] to plants at high light + ambient [CO_2] (control). The effect of low [CO_2] treatment was obtained from comparing plants at high light + low [CO_2] to plants at high light + ambient [CO_2] (control). The effect of the combination of low light and low [CO_2] treatment was obtained from comparing plants at low light + low [CO_2] to plants at high light + ambient [CO_2] (control). Under each treatment, each variable was compared among species using multiple-comparison Tukey's post-hoc test. Variable from each treatment was then compared to the control by t-test.

5.3 RESULTS

5.3.1. Leaf gas exchange under low light and low CO_2

When measured at saturating light and ambient [CO_2], the photosynthetic rates (A_{sat}) were higher in the C_4 species compared to C_3-C_4 and C_3 species (**Tables 5. 1** and **5. 2**). Among C_4 species, variation in A_{sat} was unrelated to their subtype (**Tables 5. 1** and **5. 2**). None of the treatments greatly affected A_{sat} of *P. bisulcatum* (C_3). In other species A_{sat} decreased at LL and at LL+LC (-29% to -53%) more than at LC (-8% to -14%) (**Tables 5. 1** and **5. 2**). Greatest decrease in A_{sat} at LL was observed in C_4 species, particularly *P. miliaceum* (NAD-ME) (-53%) while greatest decrease in A_{sat} at LL+LC was observed in *P. milioides* (C_3-C_4) (-45%) (**Table 5. 2).**

The CO_2-saturated rates (CSRs) were estimated from measurements at saturating light (**Figures 5. S 1A** to **5. S 1F**). In control plants, C_3 species had the lowest CSRs compared to C_3-C_4 and C_4 species (**Tables 5. 1** and **5. 2**). Greatest reductions in CSRs were observed at LL (up to -53%) and LL+LC (up to -51%) compared at LC (up to -24%) (**Tables 5. 1** and **5. 2**). Under LL, greatest decrease in CSRs were again observed in *P. milioides* (-42%) and *P. miliaceum* (-53%) (**Tables 5. 1** and **5. 2**). Under LL+LC, greatest decrease in CSRs were observed in *P. milioides* (-51%) and *P. antidotale* (-42%). *P. bisulcatum* had the greatest decrease in CSR at LC (-28%) compared to other species (**Tables 5. 1** and **5. 2**). The light-saturated photosynthesis rate, A_{max}, was estimated from the light response curves of photosynthesis measured at saturating CO_2 (**Tables 5. 1** and **5. 2**). All treatments decreased A_{max} of all species (**Tables 1** and **2**). Greatest decrease in A_{max} at LL was observed in *P. miliaceum* (-51%), while greatest decrease in A_{max} at LC was observed in *P. bisulcatum* (-50%) and *P. milioides* (-48%) compared to all C_4 species (-17% to -39%) (**Tables 5. 1** and **5. 2**). Greatest decrease at LL+LC was observed in *P. bisulcatum* (-70%) and *P. milioides* (-76%) compared to all C_4 species (-44% to -49%) (**Tables 5. 1** and **5. 2**).

5.3.2. PSII content

No significant differences were observed in the amount of functional PSII in the leaf among control plants (**Tables 5. 1** and **5. 2**). Greatest decrease in functional PSII content was observed in both *P. bisulcatum* and *P. miliaceum* at LL (-37% and -35%) and LL+LC (-32% and -55%) compared to other species (**Tables 5. 1** and **5. 2**). However, *P. milioides* acclimated by increasing PSII content in all treatments, having the greatest increase in PSII content at LL (+42%) (**Table 5. 2**).

5.3.3. Effect of low light and low [CO_2] on energy distribution of light absorbed by PSI and PSII

It was observed that dark-adapted maximum quantum yield (F_v/F_m) of all species did not significantly change at LC (**Tables 5. 1** and **5. 2**). Only *P. miliaceum* responded to all treatments by increased F_v/F_m (+7% to +19%). Significant changes in F_v/F_m were also observed in other species only at LL+LC except for *P. bisulcatum* and *M. maximus* (**Tables 5. 1** and **5. 2**).

The energy distribution in PSII and PSI in all species was greatly affected by changes in growing light intensity and [CO_2] as indicated by the decrease in effective quantum yield of PSII [Y(II)] and PSI [Y(I)] measured at HL (1000 µmol photons m^{-2} s^{-1}). Highest Y(I) was measured in *P. milioides* among all control species (**Tables 5. 1** and **5. 2**). The decrease in Y(I) in each species was observed to be greater in either LL (up to -50%) or LL+LC (up to -55%) compared to LC (up to -25%) (**Tables 5. 1** and **5. 2**). Greatest decrease in Y(I) at LL was observed in *M. maximus* (-40%) and in *Z. mays* (-50%) (**Tables 5. 1** and **5. 2**). Greatest decrease at LL+LC was observed in *P. milioides* (-55%) and again in *M. maximus* (-42%) and *Z. mays* (-37%) (**Tables 5. 1** and **5. 2**). All C_4 species increased in Y(I) (+10% to 21%) at LC except for *M. maximus* (-31%) (**Tables 5. 1** and **5. 2**).

Among all control species, Y(II) was observed to be the highest in *P. bisulcatum* (**Tables 5. 1** and **5. 2**). All the species decreased in Y(II) at LL+LC. Greatest decrease in Y(II) at LL+LC was observed in *P. bisulcatum* (-52%) and *P. milioides* (-47%) compared to C_4 species (-6% to -36%). All C_4 species showed increased Y(I) (+4% to 17%) at LC except for *M. maximus* (-22%) (**Tables 5. 1** and **5. 2**). Overall, only *P. milioides* and *M. maximus* showed reduced Y(I) and Y(II) at all treatments (**Tables 5. 1** and **5. 2**).

Photochemical quenching measured at HL (qP) decreased more at LL (up to -41%) and at LL+LC (up to -48%) compared to LC (up to -36%) in all species except for *P. antidotale* (**Tables 5. 1** and **5. 2**). A large decrease in qP at LL was observed in most C_4 species (-30% to -41%) compared to C_3 (-4%) and C_3-C_4 (-21%) species (**Tables 5. 1** and **5. 2**). Greatest decrease at LL+LC was observed in C_3-C_4 species (-48%) compared to C_3 (-33%) and C_4 species (-12% to -33%) (**Tables 5. 1** and **5. 2**). It was again observed that only *P. milioides* decreased in qP at all treatments (**Tables 5. 1** and **5. 2**).

5.3.4. Rates of various electron transports under low light and low [CO_2]

Among all control plants, *P. milioides* had the highest ETR1 measured at HL (**Figure 5. 1A**; **Table 5. 1**). Down-regulation of ETR1 was strongest in all species at LL (up to -51%) and LL+LC (up to -55%) compared to LC (up to -30%) (**Figure 5. 1A**; **Table 5. 1**). Greatest reduction in ETR1 at LL was observed in *P. milioides* (-51%) and in *Z. mays* (-50%), while greatest reduction at LL+LC was observed in *P. milioides* (-55%), *P. bisulcatum* (-42%) and *Z. mays* (-42%) (**Figure 5. 1A**; **Table 5. 1**). ETR1 of *P. milioides* and *M. maximus* were significantly down-regulated at LC with 25% and 30% reductions, respectively (**Figure 5. 1A**; **Table 5. 1**).

ETR2 was down-regulated under all three treatments in all, except the two NADP-ME, species (**Figure 5. 1B**; **Table 5. 1**). Overall, the greatest ETR2 down-regulation was observed at LL (up to -55%) and at LL+LC (up to -52%) compared at LC (up to -47%) (**Figure 5. 1B**; **Table 5. 1**). Greatest ETR2 down-regulation was observed in *P. bisulcatum* at LL (-52%) and at LL+LC (-55%) (**Figure 5. 1B**; **Table 5. 1**). Greatest down-regulation of ETR2 at LC was observed in *P. milioides* (-47%) (**Figure 5. 1B**; **Table 5. 1**).

Highest rate of CEF measured at HL was observed in both *P. milioides* and *Z. mays* among all control species (**Figure 5. 1C**; **Table 5. 1**). Rates of CEF in all species were down-regulated more at LL (up to -56%) and at LL+LC (up to -57%) compared to LC (up to 38%). Greatest down-regulation of CEF rate at LL was observed in *Z. mays* (-56%) while greatest down-regulation at LL+LC was observed in *P. milioides* (-57%) (**Figure 5. 1C**; **Table 5. 1**). Greatest down-regulation at LC was observed in *M. maximus* (-38%) (**Figure 5. 1C**; **Table 5. 1**).

5.3.5. LMA and Rubisco content

Significant decreases in LMA were observed at LL and LL+LC for all species (**Tables 5. 1** and **5. 2**). Greatest decrease in LMA at LL was observed in *P. milioides* (-64%) and *M. maximus* (-54%) (**Tables 5. 1** and **5. 2**). Greatest decrease at LL+LC was observed in *P. milioides* (-56%) and *P. bisulcatum* (-60%) (**Tables 5. 1** and **5. 2**).

Among all control plants, *P. milioides* had the highest content of leaf Rubisco (**Figure 5. 2A**; **Table 5. 1**). Only the Rubisco content of *P. bisulcatum* and *P. milioides* significantly decreased at LL (-48% and -53%) and at LL+LC (-77% and -68%) while Rubisco content of C_4 species was not affected by the treatments (**Figure 5. 2A**; **Table 5. 1**).

5.3.6. Activity of C_4 cycle enzymes in C_4 plants

Decrease in PEPC activity in all C_4 species was observed greatly at LL (up to -77%) and at LL+LC (up to -69%) than at LC (up to -24%) (**Figure 5. 2B**; **Table 5. 1**). Greatest decrease in PEPC activity at LL was observed in *M. maximus* (-77%), while greatest decrease at LL+LC was observed in *P. miliaceum* (-70%) and *P. antidotale* (-70%) (**Figure 5. 2B**; **Table 5. 1**).

NADP-ME activity decreased most at LL and at LL+LC than at LC in *P. antidotale* (-32% and -38%) and in *Z. mays* (-41% and -42%). Activity of NAD-ME in *P. miliaceum* also decreased greatly at LL (-32%) and at LL+LC (-37%) more than at LC (+3.1%). Same with PCK activity in *M. maximus* which significantly decreased at LL (-68%) and at LL+LC (-69%) more than at LC (-19%) (**Figure 5. 2C**; **Table 5. 1)**.

5.3.7. Pigment content and composition in leaves under low light and low [CO_2]

Lutein and β-carotene are the predominant carotenoids observed in all samples; the other carotenoids that accumulate, in order of abundance, are violaxanthin, neoxanthin, antheraxanthin and zeaxanthin. Individual carotenoids were expressed in mg per leaf area (**Table 5. 3**).

It was observed that all control plants had the same pigment profiles (**Tables 5. 1** and **5. 3**) and there were no significant differences observed in the content of total carotenoids and total chl in leaves (**Figures 5. 3A** and **5. 3B**). Most of the individual carotenoids decreased at LL and at LL+LC in all species except for *P. bisulcatum* (**Figures 5. 3A** and **5. 3B**; **Tables 5. 1** and **5. 3**).

The C_3 grass showed 80% reduction in total carotenoids and 77% reduction in total *chl* under LL+LC. Total carotenoids and chl also significantly decreased under LL in C_3-C_4 and NADP-ME grass species. Interestingly, significant increase in levels of total carotenoids and *chl* was observed only in C_3 grass grown at LL with 127% and 147% increase in content (**Figures 5. 3A** and **5. 3B**). Total carotenoids and total chl decreased greatly in *P. bisulcatum* at LL+LC with 80% and 77% reductions compared to other species (-4% to -50%) (**Figures 5. 3A** and **5. 3B**). All species decreased in chl a/b ratios at LL except for *Z. mays*. Significant decrease in chl *a/b* ratios was also observed at LL+LC only in *P. milioides* and *M. maximus* (**Figure 5. 3C**; **Table 5. 1**).

Ratio of total carotenoids to total chl in all species was not greatly affected by the treatments except for *P. milioides* and *M. maximus* where total carotenoids/total chl ratio decreased at LL and at LL+LC (**Figure 5. 3D**; **Table 5. 1**).

5.3.8. Leaf optical properties and the *QY* under low light and low [CO_2]

A Absorptance spectra for all plants species were typical of vascular plants where the highest total leaf-specific absorptance was observed in the blue region (400–500 nm) and around the chl *a* peak of 660–670 nm (Olle Björkman & Demmig, 1987; Knapp & Carter, 1998) (**Figures 5. 4A** to **5. 4F**). Slightly less than 80% of the incident irradiance was absorbed in this spectral region. Lowest total leaf-specific absorptance occurred around the green wavelengths (500-550 nm), the spectral region with highest transmittance and reflectance. In this region of the spectra, less than 50% of the incident irradiance was absorbed. Changes in leaf absorption were most observable around the green to yellow wavelength region (500-600 nm) (**Figures 5. 4A** to **5. 4F**).

Total leaf absorption of *P. bisulcatum* did not greatly vary at any of treatments (**Figure 5. 4A**). However, it was observed that leaf absorptance at 500-600 nm region of other species decreased more at LL and at LL+LC compared to LC. The leaf absorptance profiles of these species at LL were roughly similar with the profiles at LL+LC, while leaf absorptance profiles at LC were roughly similar with the profiles at control (**Figures 5. 4B** to **5. 4F**). Among all species at LL and at LL+LC, *P. milioides* had the greatest decrease in leaf absorptance around 500-600 nm region with 10% and 12% reduction in absorptance (**Figure 5. 4B**), followed by the two NADP-ME species with 7% and 8% reductions in absorptance **(Figures 5. 4E** to **5. 4F**). It was also observed that *M. maximus* had the greatest decrease in leaf absorptance at 500-600 nm region at LC (-8%) compared to other species (**Figure 5. 4D**).

5.3.9. Quantum yield for CO_2 uptake (*QY*) under low light and low [CO_2]

The quantum yield for CO_2 uptake at saturating irradiance (QY_{sat}) decreased significantly under the two LL treatments for all species (-30% to -50%) except for *P. bisulcatum* which showed no change in QY_{sat} across treatments (**Figure 5. 4A**; **Table 5. 1**).

When measured at growth irradiance, QY_{growth} of *P. bisulcatum* and *P. milioides* at LC was lower compared to the control and at LL+LC (-50% and -33%). However, QY_{growth} of these two species was higher at LL (**Figure 5. 4A**; **Table 5. 1**). All C_4 plants grown under the two LL treatments had significantly higher QY_{growth} compared to the control and LC plants (**Figure 5. 4B**; **Table 5. 1**).

5.4 DISCUSSIONS

To investigate how the light reactions in each of the three C_4 subtype respond to low [CO_2] alone or in combination with low light, representative species of C_3 (*Panicum bisulcatum*), C_3-C_4 (*Panicum milioides*), NADP-ME (*Panicum antidotale*), NAD-ME (*Panicum miliaceum*), PCK (*Megathyrsus maximus*), and model C_4/NADP-ME crop (*Zea mays*) species were grown in four growth chambers with different combinations of low (180 ppm) or ambient (400 ppm) [CO_2] and low (200 µmol photons m^{-2} s^{-1}) or high (1000 µmol photons m^{-2} s^{-1}) light intensity. The influence of long-term exposure to these different environmental conditions on the activity of light harvesting complexes and photosynthesis was examined using measurements of pigment content, chlorophyll fluorescence, leaf absorptance, activity of photosynthetic enzymes, and leaf gas exchange.

5.4.1. Photosynthetic rate was down-regulated in greater extent under low light than under low [CO_2]: C_3, C_3-C_4, and C_4 pathways

A_{sat} and CSRs were more down-regulated under the two LL treatments compared to LC (**Tables 5. 1** and **5. 2**). This was associated with reduced LMA under the two LL treatments (**Tables 5. 1** and **5. 2**). The down-regulation of A_{sat} and CSRs was strongest in C_4 species followed by C_3-C_4 species (**Tables 5. 1** and **5. 2**), suggesting reduced plasticity of C_4 photosynthesis compared to C_3 photosynthesis under LL environment (Björkman, 2011; Boardman, 2003; Ehleringer & Björkman, 1977; Ehleringer & Pearcy, 1983a; Ehleringer, 1978; Jensen, 2006). Down-regulation in photosynthetic rates under LL might be due to lower leaf Rubisco content, which was only observed in C_3 and C_3-C_4 species under LL treatments (**Figure 5. 2A**; **Table 5. 1**). It was expected that Rubisco content in C_4 species will also decrease under LL based on Sonawane *et al.* (2018). However, LL did not elicit any change in Rubisco content of C_4 species (**Figure 5. 2A**; **Table 5. 1**). This maybe because that the level of light used for low light treatments (200 µmol photons m^{-2} s^{-1}) in the present study was not low enough to affect Rubisco content among C_4 species. Other factors might have contributed to the observed down-regulation of photosynthetic rate in C_4 species, such as increased bundle sheath leakiness as demonstrated by increased carbon isotope discrimination (Bellasio & Griffiths, 2014c, 2014a; Bellasio & Lundgren, 2016; Henderson *et al.*, 1992; Sonawane *et al.*, 2018) Overall, my results suggest that light intensity more than [CO_2] is the main factor that controls the rate of photosynthesis especially in C_4 species..

5.4.2. Efficiency of light reactions in PSI and PSII was down-regulated in greater extent under low light than under low [CO_2]: C_3, C_3-C_4, and C_4 pathways

Rates of various photosynthetic electron transport processes were measured under high light (HL) (1000 µmol photons m^{-2} s^{-1}) (**Figures 5. 1A** to **5. 1C**). In all species, ETR1 and ETR2 were down-regulated more under the two LL treatments relative to LC treatment (**Figures 5. 1A** and **5. 1B**; **Table 5. 1**).

Under LL, ETR1 decreased most in C_3-C_4 species followed by C_4 species (**Figure 5. 1A**; **Table 5. 1**). Under LL+LC, ETR1 decreased in both C_3 and C_3-C_4 species (**Figure 5. 1A**; **Table 5. 1**). ETR2 responded similarly to ETR1 except that LL reduced ETR2 most in C_3 species followed by C_4 species (**Figure 5. 1B**; **Table 5. 1**). These results suggest that PSI of C_3-C_4 species is the most sensitive to LL among all species. For the C_3 species, the negative effect of LL on PSI was intensified under LC (**Figure 5. 1A**; **Table 5. 1**). PSII of C_3-C_4 species is more sensitive to LC than to LL according the response of ETR2 (**Figure 5. 1B**; **Table 5. 1**). However, PSII of C_3 species was affected LL independently of [CO_2] treatment (**Figure 5. 1B**; **Table 5. 1**). For the C_4 species, PSI and PSII were more sensitive to changes in light intensity than changes in [CO_2] (**Figures 5. 1A** and **5. 1B**; **Table 5. 1**). However, growth under LC might have affected the development of PSI and PSII in PCK species which might explain the significant decrease in ETR1 and ETR2 even under HL (**Figures 5. 1A** and **5. 1B**; **Table 5. 1**).

Several factors can account for reduced PSI and PSII efficiency under LL or LC. One is the decrease in the amount of functional PSII in leaves which was observed only in C_3 and NAD-ME species under the two LL treatments (**Tables 5. 1** and **5. 2**). However, this change does not explain the low ETR2 of C_3, C_3-C_4 and PCK species under other treatments (**Figure 5. 1B**; **Table 5. 1**). This suggests that light plays a more important role in regulating the synthesis, accumulation and stoichiometry of the protein components of PSII in C_3 and NAD-ME species (Anderson, 1986; Bailey *et al.*, 2001; Chow *et al.*, 1991; Leong & Anderson, 1984; Mullet, 1988).

Measurements of photochemical quenching of PSII (qP), quantum yield of PSII [Y(II)] and PSI [Y(I)] also reflect the efficiency of both photosystems. The first two parameters represent the approximate fraction of open to total PSII centers (Govindjee, 1995; Klughammer & Schreiber, 1994; Krause & Weis, 1991). A decrease in these fraction is associated with an increased risk of photoinhibition and subsequent photodamage (Baroli & Melis, 1998; Ögren & Rosenqvist, 1992; Öquist & Huner, 1993; Park *et al.*, 1996). A greater decrease in qP,

Y(II), and Y(I) was observed under the two LL treatments (**Tables 5. 1** and **5. 2**). However, qP, Y(II), and Y(I) decreased more in C_3 and C_3-C_4 species grown under LL+LC treatment (**Tables 5. 1** and **5. 2**), suggesting that LC intensified the negative effect of LL on PSI and PSII efficiency in these species.

Another factor which might have impacted the efficiency of both photosystems under LL treatments is the cyclic electron flux around PSI (CEF). This can serve as a protective mechanism which can consume excess reducing power NADPH to maintain the efficiency of photosystems during sudden exposure to very high irradiances (Shikanai, 2007). CEF decreased under the two LL treatments in C_4 species (**Figure 5. 1C**; **Table 5. 1**). This suggests that the operation of CEF under the two LL environments in C_4 species was much slower than in plants grown under HL with LC. LL during growth might down-regulate some proteins needed for the operation of CEF such as *PGR5* and *Ndh* particularly in C_4 species (Burrows *et al.*, 1998; DalCorso *et al.*, 2008; Horváth *et al.*, 2000; Munekage *et al.*, 2002; Shikanai *et al.*, 1998; Yamori & Shikanai, 2016). However, under LL+LC treatment, CEF of C_3-C_4 and PCK species also greatly declined (**Figure 5. 1C**; **Table 5. 1**) suggesting that LC during growth might also affect the development of proteins needed for CEF in these species.

5.4.3. Light-harvesting processes was down-regulated in greater extent under low light than under low [CO_2]: C_3, C_3-C_4, and C_4 pathways

In the C_3 and C_3-C_4 species and one C_4 species (*P. antidotale*), significant changes in total leaf carotenoid and chlorophyll contents were observed under the two LL treatments (**Figures 5. 3A** and **5. 3B**). These results highlight again that light intensity was mow important than atmospheric [CO_2] for leaf pigment development of these species. Under ambient [CO_2], LL greatly increased total carotenoids and total chlorophylls in the C_3 species while a decrease or no change was observed in other species (**Figures 5. 3A** and **5. 3B**; **Table 5. 1**). Under LL+LC, total leaf carotenoid and chlorophyll contents decreased similarly in the C_3 and other species. The increase in leaf pigment contents under low light and ambient CO_2 might be an acclimation response of C_3 species where some of the nitrogen resources were allocated from maximizing CO_2 fixation to maximizing light harvesting (Evans & Poorter, 2001). However, total carotenoid and total chlorophylls under low light treatment with low [CO_2] decreased in the C_3 species (**Figures 5. 3A** and **5. 3B**; **Table 5. 1**) suggesting that low [CO_2] constrained plant growth, limiting its options for optimisation between CO_2 fixation and light harvesting processes.

Lower leaf chlorophyll *a/b* ratios and lower carotenoids/chlorophyll ratios were also observed in most of the species grown under two LL treatments (**Figures 5. 3C** and **5. 3D**; **Table 5. 1**). Changes in chlorophyll *a/b* ratios may partly explain the decrease in electron transport rates under LL treatments. The chlorophyll-protein complex of both photosystems is composed of a core complex (reaction centre) and a light-harvesting complex (Thornber, 1986). The chlorophyll *a/b* ratios are greater in the core complex than the light-harvesting complex in both photosystems. A low chlorophyll *a/b* ratio could imply an increased proportion of light-harvesting complexes relative to reaction centres (Green & Durnford, 1996; Hikosaka & Terashima, 1995). The increase in light-harvesting complexes relative to reaction centres might be an adaptation to broaden the spectral range over which PSI and PSII absorb light as part of acclimation to balance energy absorption under low light environment (Yamazaki *et al.*, 2005). Lower carotenoids/chlorophyll ratios also suggest that low light grown plants prioritized light harvesting (through chlorophyll) more than photoprotection (through carotenoids).

These alterations in pigment ratios are reflected by the pronounced changes in the absorption spectra of plants under the two LL treatments (**Figures 5. 4A** to **5. 4F**). It was again observed that leaf absorptance at the visible wavelengths (400-700 nm) decreased to a greater extent under the two LL environments than under HL environment combined with LC, suggesting that growth under LL negatively affected mechanisms of light absorption in leaves. It has been shown by Carter (1993) and Carter *et al.* (1992) that increased leaf reflectance (decrease in absorptance) within the PAR wavebands, specifically 535–640 nm (green) and 685–700 nm (red) in response to environmental conditions was a result of decreased chlorophyll content and likely to indicate plant stress. Greatest decrease in absorptance under LL was observed in C_3-C_4 species (**Figure 5. 4B**) followed by C_4 species, more particularly in *P. antidotale* (NADP-ME) (**Figure 5. 4E**) which was reflected by the lower chlorophyll content (**Figure 5. 3B**). Decreased leaf absorptance can also be due to alterations in leaf morphology (e.g. reduced leaf thickness) as a result of growth under LL. This can also be an acclimation response to increase transmitted light to prevent photoinhibition (Vogelmann, 2003). Since *P. milioides* and *P. antidotale* had the greatest decrease in total absorptance under LL, it can be suggested that these species have less leaf plasticity under low light environments in comparison to other species.

The decrease in the QY_{sat} of LL-grown plants also suggests that the light-harvesting components in the leaf were down-regulated by LL more than LC (**Figure 5. 3A**; **Table 5. 1**). This down-regulation made both photosystem sensitive to saturating irradiance which might

have caused photoinhibiton during *QY* measurements thus affecting ATP production needed for CO_2 assimilation. However, at their respective growth environment, QY_{growth} was higher under low light in most of the species suggesting that these plants might have developed light reaction components that were more acclimated to low light (**Figure 5. 3B**; **Table 5. 1**).

5.4.4. Photosynthetic enzymes in the C_4 species were more affected by low light than by low CO_2

The activities of PEPC and decarboxylases in all C_4 species were greatly reduced under the two LL treatments more than under HL treatment with LC suggesting that LL down-regulated C_4 cycle enzymes more than LC (**Figures 5. 2B** and **5. 2C**; **Table 5. 1**). Similarly, Sonawane *et al.* (2018) reported that long-term exposure to low light (119 μmol photons m^{-2} s^{-1}) reduced PEPC activity by 49-84% and decarboxylases activity by 25-64% of C_4 species which caused an impairment in CCM efficiency. It has also been shown by Pinto *et al.* (2014) that PEPC and decarboxylases activities in C_4 species were unaffected by growth under low [CO_2].

5.5 CONCLUSION

Using representative grass species from C_3, C_3-C_4 and three biochemical subtypes of C_4 photosynthesis grown under high light (HL) or low light (LL) combined with low [CO_2] (LC) or ambient [CO_2] (AC), this study demonstrated that LL is the main factor that influences the regulation of the activities of photosystem complexes and the rate of photosynthesis more than LC in C_4 species. Acclimation responses brought about by LL involved decreased in the yield efficiency of PSI and PSII and down-regulation of various electron transport rates brought about by the decrease in the content of functional PSII, total leaf pigments and leaf absorptance. These resulted in the deficiency in ATP and NADPH production which in turn affected the rates of photosynthesis. Same with findings of Sonawane *et al.* (2018), low light condition also caused reduction in Rubisco content and activities of PEPC and decarboxylases thus affecting CCM which added stress on the photosynthetic rate. However, I did not find any change in PEPC activity in all C_4 species under low [CO_2] treatments which is contrary to Pinto *et al.* (2014). Among the C_4 subtypes, the PCK grass was the most sensitive under LC as seen in the slight decrease of fluorescence parameters, leaf absorptance and PCK activity. Acclimation of light reactions in the C_3-C_4 grass was the same as PCK grass but seemed that low [CO_2] caused a greater acclimation more than low light. Interestingly, light reactions of C_3 grass did not show much acclimation under LC or LL but greatly acclimated when the two factors were combined. Content and activity of photosynthetic enzymes and LMA were greatly reduced in all species under LL+LC and LL more than under LC suggesting that light is the main factor that influence proteins involved in carbon assimilation. We suggest further experiments are needed involving more representative species from each photosynthetic type and using much lower light intensity and CO_2 concentration during growth.

Table 5. 1 Statistical summary

Summary of statistical analysis using two-way ANOVA for the effects of treatments and species on various parameters collected from leaf of 24 plants grown under control (high light + ambient [CO_2]), low light + low [CO_2], high light + low [CO_2], and low light + ambient [CO_2] environments. Some of the parameters were measured at 200 µmol photons m^{-2} s^{-1} (LL) or 1000 µmol photons m^{-2} s^{-1} (HL).

Parameter	Low [CO_2] (P)			Low light (P)			Low light x low [CO_2] (P)		
	species	treatment	species x treatment	species	treatment	species x treatment	species	treatment	species x treatment
PSII content (µmol m^{-2})	0.011	0.389	0.436	0.000	0.410	0.004	0.000	0.005	0.014
LMA (g m^{-2})	0.008	0.637	0.290	0.000	0.000	0.007	0.000	0.000	0.052
A_{sat} (µmol $m^{-2}s^{-1}$)	0.000	0.696	0.581	0.000	0.000	0.003	0.000	0.000	0.061
CSR (µmol $m^{-2}s^{-1}$)	0.066	0.718	0.219	0.080	0.000	0.028	0.006	0.000	0.001
ETR1 at LL (µmol e- $m^{-2}s^{-1}$)	0.000	0.273	0.000	0.003	0.000	0.015	0.000	0.000	0.064
ETR1 at HL (µmol e^- $m^{-2}s^{-1}$)	0.000	0.001	0.000	0.000	0.000	0.000	0.000	0.000	0.000
ETR2 at LL (µmol e^- $m^{-2}s^{-1}$)	0.000	0.016	0.000	0.000	0.003	0.007	0.006	0.000	0.007
ETR2 at HL (µmol e^- $m^{-2}s^{-1}$)	0.000	0.021	0.000	0.000	0.001	0.290	0.000	0.000	0.000
CEF at LL (µmol e^- $m^{-2}s^{-1}$)	0.000	0.075	0.049	0.000	0.002	0.007	0.000	0.005	0.136
CEF at HL (µmol e^- $m^{-2}s^{-1}$)	0.000	0.017	0.054	0.000	0.000	0.000	0.000	0.000	0.000
F_v/F_m	0.000	0.283	0.219	0.000	0.417	0.003	0.000	0.473	0.000
Y(I) at LL	0.000	0.381	0.000	0.004	0.000	0.015	0.000	0.000	0.062
Y(I) at HL	0.000	0.030	0.001	0.000	0.003	0.405	0.000	0.000	0.000
Y(II) at LL	0.000	0.015	0.000	0.000	0.004	0.007	0.006	0.000	0.005
Y(II) at HL	0.000	0.001	0.000	0.000	0.000	0.000	0.000	0.000	0.000
qP at LL	0.000	0.560	0.005	0.005	0.043	0.205	0.002	0.030	0.001
qP at HL	0.000	0.897	0.000	0.000	0.005	0.124	0.001	0.000	0.060

Rubisco content (µmol LSU sites m^{-2})	0.000	0.522	0.991	0.000	0.000	0.002	0.000	0.000	0.000
PEPC activity (µmol m^{-2} s^{-1})	0.000	0.179	0.067	0.000	0.000	0.000	0.000	0.000	0.000
NADP-ME activity (µmol m^{-2} s^{-1})	0.000	0.001	0.000	0.000	0.000	0.000	0.000	0.000	0.000
NAD-ME activity (µmol m^{-2} s^{-1})	0.000	0.775	0.901	0.000	0.002	0.002	0.000	0.003	0.002
PCK activity (µmol m^{-2} s^{-1})	0.000	0.000	0.032	0.000	0.000	0.000	0.000	0.000	0.000
Absorptance at 453 nm	0.000	0.000	0.000	0.000	0.001	0.000	0.000	0.000	0.000
Absorptance at 550 nm	0.000	0.013	0.201	0.000	0.000	0.188	0.000	0.000	0.031
Absorptance at 662 nm	0.000	0.000	0.001	0.000	0.000	0.000	0.000	0.000	0.000
QY_{growth}	0.000	0.000	0.025	0.001	0.000	0.222	0.000	0.001	0.005
QY_{sat}	0.128	0.784	0.812	0.490	0.000	0.119	0.010	0.000	0.908
Neoxanthin content (mg m^{-2})	0.000	0.035	0.620	0.000	0.137	0.000	0.000	0.000	0.000
Violaxanthin content (mg m-2)	0.000	0.027	0.286	0.000	0.011	0.000	0.000	0.000	0.000
Antheraxanthin content (mg m^{-2})	0.000	0.005	0.558	0.000	0.995	0.000	0.000	0.000	0.000
Lutein content (mg m^{-2})	0.001	0.149	0.698	0.000	0.015	0.000	0.000	0.000	0.000
Zeaxanthin content (mg m^{-2})	0.003	0.338	0.157	0.054	0.000	0.029	0.056	0.000	0.039
β-Carotene content (mg m^{-2})	0.000	0.009	0.689	0.000	0.543	0.000	0.000	0.000	0.000
Chlorophyll a content (mg m^{-2})	0.001	0.009	0.557	0.000	0.010	0.000	0.000	0.000	0.000
Chlorophyll b content (mg m^{-2})	0.000	0.015	0.665	0.000	0.000	0.000	0.000	0.000	0.000
Total carotenoids content (mg m^{-2})	0.000	0.033	0.657	0.000	0.428	0.000	0.000	0.000	0.000
Total chlorophyll content (mg m^{-2})	0.000	0.009	0.593	0.000	0.005	0.000	0.000	0.000	0.000
Chlorophyll *a/b*	0.035	0.438	0.297	0.000	0.001	0.000	0.000	0.025	0.013
Total carotenoids/total chlorophyll	0.000	0.585	0.049	0.001	0.066	0.186	0.000	0.444	0.001

Table 5. 2 Parameters derived from *A–C*i curve, light response curve, Dual-PAM measurements, and LMA in leaf of C_3, C_3-C_4 and C_4 species

Parameters derived from *A–C*i curve, light response curve, Dual-PAM measurements, and LMA for *Panicum bisulcatum* (C_3); *Panicum milioides* (C_3-C_4); *Panicum miliaceum* (NAD-ME); *Megathyrsus maximus* (PCK); *Panicum antidotale* (NADP-ME); and *Zea mays* (NADP-ME) grown under control (high light + ambient [CO_2]), low light + low [CO_2], high light + low [CO_2], and low light + ambient [CO_2] environments. Each column represents the mean ± s.e. of species (n = 4 plants). Letters indicate the ranking (highest = a) within each species under each treatment using multiple-comparison Tukey's post-hoc test. Statistical significance levels (t-test) for the growth condition within each species are also shown and they are: * ≡ $p < 0.05$; ** ≡ $p < 0.01$; *** ≡ $p < 0.001$.

Parameter	Treatment	C_3	C_3-C_4	NAD-ME	PCK	NADP-ME	NADP-ME
		Panicum bisulcatum	*Panicum milioides*	*Panicum miliaceum*	*Megathyrsus maximums*	*Panicum antidotale*	*Zea mays*
A_{sat} (μmol m^{-2} s^{-1})	CONTROL	20.20 ± 0.54 a	26.31 ± 2.50 a	32.62 ± 2.45 a	39.30 ± 2.40 a	37.8 ± 1.79 a	48.89 ± 1.61 a
	Low light + Low CO_2	20.48 ± 0.27 ab	14.47 ± 2.31 b**	21.81 ± 2.69 b*	27.04 ± 1.18 ab	26.85 ± 3.88 b	34.48 ± 1.45 a***
	Low CO_2	22.11 ± 5.13 b	26.51 ± 3.07 ab	30.06 ± 9.81 b	45.05 ± 2.96 ab	34.31 ± 5.98 ab	42.26 ± 4.00 a
	Low light	21.25 ± 1.96 a	17.02 ± 1.70 ab**	15.26 ± 2.86 b**	22.58 ± 4.41 ab	25.32 ± 1.47 ab	29.61 ± 2.13 a**
CSRs (μmol m^{-2} s^{-1})	CONTROL	36.24 ± 2.96 c	43.27 ± 3.53 b	37.58 ± 2.64 b	39.11 ± 6.4 ab	38.64 ± 0.62 b	38.64 ± 0.62 a
	Low light + Low CO_2	29.92 ± 0.5 b	21.07 ± 2.28 b**	22.18 ± 1.62 a*	33.2 ± 2.12 a	22.51 ± 1.95 a**	41.79 ± 2.29 a
	Low CO_2	27.48 ± 1.34 d	38.69 ± 4.73 cd	33.29 ± 6.32 ab	39.81 ± 6.69 b	38.59 ± 4.32 bc	50.43 ± 2.37 a
	Low light	33.75 ± 2.24 d	24.85 ± 3.02 cd**	17.6 ± 1.50 d*	30.06 ± 4.74 b	31.12 ± 0.84 bc**	36.1 ± 3.39 a
PSII content (μmol m^{-2})	CONTROL	2.53 ± 0.32 a	1.77 ± 0.35 ab	1.59 ± 0.07 b	2.49 ± 0.27 a	2.27 ± 0.05 ab	2.08 ± 0.11 ab
	Low light + Low CO_2	1.71 ± 0.02 ab*	2.25 ± 0.18 ab	0.72 ± 0.06 c***	2.42 ± 0.21 a	2.10 ± 0.30 ab	1.45 ± 0.04 bc**
	Low CO_2	2.17 ± 0.21 a	2.20 ± 0.33 a	1.54 ± 0.13 a	2.03 ± 0.31 a	2.36 ± 0.13 a	1.80 ± 0.22 a
	Low light	1.59 ± 0.08 bc*	2.51 ± 0.29 a	1.03 ± 0.10 c*	2.77 ± 0.25 a	2.21 ± 0.06 ab	2.03 ± 0.15 ab
F_v/F_m	CONTROL	0.79 ± 0.01 a	0.78 ± 0 a	0.67 ± 0 c	0.79 ± 0 a	0.75 ± 0.02 b	0.76 ± 0 ab
	Low light + Low CO_2	0.77 ± 0.02 a	0.74 ± 0.01 bc*	0.72 ± 0.01 c***	0.79 ± 0.01 a	0.76 ± 0 ab*	0.77 ± 0 a*
	Low CO_2	0.77 ± 0.01 ab	0.78 ± 0 a	0.79 ± 0 c	0.78 ± 0.01 a	0.76 ± 0.01 ab	0.74 ± 0.01 b
	Low light	0.79 ± 0 a	0.78 ± 0 ab	0.71 ± 0.01 d*	0.78 ± 0.01 ab	0.74 ± 0.01 cd	0.75 ± 0.01 bc

Y(I)	CONTROL	0.19 ± 0.01 c	0.32 ± 0.02 a	0.14 ± 0.01 d	0.15 ± 0.01 cd	0.12 ± 0.01 d	0.23 ± 0.01 b
	Low light + Low CO_2	0.11 ± 0.01 ab**	0.14 ± 0.01 a**	0.11 ± 0.01 ab	0.09 ± 0.01 b*	0.09 ± 0.01 b	0.15 ± 0.01 a
	Low CO_2	0.17 ± 0.01 bc	0.24 ± 0.01 a**	0.15 ± 0 c	0.1 ± 0 d**	0.14 ± 0.01 cd	0.21 ± 0.02 ab
	Low light	0.17 ± 0.01 b	0.24 ± 0.02 a*	0.11 ± 0.01 c	0.09 ± 0 c**	0.1 ± 0 c	0.12 ± 0.01 c*
Y(II)	CONTROL	0.11 ± 0.01 a	0.09 ± 0.01 b	0.06 ± 0.01 c	0.07 ± 0 bc	0.06 ± 0 c	0.06 ± 0 c
	Low light + Low CO_2	0.05 ± 0.01 a***	0.05 ± 0.01 a*	0.04 ± 0.01 a	0.05 ± 0 a**	0.05 ± 0 a**	0.05 ± 0 a**
	Low CO_2	0.1 ± 0.01 a	0.05 ± 0.01 b**	0.07 ± 0 b	0.06 ± 0 b**	0.07 ± 0 b	0.06 ± 0 b*
	Low light	0.11 ± 0.01 a	0.06 ± 0.01 b	0.05 ± 0 b	0.05 ± 0 b**	0.05 ± 0 b	0.04 ± 0 b**
qP	CONTROL	0.33 ± 0.03 a	0.33 ± 0.02 a	0.25 ± 0.02 ab	0.18 ± 0 b	0.16 ± 0.02 b	0.23 ± 0.01 ab
	Low light + Low CO_2	0.22 ± 0.02 a**	0.17 ± 0.07 a	0.17 ± 0.02 a*	0.16 ± 0.01 a	0.17 ± 0.01 a	0.19 ± 0.02 a
	Low CO_2	0.37 ± 0.03 a	0.21 ± 0.01 bc***	0.28 ± 0.01 ab	0.16 ± 0.01 c	0.2 ± 0.02 bc	0.24 ± 0.02 bc
	Low light	0.32 ± 0.04 a	0.26 ± 0.04 ab	0.17 ± 0.03 bc*	0.12 ± 0.01 c*	0.16 ± 0.01 bc	0.14 ± 0.01 c*
LMA ($g\ m^{-2}$)	CONTROL	34.64 ± 2.05 a	28.75 ± 2.23 abc	32.47 ± 1.72 abc	26.96 ± 2.09 bc	25 ± 3.53 c	33.1 ± 0.77 ab
	Low light + Low CO_2	15.36 ± 0.68 abc**	11.58 ± 0.77 c**	20 ± 0.59 ab**	13.39 ± 1.35 bc*	16.83 ± 2.2 abc*	21.33 ± 1.01 a**
	Low CO_2	31.79 ± 3.66 ab	29.5 ± 1.72 ab	29.49 ± 1.94 ab	26.07 ± 2.71 b	31.33 ± 2.38 ab	36.52 ± 0.55 a
	Low light	12.5 ± 1.58 b**	16.5 ± 0.73 ab**	22.17 ± 1.09 a**	12.5 ± 1.22 b*	16.17 ± 1.32 ab*	21.39 ± 0.93 a**
QY_{growth} (mol CO_2 mol^{-1} photons)	CONTROL	0.02 ± 0 b	0.03 ± 0.01 ab	0.03 ± 0 ab	0.05 ± 0 a	0.03 ± 0 b	0.04 ± 0 a
	Low light + Low CO_2	0.03 ± 0 cd	0.03 ± 0 d	0.05 ± 0 bc	0.07 ± 0 ab*	0.07 ± 0.01 a	0.05 ± 0 ab
	Low CO_2	0.01 ± 0 b*	0.02 ± 0 ab*	0.03 ± 0 a	0.03 ± 0 ab	0.02 ± 0 ab	0.03 ± 0.01 a
	Low light	0.05 ± 0 ab*	0.06 ± 0 ab*	0.04 ± 0.01 b	0.06 ± 0 a*	0.05 ± 0 ab*	0.06 ± 0 ab*
QY_{sat} (mol CO_2 mol^{-1} photons)	CONTROL	0.01 ± 0 b	0.02 ± 0 ab	0.02 ± 0 b	0.02 ± 0 ab	0.02 ± 0 ab	0.03 ± 0 a
	Low light + Low CO_2	0.01 ± 0 ab	0.01 ± 0 b**	0.01 ± 0 ab*	0.01 ± 0 ab*	0.01 ± 0 ab*	0.02 ± 0 a***
	Low CO_2	0.02 ± 0 b	0.02 ± 0 ab	0.02 ± 0 ab	0.02 ± 0 a	0.02 ± 0 ab	0.02 ± 0 a
	Low light	0.01 ± 0 ab	0.01 ± 0 ab**	0.01 ± 0 b**	0.01 ± 0 ab*	0.01 ± 0 ab**	0.02 ± 0 a**

Table 5. 3 Pigment composition in leaves C_3, C_3-C_4 and C_4 species

Pigment composition in leaves of *Panicum bisulcatum* (C_3); *Panicum milioides* (C_3-C_4); *Panicum miliaceum* (NAD-ME); *Megathyrsus maximus* (PCK); *Panicum antidotale* (NADP-ME); and *Zea mays* (NADP-ME) grown under control (high light + ambient [CO_2]), low light + low [CO_2], high light + low [CO_2], and low light + ambient [CO_2] environments. Each column represents the mean ± s.e. of species (n = 4 plants Letters indicate the ranking (highest = a) within each species under each treatment using multiple-comparison Tukey's post-hoc test. Statistical significance levels (t-test) for the growth condition within each species are also shown and they are: * ≡ $p < 0.05$; ** ≡ $p < 0.01$; *** ≡ $p < 0.001$.

Parameter	Treatment	C_3	C_3-C_4	NAD-ME	PCK	NADP-ME	NADP-ME
		Panicum bisulcatum	*Panicum milioides*	*Panicum miliaceum*	*Megathyrsus maximums*	*Panicum antidotale*	*Zea mays*
Neoxanthin (mg m^{-2})	CONTROL	6.44 ± 0.27 b	12.06 ± 0.52 a	6.29 ± 0.93 b	6.87 ± 0.63 b	8.63 ± 0.37 b	8.12 ± 0.74 b
	Low light + Low CO_2	0.92 ± 0.05 c***	6.1 ± 0.85 ab*	6.18 ± 0.73 ab	9.16 ± 0.19 a*	4.77 ± 0.2 b**	7.53 ± 0.68 ab
	Low CO_2	4.65 ± 0.49 b	9.27 ± 2.34 a	6.42 ± 0.22 ab	6.07 ± 0.51 b	7.7 ± 0.49 ab	7.67 ± 0.75 ab
	Low light	13.21 ± 0.5 a**	10.24 ± 0.61 ab***	7.83 ± 0.54 bc	7.51 ± 0.96 bc	5.82 ± 0.56 c**	7.19 ± 0.72 bc
Violaxanthin (mg m^{-2})	CONTROL	18.28 ± 0.58 bc	29.06 ± 0.66 a	14.45 ± 2.73 c	15.8 ± 0.78 bc	20.7 ± 0.3 bc	23.56 ± 3.84 ab
	Low light + Low CO_2	2.7 ± 0.08 c***	11.54 ± 1.97 b**	13.66 ± 1.02 ab	14.76 ± 0.15 ab	10.2 ± 0.87 bc**	19.45 ± 1.39 a
	Low CO_2	13.8 ± 0.44 c**	21.58 ± 4.75 ab	17.58 ± 1.12 abc	11.56 ± 0.58 c*	14.94 ± 0.84 bc*	23.18 ± 4.58 a
	Low light	30.03 ± 0.78 a***	19.78 ± 1.46 b*	14.81 ± 0.65 bc	14.04 ± 0.77 bc	10.11 ± 1.26 c**	18.24 ± 1.33 b
Antheraxanthin (mg m^{-2})	CONTROL	1.38 ± 0.06 bc	2.07 ± 0.05 a	1.04 ± 0.15 c	1.81 ± 0.1 ab	1.51 ± 0.04 bc	1.8 ± 0.2 ab
	Low light + Low CO_2	0.25 ± 0.02 c***	1.04 ± 0.12 ab**	1.05 ± 0.07 ab	1.54 ± 0.02 a	0.72 ± 0.05 bc**	1.49 ± 0.16 a
	Low CO_2	1.03 ± 0.11 a	1.58 ± 0.44 a	1.15 ± 0.09 a	1.5 ± 0.03 a	1.15 ± 0.05 a**	1.53 ± 0.1 a
	Low light	2.82 ± 0.05 a***	1.75 ± 0.12 b	1.31 ± 0.09 bc	1.37 ± 0.11 bc	0.88 ± 0.08 c**	1.46 ± 0.18 b

Lutein (mg m^{-2})	CONTROL	25.97 ± 8.35 b	54.35 ± 1.45 a	31.52 ± 4.47 b	41.69 ± 2.5 ab	42 ± 2.4 ab	48.97 ± 4.65 a
	Low light + Low CO_2	6.83 ± 0.47 d	28.62 ± 3.74 bc**	31 ± 3.16 bc	51.67 ± 0.38 a*	23.01 ± 1.05 c*	41.48 ± 3.77 ab
	Low CO_2	28.6 ± 2.4 a	42.81 ± 10.9 a	32.67 ± 0.74 a	37.1 ± 1.69 a	36.07 ± 2.32 a	43.07 ± 3.13 a
	Low light	79.89 ± 1.65 a	45.21 ± 2.98 b*	39.28 ± 2.21 bc	44.75 ± 3.33 bc	28.73 ± 2.19 c*	41.24 ± 4.96 bc
Zeaxanthin (mg m^{-2})	CONTROL	2.11 ± 0.71 a	0.87 ± 0.11 ab	2.18 ± 1.06 a	1.06 ± 0.29 ab	0.17 ± 0 b	2.01 ± 0.14 a
	Low light + Low CO_2	0 ± 0 a	0.77 ± 0.14 a	0.35 ± 0.09 a	0.14 ± 0.08 a	0.06 ± 0.03 a	0.26 ± 0.11 a**
	Low CO_2	1.81 ± 0.16 ab	0.84 ± 0.33 b	1.25 ± 0.33 b	3.16 ± 0.82 a	0.28 ± 0.05 b	3.02 ± 1.18 a
	Low light	0 ± 0 a	0.81 ± 0.1 a	0.32 ± 0.04 a	0 ± 0 a*	0.06 ± 0.03 a	0.16 ± 0 a**
β-Carotene (mg m^{-2})	CONTROL	25.88 ± 0.44 bc	40.17 ± 1.08 a	22.12 ± 2.4 c	31.37 ± 2.14 abc	33.17 ± 0.84 ab	37.85 ± 3.49 a
	Low light + Low CO_2	5.05 ± 0.28 c***	19.46 ± 2.69 b**	22.33 ± 2.11 ab	31.24 ± 0.25 a	16.23 ± 1.01 b**	32.9 ± 3.41 a
	Low CO_2	20.12 ± 1.92 b	31.89 ± 8.43 a	23.75 ± 1.5 ab	26.35 ± 1.02 ab	26.95 ± 1.02 ab*	32.6 ± 2.59 a
	Low light	55.88 ± 1.33 a***	32.41 ± 2.12 b*	27.73 ± 1.46 bc	27.06 ± 2.17 bc	19.48 ± 1.48 c**	32.5 ± 3.71 b
Chlorophyll *a* (mg m^{-2})	CONTROL	364.89 ± 8.35 bc	529.24 ± 15.19 ab	286.88 ± 33.84 c	480.59 ± 23.22 ab	443.93 ± 8.75 abc	553.6 ± 60.7 a
	Low light + Low CO_2	83.68 ± 4.36 c***	281.94 ± 37.91 b**	309.1 ± 31.09 b	520.98 ± 5.64 a	238.14 ± 13.09 bc**	501.4 ± 54.46 a
	Low CO_2	310.21 ± 26.07 ab	360.15 ± 131.61 ab	300.99 ± 13.15 b	399.67 ± 19.05 ab	369.78 ± 23.66 ab	474.98 ± 32.18 a
	Low light	884.28 ± 20.1 a***	454.17 ± 34.96 b	361.32 ± 16.92 bc	479.08 ± 40.89 b	284 ± 20.44 c**	510.05 ± 60.71 b
Chlorophyll *b* (mg m^{-2})	CONTROL	88.4 ± 2.2 ab	124.51 ± 4.05 a	64.87 ± 7.18 b	119.87 ± 5.65 a	93.11 ± 4.77 ab	125.87 ± 16.83 a
	Low light + Low CO_2	20.85 ± 1.38 d***	70.88 ± 9.32 bc*	69.96 ± 7.7 bc	140.41 ± 0.86 a*	54.12 ± 3.3 cd*	106.05 ± 10.23 ab
	Low CO_2	74.98 ± 6.09 a	98.22 ± 27.92 a	68.12 ± 2.49 a	94.46 ± 4.79 a	85.8 ± 7.29 a	101.6 ± 3.85 a
	Low light	235.85 ± 6.02 a***	117.12 ± 10.63 bc	84.44 ± 4.38 cd	126.15 ± 10.27 b	65.19 ± 4.7 d*	105.87 ± 13.5 bc

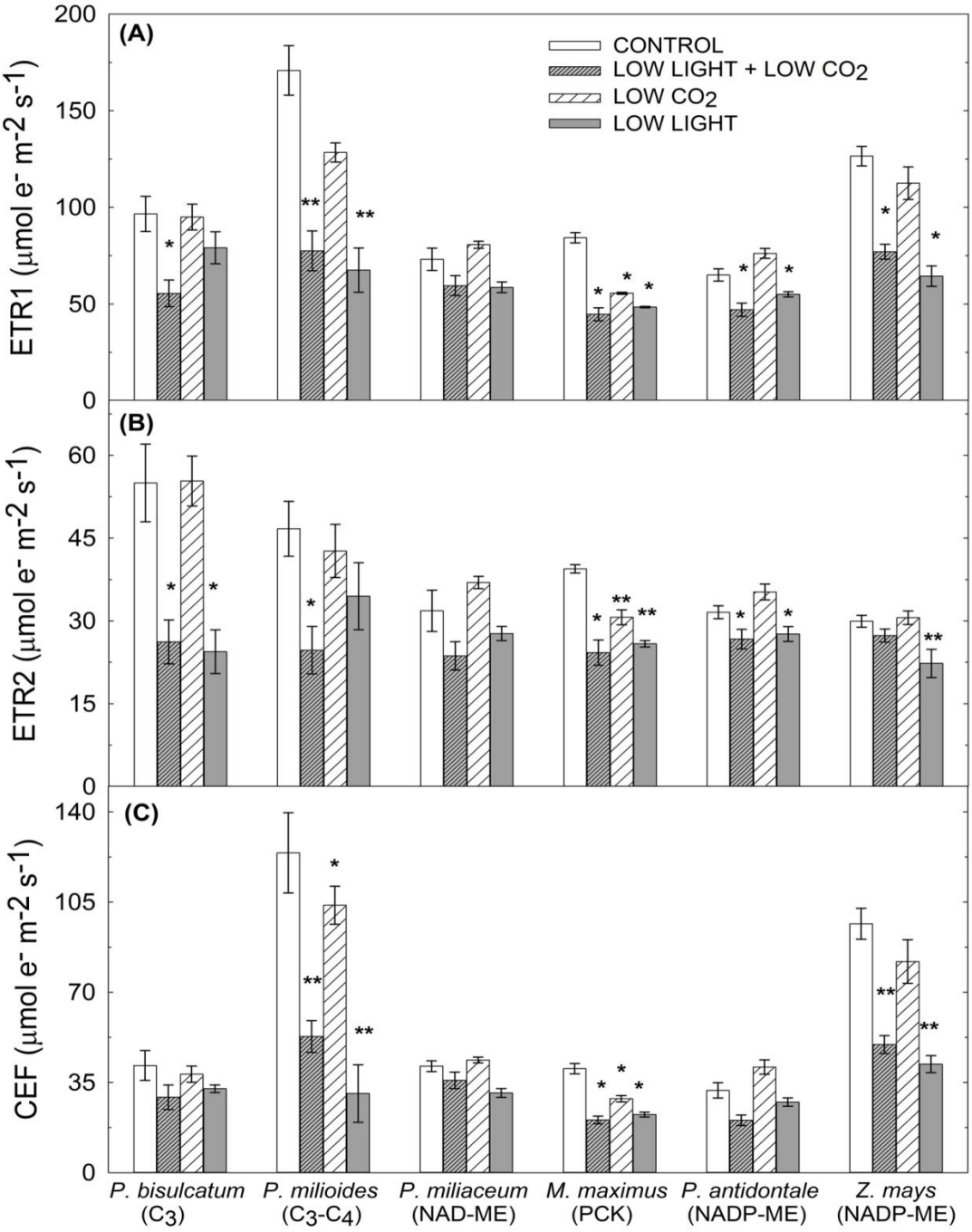

Figure 5. 1 Various electron fluxes in leaves of C_3, C_3-C_4 and C_4 species under low light and low [CO_2]

Various electron fluxes measured at 1000 µmol photons m^{-2} s^{-1} in leaves of *Panicum bisulcatum* (C_3); *Panicum milioides* (C_3-C_4); *Panicum miliaceum* (NAD-ME); *Megathyrsus maximus* (PCK); *Panicum antidotale* (NADP-ME); and *Zea mays* (NADP-ME) grown under control (high light + ambient [CO_2]), low light + low [CO_2], high light + low [CO_2], and low light + ambient [CO_2] environments. Each column represents the mean ± s.e. of species (n = 4 plants). **(A)** ETR1 and **(B)** ETR2 are the linear electron flux through PSI and PSII. **(C)** CEF is cyclic electron flux around PSI calculated by subtracting ETR2 from ETR1. Statistical significance levels (t-test) for the growth condition within each species are shown and they are: * ≡ $p < 0.05$; ** ≡ $p < 0.01$; *** ≡ $p < 0.001$.

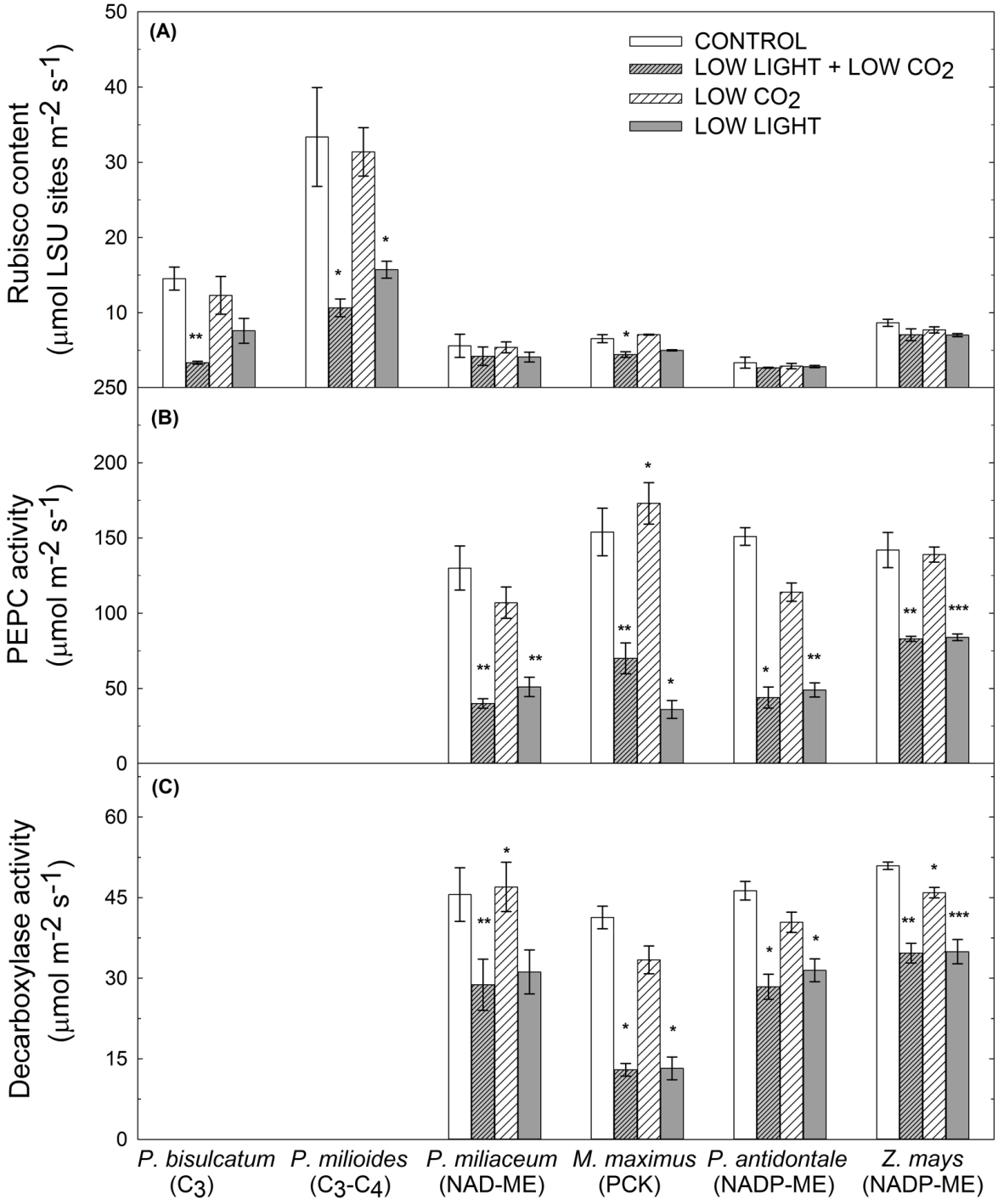

Figure 5. 2 Acclimation of photosynthetic enzymes leaf of C_3, C_3-C_4 and C_4 species under low light and low [CO_2]

Acclimation of **(A)** Rubisco; **(B)** PEPC and **(C)** decarboxylases in leaves of *Panicum bisulcatum* (C_3); *Panicum milioides* (C_3-C_4); *Panicum miliaceum* (NAD-ME); *Megathyrsus maximus* (PCK); *Panicum antidotale* (NADP-ME); and *Zea mays* (NADP-ME) grown under control (high light + ambient [CO_2]), low light + low [CO_2], high light + low [CO_2], and low light + ambient [CO_2] environments. Each column represents the mean ± s.e. of species (n = 4 plants). Statistical significance levels (t-test) for the growth condition within each species or subtype are shown and they are: * ≡ $p < 0.05$; ** ≡ $p < 0.01$; *** ≡ $p < 0.001$.

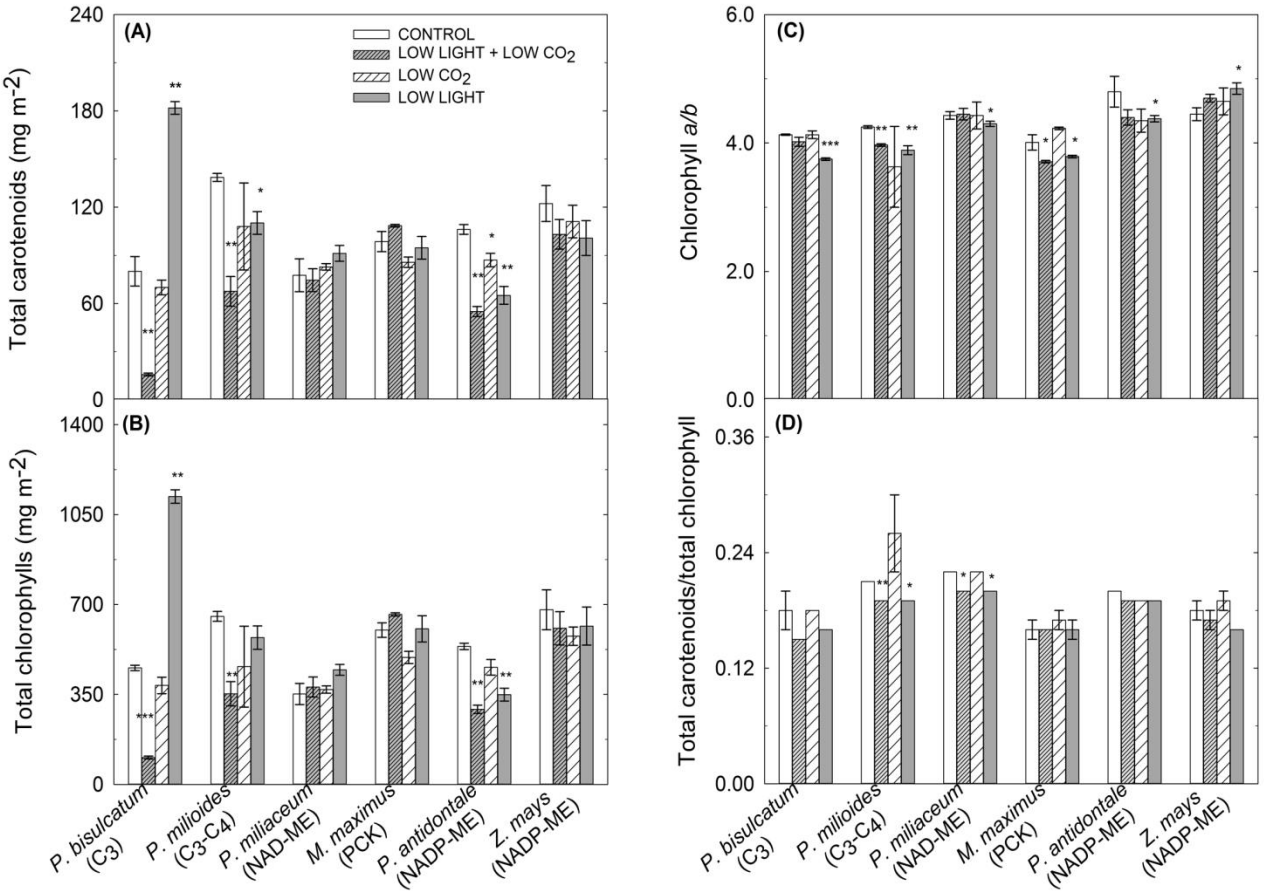

Figure 5. 3 Contents of chlorophyll and carotenoids in leaf of C_3, C_3-C_4 and C_4 species under low light and low [CO_2]

Contents of **(A)** total carotenoids and **(B)** total chlorophylls; and ratios of **(C)** chlorophyll *a* to *b* and (D) total carotenoids to total chlorophylls in leaves of *Panicum bisulcatum* (C_3); *Panicum milioides* (C_3-C_4); *Panicum miliaceum* (NAD-ME); *Megathyrsus maximus* (PCK); *Panicum antidotale* (NADP-ME); and *Zea mays* (NADP-ME) grown under control (high light + ambient [CO_2]), low light + low [CO_2], high light + low [CO_2], and low light + ambient [CO_2] environments. Each column represents the mean ± s.e. of species (n = 4 plants). Statistical significance levels (t-test) for the growth condition within each species or subtype are shown and they are: * ≡ $p < 0.05$; ** ≡ $p < 0.01$; *** ≡ $p < 0.001$.

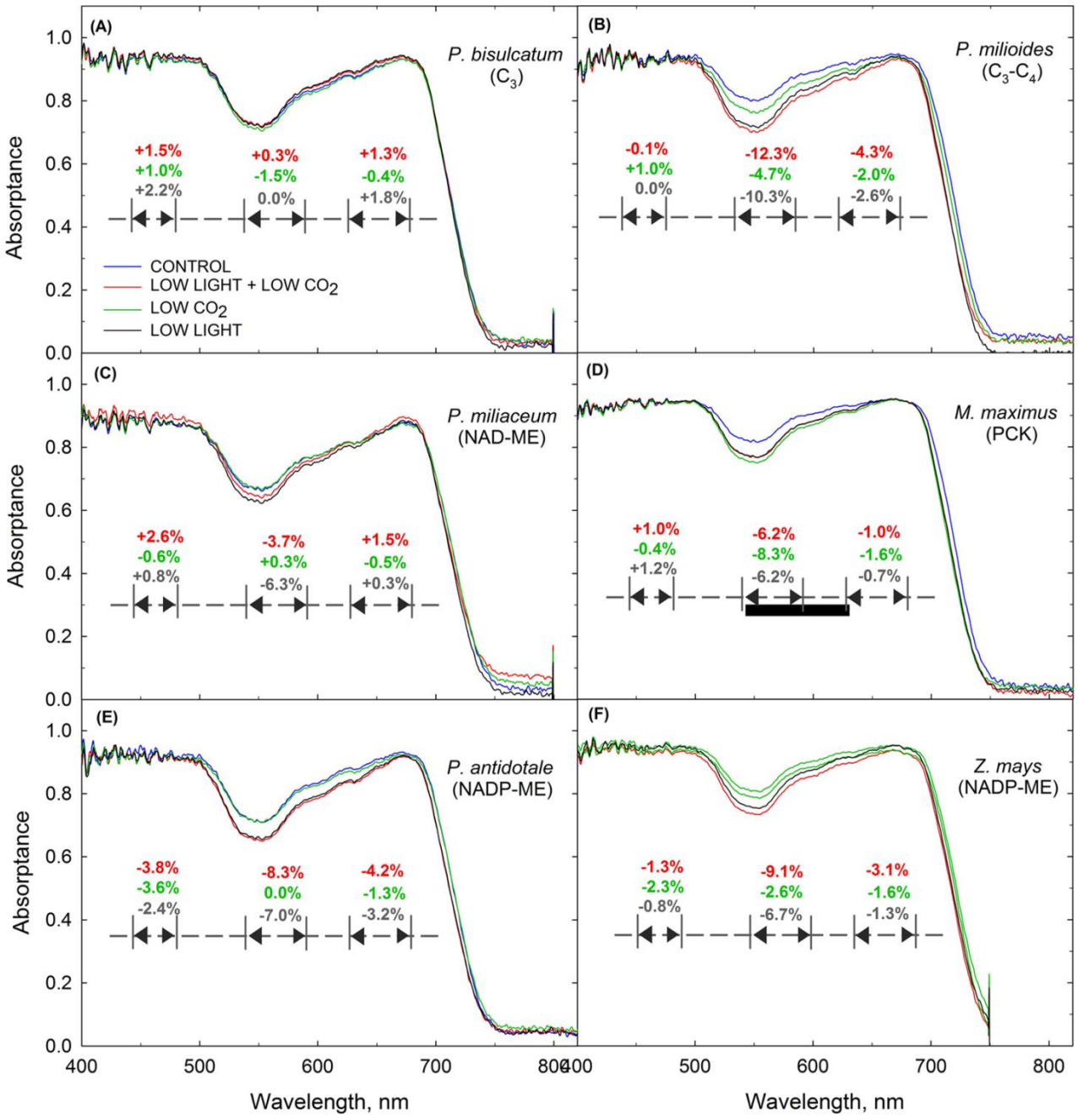

Figure 5. 4 Average leaf spectral absorptance at 400 nm to 800 nm of C_3, C_3-C_4 and C_4 species under low light and low [CO_2]

Average leaf spectral absorptance at 400 nm to 800 nm showing the percentage decrease in absorptance in the blue (430-453 nm), green (500-580 nm), and red (640-662 nm) regions in **(A)** *Panicum bisulcatum* (C_3); **(B)** *Panicum milioides* (C_3-C_4); **(C)** *Panicum miliaceum* (NAD-ME); **(D)** *Megathyrsus maximus* (PCK); **(E)** *Panicum antidotale* (NADP-ME); and **(F)** *Zea mays* (NADP-ME) grown under control (high light + ambient [CO_2]), low light + low [CO_2], high light + low [CO_2], and low light + ambient [CO_2] environments. Values are means ± s.e. of species (n = 4 plants).

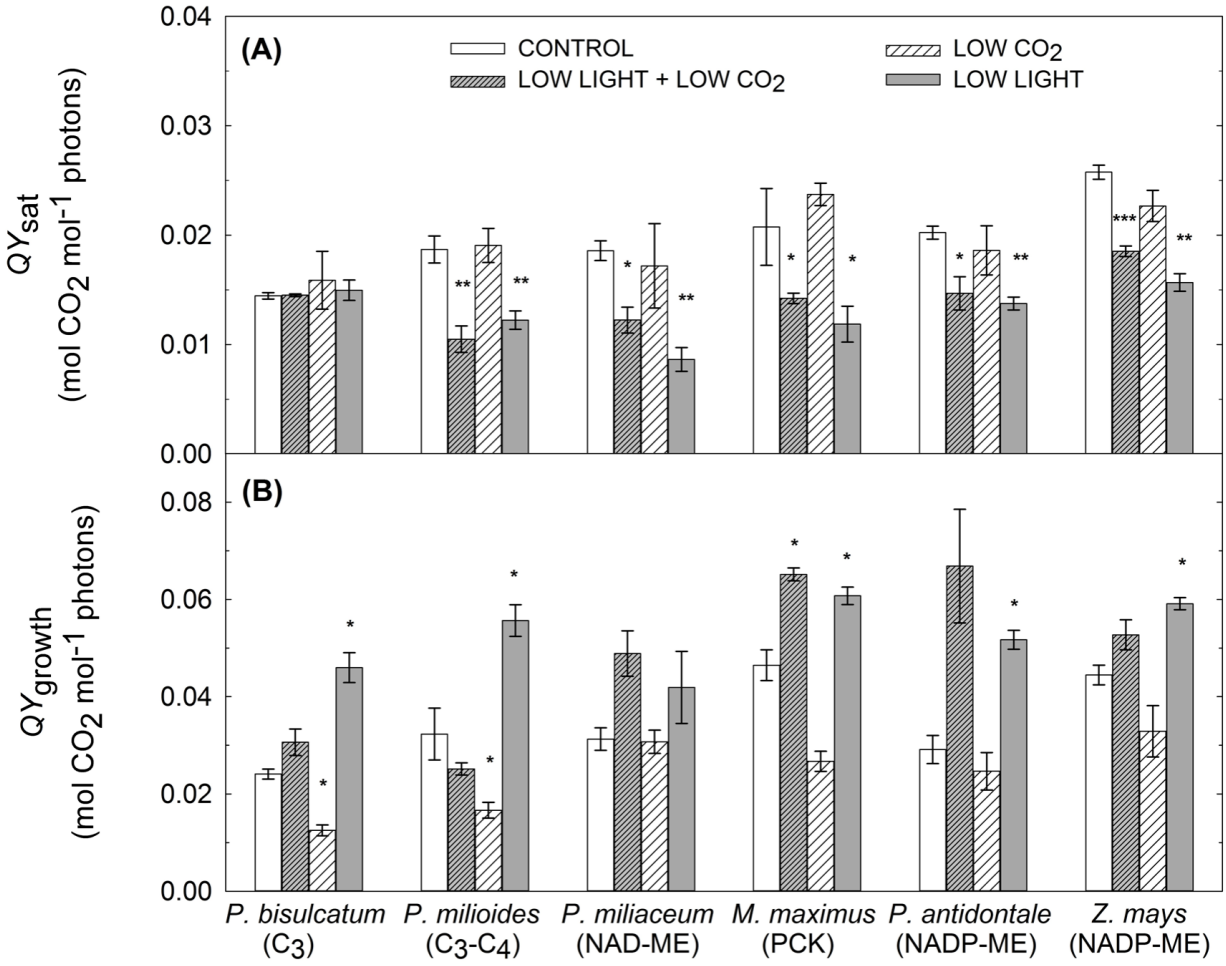

Figure 5. 5 Absorbed quantum yield for CO_2 uptake at saturating irradiance and at growth irradiance in leaf of C_3, C_3-C_4 and C_4 species under low light and low [CO_2]

Absorbed quantum yield for CO_2 uptake at **(A)** saturating irradiance (QY_{sat}) and at **(B)** growth irradiance (QY_{growth}) measured in leaves of *Panicum bisulcatum* (C_3); *Panicum milioides* (C_3-C_4); *Panicum miliaceum* (NAD-ME); *Megathyrsus maximus* (PCK); *Panicum antidotale* (NADP-ME); and *Zea mays* (NADP-ME) grown under control (high light + ambient [CO_2]), low light + low [CO_2], high light + low [CO_2], and low light + ambient [CO_2] environments. Each column represents the mean ± s.e. of species (n = 4 plants). Statistical significance levels (t-test) for the growth condition within each species or subtype are shown and they are: * ≡ p < 0.05; ** ≡ p < 0.01; *** ≡ p < 0.001.

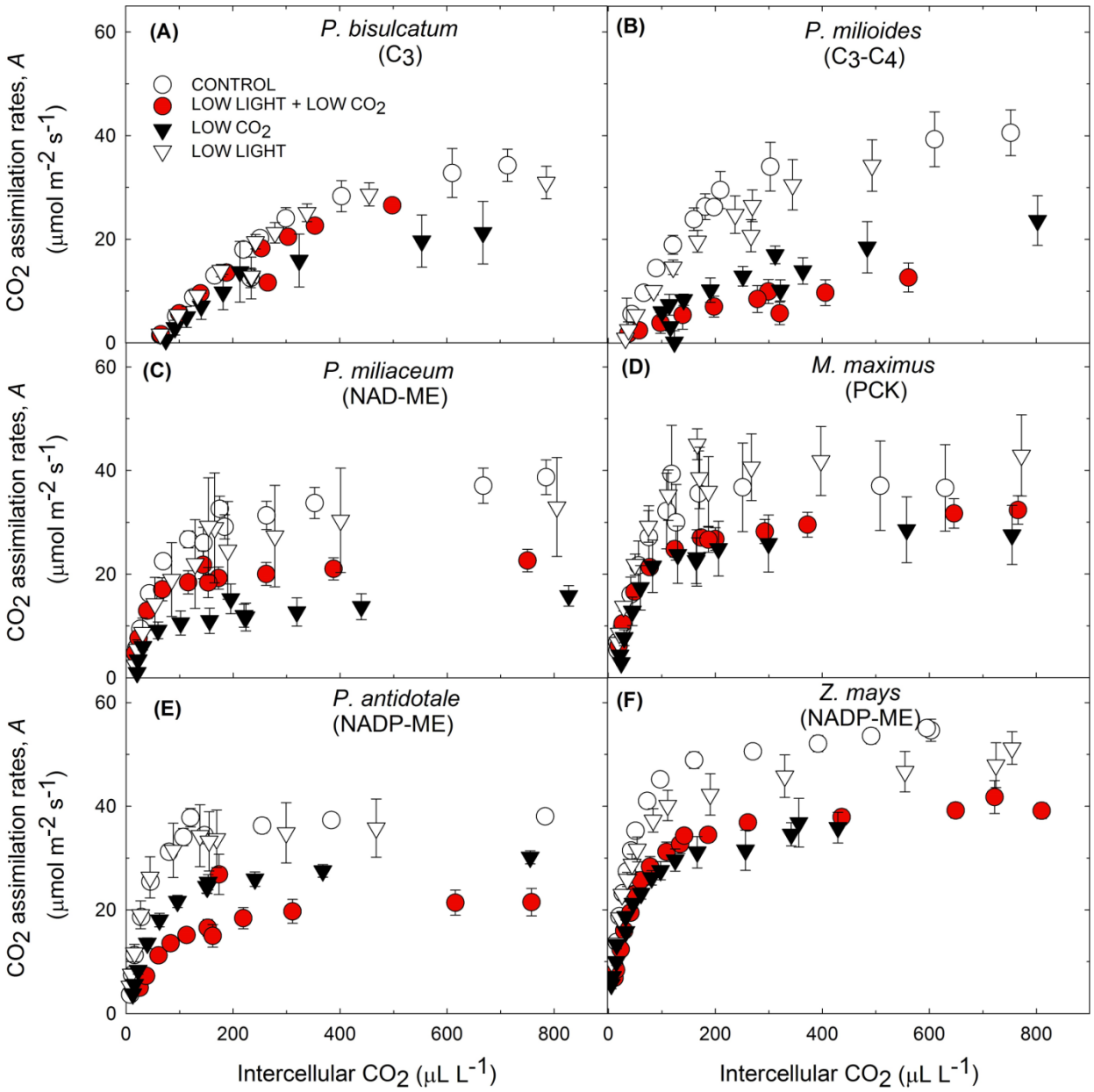

Figure 5. S 1 Photosynthetic CO_2 response curves (A-C_i) of C_3, C_3-C_4 and C_4 species under low light and low [CO_2]

Photosynthetic CO_2 response curves (A-C_i) of **(A)** *Panicum bisulcatum* (C_3); **(B)** *Panicum milioides* (C_3-C_4); **(C)** *Panicum miliaceum* (NAD-ME); (D) *Megathyrsus maximus* (PCK); **(E)** *Panicum antidotale* (NADP-ME); and **(F)** *Zea mays* (NADP-ME) grown in control (high light + ambient [CO_2]), low light + low [CO_2], high light + low [CO_2], and low light + ambient [CO_2] environments. Responses of CO_2 assimilation rate (A) to increasing intercellular [CO_2], C_i were measured at saturating light (2000 µmol photons m^{-2} s^{-1} for C_4 species and 1500 µmol photons m^{-2} s^{-1} for C_3 and C_3-C_4 species). Values are means ± s.e. of species or subtype (n = 4 plants).

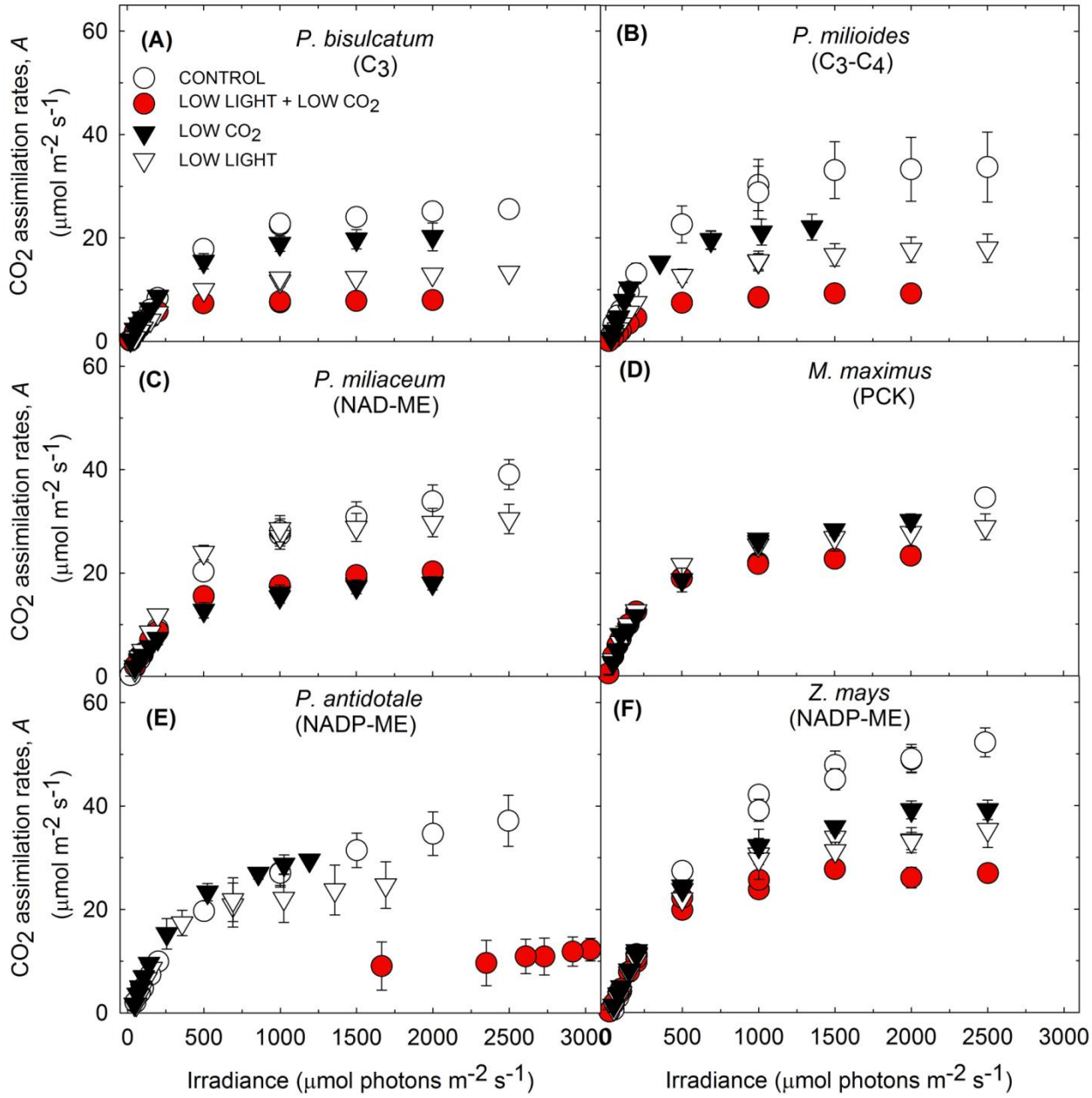

Figure 5. S 2 Photosynthetic light response curves of C_3, C_3-C_4 and C_4 species under low light and low [CO_2]

Photosynthetic light response curves of **(A)** *Panicum bisulcatum* (C_3); **(B)** *Panicum milioides* (C_3-C_4); **(C)** *Panicum miliaceum* (NAD-ME); (D*) Megathyrsus maximus* (PCK); **(E)** *Panicum antidotale* (NADP-ME); and **(F)** *Zea mays* (NADP-ME) grown in control (high light + ambient [CO_2]), low light + low [CO_2], high light + low [CO_2], and low light + ambient [CO_2] environments. Responses of CO_2 assimilation rate (*A*) to increasing irradiance were measured at saturating CO_2 (C_a = 800 ppm). Values are means ± s.e. of species or subtype (*n* = 4 plants).

CHAPTER 6

GENERAL DISCUSSIONS

6.1. Overall thesis summary

It has become well established that C_4 photosynthetic pathway enables plants to photosynthesize at a higher rate than C_3 plants under conditions of high light, temperatures and limited water supply (Edwards, *et al.*, 2010; Ehleringer & Björkman, 1977; Ehleringer & Pearcy, 1983; Pearcy *et al.*, 1981; Zhu *et al.*, 2008). This is because of the CO_2 concentrating mechanism (CCM) in C_4 photosynthesis which saturates Rubisco with CO_2 in the bundle sheath cells (BSC). The CCM minimizes photorespiration where oxygen competes with CO_2 uptake which consumes additional energy and decreases productivity. Importantly, the activity rate of C_4 photosynthesis is optimal under high light intensities, therefore it is not surprising to find C_4 plants in open and arid habitats leading to their agricultural and ecological importance in those habitats. C_4 photosynthesis is traditionally grouped into three classical subtypes based on the major C_4 acid decarboxylation step in the BSC: NADP malic enzyme (NADP-ME), NAD-malic enzyme (NAD-ME), and PEP carboxykinase (PCK). In many C_4 species, especially those using NADP-ME as a primary decarboxylase, PEP-CK operates as a secondary decarboxylase (Chapman & Hatch, 1981; Sharwood *et al.*, 2014; Wingler *et al.*, 1999).

In view of the relative abundance of C_4 plants in high light environments, it is important to ascertain what physiological factors associated with C_4 photosynthesis might make it favourable in those environments. One reason is the differences in the maximum quantum yield for CO_2 uptake (*QY*), which is the leaf-level ratio of photosynthetic carbon gain to absorbed photons. Under elevated temperature (>25^{o}C) and ambient CO_2 concentrations, previous studies showed that *QY* of C_3 species are lower compared to C_4 species, and among C_4 subtypes, NAD-ME subtype had the lowest. The lower *QY* of C_3 and C_3-C_4 species can be attributed to the energy expenditure due to higher rate of photorespiration under normal atmospheric conditions compared to C_4 plants. However, factors behind the observed differences in *QY* among the C_4 subtypes are not clear. One reason for this variation is the efficiency of light energy conversion reactions (termed energetics) in MC and BSC which is associated with distinct composition and activity of light-harvesting complexes (LHC) and electron transport reactions. Limited information is available explaining the connection between energetics under varying environmental conditions and *QY* among the C_4 subtypes. Understanding acclimation strategies, that is, how C_4 photosynthesis cope with varying environmental conditions such as light and CO_2, is therefore relevant to provide insights about the efficiency of C_4 energetics.

In this study, the components of light reactions of photosynthesis in different species of C_3, C_3-C_4 and C_4 plants were measured and compared to test whether the high photosynthetic *QY* observed in C_4 plants and the variations in *QY* among C_4 subtypes are attributed to the differences in light absorption and/or activity and stoichiometry of photosystems in the leaf. Representative species of C_3, C_3-C_4 and C_4 plants were grown under high-light (control) and shade (20% sunlight) which are also combined with either ambient or low CO_2 condition to elucidate how light intensity may affect photosystem contents and activities in chloroplasts and also to learn about the effect of low CO_2 environment on the rate of energy generation during the light reactions. In addition, relative electron fluxes in the leaf were monitored and quantified *in vivo* so they reflected functionality *in situ*, without any potential complication associated with isolation of thylakoids. This also enabled me to calculate the partitioning of the absorbed light into the two photosystems which are needed to quantitatively estimate cyclic electron flow (CEF) and Mehler reactions in the leaf. The developed methods were also applied on representative species of gymnosperm, liverwort and fern, in order to test the reliability of our screening techniques on diverse plant species.

In conclusion, this PhD project demonstrated that the observed high *QY* of C_4 species and particularly in the NADP-ME species is associated with the comparatively greater plastic adjustments of leaf energetics under varying environmental conditions. This is very important acclamatory characteristic as it maximises light energy absorption while preventing photo-inhibition under stress conditions such as long-term shade exposure. This also ensures the light reactions can still provide the right ATP/NADPH ratio even under limited supply of light energy.

6.2. Overall thesis conclusions

The current study investigated the plasticity of the components and activities of the light reactions (termed energetics) of photosynthesis in representative species of C_3, C_3-C_4, and the three subtypes of C_4 photosynthesis under environmental conditions that may affect the photosynthetic quantum yield (*QY*) such as low light and low CO_2. Based on the results reported in this thesis, I have selected to discuss five key overall findings in this general conclusion chapter (**Figures 6. 1** and **6. 2**; **Tables 6. 1** and **6. 2**).

6.2.1. Experimentally derived f_I is important for the accurate estimation of the rates of electron fluxes through PSI

Calculation of electron flow rates through PSI (ETR1) and cyclic electron flow around PSI (CEF) depends on an accurate estimation of the fraction of the absorbed white light partitioned to PSI (f_I) and PSII (f_{II}). Value of f_I is usually assumed to be 0.5 which means that 50% of the absorbed light is partitioned to (i.e., absorbed by) PSI, but it has been hypothesized that this value could be higher in C_4 plants. f_I and f_{II} are only known for a few species, commonly C_3, and f_I is always assumed to be 0.5 in untested species. It is also unknown in ferns, liverwort, gymnosperms or among the various C_4 species. Under control conditions, I showed that the majority of C_4 species examined had f_I of 0.6 which is higher than what is usually assumed (**Table 6. 1**). C_3 grass had f_I of 0.4 which is lower compared to the model C_3 species, spinach. Higher value of f_I in C_4 species compared to C_3 species validated the hypothesis that more excitation energy is distributed to PSI compared to PSII in C_4 species. Other species such as liverwort and fern had f_I of 0.5 while gymnosperms had lower f_I suggesting a greater amount of PSII components relative to PSI in mesophyll chloroplasts. It was also shown that these values can change depending on the growth irradiance. Under shade, f_I of C_3 and C_4 species increased suggesting that growth irradiance affected the distribution of excitation energy by modulating the composition of light-harvesting antennas of PSI and PSII (Anderson, 1986; Huner *et al.,* 2003; Tanaka & Melis, 1997).

Using the experimentally derived f_I values, corrected ETR1 was higher in NADP-ME and NAD-ME grasses by ~20% and lower in control PCK (~9%) and C_3 (~16%) grasses when compared to uncorrected ETR1. Using corrected ETR1, CEF rates were found to increase by ~32% and 38% in control NADP-ME and NAD-ME grass species and decreased by ~14% and ~28% in control PCK and C_3 grass species, respectively measured at ≥500 μmol photons m^{-2} s^{-1}. The calculated variations in f_I and f_{II} among species should therefore be taken into account for improved photosynthetic calculations and modelling.

6.2.2. Magnitude of Mehler reaction was negligible in high light-grown plants but was greatly stimulated in shade-grown plants

The extent to which the Mehler reaction is engaged during the light reactions may also contribute to the light use efficiency of C_4 plants (Cramer *et al.,* 2002; Rumberg *et al.,* 2013). To elucidate the physiological significance of Mehler reaction, quantitative analysis and precise evaluation of the O_2 exchange *in vivo* are important. However, the Mehler reaction is difficult to measure directly. It is commonly estimated from measurements of chlorophyll fluorescence and net CO_2 or O_2 exchange. Since it was previously demonstrated that O_2 uptakes from photorespiration, mitochondrial respiration and Mehler reaction have different isotope fractionation factors (Guy *et al.,* 2016), the method developed in Chapter 2 which uses $^{16}O/^{18}O$ isotopes was used to quantify the O_2 exchange rates in leaf.

Here, I observed that O_2 uptake of all high-light grown species measured at high light and high pCO_2 was roughly similar to that measured in the dark suggesting a low or virtually no potential for the Mehler reaction and that the O_2 uptake was mainly due to photorespiration or mitochondrial respiration (**Table 6. 2**). Among the C_4 species, O_2 uptake at high pCO_2 was not significantly different between the light and the dark, suggesting that this is mainly due to mitochondrial respiration, given that photorespiration in C_4 plants is negligible under very high pCO_2.

However, O_2 uptake of shade-grown C_4 plants under high light was significantly higher compared to dark O_2 uptake suggesting an enhanced operation of Mehler reaction (**Table 6. 2**). Since both the C_3 and C_4 cycles were compromised under shade (Sonawane *et al.,* 2018), electron flow in the thylakoid is expected to be limited at the reducing side of PSI upon exposure to high irradiance. The electron flow to PSI will be suppressed because of the increasing counter-pressure to proton release during PQH_2 oxidation at cyt b_6f (Harbinson & Hedley, 1993; Laisk *et al.,* 2005; Tsuyama & Kobayashi, 2009). Therefore, electron drain from PSI in the Mehler reaction is important in shade-grown plants to alleviate this pressure. Consequently, Mehler reaction served more as a photo-protective mechanism against photo-oxidative stress to the photosynthetic machinery under high irradiance than as support for additional ATP production in shade-grown plants. This is a new concept for C_4 plants relative to what has previously been suggested (Furbank *et al.,* 1990).

6.2.3. Efficiency of light reactions of photosynthesis in C_3, C_3-C_4 and C_4 species were down-regulated under long-term shade exposure

To determine how photosynthetic types and subtypes influence the variations in energy conversion efficiency and susceptibility to low light, measurements of leaf chlorophyll fluorescence, photosynthesis, electron transport rates, absorptance and pigment contents were compared between high light and low light-grown plants (**Figure 6. 1**).

In C_3 species, photosynthesis was least affected while CEF was virtually suppressed under shade. Further, quantum yield for CO_2 uptake (QY), leaf absorptance and total chlorophyll and carotenoid contents were unaffected in the C_3 species under shade. The response of PSII/PSI ratio, CEF rates, leaf absorptance and pigments of C_3-C_4 species under shade were closer to the C_4 species (**Figures 6. 1** and **6. 2**).

Among all C_4 species, NAD-ME species was the most negatively affected by shade in terms of reduced leaf pigments, absorptance, QY, Y(II), F_v/F_m, LEF_{O2} and PSII content. Reduced leaf PSII content under shade reflects the greater photosynthetic inhibition of NAD-ME species to low light relative to the other C_4 subtypes (Sonawane *et al.*, 2018), and might also be an acclimation response to prevent photo-inhibition (Park *et al.*, 2016).

It was also observed that long term exposure to shade reduced the activities of Rubisco, PEPC and decarboxylase the greatest in NAD-ME species, again confirming that CCM of this subtype is least efficient under shade (Sonawane *et al.*, 2018).

In conclusion, my study clearly showed that the NAD-ME subtype is less efficient under shade not only because of it less efficient CCM (Sonawane *et al.*, 2018), but also because of its less efficient and less plastic energetics (i.e., light absorption and electron transport) characteristics. This is also a novel contribution of my work.

The efficiency of PSI in the two NADP-ME species was reflected in their higher operation of ETR1 and CEF under saturating light compared to other species. This finding also supports the view that the photosynthetic apparatus of BS chloroplasts of NADP-ME species generates ATP through CEF (but not the Mehler reaction, as argued above). High operation of CEF around PSI might be one of the reasons for the observed high QY among NADP-ME species. Shade reduced ETR1 and CEF the greatest in the two NADP-ME species, which highlights the dependence of photosynthetic rates on CEF in this subtype.

6.2.4. Efficiency of photosynthesis and light reactions in PSI and PSII were down-regulated more under low light than under low CO_2 in C_3, C_3-C_4, and C_4 species

It was observed that the saturated CO_2 assimilation rate (A_{sat}), CO_2 saturated rates (CSRs), rates of various electron fluxes in PSI and PSII, contents of carotenoids and chlorophylls, QY and contents of photosynthetic enzymes were more down-regulated under low light treatments (low light + ambient [CO_2] and low light + low [CO_2]) compared at under low CO_2 treatment (high light + low [CO_2]), suggesting that light intensity more than CO_2 concentration greatly influence the efficiency of photosynthesis in C_3, C_3-C_4, and C_4 species (**Figures 6. 1** and **6. 2**). Greatest down-regulation of A_{sat}, CSR and QY under low light was observed in C_4 species followed by C_3-C_4 species may indicate the lower plasticity of C_4 photosynthesis compared to C_3 photosynthesis under low light environment (**Figures 6. 1** and **6. 2**) (Sage & McKown, 2006; Sage & Coleman, 2001; Tissue *et al.*, 1995).

Among the C_4 subtypes, the PCK grass was the most sensitive under low [CO_2] condition as seen in the slight decrease of fluorescence parameters, leaf absorptance and PCK activity. Interestingly, light reactions of the C_3 grass did not show much acclimation under high light + low [CO_2] or low light + ambient [CO_2] but greatly acclimated when the two factors were combined.

This is in contrast to the other studies showing that CO_2 starvation resulted in a dramatic decrease in photosynthetic activity in C_3 plants as shown by the down-regulation of electron transport activity (Durchan *et al.*, 2001) and reduction in stomatal and biochemical responses (Pinto *et al.*, 2014; Tissue *et al.*, 1995).

6.2.5. Simultaneous measurements of CO_2 and O_2 fluxes enabled the estimation of the capacity for the photosynthetic reduction of nitrate (NO_3^-) among plant species as reflected by the assimilation quotient (*AQ*)

According to the overall equation for photosynthesis in plants, the ratio of CO_2 taken up to O_2 evolved (assimilation quotient or *AQ*) should be in unity (Björkman, 1973; Kaplan & Bjorkman, 1980). Sustained *AQ*, consistently either above or below unity can be expected only in those cases where a substantial fraction of the organic carbon products have a reduction level that differs markedly from that of carbohydrates (Kaplan & Bjorkman, 1980). The *AQ* was also verified as a non-destructive measure of *in vivo* NO_3^- assimilation (Bloom *et al.,* 1989; Myers, 1949).

It was observed in **Chapter 3** that *AQ* values of all control species are close to 1.0 when measured at low irradiance (~200 µmol photons m^{-2} s^{-1}) and high pCO_2. Then *AQ* started to decrease under increasing irradiance (up to 0.8). This decrease in *AQ* under increasing irradiance is expected where substantial amounts of other substrates, such as NO_3^- and SO_4^{2-} are reduced during photosynthesis, or where the final carbon products of photosynthesis have an average reduction level greater than that of carbohydrates unity (Björkman, 1973; Bloom *et al.,* 1989; Bloom *et al.,* 2002; Kaplan & Bjorkman, 1980). Transfer of electrons to NO_3^- and NO_2^- during photosynthesis increases O_2 evolution from the light-dependent reactions of photosynthesis, while CO_2 consumption by the Calvin cycle continues at similar rates (Bloom *et al.,* 2002). Therefore, plants that are reducing NO_3^- and SO_4^{2-} exhibit a lower *AQ*. The observed decreased *AQ* of all control species measured at 1000 µmol photons m^{-2} s^{-1} (AQ_{1000}) indicates a high rate of electron fluxes and overall light reactions in the chloroplasts (**Figure 6. 3**).

It was also observed that shade-grown plants have higher *AQ* compared to the control plants even when measured at low irradiance. *AQ* above unity is expected where a significant fraction of the organic carbon products have a reduction level lower than that of carbohydrates (Björkman, 1973; Bloom *et al.,* 1989; Bloom *et al.,* 2002; Kaplan & Bjorkman, 1980). Greatest increase in AQ_{1000} was observed in NAD-ME species (+129%) (**Figure 6. 3**) suggesting the decrease in electron fluxes and light reactions capacities which might be due to the down-regulation of proteins and other light-harvesting complexes under long exposure to shade.

6.3. Future Outlook

Finally, several tests and experiments are still needed in the future in order to further elucidate my findings here. Future work requires more detailed analysis of the mechanisms of light reactions. Here, I outline some ideas.

- **Chapter 3** estimated the rate of Mehler reaction in leaves of several plant species based on monitoring of $^{16}O_2$ uptake under high irradiances. However, this O_2 uptake can also be due to photorespiration or mitochondrial respiration. Hence, there is a need to develop a method for monitoring different isotopes of O_2 during gas evolution in leaves to have a better estimation of the Mehler reaction rate. Developing a method to monitor the rate of CO_2 as well as O_2 isotopic exchanges in leaf discs will also help to better estimate the capacity for light respiration (R_l) under various conditions.
- It is suggested that more intensive measurements of the activities of the light-harvesting complexes should be done under varying environmental conditions such as measuring the activity and quantity of ATP synthase, cyt b_6f complex, PSI core complexes, and PSII minor antennae to have a more holistic conclusion on the effect of shade or low CO_2 on light reactions.
- **Chapters 4** and **5** measured the total leaf absorptance and it is suggested that examination of leaf morphological and anatomical characteristics will elucidate whether changes in absorptance were also due to the occurrence of other alterations in leaf structure or ultra-structure as a result of growth under shade or low CO_2 environment. These changes may include changes in leaf thickness, arrangement of cells within a leaf, chloroplast positions within cells which could influence transmitted light.
- **Chapter 4** focussed on how the whole leaf acclimated to low light. It will be necessary in the future to undertake these studies on BSC and MC such as has been previously done with thylakoid protein analysis (Hernández-Prieto *et al.,* 2019).
- It will also be useful in the future to directly measure absorbed light intensity within the leaf as has been previously done (Evans, 2006; Evans, 1986; Evans & Anderson, 1987; Vogelmann, 2003) and not just across the whole leaf as I was able to do here.

Table 6. 1 Estimated fraction of absorbed light partitioned to PSI (f_I) and PSII (f_{II})

Estimated fraction of absorbed light partitioned to PSI (f_I) and PSII (f_{II}) obtained by Chl fluorescence method under low irradiances and high CO_2 (3-4%) conditions in leaf of control and shade-grown C_3, C_4, gymnosperm, fern, and liverwort species. Values are means ± *s.e* (*n* = 4 leaf discs).

Species	f_I	f_{II}	f_I	f_{II}
	Control	Control	Shade	Shade
Panicum bisulcatum (C_3)	0.40 ± 0.02	0.60 ± 0.02	0.51 ± 0.01	0.49 ± 0.01
Panicum miliaceum (NAD-ME)	0.58 ± 0.01	0.42 ± 0.01	0.59 ± 0.01	0.41 ± 0.01
Megathyrsus maximus (PCK)	0.60 ± 0.01	0.40 ± 0.01	0.58 ± 0.02	0.42 ± 0.02
Panicum antidotale (NADP-ME)	0.60 ± 0.02	0.40 ± 0.02	0.62 ± 0.02	0.38 ± 0.02
Zea mays (NADP-ME)	0.43 ± 0.01	0.57 ± 0.01	0.54 ± 0.03	0.46 ± 0.03
Spinach (C_3)	0.58 ± 0.02	0.42 ± 0.02	0.60 ± 0.01	0.40 ± 0.01
Ginkgo biloba (Gymnosperm)	0.50 ± 0.01	0.50 ± 0.01		
Wollemi nobilis (Gymnosperm)	0.37 ± 0.01	0.63 ± 0.01		
Polypodium sp. (Fern)	0.48 ± 0.01	0.52 ± 0.01		
Marchantia polymorpha (Liverwort)	0.44 ± 0.01	0.56 ± 0.01		

Table 6. 2 Values of cyclic electron flow rates (CEF) and the estimated rates of Mehler reaction in leaf

Values of cyclic electron flow rates (CEF) calculated using the assumed f_I (uncorrected) and experimentally-derived f_I (corrected) and the estimated rates of Mehler reaction in leaf of control and shade-grown *Panicum antidotale* (NADP-ME), *Panicum miliaceum* (NAD-ME) and *Megathyrsus maximus* (PCK). Measurements were made under the temperature of 28^{o}C and high CO_2 condition (3-4%). Values are means ± s.e. (*n* = 4 leaf discs).

Irradiance (µmol photons m^{-2} s^{-1})	*P. antidotale* (NADP-ME)				*P. miliaceum* (NAD-ME)				*M. maximus* (PCK)			
	CEF (µmol e^- m^{-2} s^{-1})		Mehler reaction (µmol e^- m^{-2} s^{-1})		CEF (µmol e^- m^{-2} s^{-1})		Mehler reaction (µmol e^- m^{-2} s^{-1})		CEF (µmol e^- m^{-2} s^{-1})		Mehler reaction (µmol e^- m^{-2} s^{-1})	
	Uncorrected	Corrected	Control	Shade	Uncorrected	Corrected	Control	Shade	Uncorrected	Corrected	Control	Shade
100	-1.7 ± 3.4	3 ± 3.7	0.61 ± 0.08	0.37 ± 0.05	2.2 ± 3.4	8.8 ± 4	0.54 ± 0.16	1.34 ± 0.19	-2.9 ± 1.5	-5.1 ± 1.4	0.41 ± 0.07	0.62 ± 0.09
400	40.1 ± 8.4	61.2 ± 10.2	0.55 ± 0.17	0.53 ± 0.04	44.3 ± 13.7	71.4 ± 15.8	0.98 ± 0.27	1.77 ± 0.3	45.1 ± 8.3	35 ± 7.7	0.59 ± 0.18	0.93 ± 0.09
750	104.1 ± 12.1	142.6 ± 15	0.79 ± 0.31	0.62 ± 0.05	109.2 ± 21.9	157.2 ± 25.6	1.01 ± 0.11	1.85 ± 0.33	143.9 ± 15.9	123.8 ± 14.8	0.55 ± 0.14	0.84 ± 0.09
1000	148 ± 19.4	198.7 ± 23.8	0.63 ± 0.35	0.72 ± 0.05	151.2 ± 27.3	214.4 ± 32.2	0.84 ± 0.34	1.99 ± 0.39	205 ± 23.9	178.5 ± 22.3	0.63 ± 0.32	1 ± 0.05
2000	334.8 ± 39.1	423.8 ± 46	0.95 ± 0.41	1.25 ± 0.16	354.9 ± 51.6	463.5 ± 61.5	1.29 ± 0.45	1.84 ± 0.27	421.1 ± 46.7	375.3 ± 43.4	1.27 ± 0.13	1.28 ± 0.09

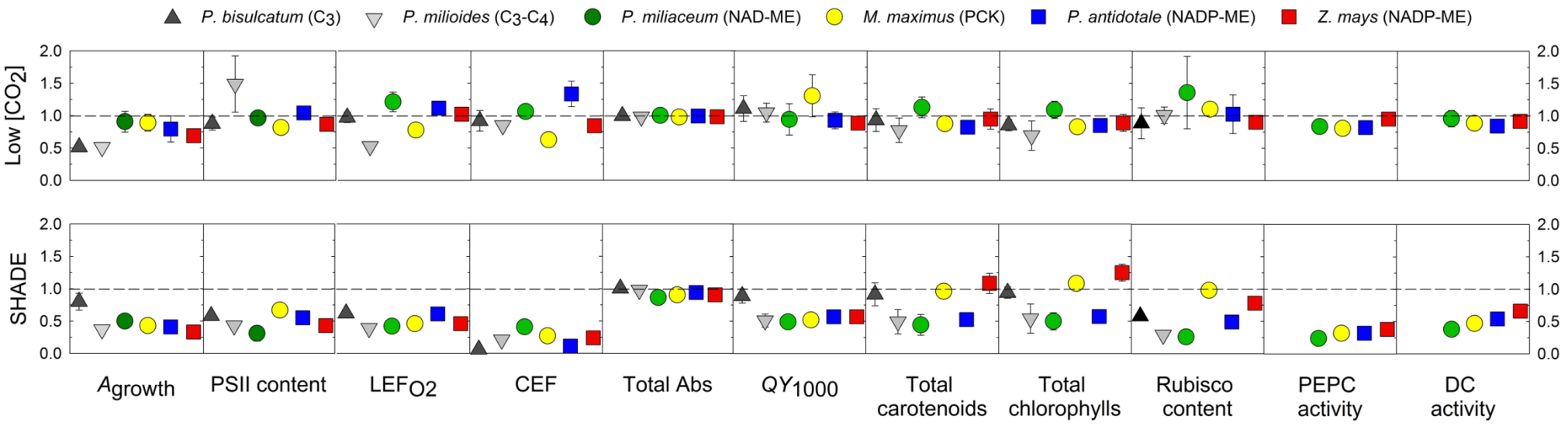

Figure 6. 1 Low [CO_2] and shade acclimation of physiological parameters in C_3, C_3-C_4 and C_4 species

Low [CO_2] and shade acclimation expressed as response ratio of CO_2 assimilation rates under growth irradiance (A_{growth}), content of functional PSII, various electron transport rates (LEF_{O2} or ETR2 and CEF), total absorptance, absorbed quantum yield for CO_2 uptake under high light (QY_{1000}), contents of total carotenoids, chlorophyll and Rubisco, PEPC and total decarboxylases activity for C_3, C_3-C_4 and C_4 species grown under ambient (400 ppm) and low (280 ppm) CO_2 conditions and high light (~900 µmol photons m^{-2} s^{-1}) and shade (~280 photons m^{-2} s^{-1}) environments.

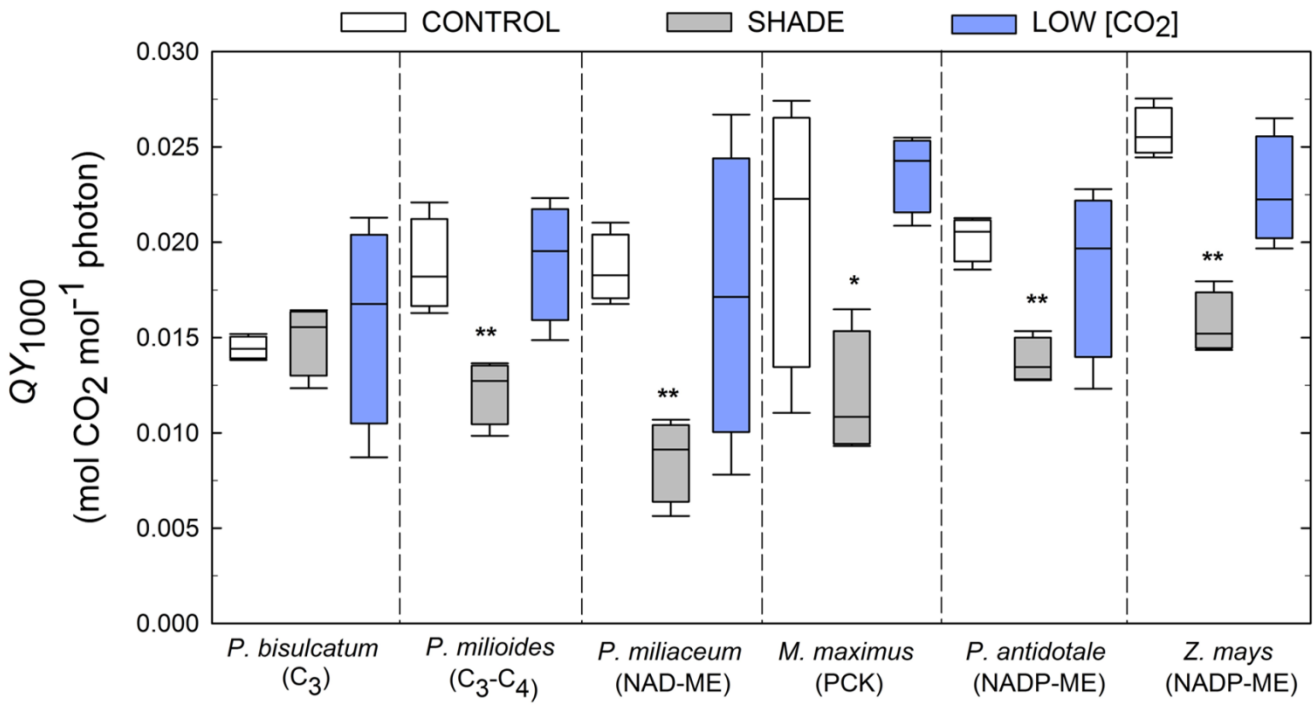

Figure 6. 2 Absorbed quantum yields for CO_2 uptake (QY_{1000}) by C_3, C_3-C_4 and C_4 species under shade and low [CO_2] environments

Absorbed quantum yields for CO_2 uptake measured at 1000 µmol photons m^{-2} s^{-1} and 400 ppm [CO_2] (QY_{1000}) by C_3, C_3-C_4 and C_4 species grown under ambient (400 ppm) and low (280 ppm) [CO_2] and high light (~900 µmol photons m^{-2} s^{-1}) and shade (~280 photons m^{-2} s^{-1}) environments. Statistical significance levels (t-test) for the growth condition within each species are shown and they are: * ≡ $p < 0.05$; ** ≡ $p < 0.01$; *** ≡ $p < 0.001$.

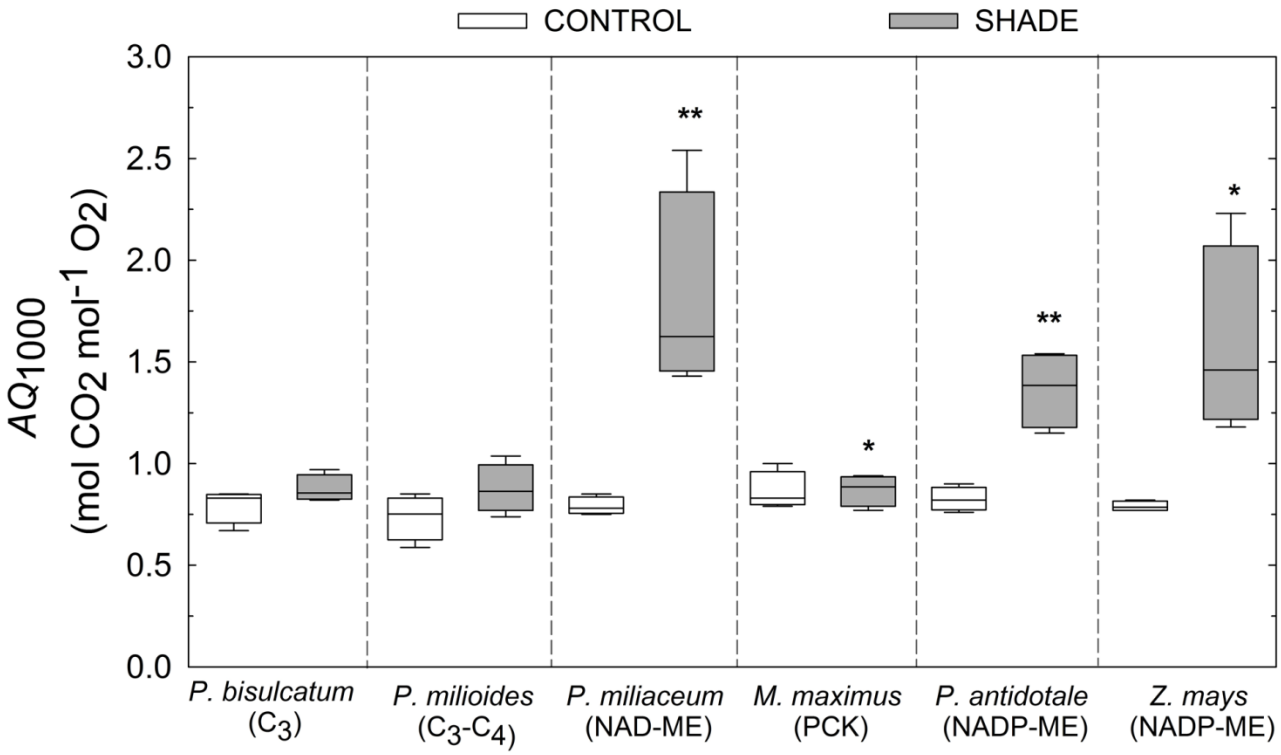

Figure 6. 3 The assimilation quotient (AQ_{1000}) of C_3, C_3-C_4 and C_4 species grown under shade

The assimilation quotient at 1000 µmol photons m^{-2} s^{-1} (AQ_{1000}) of C_3, C_3-C_4 and C_4 species grown under shade. Measurements were made at 28°C, 21% O_2 and 400 ppm [CO_2]. Statistical significance levels (t-test) for the growth condition within each species are shown and they are: * ≡ $p < 0.05$; ** ≡ $p < 0.01$; *** ≡ $p < 0.001$.Values are means ± s.e. (n = 4 leaf discs).

REFERENCES

Akoumianaki-Ioannidou, A., Georgakopoulos, J.H., Fasseas, C. & Argyroudi-Akoyunoglou, J.H. (2004). Photoacclimation in *Spathiphyllum*. *Journal of Photochemistry and Photobiology B: Biology*. ***73*(3)**: 149–158

Allen, J.F. (2003). Cyclic, pseudocyclic and noncyclic photophosphorylation: new links in the chain. *Trends in Plant Science*. ***8*(1)**: 15–19

Amthor, J.S. (2010). From sunlight to phytomass: on the potential efficiency of converting solar radiation to phyto-energy. *New Phytologist*. ***188*(4)**: 939–959

Anderson, J. M., Chow, W.S. & Goodchild, D.J. (1988). Thylakoid membrane organisation in sun/shade acclimation. *Functional Plant Biology*. ***15*(2)**: 11–26

Anderson, J.M. & Osmond, C.B. (1987). Shade-sun responses: compromises between acclimation and photoinhibition. In D. J. Kyle, C. B. Osmond & C. J. Arntzen (eds.), *Photoinhibition*. Amsterdam: Elsevier

Anderson, J. M., Chow, W.S. & Goodchild, D.J. (1988). Thylakoid membrane organisation in sun/shade acclimation. *Australian Journal of Plant Physiology*. ***15***: 11–26

Anderson, J. M., Chow, W.S. & Park, Y.-I. (1995). The grand design of photosynthesis: Acclimation of the photosynthetic apparatus to environmental cues. *Photosynthesis Research*. ***46*(1–2)**: 129–139

Anderson, J. M., Woo, K.C. & Boardman, N.K. (1971). Photochemical systems in mesophyll and bundle sheath chloroplasts of C_4 plants. *BBA - Bioenergetics*. ***245*(2)**: 398–408

Anderson, J. M. (1986). Photoregulation of the composition, function, and structure of thylakoid membranes. *Annual Review of Plant Physiology*. ***37*(1)**: 93–136

Anderson, L.E. (2003). Chloroplast and cytoplasmic enzymes III. Pea leaf ribose 5-phosphate isomerases. *BBA - Enzymology*. ***235*(1)**: 245–249

Anderson, L.J., Maherali, H., Johnson, H.B., Wayne Polley, H. & Jackson, R.B. (2001). Gas exchange and photosynthetic acclimation over subambient to elevated CO_2 in a C_3-C_4 grassland. *Global Change Biology*. ***7*(6)**: 693–707

Aro, E.-M., Virgin, I. & Andersson, B. (1993). Photoinhibition of Photosystem II. Inactivation, protein damage and turnover. *BBA - Bioenergetics*. ***1143*(2)**: 113–134

Asada, K. (1999). The water-water cycle in chloroplasts: scavenging of active oxygens and dissipation of excess photons. *Annual Review of Plant Physiology and Plant Molecular Biology*. ***50***: 601–639

Asada, K. (2000). The water-water cycle as alternative photon and electron sinks. *Philosophical Transactions of the Royal Society B: Biological Sciences*. ***355*(1402)**: 1419–1431

Atkin, O.K., Millar, A.H., Gardeström, P. & Day, D.A. (2006). Photosynthesis, carbohydrate metabolism and respiration in leaves of higher plants. In S. Leegood R.C., Sharkey T.D., von Caemmerer (ed.), *Photosynthesis. Advances in Photosynthesis and Respiration. vol 9.* Springer, Dordrecht

Avelange, M.H., Thiéry, J.M., Sarrey, F., Gans, P. & Rébeillé, F. (1991). Mass-spectrometric determination of O_2 and CO_2 gas exchange in illuminated higher-plant cells. Evidence for light-inhibition of substrate decarboxylations. *Planta*. ***183*(2)**: 150–157

Azcón-Bieto, J., Farquhar, G.D. & Caballero, A. (1981). Effects of temperature, oxygen concentration, leaf age and seasonal variations on the CO_2 compensation point of *Lolium perenne* L. *Planta*. ***152*(6)**: 497–504

Badger, M.R. (1985). Photosynthetic oxygen exchange. *Annual Review of Plant Physiology*. ***36*(1)**: 27–53

Badger, M.R., von Caemmerer, S., Ruuska, S. & Nakano, H. (2000). Electron flow to oxygen in higher plants and algae: rates and control of direct photoreduction (Mehler reaction) and rubisco oxygenase. *Philosophical Transactions of the Royal Society B: Biological Sciences*. ***355*(1402)**: 1433–1446

Bailey, S., Walters, R.G., Jansson, S. & Horton, P. (2001). Acclimation of *Arabidopsis thaliana* to the light environment: the existence of separate low light and high light responses. *Planta*. ***213*(5)**: 794–801

Ballaré. (1999). Keeping up with the neighbours: phytochrome sensing and other signalling mechanisms. *Trends in Plant Science*. ***4*(3)**: 97–102

Baroli, I. & Melis, A. (1998). Photoinhibitory damage is modulated by the rate of photosynthesis and by the photosystem II light-harvesting chlorophyll antenna size. *Planta*. ***205*(2)**: 288–296

Bartoli, C.G., Gomez, F., Gergoff, G., Guiamét, J.J. & Puntarulo, S. (2005). Up-regulation of the mitochondrial alternative oxidase pathway enhances photosynthetic electron transport under drought conditions. *Journal of Experimental Botany*. ***56*(415)**: 1269–1276

Bassi, R., Pineau, B., Dainese, P. & Marquardt, J. (1993). Carotenoid-binding proteins of photosystem II. *European Journal of Biochemistry*. ***212*(2)**: 297–303

Batanouny, K.H., Stichler, W. & Ziegler, H. (1988). Photosynthetic pathways, distribution, and ecological characteristics of grass species in Egypt. *Oecologia*. ***75*(4)**: 539–548

Beckmann, K., Messinger, J., Badger, M.R., Wydrzynski, T. & Hillier, W. (2009). On-line mass spectrometry: membrane inlet sampling. *Photosynthesis Research*. ***102*(2)**: 511–522

Bellasio, C. & Griffiths, H. (2014a). Acclimation of C_4 metabolism to low light in mature maize leaves could limit energetic losses during progressive shading in a crop canopy. *Journal of Experimental Botany*. ***65*(13)**: 3725–3736

Bellasio, C. & Griffiths, H. (2014b). The operation of two decarboxylases, transamination, and partitioning of C_4 metabolic processes between mesophyll and bundle sheath cells allows light capture to be balanced for the maize C_4 pathway. *Plant Physiology*. ***164*(1)**: 466–80

Bellasio, C. & Griffiths, H. (2014c). Acclimation to low light by C_4 maize: implications for bundle sheath leakiness. *Plant, Cell and Environment*. ***37*(5)**: 1046–1058

Bellasio, C. & Lundgren, M.R. (2016). Anatomical constraints to C_4 evolution: light harvesting capacity in the bundle sheath. *New Phytologist*. ***212*(2)**: 485–496

Berner, R.A. & Kothavala, Z. (2001). GEOCARB III: A revised model of atmospheric CO_2 over Phanerozoic time. *American Journal of Science*. ***301*(2)**: 182–204

Biehler, K. & Fock, H. (2016). Evidence for the contribution of the Mehler-peroxidase reaction in dissipating excess electrons in drought-stressed wheat. *Plant Physiology*. ***112*(1)**: 265–272

Björkman, O. (2011). Responses to different quantum flux densities. In O. L. Lange, P. S. Nobel, C. B. Osmond & H. Ziegler (eds.), *Physiological Plant Ecology I. Encyclopedia of Plant*

Physiology (New Series), vol. 12. Berlin, Heidelberg: Springer Berlin Heidelberg

Björkman, O. (1973). Comparative studies on photosynthesis in higher plants. In A. C. Giese (ed.), *Photophysiology*. New York: Elsevier

Björkman, O. & Demmig, B. (1987). Photon yield of O_2 evolution and chlorophyll fluorescence characteristics at 77K among vascular plants of diverse origins. *Planta*. ***170*(4)**: 489–504

Bloom, A J, Caldwell, R.M., Finazzo, J., Warner, R.L. & Weissbart, J. (1989). Oxygen and carbon dioxide fluxes from barley shoots depend on nitrate assimilation. *Plant physiology*. ***91*(1)**: 352–6

Bloom, A.J., Smart, D.R., Nguyen, D.T. & Searles, P.S. (2002). Nitrogen assimilation and growth of wheat under elevated carbon dioxide. *Proceedings of the National Academy of Sciences of the United States of America*. ***99*(3)**: 1730–5

Boardman, N.K. (1977). Comparative photosynthesis of sun and shade plants. *Annual Review of Plant Physiology*. ***28*(1)**: 355–377

Boardman, N.K. (2003). Comparative photosynthesis of sun and shade plants. *Annual Review of Plant Physiology*. ***28*(1)**: 355–377

Brooks, A. & Farquhar, G.D. (1985). Effect of temperature on the CO_2/O_2 specificity of ribulose-1,5-bisphosphate carboxylase/oxygenase and the rate of respiration in the light. *Planta*. ***165*(3)**: 397–406

Burnell, J.N. & Hatch, M.D. (1988). Photosynthesis in phosphoenolpyruvate carboxykinase-type C_4 plants: pathways of C_4 acid decarboxylation in bundle sheath cells of Urochloa panicoides. *Archives of Biochemistry and Biophysics*. ***260*(1)**: 187–99

Burrows, P.A., Sazanov, L.A., Svab, Z., Maliga, P. & Nixon, P.J. (1998). Identification of a functional respiratory complex in chloroplasts through analysis of tobacco mutants containing disrupted plastid *ndh* genes. *The EMBO Journal*. ***17*(4)**: 868–876

Byrd, G.T. & Brown, R.H. (2008). Environmental effects on photorespiration of C_3-C_4 species : I. Influence of CO_2 and O_2 during growth on photorespiratory characteristics and leaf anatomy. *Plant Physiology*. ***90*(3)**: 1022–1028

Calvin, M. (1962). The Path of Carbon in Photosynthesis. *Angewandte Chemie International Edition in English*. ***1*(2)**: 65–75

Cammarata, K., Plumley, F.G. & Schmidt, G.W. (2013). Reconstitution of light harvesting complexes: a single apoprotein binds chl*a*, chl*b*, and xanthophylls. In M. Baltscheffsky (ed.), *Current Research in Photosynthesis*. Dordrecht: Springer Netherlands

Campbell, C.D., Sage, R.F., Kocacinar, F. & Way, D.A. (2005). Estimation of the whole-plant CO_2 compensation point of tobaco (*Nicotiana tabacum* L.). *Global Change Biology*. ***11*(11)**: 1956–1967

Canvin, D.T., Berry, J. a, Badger, M.R., Fock, H. & Osmond, C.B. (1980). Oxygen exchange in leaves in the light. *Plant Physiology*. ***66*(2)**: 302–307

Carlquist, S. & Schneider, E.L. (2001). Vessels in ferns: structural, ecological, and evolutionary significance. *American Journal of Botany*. ***88*(1)**: 1–13

Carnal, N.W., Agostino, A. & Hatch, M.D. (1993). Photosynthesis in phosphoenolpyruvate carboxykinase-type C_4 plants: Mechanism and regulation of C_4 acid decarboxylation in bundle sheath cells. *Archives of Biochemistry and Biophysics*. ***306*(2)**: 360–367

Carter, G.A. (2006). Responses of leaf spectral reflectance to plant stress. *American Journal of Botany*. ***80*(3)**: 239

Carter, G.A., Mitchell, R.J., Chappelka, A.H. & Brewer, C.H. (1992). Response of leaf spectral reflectance in loblolly pine to increased atmospheric ozone and precipitation acidity. *Journal of Experimental Botany*. ***43*(4)**: 577–584

Casano, L.M., Zapata, J.M., Martín, M. & Sabater, B. (2000). Chlororespiration and poising of cyclic electron transport. Plastoquinone as electron transporter between thylakoid NADH dehydrogenase and peroxidase. *The Journal of biological chemistry*. ***275*(2)**: 942–8

Chapman, K.S.R., Berry, J.A. & Hatch, M.D. (1980). Photosynthetic metabolism in bundle sheath cells of the C_4 species *Zea mays*: sources of ATP and NADPH and the contribution of photosystem II. *Archives of Biochemistry and Biophysics*. ***202*(2)**: 330–341

Chapman, K.S.R. & Hatch, M.D. (1981). Aspartate decarboxylation in bundle sheath cells of *Zea mays* and its possible contribution to C_4 photosynthesis. *Aust. J. Plant Physiol*. ***8***: 237–248

Chow, W., Hope, A. & Anderson, J. (2006). Further studies on quantifying photosystem II *in vivo* by flash-induced oxygen yield from leaf discs. *Functional Plant Biology*. ***18*(4)**: 397

Chow, W. S., Anderson, J.M. & Melis, A. (1990). The photosystem stoichiometry in thylakoids of some Australian shade-adapted plant-species. *Australian Journal of Plant Physiology*. ***17*(6)**: 665–674

Chow, W. S. & Hope, A.B. (2004). Kinetics of reactions around the cytochrome *bf* complex studied in intact leaf disks. *Photosynthesis Research*. ***81*(2)**: 153–163

Chow, W. S., Hope, A.B. & Anderson, J.M. (1989). Oxygen per flash from leaf disks quantifies photosystem II. *BBA - Bioenergetics*. ***973*(1)**: 105–108

Chow, W. S., Melis, A. & Anderson, J.M. (1990). Adjustments of photosystem stoichiometry in chloroplasts improve the quantum efficiency of photosynthesis. *PNAS*. ***87*(19)**: 7502–7506

Chow, W. S. & Anderson, J.M. (1987). Photosynthetic responses of *Pisum sativum* to an increase in irradiance during growth. *Australian Journal of Plant Physiology*. **14**: 1-8

Chow, W. S., Fan, D.-Y., Oguchi, R., Jia, H., Losciale, P., Park, Y.-I., … Anderson, J.M. (2012). Quantifying and monitoring functional photosystem II and the stoichiometry of the two photosystems in leaf segments: approaches and approximations. *Photosynthesis Research*. ***113*(1–3)**: 63–74

Christin, P.-A., Besnard, G., Samaritani, E., Duvall, M.R., Hodkinson, T.R., Savolainen, V. & Salamin, N. (2008). Oligocene CO_2 decline promoted C_4 photosynthesis in grasses. *Current Biology*. ***18*(1)**: 37–43

Collatz, G.J., Berry, J.A. & Clark, J.S. (1998). Effects of climate and atmospheric CO_2 partial pressure on the global distribution of C_4 grasses: present, past, and future. *Oecologia*. ***114*(4)**: 441–454

Cousins, A.B., Badger, M.R. & von Caemmerer, S. (2008). C_4 photosynthetic isotope exchange in NAD-ME- and NADP-ME-type grasses. *Journal of Experimental Botany*. ***59*(7)**: 1695–1703

Cramer, W.A., Soriano, G.M., Ponomarev, M., Huang, D., Zhang, H., Martinez, S.E. & Smith, J.L. (2002). Some new structural aspects and old controversies concerning the

cytochrome b_6f complex of oxygenic photosynthesis. *Annual Review of Plant Physiology and Plant Molecular Biology*. ***47*(1)**: 477–508

Cuttriss, A.J., Chubb, A.C., Alawady, A., Grimm, B. & Pogson, B.J. (2007). Regulation of lutein biosynthesis and prolamellar body formation in *Arabidopsis*. *Functional Plant Biology*. ***34*(8)**: 663–672

DalCorso, G., Pesaresi, P., Masiero, S., Aseeva, E., Schünemann, D., Finazzi, G., … Leister, D. (2008). A complex containing PGRL1 and PGR5 is involved in the switch between linear and cyclic electron flow in *Arabidopsis*. *Cell*. ***132*(2)**: 273–285

Daniel, E. (1997). The temperature dependence of photoinhibition in leaves of *Phaseolus vulgaris* (L.) Influence of CO_2 and O_2 concentrations. *Plant Science*. ***124*(1)**: 1–8

Danielsson, R., Albertsson, P.Å., Mamedov, F. & Styring, S. (2004). Quantification of photosystem I and II in different parts of the thylakoid membrane from spinach. *BBA - Bioenergetics*. ***1608*(1)**: 53–61

De la Torre, W.R. & Burkey, K.O. (1990a). Acclimation of barley to changes in light intensity: chlorophyll organization. *Photosynthesis Research*. ***24*(2)**: 117–125

De la Torre, W.R. & Burkey, K.O. (1990b). Acclimation of barley to changes in light intensity: photosynthetic electron transport activity and components. *Photosynthesis Research*. ***24*(2)**: 127–136

Demmig-Adams, B. (1998). Survey of thermal energy dissipation and pigment composition in sun and shade leaves. *Plant and Cell Physiology*. ***39*(5)**: 474–482

Demmig-Adams, B. & Adams, W.W. (1992). Carotenoid composition in sun and shade leaves of plants with different life forms. *Plant, Cell & Environment*. ***15*(4)**: 411–419

Demmig-Adams, B. & Adams, W.W. (1996). Xanthophyll cycle and light stress in nature: uniform response to excess direct sunlight among higher plant species. *Planta*. ***198***: 460–470

Demmig, B. & Björkman, O. (1987). Comparison of the effect of excessive light on chlorophyll fluorescence (77K) and photon yield of O_2 evolution in leaves of higher plants. *Planta*. ***171*(2)**: 171–184

Dengler, N.G., Dengler, R.E., Donnelly, P.M. & Hattersley, P.W. (1994). Quantitative leaf anatomy of C_3 and C_4 grasses (Poaceae): bundle sheath and mesophyll surface area relationships. *Annals of Botany*. ***73*(3)**: 241–255

Drozak, A. & Romanowska, E. (2006). Acclimation of mesophyll and bundle sheath chloroplasts of maize to different irradiances during growth. *BBA - Bioenergetics*. ***1757*(11)**: 1539–1546

Ducruet, J.M., Roman, M., Havaux, M., Janda, T. & Gallais, A. (2005). Cyclic electron flow around PSI monitored by afterglow luminescence in leaves of maize inbred lines (*Zea mays* L.): correlation with chilling tolerance. *Planta*. ***221*(4)**: 567–579

Durchan, M., Vácha, F. & Krieger-Liszkay, A. (2001). Effects of severe CO_2 starvation on the photosynthetic electron transport chain in tobacco plants. *Photosynthesis Research*. ***68*(3)**: 203–213

Edwards, E.J. (2012). New grass phylogeny resolves deep evolutionary relationships and discovers C_4 origins. *New Phytologist*. ***193***: 304–312

Edwards, E.J. & Ogburn, R.M. (2012). Angiosperm responses to a low-CO_2 world: CAM and

C_4 photosynthesis as parallel evolutionary trajectories. *International Journal of Plant Sciences*. ***173*(6)**: 724–733

Edwards, E.J., Osborne, C.P., Strömberg, C.A.E., Smith, S.A., Bond, W.J., Christin, P.A., … Tipple, B. (2010). The origins of C_4 grasslands: integrating evolutionary and ecosystem science. *Science*. ***328*(5978)**: 587–591

Edwards, E.J., Osborne, C.P., Strömberg, C.A.E., Smith, S.A. & Consortium, C.G. (2010). The origins of C_4 grasslands: Integrating evolutionary and ecosystem science. *Science*. ***328***: 587–592

Edwards, G. & Walker, D.A. (1983). *C_3 C_4: Mechanisms, and cellular and environmental regulation of photosynthesis*. *Plant, Cell and Environment*. Oxford: Blackwell

Edwards, G.E., Franceschi, V.R. & Voznesenskaya, E. V. (2004). Single-cell C_4 photosynthesis versus the dual-cell (kranz) paradigm. *Annual Review of Plant Biology*. ***55*(1)**: 173–196

Ehleringer, J. & Björkman, O. (1977). Quantum yields for CO_2 uptake in C_3 and C_4 plants: dependence on temperature, CO_2 and O_2 concentration. *Plant Physiology*. ***59*(1)**: 86–90

Ehleringer, J. & Pearcy, R.W. (1983). Variation in quantum yield for CO_2 uptake among C_3 and C_4 plants. *Plant Physiology*. ***73*(3)**: 555–9

Ehleringer, J.R. (1978). Implications of quantum yield differences on the distributions of C_3 and C_4 grasses. *Oecologia*. ***31*(3)**: 255–267

Ehleringer, J.R., Cerling, T.E. & Helliker, B.R. (1997). C_4 photosynthesis, atmospheric CO_2, and climate. *Oecologia*. ***112*(3)**: 285–299

Ehleringer, J.R., Sage, R.F., Flanagan, L.B. & Pearcy, R.W. (1991). Climate change and the evolution of C_4 photosynthesis. *Trends in ecology & evolution*. ***6*(3)**: 95–9

Evans, J. R. (2006). Acclimation by the thylakoid membranes to growth irradiance and the partitioning of nitrogen between soluble and thylakoid proteins. *Functional Plant Biology*. ***15*(2)**: 93

Evans, J. R. (1987). The relationship between electron transport components and photosynthetic capacity in pea leaves grown at different irradiances. *Functional Plant Biology*. ***14*(2)**: 157–170

Evans, J. R. (1989). Partitioning of nitrogen between and within leaves grown under different irradiances. *Australian Journal of Plant Physiology*. ***16*(6)**: 533–548

Evans, J. R. (2006a). The dependence of quantum yield on wavelength and growth irradiance. *Functional Plant Biology*. ***14*(1)**: 69–79

Evans, J. R. (2006b). Photosynthetic acclimation and nitrogen partitioning within a lucerne canopy. II. Stability through time and comparison with a theoretical optimum. *Functional Plant Biology*. ***20*(1)**: 69–82

Evans, J. R. & Poorter, H. (2001). Photosynthetic acclimation of plants to growth irradiance: the relative importance of specific leaf area and nitrogen partitioning in maximizing carbon gain. *Plant, Cell and Environment*. ***24*(8)**: 755–767

Evans, J. R. (1986). A quantitative analysis of light distribution between the two photosystems, considering variation in both the relative amounts of the chlorophyll-protein complexes and the spectral quality of light. *Photobiochemistry and Photobiophysics*. ***10***: 135–147

Evans, J. R. & Anderson, J.M. (1987). Absolute absorption and relative fluorescence excitation spectra of the five major chlorophyll-protein complexes from spinach thylakoid membranes. *BBA - Bioenergetics*. ***892(1)***: 75-82

Fan, D.Y., Fitzpatrick, D., Oguchi, R., Ma, W., Kou, J. & Chow, W.S. (2016). Obstacles in the quantification of the cyclic electron flux around photosystem I in leaves of C_3 plants. *Photosynthesis Research*. ***129*(3)**: 239–251

Fan, D.Y., Hope, A.B., Smith, P.J., Jia, H., Pace, R.J., Anderson, J.M. & Chow, W.S. (2007). The stoichiometry of the two photosystems in higher plants revisited. *BBA - Bioenergetics*. ***1767*(8)**: 1064–1072

Flexas, J., Ortuño, M.F., Ribas-Carbo, M., Diaz-Espejo, A., Flórez-Sarasa, I.D. & Medrano, H. (2007). Mesophyll conductance to CO_2 in *Arabidopsis thaliana*. *New Phytologist*. ***175*(3)**: 501–511

Foyer, C.H. & Noctor, G. (2000). Oxygen processing in photosynthesis: regulation and signalling. *New Phytologist*. ***146*(3)**: 359–388

Friso, G., Majeran, W., Huang, M., Sun, Q. & van Wijk, K.J. (2010). Reconstruction of metabolic pathways, protein expression, and homeostasis machineries across maize bundle sheath and mesophyll chloroplasts: large-scale quantitative proteomics using the first maize genome assembly. *Plant Physiology*. ***152*(3)**: 1219–50

Furbank, R., Jenkins, C. & Hatch, M. (1990). C_4 photosynthesis: quantum requirement, C_4 and overcycling and Q-cycle involvement. *Australian Journal of Plant Physiology*. ***17*(1)**: 1–7

Furbank, R.T. (2011). Evolution of the C_4 photosynthetic mechanism: are there really three C_4 acid decarboxylation types? *Journal of Experimental Botany*. ***62*(9)**: 3103–3108

Furbank, R.T., Badger, M.R. & Osmond, C.B. (1983). Photoreduction of oxygen in mesophyll chloroplasts of C_4 plants: a model system for studying an *in vivo* Mehler reaction. *Plant Physiology*. ***73*(4)**: 1038–41

Genty, B., Briantais, J.-M. & Baker, N.R. (1989). The relationship between the quantum yield of photosynthetic electron transport and quenching of chlorophyll fluorescence. *BBA - General Subjects*. ***990***: 87–92

Gerotto, C., Alboresi, A., Meneghesso, A., Jokel, M., Suorsa, M., Aro, E.-M. & Morosinotto, T. (2016). Flavodiiron proteins act as safety valve for electrons in *Physcomitrella patens*. *PNAS*. ***113*(43)**: 12322–12327

Gerst, A.N.J. (1995). Coupled cyclic electron transport in intact chloroplasts and leaves of C_3 plants: Does it exist? if so, what is its function? *Photosynthesis Research*. ***46***: 269–275

Gesch, R.W., Vu, J.C.V., Boote, K.J., Allen, L.H. & Bowes, G. (2000). Subambient growth CO_2 leads to increased Rubisco small subunit gene expression in developing rice leaves. *Journal of Plant Physiology*. ***157*(2)**: 235–238

Ghannoum, O., Evans, J.R., Chow, W.S., Andrews, T.J., Conroy, J.P. & von Caemmerer, S. (2005). Faster rubisco is the key to superior nitrogen-use efficiency in NADP-malic enzyme relative to NAD-malic enzyme C_4 grasses. *Plant Physiology*. ***137*(2)**: 638–650

Ghannoum, O., Evans, J.R. & von Caemmerer, S. (2011). Nitrogen and water use efficiency of C_4 plants. In A. S. Raghavendra & R. F. Sage (eds.), *C_4 Photosynthesis and Related CO_2 Concentrating Mechanisms*. Springer, Dordrecht

Gill, R.A., Polley, H.W., Johnson, H.B., Anderson, L.J., Maherali, H. & Jackson, R.B. (2002). Nonlinear grassland responses to past and future atmospheric CO_2. *Nature*. ***417*(6886)**: 279–282

Godde, D. (1982). Evidence for a membrane bound NADH-plastoquinone-oxidoreductase in *Chlamydomonas reinhardii* CW-15. *Arch. Microbiol.* ***131***: 197–202

Golding, A.J. & Johnson, G.N. (2003). Down-regulation of linear and activation of cyclic electron transport during drought. *Planta*. ***218*(1)**: 107–114

Gould, K.S., Kuhn, D.N., Lee, D.W. & Oberbauer, S.F. (1995). Why leaves are sometimes red? *Nature*. ***378*(6554)**: 241–242

Govindjee. (1995). Sixty-three years since Kautsky: Chlorophyll *a* fluorescence. *Functional Plant Biology*. ***22*(2)**: 131

Gowik, U. & Westhoff, P. (2011). The path from C_3 to C_4 photosynthesis. *Plant Physiology*. ***155*(1)**: 56–63

Green, B.R. & Durnford, D.G. (2002). The chlorophyll-carotenoid proteins of oxygenic photosynthesis. *Annual Review of Plant Physiology and Plant Molecular Biology*. ***47*(1)**: 685–714

Gutierrez, M., Gracen, V.E. & Edwards, G.E. (1974). Biochemical and cytological relationships in C_4 plants. *Planta*. ***119*(4)**: 279–300

Guy, R.D., Fogel, M.L. & Berry, J.A. (2016). Photosynthetic fractionation of the stable isotopes of oxygen and carbon. *Plant Physiology*. ***101*(1)**: 37–47

Hanawa, H., Ishizaki, K., Nohira, K., Takagi, D., Shimakawa, G., Sejima, T., … Miyake, C. (2017). Land plants drive photorespiration as higher electron-sink: comparative study of post-illumination transient O_2 -uptake rates from liverworts to angiosperms through ferns and gymnosperms. *Physiologia Plantarum*. ***161*(1)**: 138–149

Harbinson, J. & Hedley, C.L. (1993). Changes in P-700 oxidation during the early stages of the induction of photosynthesis. *Plant Physiology*. ***103*(2)**: 649–660

Hatch, M.D. (1987). C_4 photosynthesis: a unique blend of modified biochemistry, anatomy and ultrastructure. *BBA - Reviews on Bioenergetics*. ***895*(2)**: 81–106

Hatch, M.D., Agostino, A. & Jenkins, C. (1995). Measurement of the leakage of CO_2 from bundle-sheath cells of leaves during C_4 photosynthesis. *Plant Physiology*. ***108*(1)**: 173–181

Hattersley, P.W. (1983). The distribution of C_3 and C_4 grasses in Australia in relation to climate. *Oecologia*. ***57*(1–2)**: 113–128

Hattersley, P.W. (1992). C_4 photosynthetic pathway variation in grasses (Poaceae): Its significance for arid and semi-arid lands. In G. P. Chapman (ed.), *Desertified grasslands: their biology and management*. London: Academic Press

Heber, U. & Walker, D. (2008). Concerning a dual function of coupled cyclic electron transport in leaves. *Plant Physiology*. ***100*(4)**: 1621–1626

Henderson, S., von Caemmerer, S. & Farquhar, G. (1992). Short-term measurements of carbon isotope discrimination in several C_4 species. *Functional Plant Biology*. ***19*(3)**: 263

Hernández-Prieto, M.A., Foster, C., Watson-Lazowski, A., Ghannoum, O. & Chen, M. (2019). Comparative analysis of thylakoid protein complexes in the mesophyll and bundle

sheath cells from C_3, C_4 and C_3-C_4 Paniceae grasses. *Physiologia Plantarum*. https://doi.org/10.1111/ppl.12956

Hihara, Y. & Sonoike, K. (2006). Regulation, inhibition and protection of photosystem I. In E. M. Aro & B. Andersson (eds.), *Regulation of Photosynthesis. Advances in Photosynthesis and Respiration, vol 11*. Dordrecht: Springer, Dordrecht

Hikosaka, K. & Terashima, I. (1995). A model of the acclimation of photosynthesis in the leaves of C_3 plants to sun and shade with respect to nitrogen use. *Plant, Cell & Environment*. ***18*(6)**: 605–618

Hoefnagel, M.H.N., Atkin, O.K. & Wiskich, J.T. (1998). Interdependence between chloroplasts and mitochondria in the light and the dark. *BBA*. ***1366***: 235–255

Hogewoning, S.W., Wientjes, E., Douwstra, P., Trouwborst, G., van Ieperen, W., Croce, R. & Harbinson, J. (2012). Photosynthetic quantum yield dynamics: from photosystems to leaves. *The Plant Cell*. ***24*(5)**: 1921–1935

Hormann, H., Neubauer, C. & Schreiber, U. (1994). An active Mehler-peroxidase reaction sequence can prevent cyclic PSI electron transport in the presence of dioxygen in intact spinach chloroplasts. *Photosynthesis Research*. ***41*(3)**: 429–437

Horton, J.L. & Neufeld, H.S. (1998). Photosynthetic responses of *Microstegium vimineum* (Trin.) A. Camus, a shade-tolerant, C_4 grass, to variable light environments. *Oecologia*. ***114*(1)**: 11–19

Horton, P., Ruban, A. V., Rees, D., Pascal, A.A., Noctor, G. & Young, A.J. (1991). Control of the light-harvesting function of chloroplast membranes by aggregation of the LHCII chlorophyll-protein complex. *Federation of European Biochemical Societies*. ***292*(1)**: 1–4

Horváth, E.M., Peter, S.O., Joët, T., Rumeau, D., Cournac, L., Horváth, G. V, … Medgyesy, P. (2000). Targeted inactivation of the plastid *ndhB* gene in tobacco results in an enhanced sensitivity of photosynthesis to moderate stomatal closure. *Plant Physiology*. ***123*(4)**: 1337–1350

Huang, W., Yang, S.J., Zhang, S.B., Zhang, J.L. & Cao, K.F. (2012). Cyclic electron flow plays an important role in photoprotection for the resurrection plant *Paraboea rufescens* under drought stress. *Planta*. ***235*(4)**: 819–828

Huner, N.P.A., Öquist, G. & Melis, A. (2003). Photostasis in plants, green algae and cyanobacteria: the role of light-harvesting antenna complexes. In B. R. Green & P. W.W. (eds.), *Light-harvesting antennas in photosynthesis*. Springer, Dordrecht

Ikezawa, N., Ifuku, K., Endo, T. & Sato, F. (2003). Inhibition of photosystem II of spinach by the respiration inhibitors piericidin A and thenoyltrifluoroacetone. *Bioscience, Biotechnology, and Biochemistry*. ***66*(9)**: 1925–1929

Inc., L.-C. (1984). Integrating Sphere, Instruction manual

Ivanov, B., Asada, K. & Edwards, G.E. (2007). Analysis of donors of electrons to photosystem I and cyclic electron flow by redox kinetics of P700 in chloroplasts of isolated bundle sheath strands of maize. *Photosynthesis Research*. ***92*(1)**: 65–74

Jensen, R.G. (2006). Photosynthesis: C_3, C_4. Mechanisms, and cellular and environmental regulation, of photosynthesis. *Science*. ***222*(4627)**: 1009–1009

Jin, E. (2003). Role of the reversible xanthophyll cycle in the photosystem II damage and repair

cycle in *Dunaliella salina*. *Plant Physiology*. ***132*(1)**: 352–364

Johnson, G.N. (2011). Reprint of: physiology of PSI cyclic electron transport in higher plants. *BBA - Bioenergetics*. ***1807*(8)**: 906–911

Joliot, P. & Joliot, A. (2002). Cyclic electron transfer in plant leaf. *PNAS*. ***99*(15)**: 10209–14

Joliot, P. & Joliot, A. (2006). Cyclic electron flow in C_3 plants. *BBA - Bioenergetics*. ***1757*(5–6)**: 362–368

Kanai, R. & Edwards, G.E. (1999). The biochemistry of C_4 photosynthesis. In Rowan F. Sage & R. K. Monson (eds.), *C_4 Plant Biology*. San Diego: Academic Press

Kaplan, A. & Bjorkman, O. (1980). Ratio of CO_2 uptake to O_2 evolution during photosynthesis in higher plants. *Z Planzenphysiol*. ***96*(623)**: 185–188

Kiirats, O. (2002). Bundle sheath diffusive resistance to CO_2 and effectiveness of C_4 photosynthesis and refixation of photorespired CO_2 in a C_4 cycle mutant and wild-type *Amaranthus edulis*. *Plant Physiology*. ***130*(2)**: 964–976

Kirchhoff, H., Sharpe, R.M., Herbstova, M., Yarbrough, R. & Edwards, G.E. (2013). Differential mobility of pigment-protein complexes in granal and agranal thylakoid membranes of C_3 and C_4 plants. *Plant physiology*. ***161*(1)**: 497–507

Klughammer, C. & Schreiber, U. (1994). An improved method, using saturating light-pulses, for the determination of photosystem-I quantum yield via $P700^+$-absorbency changes at 830 nm. *Planta*. ***192*(2)**: 261–268

Klughammer, C. & Schreiber, U. (2008). Saturation pulse method for assessment of energy conversion in PSI. *PAM Application Notes*. ***1***: 11–14

Knapp, A.K. & Carter, G.A. (1998). Variability in leaf optical properties among 26 species from a broad range of habitats. *American Journal of Botany*. ***85*(7)**: 940–946

Kok, B. (1948). A critical consideration of the quantum yield of *Chlorella*-photosynthesis. *Enzymologia [Hague]*. ***13*(1)**: 1–56

Kono, M., Noguchi, K. & Terashima, I. (2014). Roles of the cyclic electron flow around PSI (CEF-PSI) and O_2-dependent alternative pathways in regulation of the photosynthetic electron flow in short-term fluctuating light in *Arabidopsis thaliana*. *Plant and Cell Physiology*. ***55*(5)**: 990–1004

Koteyeva, N.K., Voznesenskaya, E. V. & Edwards, G.E. (2015). An assessment of the capacity for phosphoenolpyruvate carboxykinase to contribute to C_4 photosynthesis. *Plant Science*. ***235***: 70–80

Kou, J., Takahashi, S., Fan, D.-Y., Badger, M.R. & Chow, W.S. (2015). Partially dissecting the steady-state electron fluxes in photosystem I in wild-type and pgr5 and *ndh* mutants of Arabidopsis. *Frontiers in Plant Science*. ***6***: 1–9

Kou, J., Takahashi, S., Oguchi, R., Badger, M.R. & Chow, W.S. (2013a). Estimation of the steady-state cyclic electron flux around PSI in spinach leaf discs in white light, CO_2-enriched air and other varied conditions. *Fuctional Plant Biology*. ***40***: 1018–1028

Kou, J., Takahashi, S., Oguchi, R., Badger, M.R. & Chow, W.S. (2013b). Quantification of cyclic electron flow in spinach leaf discs. In *Photosynthesis research for food, fuel and the future. Advanced topics in science and technology in China*. Springer, Berlin, Heidelberg

Kozaki, A. & Takeba, G. (1996). Photorespiration protects C_3 plants from photooxidation. *Nature*. ***384*(6609)**: 557–560

Krall, J.P. & Pearcy, R.W. (1993). Concurrent measurements of oxygen and carbon dioxide exchange during lightflecks in Maize (*Zea mays* L.). *Plant Physiology*. ***103*(3)**: 823–828

Kramer, D. M. & Evans, J.R. (2011). The importance of energy balance in improving photosynthetic productivity. *Plant Physiology*. ***155*(1)**: 70–78

Kramer, D. M., Johnson, G., Kiirats, O. & Edwards, G.E. (2004). New fluorescence parameters for the determination of QA redox state and excitation energy fluxes. *Photosynthesis Research*. ***79*(2)**: 209–218

Krause, G.H. & Weis, E. (1991). Chlorophyll fluorescence and photosynthesis: the basics. *Annual Review of Plant Physioliogy and Plant Molecular Biology*. ***42***: 313–49

Kromdijk, J, Ubierna, N., Cousins, A.B. & Griffiths, H. (2014). Bundle-sheath leakiness in C_4 photosynthesis: a careful balancing act between CO_2 concentration and assimilation. *Journal of Experimental Botany*. ***65*(13)**: 1–15

Kromdijk, Johannes, Griffiths, H. & Schepers, H.E. (2010). Can the progressive increase of C_4 bundle sheath leakiness at low PFD be explained by incomplete suppression of photorespiration? *Plant, Cell and Environment*. ***33*(11)**: 1935–1948

Ku, S.B. & Edwards, G.E. (2004). Oxygen inhibition of photosynthesis. *Planta*. ***140*(1)**: 1–6

Ku, S.B., Gutierrez, M., Kanai, R., Edwards, G.E. & Ku, S.B. (1974). Photosynthesis in mesophyll protoplasts and bundle sheath cells of various types of C_4 plants II. Chlorophyll and hill reaction studies. *Zeitschrift für Pflanzenphysiologie*. ***72*(4)**: 320–337

Kubásek, J., Šetlík, J., Dwyer, S. & Šantrůček, J. (2007). Light and growth temperature alter carbon isotope discrimination and estimated bundle sheath leakiness in C_4 grasses and dicots. *Photosynthesis Research*. ***91*(1)**: 47–58

Kühlbrandt, W., Wang, D.N. & Fujiyoshi, Y. (1994). Atomic model of plant light-harvesting complex by electron crystallography. *Nature*. ***367*(6464)**: 614–621

Laisk, A. & Edwards, G.E. (1998). Oxygen and electron flow in C_4 photosynthesis: Mehler reaction, photorespiration and CO_2 concentration in the bundle sheath. *Planta*. ***205*(4)**: 632–645

Laisk, A., Eichelmann, H., Oja, V. & Peterson, R.B. (2005). Control of cytochrome b_6f at low and high light intensity and cyclic electron transport in leaves. *BBA - Bioenergetics*. ***1708*(1)**: 79–90

Laisk, A., Eichelmann, H., Oja, V., Rasulov, B. & Rämma, H. (2006). Photosystem II cycle and alternative electron flow in leaves. *Plant and Cell Physiology*. ***47*(7)**: 972–983

Laisk, A., Eichelmann, H., Oja, V., Talts, E. & Scheibe, R. (2007). Rates and roles of cyclic and alternative electron flow in potato leaves. *Plant and Cell Physiology*. ***48*(11)**: 1575–1588

Laisk, A. & Loreto, F. (1996). Determining photosynthetic parameters from leaf CO_2 exchange and chlorophyll fluorescence. *Plant Physiology*. ***110*(3)**: 903–912

Laisk, A., Oja, V., Eichelmann, H. & Dall'Osto, L. (2014). Action spectra of photosystems II and I and quantum yield of photosynthesis in leaves in state 1. *BBA - Bioenergetics*. ***1837*(2)**: 315–325

Leegood, R.C. & Walker, R.P. (2003). Regulation and roles of phosphoenolpyruvate carboxykinase in plants. *Archives of Biochemistry and Biophysics*. ***414*(2)**: 204–210

Leegwood, R.C., Sharkey, T.D. & Caemmerer, S. Von. (2000). Photosynthesis Physiology and Metabolism. *Book*. Springer, Dordrecht

Lei, T.T. & Lechowicz, M.J. (1997). Functional responses of *Acer* species to two simulated forest gap environments: leaf-level properties and photosynthesis. *Photosynthetica*. ***33*(2)**: 277–289

Lei, Thomas T., Tabuchi, R., Kitao, M. & Koike, T. (1996). Functional relationship between chlorophyll content and leaf reflectance, and light-capturing efficiency of Japanese forest species. *Physiologia Plantarum*. ***96*(3)**: 411–418

Leong, T.-Y. & Anderson, J.M. (1984). Adaptation of the thylakoid membranes of pea chloroplasts to light intensities. I. Study on the distribution of chlorophyll-protein complexes. *Photosynthesis Research*. ***5*(2)**: 105–115

Li, Y., Xu, J., Haq, N.U., Zhang, H. & Zhu, X.G. (2014). Was low CO_2 a driving force of C_4 evolution: *Arabidopsis* responses to long-term low CO_2 stress. *Journal of Experimental Botany*. ***65*(13)**: 3657–3667

Lichtenthaler, H. K., Buschmann, C., D  **ll, M., Fietz, H.-J., Bach, T., Kozel, U., … Rahmsdorf, U.** (1981). Photosynthetic activity, chloroplast ultrastructure, and leaf characteristics of high-light and low-light plants and of sun and shade leaves. *Photosynthesis Research*. ***2*(2)**: 115–141

Lichtenthaler, H.K., Meier, D. & Buschmann, C. (1984). Development of chloroplasts at high and low light quanta fluence rates. *Israel Journal of Botany*. ***33***: 185–194

Lichtenthaler, Hartmut K., Ač, A., Marek, M. V., Kalina, J. & Urban, O. (2007). Differences in pigment composition, photosynthetic rates and chlorophyll fluorescence images of sun and shade leaves of four tree species. *Plant Physiology and Biochemistry*. ***45*(8)**: 577–588

Lichtenthaler, Hartmut K., Kuhn, G., Prenzel, U. & Meier, D. (1982). Chlorophyll-protein levels and degree of thylakoid stacking in radish chloroplasts from high-light, low-light and bentazon-treated plants. *Physiologia Plantarum*. ***56*(2)**: 183–188

Lin, Z.F. & Ehleringer, J. (1983). Epidermis effects on spectral properties of leaves of four herbaceous species. *Physiologia Plantarum*. ***59*(1)**: 91–94

Liu, H., Edwards, E.J., Freckleton, R.P. & Osborne, C.P. (2012). Phylogenetic niche conservatism in C_4 grasses. *Oecologia*. ***170*(3)**: 835–845

Lodish, H.F., Berk, A., Kaiser, C., Krieger, M., Scott, M.P., Bretscher, A., … Matsudaira, P.T. (2008). *Molecular cell biology* (6th ed.). New York: W.H. Freeman

Long, S.P. (1999). Environmental response. In R. F. Sage & R. K. Monson (eds.), *C_4 plant biology*. San Diego: Academic Press

Loreto, F., Tsonev, T. & Centritto, M. (2009). The impact of blue light on leaf mesophyll conductance. *Journal of Experimental Botany*. ***60*(8)**: 2283–2290

Lovelock, C.E. & Winter, K. (1996). Oxygen-dependent electron transport and protection from photoinhibition in leaves of tropical tree species. *Planta*. ***198*(4)**: 580–587

Ludlow, M.M. & Wilson, G.L. (1971). Photosynthesis of tropical pasture plants. I. Illuminance, carbon dioxide concentration, leaf temperature, and leaf-air vapour pressure difference.

Australian Journal of Biological Science. ***24***: 449–470

Mäenpää, P. & Andersson, B. (1989). Photosystem II heterogeneity and long-term acclimation of light-harvesting. *Zeitschrift für Naturforschung C*. ***44*****(5–6)**: 403–406

Maherali, H., Reid, C.D., Polley, H.W., Johnson, H.B. & Jackson, R.B. (2002). Stomatal acclimation over a subambient to elevated CO_2 gradient in a C_3/C_4 grassland. *Plant, Cell and Environment*. ***25*****(4)**: 557–566

Majeran, W., Cai, Y., Sun, Q. & van Wijk, K.J. (2005). Functional differentiation of bundle sheath and mesophyll maize chloroplasts determined by comparative proteomics. *The Plant cell*. ***17*****(11)**: 3111–3140

Makino, A., Miyake, C. & Yokota, A. (2002). Physiological functions of the water-water cycle (Mehler reaction) and the cyclic electron flow around PSI in rice leaves. *Plant and Cell Physiology*. ***43*****(9)**: 1017–1026

Maroco, J., Ku, M., Lea, P., Dever, L., Leegood, R., Furbank, R. & Edwards, G. (1998). Oxygen requirement and inhibition of C_4 photosynthesis. An analysis of C_4 plants deficient in the C_3 and C_4 cycles. *Plant Physiology*. ***116*****(2)**: 823–32

Maroco, J.P., Ku, M.S.B. & Edwards, G.E. (1997). Oxygen sensitivity of C_4 photosynthesis: evidence from gas exchange and chlorophyll fluorescence analyses with different C_4 subtypes. *Plant, Cell and Environment*. ***20***: 1525–1533

Maxwell, K., Badger, M.R. & Osmond, C.B. (1998). A comparison of CO_2 and O_2 exchange patterns and the relationship with chlorophyll fluorescence during photosynthesis in C_3 and CAM plants. *Australian Journal of Plant Physiology*. ***27*****(6)**: 45–52

McDonald, A.E., Ivanov, A.G., Bode, R., Maxwell, D.P., Rodermel, S.R. & Hüner, N.P.A. (2011). Flexibility in photosynthetic electron transport: the physiological role of plastoquinol terminal oxidase (PTOX). *BBA - Bioenergetics*. ***1807*****(8)**: 954–967

Mehler, A.H. (1951). Studies on reactions of illuminated chloroplasts. II. Stimulation and inhibition of the reaction with molecular oxygen. *Archives of Biochemistry and Biophysics*. ***34*****(2)**: 339–351

Melis, A. (1991). Dynamics of photosynthetic membrane composition and function. *BBA - Bioenergetics*. ***1058*****(2)**: 87–106

Miyake, C. & Yokota, A. (2000). Determination of the rate of photoreduction of O_2 in the water-water cycle in watermelon leaves and enhancement of the rate by limitation of photosynthesis. *Plant and Cell Physiology*. ***41*****(3)**: 335–343

Miyake, C. (2010). Alternative electron flows (water-water cycle and cyclic electron flow around PSI) in photosynthesis: molecular mechanisms and physiological functions. *Plant and Cell Physiology*. ***51*****(12)**: 1951–1963

Miyake, C., Miyata, M., Shinzaki, Y. & Tomizawa, K.I. (2005). CO_2 response of cyclic electron flow around PSI (CEF-PSI) in tobacco leaves - relative electron fluxes through PSI and PSII determine the magnitude of non-photochemical quenching (NPQ) of chl fluorescence. *Plant and Cell Physiology*. ***46*****(4)**: 629–637

Miyake, C. & Okamura, M. (2003). Cyclic electron flow within PSII protects PSII from its photoinhibition in thylakoid membranes from spinach chloroplasts. *Plant and Cell Physiology*. ***44*****(4)**: 457–462

Miyake, C., Shinzaki, Y., Miyata, M. & Tomizawa, K.-I. (2004). Enhancement of cyclic electron flow around PSI at high light and its contribution to the induction of non-photochemical quenching of chl fluorescence in intact leaves of tobacco plants. *Plant and Cell Physiology*. ***45*(10)**: 1426–1433

Müller, P., Li, X.P. & Niyogi, K.K. (2001). Non-photochemical quenching. A response to excess light energy. *Plant Physiology*. ***125*(4)**: 1558–1566

Mullet, J.E. (2003). Chloroplast development and gene expression. *Annual Review of Plant Physiology and Plant Molecular Biology*. ***39*(1)**: 475–502

Munekage, Y., Hashimoto, M., Miyake, C., Tomizawa, K.-I., Endo, T., Tasaka, M. & Shikanai, T. (2004). Cyclic electron flow around photosystem I is essential for photosynthesis. *Nature*. ***429*(6991)**: 579–582

Munekage, Y., Hojo, M., Meurer, J., Endo, T., Tasaka, M. & Shikanai, T. (2002). *PGR5* is involved in cyclic electron flow around photosystem I and is essential for photoprotection in *Arabidopsis*. *Cell*. ***110*(3)**: 361–371

Murakami, K., Matsuda, R. & Fujiwara, K. (2016). Interaction between the spectral photon flux density distributions of light during growth and for measurements in net photosynthetic rates of cucumber leaves. *Physiologia Plantarum*. ***158*(2)**: 213–224

Murakami, K., Matsuda, R. & Fujiwara, K. (2017). Quantification of excitation energy distribution between photosystems based on a mechanistic model of photosynthetic electron transport. *Plant, Cell and Environment*. ***41***: 148–159

Myers, J. (1949). The pattern of photosynthesis in *Chlorella*. In J. Franck & W. E. Loomis (eds.), *Photosynthesis in Plants*. Ames, Iowa: Iowa State College Press

Niyogi, K.K. (1998). *Arabidopsis* mutants define a central role for the xanthophyll cycle in the regulation of photosynthetic energy conversion. *The Plant Cell*. ***10*(7)**: 1121–1134

Niyogi, K.K. (2002). Photoprotection revisited: genetic and molecular approaches. *Annual Review of Plant Physiology and Plant Molecular Biology*. ***50*(1)**: 333–359

Oaks, A. (1994). Efficiency of nitrogen utilization in C_3 and C_4 cereals. *Plant Physiology*. ***106*(2)**: 407–414

Ögren, E. & Rosenqvist, E. (1992). On the significance of photoinhibition of photosynthesis in the field and its generality among species. *Photosynthesis Research*. ***33*(1)**: 63–71

Okegawa, Y., Kagawa, Y., Kobayashi, Y. & Shikanai, T. (2008). Characterization of factors affecting the activity of photosystem I cyclic electron transport in chloroplasts. *Plant and Cell Physiology*. ***49*(5)**: 825–834

Öquist, G. & Huner, N.P.A. (1993). Cold-hardening-induced resistance to photoinhibition of photosynthesis in winter rye is dependent upon an increased capacity for photosynthesis. *Planta*. ***189*(1)**: 150–156

Ort, D.R. & Baker, N.R. (2002). A photoprotective role for O_2 as an alternative electron sink in photosynthesis? *Current Opinion in Plant Biology*. ***5*(3)**: 193–198

Osmond, B., Badger, M., Maxwell, K., Björkman, O. & Leegood, R. (1997). Too many photons: photorespiration, photoinhibition and photooxidation. *Trends in Plant Science*. ***2*(4)**: 119–121

Osmond, C.B. & Grace, S.C. (1995). Perspectives on photoinhibition and photorespiration in the

field: quintessential inefficiencies of the light and dark reactions of photosynthesis? *Journal of Experimental Botany*. ***46*(special)**: 1351–1362

Osmond, C.B., Winter, K. & Ziegler, H. (1982). Functional Significance of Different Pathways of CO2 Fixation in Photosynthesis. In *Physiological Plant Ecology II*. Berlin, Heidelberg: Springer Berlin Heidelberg

Paradiso, R., Meinen, E., Snel, J.F.H., De Visser, P., Van Ieperen, W., Hogewoning, S.W. & Marcelis, L.F.M. (2011). Spectral dependence of photosynthesis and light absorptance in single leaves and canopy in rose. *Scientia Horticulturae*. ***127*(4)**: 548–554

Park II, Y., Chow, W.S. & Anderson, J.M. (2016). Antenna size dependency of photoinactivation of photosystem II in light-acclimated pea leaves. *Plant Physiology*. ***115*(1)**: 151–157

Park, Y.-I., Chow, W.S., Osmond, C.B. & Anderson, J.M. (1996). Electron transport to oxygen mitigates against the photoinactivation of Photosystem II *in vivo*. *Photosynthesis Research*. ***50*(1)**: 23–32

Pearcy, R.W., Tumosa, N. & Williams, K. (1981). Relationships between growth, photosynthesis and competitive interactions for a C_3 and C_4 plant. *Oecologia*. ***48*(3)**: 371–376

Peisker, M. & Apel, H. (2001). Inhibition by light of CO_2 evolution from dark respiration: comparison of two gas exchange methods. *Photosynthesis Research*. ***70*(3)**: 291–298

Peltier, G & Thibault, P. (1985). O_2 uptake in the light in *Chlamydomonas:* evidence for persistent mitochondrial respiration. *Plant Physiology*. ***79*(1)**: 225–230

Peltier, Gilles & Cournac, L. (2002). Chlororespiration. *Annual Review of Plant Biology*. ***53*(1)**: 523–550

Pfundel, E., Nagel, E. & Meister, A. (1996). Analyzing the light energy distribution in the photosynthetic apparatus of C_4 plants using highly purified mesophyll and bundle-sheath thylakoids. *Plant Physiology*. ***112*(3)**: 1055–1070

Pinto, H., Sharwood, R.E., Tissue, D.T. & Ghannoum, O. (2014). Photosynthesis of C_3, C_3-C_4, and C_4 grasses at glacial CO_2. *Journal of Experimental Botany*. ***65*(13)**: 3669–3681

Pinto, H., Tissue, D.T. & Ghannoum, O. (2011). *Panicum milioides* (C_3-C_4) does not have improved water or nitrogen economies relative to C_3 and C_4 congeners exposed to industrial-age climate change. *Journal of Experimental Botany*. ***62*(9)**: 3223–3234

Plumley, F.G. & Schmidt, G.W. (2006). Reconstitution of chlorophyll a/b light-harvesting complexes: xanthophyll-dependent assembly and energy transfer. *PNAS*. ***84*(1)**: 146–150

Pogson, B., McDonald, K.A., Truong, M., Britton, G. & DellaPenna, D. (1996). *Arabidopsis* carotenoid mutants demonstrate that lutein is not essential for photosynthesis in higher plants. *Plant Cell*. ***8*(9)**: 1627–1639

Porra, R.J., Thompson, W. a. & Kriedemann, P.E. (1989). Determination of accurate extinction coefficients and simultaneous equations for assaying chlorophylls *a* and *b* extracted with four different solvents: verification of the concentration of chlorophyll standards by atomic absorption spectrosco. *BBA - Bioenergetics*. ***975*(3)**: 384–394

Prendergast, H., Hattersley, P. & Stone, N. (2006). New structural/biochemical associations in leaf blades of C_4 grasses (Poaceae). *Functional Plant Biology*. ***14*(4)**: 403

Priault, P., Tcherkez, G., Cornic, G., De Paepe, R., Naik, R., Ghashghaie, J. & Streb, P. (2006). The lack of mitochondrial complex I in a CMSII mutant of *Nicotiana sylvestris* increases photorespiration through an increased internal resistance to CO_2 diffusion. *Journal of Experimental Botany*. ***57*(12)**: 3195–3207

Quiles, M.J. (2006). Stimulation of chlororespiration by heat and high light intensity in oat plants. *Plant, Cell and Environment*. ***29*(8)**: 1463–1470

Raghavendra, A.S. & Padmasree, K. (2003). Beneficial interactions of mitochondrial metabolism with photosynthetic carbon assimilation. *Trends in Plant Science*. ***8*(11)**: 546–553

Renou, J.-L., Gerbaud, A., Just, D. & Andrc, M. (1990). Differing substomatal and chloroplastic CO_2 concentrations in water-stressed wheat. *Planta*. ***182***: 415–434

Roberty, S., Bailleul, B., Berne, N., Franck, F. & Cardol, P. (2014). PSI Mehler reaction is the main alternative photosynthetic electron pathway in *Symbiodinium* sp., symbiotic dinoflagellates of cnidarians. *New Phytologist*. ***204*(1)**: 81–91

Romanowska, E. & Albertsson, P.A. (1994). Isolation and characterization of the cytochrome *bf* complex from whole thylakoids, grana, and stroma lamellae vesicles from spinach chloroplasts. *Plant and Cell Physiology*. ***35*(4)**: 557–568

Romanowska, E. & Drożak, A. (2006). Comparative analysis of biochemical properties of mesophyll and bundle sheath chloroplasts from various subtypes of C_4 plants grown at moderate irradiance. *Acta Biochimica Polonica*. ***53*(4)**: 709–719

Romanowska, E., Drozak, A., Pokorska, B., Shiell, B.J. & Michalski, W.P. (2006). Organization and activity of photosystems in the mesophyll and bundle sheath chloroplasts of maize. *Journal of Plant Physiology*. ***163*(6)**: 607–18

Romanowska, E., Kargul, J., Powikrowska, M., Finazzi, G., Nield, J., Drozak, A. & Pokorska, B. (2008). Structural organization of photosynthetic apparatus in agranal chloroplasts of maize. *Journal of Biological Chemistry*. ***283*(38)**: 26037–26046

Ruban, A. V., Johnson, M.P. & Duffy, C.D.P. (2012). The photoprotective molecular switch in the photosystem II antenna. *BBA - Bioenergetics*. ***1817*(1)**: 167–181

Rumberg, B., Schubert, K., Strelow, F. & Tran-Anh, T. (2013). The H^+/ATP coupling ratio at the H^+-ATP-synthase of spinach chloroplasts is four. In *Current Research in Photosynthesis*. Dordrecht: Springer Netherlands

Rumeau, D., Peltier, G. & Cournac, L. (2007). Chlororespiration and cyclic electron flow around PSI during photosynthesis and plant stress response. *Plant, Cell and Environment*. ***30*(9)**: 1041–1051

Ruuska, S.A., Badger, M.R., Andrews, T.J. & von Caemmerer, S. (2000). Photosynthetic electron sinks in transgenic tobacco with reduced amounts of rubisco: little evidence for significant Mehler reaction. *Journal of Experimental Botany*. ***51***: 357–368

Sage, R. F. & McKown, A.D. (2006). Is C_4 photosynthesis less phenotypically plastic than C_3 photosynthesis? *Journal of Experimental Botany*. ***57*(2)**: 303–317

Sage, R. F., Monson, R.K., Leegood, R.C. & Walker, R.P. (1999). Regulation of the C_4 Pathway. *C_4 Plant Biology*. 89–131

Sage, R. F., Sage, T.L. & Kocacinar, F. (2012). Photorespiration and the evolution of C_4

photosynthesis. *Annual Review of Plant Biology*. ***63*(1)**: 19–47

Sage, R. F. (2004). The evolution of C_4 photosynthesis. *New Phytologist*. ***161*(2)**: 341–370

Sage, R. F & Coleman, J.R. (2001). Effects of low atmospheric CO_2 on plants: More than a thing of the past. *Trends in Plant Science*. ***6*(1)**: 18–24

Sage, R. F, Li, M. & Monson, R.K. (1999). The taxonomic distribution of C_4 photosynthesis. In Rowan F. Sage & R. K. Monson (eds.), *C_4 Plant Biology*. San Diego, California: Academic Press

Sagun, J. V., Badger, M.R., Chow, W.S. & Ghannoum, O. (2019). Cyclic electron flow and light partitioning between the two photosystems in leaves of plants with different functional types. *Photosynthesis Research*.

Sato, Y. & Kadota, A. (2006). Chloroplast movements in response to environmental signals. In R. R. Wise & J. K. Hoober (eds.), *The Structure and Function of Plastids. Advances in Photosynthesis and Respiration, vol 23*. Springer, Dordrecht

Scheibe, R. (2004). Malate valves to balance cellular energy supply. *Physiologia Plantarum*. ***120*(1)**: 21–26

Schreiber, U. & Neubauer, C. (1990). O_2-dependent electron flow, membrane energization and the mechanism of non-photochemical quenching of chlorophyll fluorescence. *Photosynthesis Research*. ***25*(3)**: 279–293

Schulze, E.D., Ellis, R., Schulze, W., Trimborn, P. & Ziegler, H. (1996). Diversity, metabolic types and $\delta^{13}C$ carbon isotope ratios in the grass flora of Namibia in relation to growth form, precipitation and habitat conditions. *Oecologia*. ***106*(3)**: 352–369

Schuster, G., Ohad, I., Martineau, B. & Taylor, W.C. (1985). Differentiation and development of bundle sheath and mesophyll thylakoids in maize. Thylakoid polypeptide composition, phosphorylation, and organization of photosystem II. *Journal of Biological Chemistry*. ***260*(21)**: 11866–11873

Sejima, T., Hanawa, H., Shimakawa, G., Takagi, D., Suzuki, Y., Fukayama, H., … Miyake, C. (2016). Post-illumination transient O_2 -uptake is driven by photorespiration in tobacco leaves. *Physiologia Plantarum*. ***156*(2)**: 227–238

Setién, I., Vega-Mas, I., Celestino, N., Calleja-Cervantes, M.E., González-Murua, C., Estavillo, J.M. & González-Moro, M.B. (2014). Root phosphoenolpyruvate carboxylase and NAD-malic enzymes activity increase the ammonium-assimilating capacity in tomato. *Journal of Plant Physiology*. ***171*(5)**: 49–63

Sharkey, T.D. (1988). Estimating the rate of photorespiration in leaves. *Physiologia Plantarum*. ***73*(1)**: 147–152

Sharwood, R. E., Sonawane, B. V. & Ghannoum, O. (2014). Photosynthetic flexibility in maize exposed to salinity and shade. *Journal of Experimental Botany*. ***65*(13)**: 3715–3724

Sharwood, R. E., Sonawane, B. V., Ghannoum, O. & Whitney, S.M. (2016). Improved analysis of C_4 and C_3 photosynthesis via refined in vitro assays of their carbon fixation biochemistry. *Journal of Experimental Botany*. ***67*(10)**: 3137–3148

Shikanai, T. (2014). Central role of cyclic electron transport around photosystem I in the regulation of photosynthesis. *Current Opinion in Biotechnology*. ***26*(Figure 1)**: 25–30

Shikanai, T, Endo, T., Hashimoto, T., Yamada, Y., Asada, K. & Yokota, A. (1998). Directed

disruption of the tobacco *ndhB* gene impairs cyclic electron flow around photosystem I. *PNAS*. ***95*(16)**: 9705–9709

Shikanai, T. (2007). Cyclic electron transport around photosystem I: genetic approaches. *Annual Review of Plant Biology*. ***58***: 199–217

Shikanai, T. (2016). Chloroplast NDH: A different enzyme with a structure similar to that of respiratory NADH dehydrogenase. *BBA - Bioenergetics*. ***1857*(7)**: 1015–1022

Shikanai, T., Takeda, T., Yamauchi, H., Sano, S., Tomizawa, K.I., Yokota, A. & Shigeoka, S. (1998). Inhibition of ascorbate peroxidase under oxidative stress in tobacco having bacterial catalase in chloroplasts. *FEBS Letters*. ***428*(1–2)**: 47–51

Shimakawa, G., Ishizaki, K., Tsukamoto, S., Tanaka, M., Sejima, T. & Miyake, C. (2017). The liverwort, *Marchantia*, drives alternative electron flow using a flavodiiron protein to protect PSI. *Plant Physiology*. ***173*(3)**: 1636–1647

Shimakawa, G., Matsuda, Y., Nakajima, K., Tamoi, M., Shigeoka, S. & Miyake, C. (2017). Diverse strategies of O_2 usage for preventing photo-oxidative damage under CO_2 limitation during algal photosynthesis. *Scientific Reports*. ***7*(1)**: 41022

Shirao, M., Kuroki, S., Kaneko, K., Kinjo, Y., Tsuyama, M., Förster, B., … Badger, M.R. (2013). Gymnosperms have increased capacity for electron leakage to oxygen (Mehler and PTOX reactions) in photosynthesis compared with angiosperms. *Plant and Cell Physiology*. ***54*(7)**: 1152–1163

Siebke, K., von Caemmerer, S., Badger, M. & Furbank, R.T. (1997). Expressing an RbcS antisense gene in transgenic Flaveria bidentis leads to an increased quantum requirement for CO_2 fixed in photosystems I and II. *Plant Physiology*. ***115*(3)**: 1163–1174

Siebke, K., Ghannoum, O., Conroy, J.P., Badger, M.R. & von Caemmerer, S. (2003). Photosynthetic oxygen exchange in C_4 oxygen as electron acceptor grasses: the role of oxygen as electron acceptor. *Plant, Cell and Environment*. ***26***: 1963–1972

Smillie, R.M. & Hetherington, S.E. (1999). Photoabatement by anthocyanin shields photosynthetic systems from light stress. *Photosynthetica*. ***36*(3)**: 451–463

Smith, M. & Martin, C.E. (1987). Photosynthetic responses to irradiance in three forest understory species of the C 4 grass genus *Muhlenbergia*. *Botanical Gazette*. ***148*(3)**: 275–282

Sonawane, B. V, Sharwood, R.E., Whitney, S. & Ghannoum, O. (2018). Shade compromises the photosynthetic efficiency of NADP-ME less than that of PEP-CK and NAD-ME C_4 grasses. *Journal of Experimental Botany*. ***69*(12)**: 3053–3068

Still, C.J., Berry, J.A., Collatz, G.J. & DeFries, R.S. (2003). Global distribution of C_3 and C_4 vegetation: Carbon cycle implications. *Global Biogeochemical Cycles*. ***17*(1)**: 6-1-6–14

Strand, D.D., Fisher, N., Davis, G.A. & Kramer, D.M. (2016). Redox regulation of the antimycin A sensitive pathway of cyclic electron flow around photosystem I in higher plant thylakoids. *BBA - Bioenergetics*. ***1857*(1)**: 1–6

Streb, P., Josse, E.M., Gallouët, E., Baptist, F., Kuntz, M. & Cornic, G. (2005). Evidence for alternative electron sinks to photosynthetic carbon assimilation in the high mountain plant species *Ranunculus glacialis*. *Plant, Cell and Environment*. ***28*(9)**: 1123–1135

Takabayashi, A., Kishine, M., Asada, K., Endo, T. & Sato, F. (2005). From the cover: Differential use of two cyclic electron flows around photosystem I for driving CO_2-

concentration mechanism in C_4 photosynthesis. *PNAS*. ***102*(46)**: 16898–16903

Takabayashi, A., Kishine, M., Asada, K., Endo, T. & Sato, F. (2005). Differential use of two cyclic electron flows around photosystem I for driving CO_2-concentration mechanism in C_4 photosynthesis. *PNAS*. ***102*(46)**: 16898–16903

Takagi, D., Ishizaki, K., Hanawa, H., Mabuchi, T., Shimakawa, G., Yamamoto, H. & Miyake, C. (2017). Diversity of strategies for escaping reactive oxygen species production within photosystem I among land plants: P700 oxidation system is prerequisite for alleviating photoinhibition in photosystem I. *Physiologia Plantarum*. ***161*(1)**: 56–74

Takahashi, H., Clowez, S., Wollman, F.A., Vallon, O. & Rappaport, F. (2013). Cyclic electron flow is redox-controlled but independent of state transition. *Nature Communications*. ***4***: 1–8

Takahashi, S., Bauwe, H. & Badger, M. (2007). Impairment of the photorespiratory pathway accelerates photoinhibition of photosystem II by suppression of repair but not acceleration of damage processes in *Arabidopsis*. *Plant Physiology*. ***144*(1)**: 487–494

Takahashi, S. & Badger, M.R. (2011). Photoprotection in plants: a new light on photosystem II damage. *Trends in Plant Science*. ***16*(1)**: 53–60

Takahashi, S., Milward, S.E., Fan, D.-Y., Chow, W.S. & Badger, M.R. (2009). How does cyclic electron flow alleviate photoinhibition in *Arabidopsis*? *Plant Physiology*. ***149*(3)**: 1560–1567

Tanaka, A. & Melis, A. (1997). Irradiance-dependent changes in the size and composition of the chlorophyll a-b light-harvesting complex in the green alga *Dunaliella salina*. *Plant and Cell Physiology*. ***38*(1)**: 17–24

Tazoe, Y. (2008). Relationships between quantum yield for CO_2 assimilation , activity of key enzymes and CO_2 leakiness in *Amaranthus cruentus*, a C_4 dicot , grown in high or low light ***49*(1)**: 19–29

Tcherkez, G., Gauthier, P., Buckley, T.N., Busch, F.A., Barbour, M.M., Bruhn, D., … Cornic, G. (2017). Leaf day respiration: low CO_2 flux but high significance for metabolism and carbon balance. *New Phytologist*. ***216*(4)**: 986–1001

Tcherkez, G., Farquhar, G.D. & Andrews, T.J. (2006). Despite slow catalysis and confused substrate specificity, all ribulose bisphosphate carboxylases may be nearly perfectly optimized. *Proceedings of the National Academy of Sciences of the United States of America*. ***103*(19)**: 7246–51

Thornber, J.P. (1986). Biochemical characterization and structure of pigment-proteins of photosynthetic organism. In L. A. Staehelin & C. J. Arntzen (eds.), *Photosynthesis III. Encyclopedia of Plant Physiology (New Series), vol 19*. Berlin, Heidelberg: Springer Berlin Heidelberg

Tissue, D.T., Griffin, K.L., Thomas, R.B. & Strain, B.R. (1995). Effects of low and elevated CO_2 on C_3 and C_4 annuals. II. Photosynthesis and leaf biochemistry. *Oecologia*. ***101*(1)**: 21–28

Tsuyama, M. & Kobayashi, Y. (2009). Reduction of the primary donor P700 of photosystem I during steady-state photosynthesis under low light in *Arabidopsis*. *Photosynthesis Research*. ***99*(1)**: 37–47

Turpin, D.H., Elrifi, I.R., Birch, D.G., Weger, H.G. & Holmes, J.J. (1988). Interactions

between photosynthesis, respiration, and nitrogen assimilation in microalgae. *Canadian Journal of Botany*. ***66*(10)**: 2083–2097

Van Lis, R. & Atteia, A. (2004). Control of mitochondrial function via photosynthetic redox signals. *Photosynthesis Research*. ***79*(2)**: 133–148

Vogel, J.C., Fuls, A. & Danin, A. (1986). Geographical and environmental distribution of C_3 and C_4 grasses in the Sinai, Negev, and Judean deserts. *Oecologia*. ***70*(2)**: 258–265

Vogelmann, T.C. (2003). Plant tissue optics. *Annual Review of Plant Physiology and Plant Molecular Biology*. ***44*(1)**: 231–251

von Caemmerer, S., Evans, J.R., Hudson, G.S. & Andrews, T.J. (1994). The kinetics of ribulose-1,5-bisphosphate carboxylase/oxygenase *in vivo* inferred from measurements of photosynthesis in leaves of transgenic tobacco. *Planta*. ***195*(1)**: 88–97

von Caemmerer, S. & Furbank, R.T. (1999). Modeling C_4 photosynthesis. In R. K. Monson (ed.), *C_4 Plant Biology*. San Diego: Academic Press

von Caemmerer, S. (2000). Biochemical models of leaf photosynthesis. *Techniques in Plant Sciences*. ***53*(9)**: 1689–1699

von Caemmerer, S. & Quick, W.P. (2006). Rubisco: physiology *in vivo*. In Leegood, T. D. Sharkey & S. von Caemmerer (eds.), *Photosynthesis. Advances in Photosynthesis and Respiration. vol 9*. Springer, Dordrecht

Walters, R. & Horton, P. (1995). Acclimation of *Arabidopsis thaliana* to the light environment: changes in photosynthetic function. *Planta*. ***197*(2)**: 306–312

Wang, Y., Bräutigam, A., Weber, A.P.M. & Zhu, X.G. (2014). Three distinct biochemical subtypes of C_4 photosynthesis? A modelling analysis. *Journal of Experimental Botany*. ***65*(13)**: 3567–3578

Ward, D.A. & Woolhouse, H.W. (1986). Comparative effects of light during growth on the photosynthetic properties of NADP-ME type C_4 grasses from open and shaded habitats. I. Gas exchange, leaf anatomy and ultrastructure. *Plant, Cell and Environment*. ***9*(4)**: 261–270

Ward, J.K., Antonovics, J., Thomas, R.B. & Strain, B.R. (2000). Is atmospheric CO_2 a selective agent on model C_3 annuals? *Oecologia*. ***123*(3)**: 330–341

Ward, J.K., Myers, D.A. & Thomas, R.B. (2008). Physiological and growth responses of C_3 and C_4 plants to reduced temperature when grown at low CO_2 of the last ice age. *Journal of Integrative Plant Biology*. ***50*(11)**: 1388–1395

Watkins, J.E., Mack, M.C., Sinclair, T.R. & Mulkey, S.S. (2007). Ecological and evolutionary consequences of desiccation tolerance in tropical fern gametophytes. *New Phytologist*. ***176*(3)**: 708–717

Weston, E., Thorogood, K., Vinti, G. & López-Juez, E. (2000). Light quantity controls leaf-cell and chloroplast development in *Arabidopsis* thaliana wild type and blue-light-perception mutants. *Planta*. ***211*(6)**: 807–815

Whitney, S.M., Baldet, P., Hudson, G.S. & John Andrews, T. (2001). Form I rubiscos from non-green algae are expressed abundantly but not assembled in tobacco chloroplasts. *Plant Journal*. ***26*(5)**: 535–547

Wingler, A., Walker, R.P., Chen, Z.-H. & Leegood, R.C. (1999). Phosphoenolpyruvate carboxykinase is involved in the decarboxylation of aspartate in the bundle sheath of maize.

Plant Physiology. ***120*(2)**: 539–46

Witt, H.T. (1979). Energy conversion in the functional membrane of photosynthesis. Analysis by light pulse and electric pulse methods. The central role of the electric field. *BBA - Bioenergetics*. ***505*(3–4)**: 355–427

Woo, K.C., Anderson, J.M., Boardman, N.K., Downton, W.J., Osmond, C.B. & Thorne, S.W. (1970). Deficient photosystem II in agranal bundle sheath chloroplasts of C_4 plants. *PNAS*. ***67*(1)**: 18–25

Xue, X., Gauthier, D.A., Turpin, D.H. & Weger, H.G. (2016). Interactions between photosynthesis and respiration in the green alga *Chlamydomonas reinhardtii* (characterization of light-enhanced dark respiration). *Plant Physiology*. ***112*(3)**: 1005–1014

Yamamoto, H.Y. (1979). Biochemistry of the violaxanthin cycle in higher plants. *Pure and Applied Chemistry*. ***51*(3)**: 639–648

Yamazaki, J.Y., Suzuki, T., Maruta, E. & Kamimura, Y. (2005). The stoichiometry and antenna size of the two photosystems in marine green algae, *Bryopsis maxim* and *Ulva pertusa*, in relation to the light environment of their natural habitat. *Journal of Experimental Botany*. ***56*(416)**: 1517–1523

Yamori, W., Sakata, N., Suzuki, Y., Shikanai, T. & Makino, A. (2011). Cyclic electron flow around photosystem I via chloroplast NAD(P)H dehydrogenase (NDH) complex performs a significant physiological role during photosynthesis and plant growth at low temperature in rice. *The Plant Journal*. ***68*(6)**: 966–976

Yamori, W. & Shikanai, T. (2016). Physiological functions of cyclic electron transport around photosystem I in sustaining photosynthesis and plant growth. *Annual Review of Plant Biology*. ***67***: 81–106

Yin, X. & Struik, P.C. (2015). Constraints to the potential efficiency of converting solar radiation into phytoenergy in annual crops: From leaf biochemistry to canopy physiology and crop ecology. *Journal of Experimental Botany*. ***66*(21)**: 6535–6549

Yin, X. & Struik, P.C. (2018). The energy budget in C_4 photosynthesis: insights from a cell-type-specific electron transport model. *New Phytologist*. ***218*(3)**: 986–998

Yin, X., Sun, Z., Struik, P.C. & Gu, J. (2011). Evaluating a new method to estimate the rate of leaf respiration in the light by analysis of combined gas exchange and chlorophyll fluorescence measurements. *Journal of Experimental Botany*. ***62*(10)**: 3489–3499

Yoshida, K., Terashima, I. & Noguchi, K. (2006). Distinct roles of the cytochrome pathway and alternative oxidase in leaf photosynthesis. *Plant and Cell Physiology*. ***47*(1)**: 22–31

Yoshida, K., Terashima, I. & Noguchi, K. (2007). Up-regulation of mitochondrial alternative oxidase concomitant with chloroplast over-reduction by excess light. *Plant and Cell Physiology*. ***48*(4)**: 606–614

Yoshida, K., Watanabe, C., Kato, Y., Sakamoto, W. & Noguchi, K. (2008). Influence of chloroplastic photo-oxidative stress on mitochondrial alternative oxidase capacity and respiratory properties: a case study with arabidopsis *yellow variegated 2*. *Plant and Cell Physiology*. ***49*(4)**: 592–603

Yoshida, K., Watanabe, C.K., Hachiya, T., Tholen, D., Shibata, M., Terashima, I. & Noguchi, K. (2011). Distinct responses of the mitochondrial respiratory chain to long- and short-term high-light environments in *Arabidopsis thaliana*. *Plant, Cell and Environment*.

***34*(4)**: 618–628

Zhang, M.-M., Fan, D.-Y., Sun, G.-Y. & Chow, W.S. (2018). Optimising the linear electron transport rate measured by chlorophyll a fluorescence to empirically match the gross rate of oxygen evolution in white light: towards improved estimation of the cyclic electron flux around photosystem I in leaves. *Functional Plant Biology*. ***45*(11)**: 1138

Zhu, X.-G., Long, S.P. & Ort, D.R. (2008). What is the maximum efficiency with which photosynthesis can convert solar energy into biomass? *Current Opinion in Biotechnology*. ***19*(2)**: 153–159